UNIVERSITY OF CAMBRIDGE

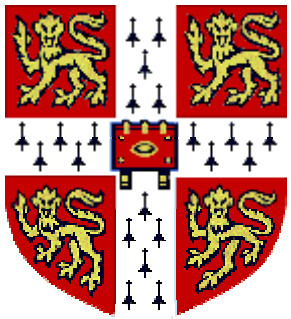

The role of the CapZ complex in vertebrate sarcomere integrity

Submitted in accordance with the requirements of the University of Cambridge for the degree of Doctor of Philosophy by

Annabelle Scott

The Wellcome Trust Sanger Institute

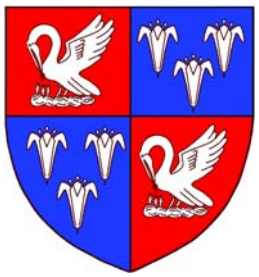

Corpus Christi College

Declaration

This thesis describes work undertaken in the laboratory of Dr Derek Stemple, at the Wellcome Trust Sanger Institute, in fulfillment of the requirements for the degree of Doctor of Philosophy, at Corpus Christi College, the University of Cambridge. This dissertation is entirely my own work and contains nothing that is the outcome of work done in collaboration with others, except as specified in the text. The material described here has not been submitted for a degree or diploma or any other qualification at any other University or Institution. I confirm that this thesis does not exceed 300 single sided pages of double spaced text, or 80,000 words.

Annabelle Scott

October 2007

Summary

Muscle cells provide the contractile force essential for internal organ function and body movement in all complex animals. Skeletal and cardiac muscle are composed of bundles of myofibrils containing highly organized arrays of individual contractile units called sarcomeres. Although many myofibrillar and sarcomeric proteins have been identified, we are only just beginning to elucidate the complex processes and interactions required for muscle formation and function. Mutations in components of the myofibril are responsible for a large proportion of human myopathies, therefore determining how the muscle develops and is maintained will be crucial for understanding the pathology of myopathies and developing treatments for these debilitating disorders.

The analyses of model organisms that carry mutations in sarcomeric and myofibrillar components can assist in our current understanding of muscle development and function. The aim of my project was to positionally clone and characterize the zebrafish (*Danio rerio)* muscle mutant *schnecke*, in order to investigate myofibrillogenesis *in vivo*. I identified a mutation in the *schnecke* locus at the exon 9 donor splice site of *capZα1*. CapZα1 is a subunit of the heterodimer CapZ, which caps the barbed end of polymerizing actin filaments at the sarcomeric Z-line. Characterization of the *schnecke* mutant and morpholino oligonucleotide knockdowns of the other CapZ subunits (CapZα2 and CapZβ) suggests that although loss of CapZ function alone does not affect sarcomere assembly, it is essential for the integrity of the myofibrillar and sarcomeric structure of zebrafish skeletal muscle. Additional double knockdown studies with the other components associated with the actin thin filament (Nebulin and Tropomodulin) indicate that CapZ is required in conjunction with these proteins for maintenance of the Z-line and thin filament assembly. The results presented in this thesis describe an additional role for CapZ in maintaining the stability of the sarcomeric and myofibrillar architecture and provides further insight into muscle integrity and function in vertebrates.

Acknowledgements

Firstly, I would like to thank my supervisor Derek Stemple, for allowing me to do a PhD in his lab, and providing me with guidance, encouragement and a fountain of ideas over the past three and a half years. I would also like to convey special thanks to Elisabeth Busch-Nentwich for assisting me in all aspects of the 'muscle' project, teaching me the art of positional cloning and collaborating on the double knockdown experiments. Thanks to past and present members of Team 31 and Team 30: Gareth, Steve, Huw, Yung Yao, Mariella, Christian, Carlos, Richard, Amanda, Fruzsina, John, Kevin, Emma, Kathy H, Kathy J, Evelyn, Ho-Yon, Ross, Colin, Marie, Isabel, Sam, Wei and Matt for help in proof reading this thesis, as well as plenty of experimental advice and lots of laughs over the years. A special mention to Morgan building friends Arun and Song for always cheering me up and sorting me out in computer crises!! Thanks to the staff in the RSF who have done a great job of keeping my lines healthy and happy: Dee, Rory, Davyd, Paul, Carl and Nick. Thanks to my committee members: Jim Smith, Jyoti Choudhary, John McCafferty and Gavin Wright, who have made me a better scientist (I hope!!!) and taught me how to be more organized and focused. I would also like to thank the Wellcome Trust and the Sanger for giving me the opportunity to work in a fantastic environment. Finally, the biggest thank you goes out to my husband Vardhman, who has supported me through all the ups and downs of this project and never lost faith in me.

Contents

List of Figures

Chapter 1

Chapter 3

Chapter 4

Chapter 5

Chapter 6

Appendix

List of Tables

Appendix

Chapter 1

Introduction

Chapter 1: Introduction

Muscle is one of the most extensively studied tissues in biological and medical science. Our fascination with how muscle is responsible for movement in humans and other animals has existed for thousands of years. Erasistratus (315-240BC) was one of the first Greek practitioners to examine the structure of skeletal muscle. He proposed that muscle was like an inflatable bag surrounded by inextensible but flexible cords. A few hundred years later another Greek physician, Galen, came to prominence and his findings on the anatomy of various mammals were widely publicized. However, it was not until the sixteenth century that a complete investigation on the anatomy of the human body was performed by the Belgian physician, Andreas Vesalius. In 1543 he published one of the landmark books in the history of medical science, De Humani Corporis Fabrica (On the Structure of the Human Body), which proved to be extremely influential in inspiring further research on many different organs of the body, including muscle. Today muscle research is carried out in a wide range of species from invertebrates, such as *Drosophila*, to mammals. Recently, the teleost *Danio rerio* (more commonly known as the zebrafish) was discovered as an ideal model organism for studying many aspects of development, including myogenesis.

In this chapter I begin by introducing the different muscle types that exist in vertebrates and highlight some common human myopathies that arise from mutations in muscle genes. I then explain why zebrafish is an ideal model organism for studying muscle development and myogenic disorders, before describing how mesoderm eventually gives rise to differentiated skeletal myocytes in the zebrafish embryo. Finally, I describe the main components of striated muscle, in addition to the mechanics of actin thin filament and sarcomere assembly.

1.1 General overview of muscle

1.1.1 Muscle types

The principal function of muscle is to convert chemical energy into mechanical energy. The force generated from this process is essential for the function of multiple internal organs and body movement in all animals. In humans, almost half of the total body mass is comprised of muscle tissues that are involved in a variety of functions such as regulating organ volume, generating heat and moving fluids and nutrients through various systems. In vertebrates, muscle is classified into three types; smooth, skeletal and cardiac. Smooth muscle is made of short, spindle shaped fibres packed together in layers (Fig. 1.1A) and is found in the walls of internal organs such as the intestines, blood vessels and stomach. Skeletal muscle is composed of bundles of long, almost cylindrical shaped fibres that are multinucleated and are attached to the skeleton (Fig. 1.1B). Skeletal muscle is composed of two fibre types: slow (Type I) and fast (Type II). Slow twitch fibres contract slowly and have a higher resistance to fatigue than fast twitch fibres which are used for short bursts of speed and power. Cardiac muscle is located in the walls of the heart and is made of short interconnecting fibres that are mononucleated (Fig. 1.1C). Although the structure of skeletal and cardiac muscle fibres are not identical, they are both striated (i.e. the fibres contain alternating light and dark bands (striations) that are visible under a light microscope). These striations are due to the ordered arrangement of sarcomeres that make up all cardiac and skeletal muscle fibres.

Striated muscle cells are composed of a multitude of interconnected components that form the complex dynamic framework which is integral to muscle function. The bulk of each muscle cell (myotube) is comprised of bundles of myofibrils which are made up of highly ordered arrays of sarcomeres that are the basic contractile units within striated muscle (Fig. 1.2). The myofibrils

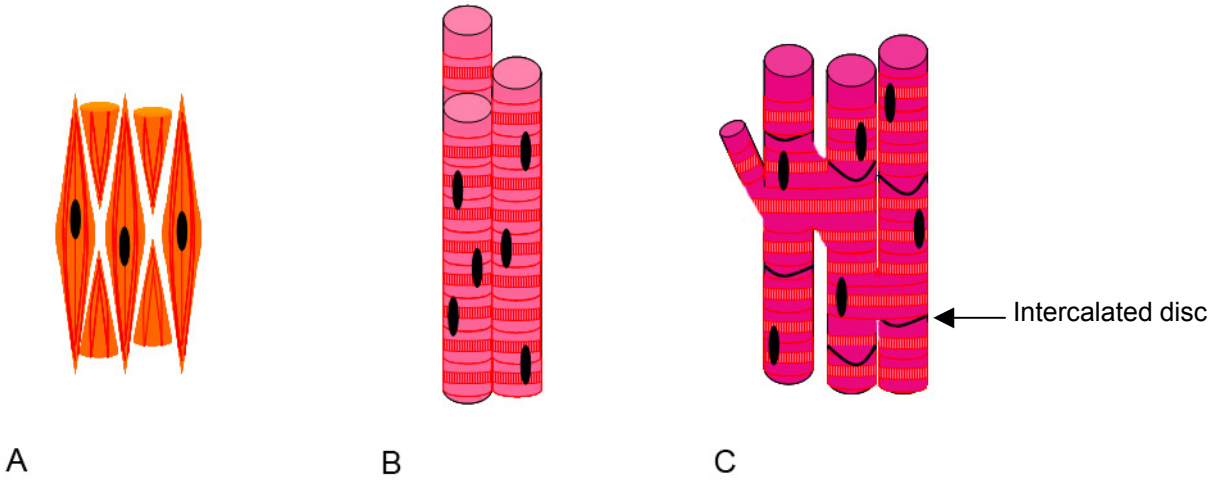

Fig. 1.1. Illustration of smooth, skeletal and cardiac muscle fibres. A) Each smooth muscle fibre is smaller than a cardiac or skeletal fibre and contains a single, centrally located nucleus. B) The skeletal muscle fibre has a very long and roughly cylindrical shape. Fibres run parallel to each other within the muscle and are multinucleated. C) Cardiac fibres have a similar shape to skeletal muscle fibres, however, are also branched and tend to join with each other end to end via intercalated discs (transverse thickenings of the membrane), which are unique to cardiac muscle. Additionally, each muscle fibre tends to be mononucleated. Cardiac and skeletal muscle fibres are composed of sarcomeres (the basic contractile unit) which give rise to the striated pattern observed in these fibres. Smooth muscle is not made up of sarcomeres and thus is not striated. However, it does contains the same elements for contraction i.e. myosin and actin filaments, but they are not regularly organized.

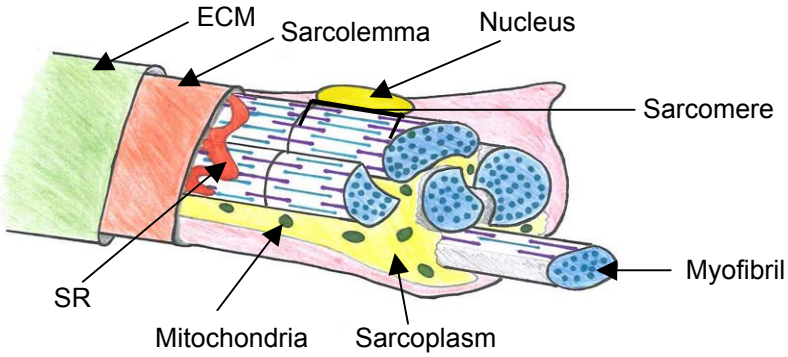

Fig.1.2. Schematic of a stereotypical striated muscle fibril. The striated fibril is composed of many bundles of myofibrils that are surrounded by a specialized plasma membrane (sarcolemma) and an overlaying ECM. The sarcoplasm (muscle cell cytoplasm) that surrounds the myofibrillar bundles contains the primary energy source (glycogen) for muscle contraction. Additionally, it is composed of organelles such as nuclei, the golgi apparatus, mitochondria and sarcoplasmic reticulum (SR). The SR is a fluid filled system of membranous sacs that encircle each myofibril and is the main store of calcium ions. Each myofibril is composed of repeating contractile units called sarcomeres which are primarily composed of myosin and actin filaments that are integral to generating force.

are surrounded by a sarcolemma (plasma membrane) and an overlaying extracellular matrix (ECM). The sarcolemma acts as an adherent substratum that the myofibrils are attached to via a costameric network that is comprised of intermediate filament and cytoskeletal elements. These structures facilitate the transduction of force between the myofibrils and the sarcolemma. The sarcolemma in turn is important for transducing the force along the entire length of the fibril by its connections to the ECM. These connections are also crucial for signaling between the underlying myofibrils and ECM, and primarily occur via the dystrophin glycoprotein complex (DGC) and focal adhesions. It is clear that an immense number of components are involved in the formation and function of striated muscle. It is not surprising therefore, that a large number of human genetic diseases have been attributed to mutations in muscle components. These diseases are debilitating and often fatal.

1.1.2 Human muscular disorders

Human myopathies (diseases of the muscle) are classified into a number of subgroups. Two major categories are dystrophies and congenital myopathies. Over 30 different inherited diseases have been classified within the muscular dystrophy subgroup, and are characterized by a progressive weakness and degeneration of skeletal muscle. Mutations in structural elements of the myofibre, in addition to regulatory components such as enzymes and signaling molecules give rise to various dystrophies (reviewed in Davies and Nowak, 2006). Duchenne muscular dystrophy is one of the most common forms of muscular dystrophy that affects 1 in 3500 males. This fatal, hereditary disorder is due to mutations in the *dystrophin* gene (Hoffman et al., 1987) and is characterized by gradual muscle weakness and degeneration. The absence of dystrophin disrupts the connection between the costameric network and the sarcolemma. Thus the link

between the force generating myofibrils and the membrane is weakened, making the myofibres susceptible to damage during contraction (Beam, 1988; Petrof et al., 1993).

Originally, any muscle disorder present at birth was classified as a congenital myopathy. Today, the accepted definition of a congenital myopathy describes a subset of disorders that include nemaline myopathy, actin myopathy and intranuclear rod myopathy (Sparrow et al., 2003). Congenital myopathies are heterogeneous disorders characterized by loss of muscle tone and muscle weakness at infancy, however, unlike dystrophic diseases there are no signs of muscle fibre degeneration, cell death or inflammation. Instead, characteristic changes in muscle morphology such as the presence of rods and aggregates of protein are used to distinguish congenital myopathies from other neuromuscular disorders.

Nemaline myopathy is one of the most common forms of congenital myopathy. It is an autosomal dominant or recessive disorder and is characterized by muscle weakness, loss of muscle tone and delayed motor development. Additionally, muscle tissues contain nemaline rods or bodies, which are electron dense structures emanating from Z-lines of the sarcomere that extend along the axis of thin filaments. Nemaline rods are thought to be primarily composed of the Z-disc protein α-actinin as well as other Z-line proteins. Genetic mutations responsible for this disease have been found in *α-actin*, *nebulin*, *α-slow tropomyosin*, *β-tropomyosin*, and *slow troponinT* (Donner et al., 2002; Johnston et al., 2000; Laing et al., 1995; Nowak et al., 1999; Pelin et al., 1999). How nemaline rods form is unknown, however, they are thought to arise from abnormal ratios of functional actin and actin binding proteins, and alterations in the interactions between these proteins (Karpati, 2002).

Currently there is no treatment for sufferers of the various forms of muscular dystrophy or congenital myopathy. However, gene therapy trials are proving somewhat successful (Foster et al., 2006). To establish better treatment strategies for these disorders, further understanding of their pathology is required. A number of mammalian models for muscular dystrophies do exist; most notably the mdx mouse and the golden retriever Duchenne muscular dystrophy dog (Bulfield et al., 1984; Cooper et al., 1988; Sicinski et al., 1989; Watchko et al., 2002). These models have been used to investigate potential treatments, including gene replacement and cell transplantation (Nowak and Davies, 2004). Zebrafish is becoming an attractive model to study the pathology of muscular disorders. Moreover, this organism is ideally suited for studying various aspects of muscle development. The advantages of using zebrafish as a model organism are described in the following section.

1.2 The advantages of using zebrafish to study muscle development and muscular disorders

Zebrafish are a freshwater species that originated from the Ganges. They are commonly found in home aquariums and are widely available in pet stores around the world. It was not until the 1970s that a scientist in Oregon, George Streisinger, discovered that this small teleost could be an extremely powerful model organism for studying development. Zebrafish have many qualities that make them an ideal model organism for research on various aspects of development, including myogenesis. They have a short generation time (two to three months) and hundreds of embryos are produced per mating making them highly amenable to genetic analysis. The embryos develop *ex utero* and are transparent, allowing all stages of development to be visualized and the fate of all cells in the embryo to be mapped. For example, single cells can be injected with a lineage tracer dye and their movement monitored over time (Kimmel and Law, 1985a). Moreover, zebrafish embryos are anatomically simpler than other vertebrate model organisms and a relatively small number of cells contribute to each tissue type. These advantages have made zebrafish a popular organism to study numerous developmental processes, and in the last decade an overwhelming amount of research has been performed using this species.

Zebrafish are particularly useful to study the development of muscle. As they are aquatic organisms, zebrafish do not require a robust skeletal system and as a result muscle tissue contributes to 60% of their total body weight. Therefore, a large proportion of cells in the developing embryo give rise to muscle tissues. Moreover, zebrafish have a relatively simple muscle system comprised of separate slow and fast myofibres. In higher vertebrates slow and fast myofibres are mixed. This feature, coupled with the transparency of the zebrafish embryo has

made studying the formation, migration and differentiation of each muscle fibre type particularly amenable to researchers.

Large scale mutagenesis screens were performed in the early 1990s to identify zygotic-effect embryonic lethal mutants and subsequent studies of these mutants have enriched our understanding of zebrafish development (Driever et al., 1996; Haffter et al., 1996). In particular, mutants with defects in somitogenesis and muscle subtype specification have been invaluable in understanding how the muscle develops (Stickney et al., 2000). An additional group of 63 mutants with defects in muscle motility were also isolated (Granato et al., 1996), however, less than 10% have been positionally cloned and characterized (Table 1.1). Research on the remaining zebrafish muscle mutants will be beneficial in extending our knowledge of muscle development and disease. Indeed, a number of the currently characterized zebrafish mutants are now being used as models to study muscular disorders.

Many of the genes associated with muscular dystrophy in humans are also found in zebrafish, and mutations in these genes cause phenotypes similar to what is observed in the skeletal muscle of human patients (reviewed in Bassett and Currie, 2003). The first dystrophic zebrafish mutant, *sapje*, was mapped to the *dystrophin* gene in 2003 (Bassett et al., 2003). It was demonstrated that the muscle in *sapje* mutant embryos degenerates due to weak somitic muscle attachments at the myotendinous junctions. Antisense morpholino oligonucleotides (MOs) have also been used to knockdown other zebrafish sarcolemmal proteins such as Caveolin and δ-Sarcoglycan (Guyon et al., 2005; Nixon et al., 2005) and similar skeletal muscle defects are observed to human patients with defects in these genes (McNally et al., 1998; Nigro et al., 1996). A number of research groups and biotechnology companies are now using MO injected embryos and mutants in high-throughput screens to discover novel pharmacological

Table 1.1 List of zebrafish muscle motility mutants identified by Granato et al., 1996. Asterisk indicates the positionally cloned mutants described in this thesis.

Zebrafish mutant	Number of alleles	Mutated gene	Related Human Muscular disorder
sloth	2		
frozen	1		
fibrils unbundled	2		
turtle	22		
buzz off	5	*nebulin**	Nemaline myopathy [1]
faulpelz	2		
slow motion	1		
schnecke	1	*capzα1**	
hermes	2		
Duesentreib	1		
mach two	1		
slop	1		
jam	1		
slinky	1		
sapje	2	*Dystrophin*[2]	Duchenne and Becker muscular dystrophy [3]
softy	3		
schwammerel	2		
runzel	1	*Titin*[4]	Titinopathy [5]
candyfloss	2	*laminin α2*[6]	Merosin-deficient muscular dystrophy [7]
Unresolved	10		

1. **Pelin, K. et al**. (1999). Mutations in the nebulin gene associated with autosomal recessive nemaline myopathy. *Proc. Natl. Acad. Sci.* **96**, 2305-2310.

2. **Bassett, D. I., Bryson-Richardson, R. J., Daggett, D. F., Gautier, P., Keenan, D. G. and Currie, P. D.** (2003). Dystrophin is required for the formation of stable muscle attachments in the zebrafish embryo. *Development* **130**, 5851-60.

3. **Koenig, M., Monaco, A. P., and Kunkel, L. M.** (1988). The complete sequence of dystrophin predicts a rod-shaped cytoskeletal protein. *Cell* **53**, 219-226.

4. **Steffen, L. S., Guyon, J.R**., **Vogel, E.D**., **Howell, M.H**., **Zhou, Y**., **Weber, G.J**., **Zon, L.I**. **and Kunkel, L.M**. (2007). The zebrafish runzel muscular dystrophy is linked to the titin gene. *Dev Biol.* **309** (2), 80-92.

5. **Hackmann, P. et al**. (2002). Tibial muscular dystrophy is a titinopathy caused by mutation in TTN, the gene encoding the giant skeletal-muscle protein titin. *Am. J. Hum. Genet.* **71**, 492-500.

6. **Hall, T.E., Bryson-Richardson, R.J., Berger, S., Jacoby, A.S., Cole, N.J., Hollway, G.E., Berger, J. and Currie, P.D. (**2007). The zebrafish *candyfloss* mutant implicates extracellular matrix adhesion failure in laminin α2-deficient congenital muscular dystrophy. *Proc. Natl. Acad. Sci.* **104** (17), 7092-7.

7. **Helbling-Leclerc, A. et al.** (1995). Mutations in the laminin α2-chain gene (LAMA2) cause merosin-deficient congenital muscular dystrophy. *Nature Genet.* **11**, 216-218.

and genetic therapies for muscular dystrophy . Zebrafish are advantageous for these types of screens as a large number of compounds can be tested on many embryos and the chemicals easily diffuse into the embryo. A number of drug screens have been successfully carried out in zebrafish and have shown that small molecules are able to alter the development of several organ systems such as ear, central nervous system and eye (den Hertog, 2005). Moreover, two screens have been carried out on mutants with cardiac and cell cycle defects and compounds that ameliorated the mutant phenotype were identified (Peterson et al., 2004; Stern et al., 2005). These drug screens demonstrate the feasibility of using zebrafish models of human disorders to screen for potential pharmacological treatments. Additionally, they could dramatically reduce the time and cost of drug discovery and assist in identification of novel treatments of human diseases, including myopathies.

1.3 Skeletal muscle development in zebrafish

1.3.1 Mesoderm induction and formation of the three germ layers

Striated muscle in vertebrates arises from mesoderm. Mesoderm is one of three germ layers that give rise to specific tissue types within the embryo. Mesoderm develops into a diverse variety of organs such as the notochord, muscle, blood, heart and kidneys. Ecotoderm and endodermal layers differentiate into epidermis and gut epithelia respectively. In zebrafish, cells fated to become mesoderm arise prior to gastrulation and are located in a ring on top of an extra-embryonic structure called the yolk syncytial layer (YSL) (Fig. 1.3). The YSL separates the yolk from the cells that form the embryo proper and has several important functions, including inducing the formation of the mesoderm and endoderm (Mizuno et al., 1999; Ober and Schulte-Merker, 1999; Rodaway et al., 1999). The cells closest to the YSL develop into the mesendodermal layer (a mixture of cells fated to become mesoderm and endoderm). Cells slightly further away from the YSL develop into mesoderm and cells furthest away from the YSL are fated to become ectoderm (Fig. 1.3) (Kimmel et al., 1990; Warga and Nusslein-Volhard, 1999).

The ability of the YSL to induce the formation of germ layers was initially discovered by transplantation of the yolk cell into the animal region of the blastoderm. This procedure ectopically induced genes normally expressed in the mesendoderm (Mizuno et al., 1999). Also, addition of RNAse to the YSL blocked expression of ventral and lateral mesendodermal markers (Chen and Kimelman, 2000). These findings lead to a hypothesis that secretion of signaling molecules from the YSL induces the formation of mesendoderm and mesoderm, and cells furthest away from the YSL, which are not affected by these signals, become ectoderm. In

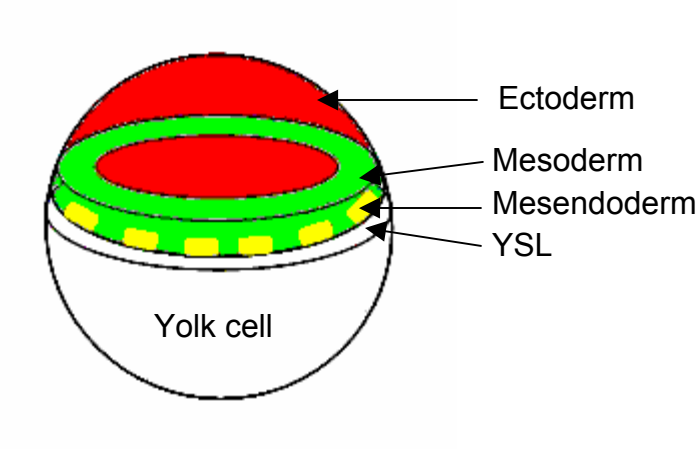

Fig. 1.3. Fate map of the three germ layers prior to gastrulation (30% epiboly). Signals from the YSL induce the formation of cells fated to become mesoderm (green) and endoderm (yellow) (mesendodermal layer) immediately adjacent to the YSL. Cells on top of the mesendodermal layer are fated to become mesoderm only, and cells furthest away from the signaling emitted by the YSL are fated to become ectoderm (red). The cells in the centre of the ring also develop into ectoderm.

Xenopus the maternal transcription factor VegT is able to induce the formation of germ layers.VegT is localized to the vegetal region of the embryo and is able to activate members of the Nodal gene family and induce mesoderm and endoderm formation (Zhang and King, 1996). Interestingly, in zebrafish the orthologue of *vegT* (*spadetail*) is only expressed zygotically. Moreover, mutations in this gene do not prevent formation of mesendoderm (Kimmel et al., 1989). The putative signal emitted by the YSL in teleosts remains to be determined.

Once mesoderm, ectoderm and endodermal fates are established they are organized into distinct layers in a process known as gastrulation. Gastrulation relies on the coordinated movement of cells so that the endoderm and mesoderm are located within the interior of the embryo and ectoderm forms the outer layer of the embryo. In zebrafish, gastrulation extends from approximately 5.5 hours post fertilization (hpf) to 10 hpf and can be divided into three movements: epiboly, involution and convergence and extension. These movements occur concurrently during this period.

Epiboly begins prior to gastrulation (4-4.5 hpf) and is characterized by the spread and movement of the blastoderm cells (which include cells that form the embryo proper) over the yolk cell towards the vegetal axis (Kimmel and Law, 1985b; Trinkaus, 1993)(Fig. 1.4A). The continual movement of these cells across the surface of the yolk enables gastrulation to proceed. Gastrulation begins just after 50% epiboly (when half the yolk is covered by blastoderm) and is marked by the formation of the germ ring.

The germ ring arises from involution (the internalization of cells). This type of cell movement induces the rim of the blastoderm (the margin adjacent to the YSL) to thicken as the mesodermal and endodermal cells start to migrate from the outside to the inside of the embryo

(Fig.1.4B). The internalization of these cells results in the division of the blastoderm into an outer layer of epiblast (ectoderm) and an inner layer of hypoblast (mesoderm and endoderm) (Warga and Kimmel, 1990). Involution occurs throughout the gastrula period and somitogenesis until all cells are internalized (Kanki and Ho, 1997).

A thickening on one side of the germ ring (the shield) is also observed almost simultaneously to germ ring formation (Fig. 1.4B), and arises from involution and convergence of mesodermal cells to the dorsal side of the embryo (Warga and Kimmel, 1990). The shield is the first morphological structure that indicates the establishment of a dorsoventral (DV) axis and is composed of cells of the dorsal YSL and part of the dorsal blastomere. It is equivalent to the Spemann-Mangold organizer in the blastopore lip of amphibians, the node in the mouse and Henson's node in the chick (Oppenheimer, 1936; Saude et al., 2000; Shih and Fraser, 1996). An organizer is present in all vertebrates and eventually differentiates into dorsal mesodermal structures such as the notochord, the defining feature of the vertebrate phylum. The organizer functions as a signaling centre and secretes multiple signaling factors that can change the fate of the surrounding cells. This property enables the organizer to initiate a secondary axis when transplanted to an ectopic position within the embryo (Ho, 1992; Saude et al., 2000; Shih and Fraser, 1996; Spemann, 1924).

Gastrulation movements persist after formation of the shield. The medosermal cells continue to converge to the dorsal side of the embryo and intercalate with dorsal blastomeres, resulting in narrowing of embryonic tissues mediolaterally. These cells then undergo extension movements and spread along the animal-vegetal axis, driving elongation along the anteroposterior (AP) axis (Fig. 1.4C). By the end of gastrulation the progenitors of all cell types are correctly positioned and arranged along the fully established DV and AP axis.

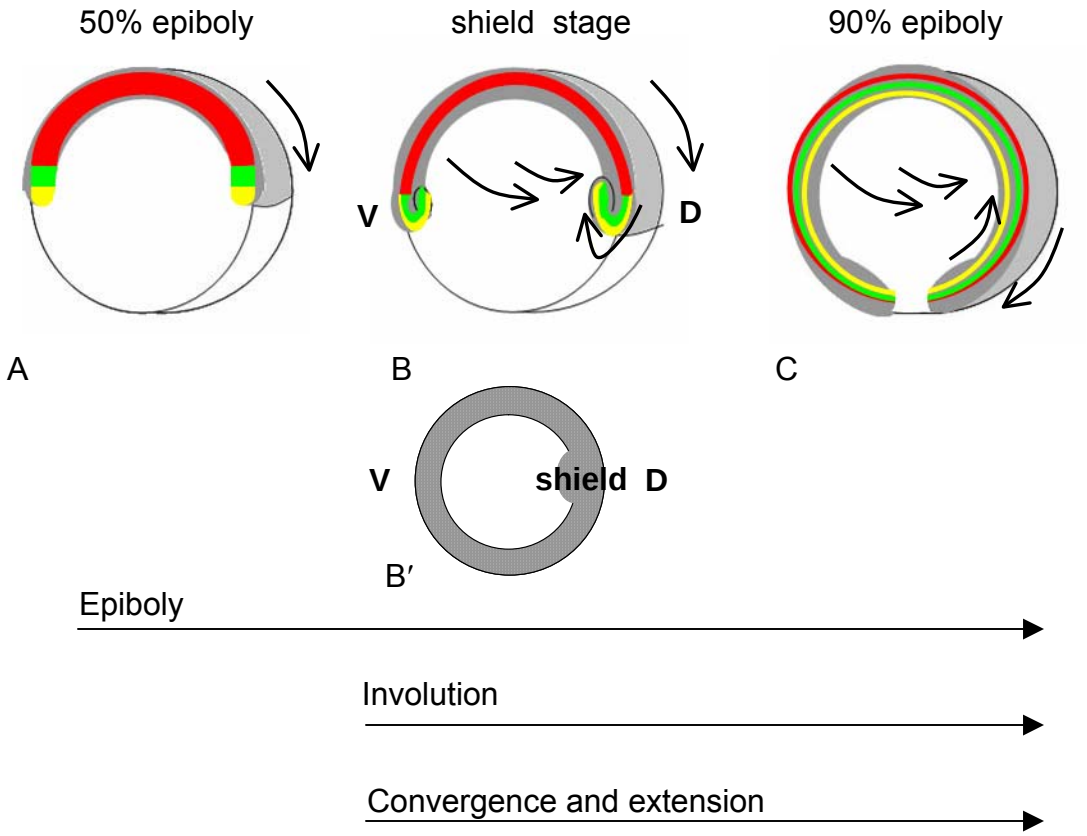

Fig. 1.4. Diagram of the three types of cell movement involved in gastrulation. A) Epiboly movements begin prior to gastrulation and move cells over the yolk towards the vegetal axis. At this stage cells fated to become endoderm (yellow), mesoderm (green) and ectoderm (red) are located on the outer surface of the embryo. B) Once just over half the yolk is covered (60% epiboly) gastrulation begins with involution and the formation of the germ ring (animal pole view shown in B′) as mesodermal and endodermal cells move from the outer edge of the embryo to the inside of the embryo. Concurrently, convergence movements result in a thickening on the dorsal side of the germ ring known as the shield. C) Epiboly, involution and convergence and extension movements continue until all three germ layers are positioned correctly along the DV and AP axis. Arrows indicate the movement of cells at each stage and D and V indicate the dorsal and ventral axis respectively.

1.3.2 Origin and specification of muscle progenitor tissues

1.3.2.1 Paraxial mesoderm

The predominant feature along the AP axis is the segmental plate, which is comprised of paraxial mesoderm that flanks either side of the axial mesoderm (derived from the shield) and forms towards the end of gastrulation (Fig. 1.5A). Axial mesoderm differentiates into notochord and paraxial mesoderm eventually gives rise to somites. One of the main questions that has intrigued developmental biologists is how mesoderm is patterned into these two different tissues. This question was primarily addressed by using various zebrafish mutants: the T-box transcription factor mutant *spadetail* (*spt*) and the Not-type homeobox transcription factor *floating head* (*flh*) were found to be the main instigators in patterning of the mesoderm. *spt* mutants lack trunk somites (Kimmel et al., 1989), while in *flh* mutants, a notochord does not form and instead axial mesoderm is converted into somitic tissues (Halpern et al., 1995; Melby et al., 1996). The loss of *spt* in *flh* mutants rescues many aspects of the *flh* phenotype and in these double mutants the axial mesoderm is still able to differentiate into notochord. These results indicated that *spt* controls paraxial mesoderm formation while *flh* represses *spt* expression in the axial mesoderm. Thus muscle differentiation is blocked at the midline, however, not in the surrounding paraxial mesoderm (Amacher and Kimmel, 1998).

Once the axial and paraxial mesoderm are established, axial mesoderm forms prechordal plate and notochord while paraxial mesoderm segregates into two cell types: adaxial cells and lateral presomitic mesoderm cells (Fig. 1.5B). Adaxial cells form a monolayer adjacent to the

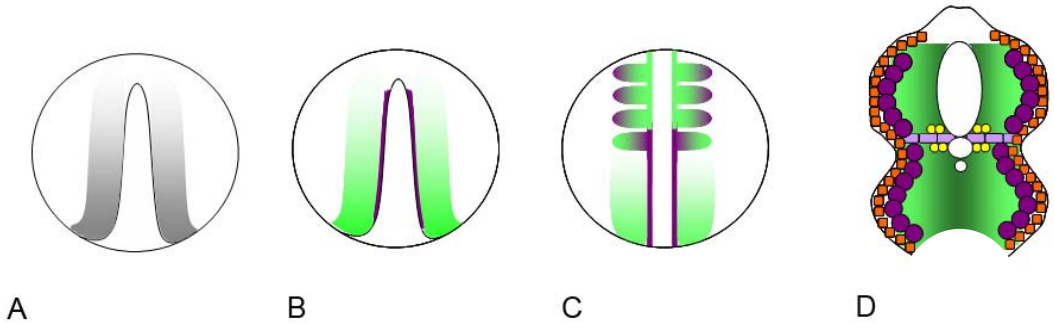

Fig. 1.5. Illustrations depicting the position of muscle precursors during zebrafish embryonic development. A) Dorsal view of embryo at 90% epiboly illustrating the notochord precursor tissue (axial mesoderm) flanked by the segmental plate containing paraxial mesoderm (grey). B) Dorsal view of bud stage embryo (~10hpf). Slow muscle precursors (adaxial cells) are positioned in a single layer (purple stripe) adjacent to the notochord while fast muscle precursors reside in lateral paraxial mesoderm on either side of the notochord (green). C). During somitogenesis, the majority of the adaxial cells migrate to the lateral edge of each somite and differentiate into superficial slow fibres. D) Transverse section through the trunk of a 24 hpf embryo showing all the differentiated muscle fibre types. Adaxial cells that do not migrate to the surface of the muscle become muscle pioneers (light purple). The bulk of the fast muscle cells differentiate into fast muscle fibres (green). A subset of the fast muscle cells located adjacent to the muscle pioneers become medial fast fibres (yellow). Superficial slow fibres (purple) are located between the fast muscle fibres and the dermomyotomal like layer of external cells (orange).

notochord. They are a specialized group of cuboidal mesodermal cells that are the precursors to all slow muscle lineages (Devoto et al., 1996; Weinberg et al., 1996). Adaxial cells arise from Sonic hedgehog signals emitted by the notochord (Barresi et al., 2000; Du et al., 1997; Wolff et al., 2003) before paraxial mesoderm segments into somites.

1.3.2.2 Somitogenesis

One of the first most striking morphological muscle structures that can be visualized in the developing zebrafish embryo are the somites. Somites are the main progenitors of skeletal muscle in vertebrates and are formed when groups of paraxial mesodermal cells on either side of the notochord separate, and form blocks of epithelial tissue at regular intervals along the AP axis. The first pair of somites are observed at 10.5 hpf and each subsequent pair forms approximately every 30 min in an AP wave until 26-30 somites have formed. Each somite is composed of an epithelioid sheet surrounded by a core of mesenchymal cells. The boundary of each somite acts as a positional template for the formation of the myotome boundary (the myoseptum).

One of the unsolved mysteries of somitogenesis is how the somites are formed in such a regulated and precise manner. This topic has been subject to extensive research and mounting evidence is emerging that supports the clock and wavefront model (for review see Pourquie, 2001; Pourquie, 2003). Briefly, this model firstly proposes the existence of a molecular clock or oscillator (e.g. a cyclic wave of gene expression) that functions with temporal periodicity. Therefore groups of paraxial mesodermal cells are only able to form a segment during a brief period of time within each cycle of the somite clock. Secondly, the wavefront, a gradient of either positional or developmental information, induces the formation of each somite when it encounters a group of cells that are cycling in the permissive phase of the clock. The wavefront

first emerges in the anterior presomitic mesoderm and gradually moves at a constant speed as somitogenesis proceeds, thus the somites form and differentiate in an anterior to posterior manner along the primary axis of the embryo. The stepwise interaction between the clock and the wavefront leads to regularly spaced furrow formation in the anterior presomitic mesoderm. Moreover, somite length and the rate of formation are dependent on the frequency of the clock or oscillator and the velocity of the wavefront.

Once each somite has formed, it is subsequently patterned by signals emitted from the adjacent notochord, neural tube, lateral plate mesoderm and surface ectoderm. Each somite in vertebrates is initially subdivided into sclerotome, myotome and dermomyotome, which give rise to the vertebral column, skeletal muscle and dermis respectively. In all vertebrates, muscle is derived mostly from the myotome. Myotome is specified by dermomyotome in chick and mouse embryos, however, a consensus has not been reached as to how this occurs (for review see Hollway and Currie, 2003). In zebrafish, the existence of a dermomyotome was only recently established when laterally located cells between the slow muscle and the dermis (known as external cells) were found to express the paired type homeobox transcription factors *pax3* and *pax7* (Devoto et al., 2006). The transcripts for both these genes are found in the dermomyotomal cells of chick and mouse (Gros et al., 2005; Relaix et al., 2005), therefore the external cell layer in zebrafish is proposed to be homologous to the dermomyotome. Moreover, the external cell layer expresses the myogenic regulatory factors *myf5* and *myogenin*, which are indicative of myogenic precursor cells in other vertebrates (Groves et al., 2005; Steinbacher et al., 2006). These properties suggest that the external cell layer may contain myogenic precursors that are able to migrate and differentiate into muscle cells. Indeed, a recent study has shown that external cells are able to incorporate and differentiate into fast muscle fibres (Stellabotte et al., 2007).

1.3.2.3 Myogenic regulatory factors: Myf5 and MyoD

The first significant indication of a commitment of mesoderm to a muscle specific lineage is detected with the expression of MyoD and Myf5. MyoD and Myf5 are myogenic regulatory factors (MRFs) of the basic-helix-loop-helix transcription factor family. They are expressed in proliferative myoblasts and have been implicated in the establishment and maintenance of muscle progenitors, as well as being involved in the terminal differentiation of myofibres (Choi et al., 1990; Davis et al., 1987; Pownall et al., 2002; Weintraub et al., 1991). In zebrafish, *myoD* is first expressed in the presomitic mesoderm (paraxial mesoderm) at 70-75% epiboly (Weinberg et al., 1996) and is closely followed by *myf 5* at 80% epiboly (Coutelle et al., 2001). The monolayer of adaxial cells that arises adjacent to the notochord exclusively expresses *myoD*. Subsequently, *myoD* is expressed in the posterior region within each newly formed somite until the cells begin to differentiate into fast muscle at the 15 somite stage. *myf5* is initially expressed in the posterior presomitic mesoderm in presumptive fast muscle cell precursors. Its expression declines in anterior presomitic mesoderm but is transiently re-expressed in the posterior border of each somite (Chen et al., 2001; Coutelle et al., 2001).

The expression of *myf5* and *myoD* are regulated by a host of factors that are expressed in the surrounding tissues. Experiments performed on two T-box transcription factor mutants *no tail* (*ntl*, homologue of *brachyury*) and *spt* indicate that both these factors are required to initially activate the expression of *myoD* in the paraxial mesoderm. As previously mentioned, *spt* is important in formation of the paraxial mesoderm and loss of this factor results in a lack of trunk somites. In *ntl* mutants the notochord and tail do not form. In each of these mutants *myoD* expression is delayed, but recovers during segmentation (Amacher et al., 2002; Weinberg et al., 1996). In *ntl* and *spt* double mutants *myoD* expressing cells are never detected (Amacher et al.,

2002), indicating the importance of these transcription factors in the induction of myogenesis. Many other factors including signalling molecules, such as Hedgehogs, Wnts, Noggin and BMPs work in concert to regulate transcription of MRFs and are essential for myogenesis to proceed (reviewed in Pownall et al., 2002).

1.3.3 Muscle differentiation

Formation of differentiated skeletal muscle in vertebrate embryos is a tightly regulated process involving cell migration and differentiation of muscle precursor cells, followed by myoblast fusion. Zebrafish contain four different types of muscle fibre: slow muscle fibres (superficial slow fibres), muscle pioneers, fast muscle fibres and medial fast fibres (Fig.1.5D). Each fibre type has unique morphological and developmental properties and is located in distinct regions within the muscle.

1.3.3.1 Slow and fast muscle fibre formation

All slow muscle fibres are derived from the adaxial cells adjacent to the notochord and fast muscle fibres are derived from lateral paraxial mesoderm. However, fate mapping studies have shown that prior to gastrulation, slow and fast muscle precursor cells occupy distinct locations within the mesoderm that is located at the margin (Hirsinger et al., 2004; Kimmel et al., 1990). At 50% epiboly slow muscle precursors are located close to the shield (on the dorsal side) and fast muscle precursors are located towards the ventral side. At this stage it was found that muscle precursor cells can still readily change fate if transplanted into another domain. Therefore they are not committed to forming a particular muscle subtype until after they enter the segmental plate and become exposed to signals emitted from the notochord (Hirsinger et al., 2004).

Shortly after somite formation, most of the adaxial cells elongate before migrating to the lateral part of the myotome to form a subcutaneous layer, where they differentiate into mononucleated slow twitch myofibres that span the somite (Blagden et al., 1997; Devoto et al., 1996; Roy et al., 2001). The migration of adaxial cells is dependent on the differential expression of the cell adhesion molecules M- and N-Cadherin (Cortes et al., 2003). The subset of adaxial cells that do not migrate, differentiate into medially located muscle pioneer cells, which are a distinct population of slow twitch fibres. They are the first cells to become terminally differentiated and are responsible for producing the horizontal myoseptum that subdivides the myotome into dorsal and ventral halves. All slow twitch fibres are characterized by the expression of the *slow myosin heavy chain* (*slow myhc*) and the homeodomain gene *prox1* (Blagden et al., 1997; Roy et al., 2001). Muscle pioneers also express genes of the *engrailed* (*eng*) homeobox protein family (Ekker et al., 1992; Felsenfeld et al., 1990; Hatta, 1992; Hatta et al., 1991).

The remaining bulk of the muscle cells differentiate into fast muscle fibres that are localized medially to the overlaying slow muscle. A subset of the fast fibres that surround the adjacent slow muscle cell pioneers form medial fast fibres. Intriguingly, although these cells express *fast muscle myosin heavy chain* (*fast myhc*) they also express *eng*, which is a characteristic of the muscle pioneers (Wolff et al., 2003). The function of these fibres remains unknown.

1.3.3.2 Hedgehog signalling

The primary signaling factor responsible for the differentiation of the four muscle subtypes, and in particular the slow myofibres, is Sonic hedgehog (Shh). *shh* and the two related *hedgehog* (*hh*) genes, *echidna hedgegog* (*ehh*) and *tiggywinkle hedgehog* (*twhh*) are expressed in axial structures. *ehh* and *shh* are expressed in the notochord (Currie and Ingham, 1996) and *twhh* is expressed in the overlying floorplate of the neural tube (Ekker et al., 1995). Hedgehog (Hh) proteins are essential for inducing the formation of slow muscle and muscle pioneers *in vivo* and *in vitro* (Du et al., 1997; Norris et al., 2000; Weinberg et al., 1996; Wolff et al., 2003). Pioneering studies in chick first demonstrated that *myoD* is activated by both Shh and Wnt signaling in the pre-segmental plate (Munsterberg et al., 1995). In zebrafish, Hh signals have also been found to drive the expression of MRFs in slow muscle precursors (Coutelle et al., 2001; Lewis et al., 1999).

Hh signalling acts through two receptor transmembrane proteins, Patched (Ptc) and Smoothened (Smo). Ptc negatively regulates Hh signalling by inhibiting Smo activity. However, once Hh binds to Ptc, Smo dissociates from Ptc and is able to transduce the Hh signal (Ingham and McMahon, 2001). In zebrafish *smoothened* mutants (*smooth muscle omitted* (*smu*)), adaxial cells do not express *myoD* and slow muscle fibres and muscle pioneers do not form. All somitic tissues differentiate into fast muscle fibres (Chen et al., 2001). It has been proposed that Hh signalling is required for slow fibre specification and acts as a gradient, whereby different levels of Hh induce the formation of different muscle subtypes.

The gradient model for Hh activity was proposed by treating zebrafish embryos with cyclopamine, a small molecule inhibitor of Hh signaling, in a dose dependent manner (Wolff et al., 2003). When Hh signaling is completely inhibited by high concentrations of cyclopamine, muscle pioneers, slow muscle myofibres and medial fast fibres are eliminated. At intermediate concentrations muscle pioneers and medial fast fibres are absent, and at the lowest concentrations only the muscle pioneers are disrupted. These findings indicate that Hh signals act as a gradient i.e. those cells that are closest to the source of Hh emanating from the notochord are exposed to high levels of Hh activity and commit to form muscle pioneers and *eng* positive medial fast fibres. Those cells that are located further away from the source of the gradient are exposed to lower levels of Hh which induces the specification of the superficial slow muscle fibre cell fate.

Fast muscle fibres derived from lateral paraxial mesoderm are still able to form in the absence of Hh signaling (Chen et al., 2001). This indicates that Hh signals are not the only governing factor in specifying muscle cell fate. The gradient of activity and threshold response to specific levels of Hh may be provided by a combination of the spatial locations of precursor cells, the timing of exposure to Hh signalling and other factors that interact with Hh signals. Indeed, a number of accessory proteins have been identified that may be required to fine tune Hh signaling and specify the differentiation of slow precursor muscle fibres (e.g. Dzip1 (DAZ interacting protein 1) (Wolff et al., 2004) and Blimp1 (Baxendale et al., 2004)). Blimp1 is one of the key Hh target genes that controls slow muscle differentiation and is mutated in the *u-boot* (*ubo*) mutant. In this mutant all slow muscle fibre cell types are lost (Roy et al., 2001). Blimp 1 is a transcription factor that is specifically expressed in adaxial cells (Baxendale et al., 2004). It is necessary for slow muscle induction and is required for the repression of *fast myhc* and activation of the *slow myhc* and *prox1* genes. It has therefore been proposed that Blimp1 may set the transcriptional status of key genes required for differentiation of the slow muscle lineage.

It is still not clear what molecules induce the formation of fast muscle fibres. However, signaling factors such as Tgf-β family members (which can inhibit slow fibre formation) and Wnts may be involved (Du et al., 1997; Makita et al., 1998). Although Hh signals are integral to the specification of the muscle fibre subtypes many other components are involved in patterning of the myotome. Further exploration of this field is necessary to conclusively determine how paraxial mesoderm differentiates into the four main classes of myofibres.

1.3.3.3 Fast fibre elongation

Once the fast fibres have been specified they elongate prior to fusion. Surprisingly, the morphogenesis of these fast fibres is triggered by the migration of slow fibres (Henry and Amacher, 2004). As the slow twitch cells migrate laterally they induce fast fibre elongation in a medial-to-lateral wave (Henry and Amacher, 2004). So although fast muscle fibres do not directly require Hh signals to elongate they need the slow muscles to migrate, which is induced by Hh signaling. The molecular mechanisms responsible for fast fibre elongation are unknown, though it has been postulated that the slow muscle cells could secrete a factor that promotes elongation. Alternatively, direct cell-to-cell contact may induce the elongation of some of the fast fibres, which subsequently activates elongation in adjacent fast muscle fibres. After the fast fibres elongate they fuse to form around 80 multinucleated fast twitch fibres per somite.

1.3.3.4 Myoblast fusion and terminal differentiation of myofibres

During myoblast fusion mononucleated myoblasts fuse to form multinucleated muscle fibres. In zebrafish, only the fast muscle cells fuse while the slow muscle fibres remain mononucleated. This process has been most extensively studied in mammalian cell cultures

where fusion can be synchronized (Knudsen, 1992; Wakelam, 1985). These studies have identified a number of cell adhesion molecules (e.g. calmodulin and protein kinases) that may be involved in myoblast fusion. However, the role of these proteins *in vivo* has still not been thoroughly investigated and how myoblast fusion is regulated in vertebrates is poorly understood.

Mechanisms of myoblast fusion *in vivo* have primarily been elucidated by studies in *Drosophila*. In *Drosophila*, founder myoblasts prefigure the position, orientation and identity of individual muscles, and fusion competent myoblasts fuse with founders and convert them into syncytia (for review see Chen and Olson, 2004)). Central to the fusion process is a signaling pathway involving *dumbfounded* (*kirre*) and *roughest*, which are both Ig-domain containing membrane receptors (Ruiz-Gomez et al., 2000; Strunkelnberg et al., 2001). A recent report has identified the first vertebrate homologue of *kirre* in zebrafish, *kirrel* (Srinivas et al., 2007). *kirrel* is required for muscle precursor fusion in zebrafish and is expressed in all fast myoblasts. Knockdown of Kirrel with a MO produced embryos with unfused fast muscle cells. However, MRFs were still expressed in these cells, suggesting that myoblast differentiation is unaffected (i.e. formation of sarcomeres and myofibrils). Thus muscle differentiation and fusion appear to be independent of each other. Inhibition of the most downstream intracellular transducer of the fusion signal in *Drosophila*, Rac, also compromised fast muscle fusion in zebrafish. However, unlike *Drosophila*, constitutively active Rac led to hyperfused giant syncytia. Therefore Rac could potentially be important for limiting the number of fusion events and the polarity of the fast muscle cells.

Caveolin-3, a sarcolemmal protein expressed in skeletal and cardiac muscle (Tang et al., 1996; Way and Parton, 1995) may also be involved in myoblast fusion. Studies of muscle cell lines extracted from transgenic mice found that overexpression of Caveolin-3 reduces fusion,

while loss of Caveolin-3 enhances myoblast fusion (Volonte et al., 2003). In contrast, in the Caveolin-3 mouse knock out myoblast fusion is not defective (Galbiati et al., 2001; Hagiwara et al., 2000). In zebrafish, myoblast fusion is reduced in muscle fibres isolated from caveolin-3 MO injected embryos (Nixon et al., 2005). Due to the contradictary results of Caveolin-3 to date, further studies are required to elucidate its function. However, it will be interesting to determine how this protein is involved in controlling myoblast fusion.

Both slow and fast muscle cells terminally differentiate into striated muscle fibres which must contain all the basic elements to enable muscle contraction to take place. Very little is known about these last stages of muscle development, especially *in vivo*. However, it is likely that the master MRFs MyoD and Myf5, as well as Myogenin and Mrf4, play roles in regulating the expression of myofibril components (Edmondson and Olson, 1989; Lassar et al., 1989; Rhodes and Konieczny, 1989; Wright et al., 1989). Retinoic acid is also thought to be involved in differentiation of fast muscle fibres, and has been shown to inhibit proliferation and induce fast muscle fibre differentiation (Alric et al., 1998). Moreover, it has been shown that zebrafish retinaldehyde dehydrogenase 2, the main retinoic acid synthesizing enzyme, is expressed in the somites where it activates FGF8 expression and consequently fast muscle differentiation (Hamade et al., 2006).

As myoblasts become terminally differentiated, a wide range of different transcription factors are expressed (Tapscott, 2005) e.g. Mef2 and SRF. Mef2 has been shown to be co-expressed with MyoD to enhance the conversion of non-muscle cells into myogenic cells *in vivo* (Molkentin et al., 1995) and both Mef2 and SRF have been shown to regulate many heart and skeletal muscle genes (Balza and Misra, 2006; Black and Olson, 1998). In addition, it has been

demonstrated that Mef2 family proteins are required to upregulate thick filament components, such as myosin, in the zebrafish embryo (Hinits and Hughes, 2007).

The exact mechanisms that drive terminal differentiation of myofibres in zebrafish and other vertebrates are still unknown. Preliminary antibody stainings of some sarcomeric components in zebrafish embryonic muscle indicate that sarcomeric assembly begins around 24 hpf and myofibres are fully differentiated by 48 hpf (Costa et al., 2002). However, how the muscle components are temporally and spatially regulated to result in the formation of a fully functioning contractile unit is yet to be elucidated. Thus further detailed analysis of sarcomere and myofibril formation in zebrafish embryos will be beneficial in understanding the later aspects of muscle development in vertebrates. Moreover, this information will be invaluable to unraveling the mechanisms underlying many human muscular disorders.

1.4 Components of striated muscle

1.4.1 The sarcomere

The sarcomere is the fundamental contractile unit of all striated muscles and is composed of an elaborate array of elements that are precisely assembled and maintained. The ultrastructural arrangement of sarcomeric components is clearly illustrated by transmission electron microscopy (TEM), and defined regions of the sarcomere including the A-band, I-band, Z-band and M-band are readily visualized (Fig. 1.6). The thick and thin filaments that are integral to the generation of force are located within the A- and I-bands. The thick filament is comprised of bundles of myosin which are located primarily within the A-band. Within this region, the globular head of the myosin chains are able to interact with actin containing thin filaments, which interdigitate with the thick filaments. The small region where the thick filaments no longer contact the thin filament is called the bare zone. Within the middle of this region, the M-band (M-line) is where the myosin bundles are anchored to the middle of the sarcomere. The M-band ensures the regular packing of myosin filaments and is important in maintaining sarcomeric stability during contraction. The Z-band (also known as the Z-line or Z-disc) forms the lateral boundary of each sarcomere and contains proteins that crosslink components of adjacent sarcomeres, such as titin, nebulin and antiparallel thin filaments.

Muscle contracts by a sliding filament mechanism. This mechanism was first hypothesized from TEM images of the sarcomere, which showed that the lengths of the thick and thin filaments did not change during muscle contraction. Instead, the sarcomere appeared shortened, suggesting that the thick and thin filaments slide past each other (Huxley and Niedergerke, 1954; Huxley and Hanson, 1954). This movement draws the Z-discs to the middle

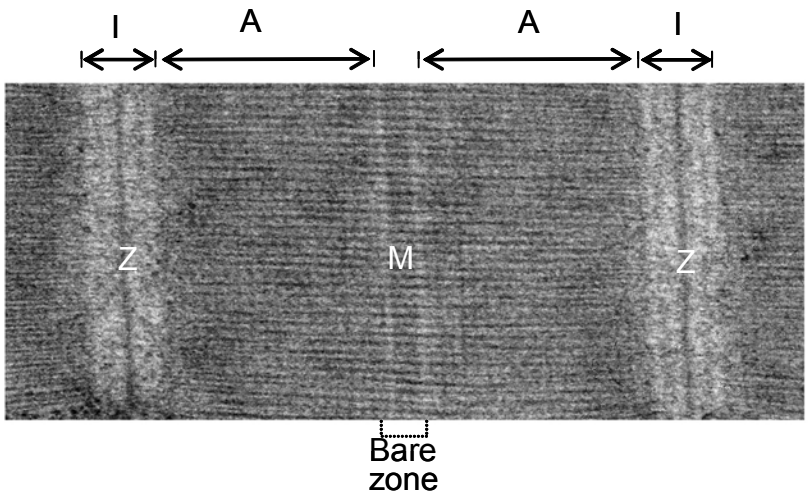

Fig. 1.6. Transmission electron microscope image of a zebrafish sarcomere. The Z-lines (Z) form the boundary of each sarcomere. The M-band (M) is located within the bare zone at the centre of the sarcomere. The I-band (I) is positioned between sarcomeres and spans the region of the thin filament attached to the Z-line. The A-bands (A) form the bulk of the sarcomere and consist of interdigitated thin and thick filaments.

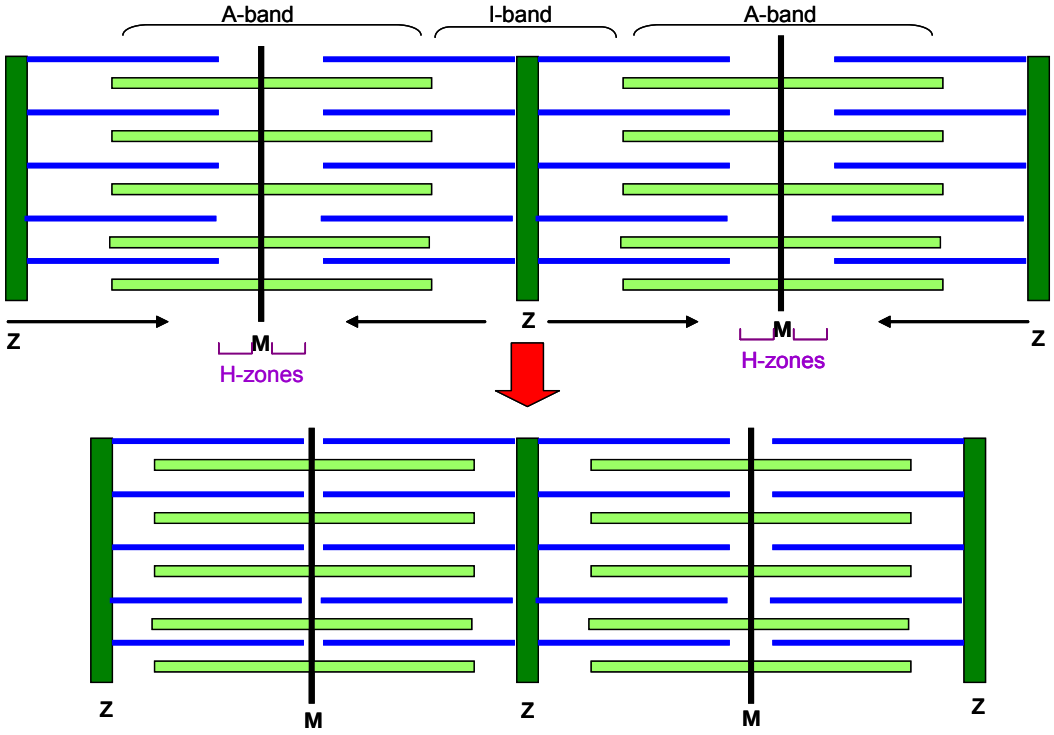

Fig. 1.7. Schematic illustration of the sliding filament mechanism for sarcomere contraction. As the thick (light green rods) and thin filaments (blue rods) slide past each other, the Z-lines (dark green bars) move closer together, thereby decreasing the width of the I-bands and H-zones (region between the M-band and the edge of the thin filament), however the width of the A-band remains constant. M indicates the M-line.

of each sarcomere so that the I-bands and H-zone narrow, however, the A-band remains constant (Fig. 1.7).

It is apparent that large forces are placed on the sarcomere during contraction, therefore it is not surprising that this contractile unit is composed of a multitude of interconnected structural elements. The major components of the sarcomere are illustrated in Fig. 1.8 and will be described herein.

1.4.1.1 The actin thin filament and its associated proteins

Filamentous actin (F-actin) is involved in numerous functions including cell motility, cytokinesis, formation of stress fibres and muscle contraction (Carlier, 1998). In different cell types actin filaments form specialized structures, such as thin filaments within the sarcomeres of striated muscle, internal stiffening rods in the microvilli of intestinal brush borders and the membrane skeleton within erythrocytes. There are at least six isoforms of actin in mammals and birds, and these are grouped into three classes by their isoelectric points: α-actin is found in muscle and the β- and γ-actins are primarily found in non-muscle cells. Each actin monomer is tightly associated with a molecule of ATP, enabling it to polymerize by ATP hydrolysis. Actin filament formation begins with nucleation. This involves the association of three or four monomers that form a stable oligomer (nucleus) from which polymerization can proceed. Once polymerized, each actin filament appears as two twisted strands of actin monomers and has a barbed and pointed end. The designation of barbed and pointed is derived from TEM images of actin filament decorated with myosin heads, which give the appearance of arrowheads along the length of the filament.

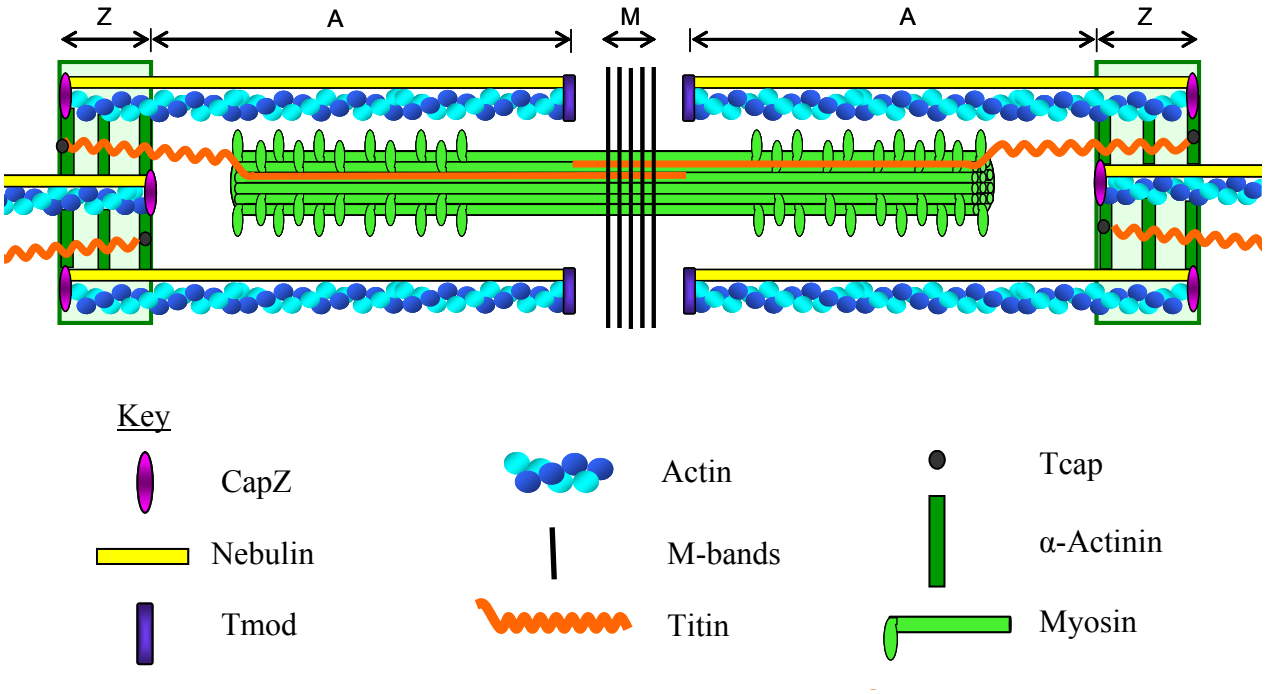

Fig 1.8. Diagram of the sarcomere illustrating the major components. The thin filament is made up of filamentous actin which is capped at each end by capZ and Tmod. Nebulin spans the length of the thin filament. The thick filament is composed of myosin bundles which are cross-linked at the M-band. Titin centres myosin to the middle of the sarcomere and is anchored to the Z-line by telethonin (Tcap). α-Actinin links thin filaments between adjacent sarcomeres and is one of the major components of the Z-line.

Within the sarcomere, each actin filament spans half of the I-band and part of the A-band. The pointed end extends towards the M-line and interdigitates and associates with the thick filament within the A-band region, while the barbed end is anchored to the Z-line (Fig. 1.8 light and dark blue helix). Regulation of actin filament formation, dynamics, maintenance and stability is very tightly controlled and this is reflected by the vast number of distinct actin binding proteins that cap, sever and crosslink the actin filament (dos Remedios et al., 2003).

CapZ and tropomodulin (Tmod) are the major capping proteins that cap the barbed and pointed end of the actin thin filament in striated muscle respectively (Fig. 1.8, capZ is represented as a pink disc and Tmod is represented as a purple rectangle). They are both important factors in actin dynamics and are able to regulate and maintain the uniform length of the actin filament. CapZ is a heterodimer composed of α and β subunits and is present in all eukaryotic cells (Cooper and Schafer, 2000). In skeletal muscle, capZ is localized at the Z-line of the sarcomere. A number of biological roles for capZ have been reported. Firstly, it can nucleate actin filament assembly *in vitro* (Fowler, 1996; Schafer et al., 1995). Secondly, its binding affinity for actin filament ends appears to be regulated by Phosphatidylinositol 4,5-bisphosphate (PIP_2) and increases in PIP_2 levels causes rapid disassociation of capZ from actin filament barbed ends *in vitro* (Schafer et al., 1996). Another candidate for regulating capZ's affinity for the barbed end is S100, a Z-line associated protein that binds to capZ in a calcium dependent manner (Ivanenkov et al., 1995; Kilby et al., 1997). S100 has been proposed modulate the function of capZ indirectly, by affecting its interaction with other Z-line components and regulating barbed end alignments at the Z-line (Littlefield and Fowler, 1998). Thirdly, capZ is thought to directly regulate isometric tension of sarcomeres in cardiomyocytes and is involved in the binding of protein kinase C to the myofibrils (Pyle et al., 2002; Pyle et al., 2006). Fourthly, capZ binds to α-actinin (Papa et al.,

1999) and nebulin (Witt et al., 2006) and is thought to anchor the actin thin filament to the Z-line. Finally, from *in vitro* studies, capZ is proposed to organize and align the barbed end of thin filaments at the Z-line (Schafer et al., 1995; Schafer et al., 1993).

At present four vertebrate Tmod isoforms (Tmod-1-4) are known and are referred to as E, N, U and Sk-Tmod respectively (Conley et al., 2001; Cox and Zoghbi, 2000; Fowler, 1990). Each isoform is encoded on a separate gene and all isoforms have unique expression profiles. Two of the Tmod isoforms are expressed in muscle: Tmod-1 is expressed in the heart and slow-twitch skeletal muscle and Tmod-4 (Sk-Tmod) is expressed in fast-twitch skeletal muscle. In addition to capping the actin filament, Tmod can simultaneously bind to nebulin (the thin filament ruler, see below) and Tropomyosin (Tm) (Greenfield and Fowler, 2002; Kostyukova et al., 2006; Vera et al., 2000). Within striated myofibrils Tmod is regarded as one of the key elements in maintaining sarcomeric structure and regulating actin filament length (Fischer and Fowler, 2003; Gregorio et al., 1995; Littlefield et al., 2001; Sussman et al., 1998; Ursitti and Fowler, 1994).

Nebulin is one of the largest proteins identified in vertebrates. It is encoded on one gene and is extensively alternately spliced to produce isoforms varying in size between 500 – 900 kDa (McElhinny et al., 2003). Over 95% of the protein consists of 35 residue repeat modules that function as actin binding domains (Horowits et al., 1996; McElhinny et al., 2003; Wang, 1996). Each group of seven 35 residue repeat modules are arranged into a higher order repeating unit termed a super-repeat. Nebulin is anchored to the Z-line at its C-terminus and extends the length of the thin filament (Fig. 1.8, yellow rod). It binds to many different components of the sarcomere such as myopalladin and the actin capping proteins capZ and Tmod (Bang et al., 2001a; McElhinny et al., 2001; Witt et al., 2006). Modules that span the A-I junction bind to actin, myosin and calmodulin (Jin and Wang, 1991; Lukoyanova et al., 2002; Root and Wang,

2001; Wang, 1996). Nebulin (also known as nebulette in the heart) is expressed in the heart but at much lower levels than in skeletal muscle (Kazmierski et al., 2003). It appears to assemble early in myofibrillogenesis before actin filaments attain their mature lengths and organization (Ojima et al., 1999).

Nebulin is predicted to act as a molecular ruler for defining the length of thin filaments in striated muscle (Wang and Wright, 1988). A number of properties of this protein make it an ideal candidate for a ruler. Firstly, the entire protein spans the length of the actin filament. Secondly, it binds to both actin thin filament capping proteins (capZ and Tmod) and thirdly it is able to associate with the actin filament along its entire length. Indeed, loss of nebulin in cultured rat cardiomyocytes resulted in longer actin filaments (McElhinny et al., 2005). However, in contrast to this finding, two separate studies that generated a nebulin targeted mouse mutant suggested that actin filaments were shorter as a result of a lack of nebulin (Bang et al., 2006; Witt et al., 2006). Although nebulin has a role in maintaining the length of the thin filament, the precise mechanism of how it contributes to this process remains unknown. However, it is likely to involve a number of other sarcomeric components which act in concert to precisely regulate actin dynamics and thereby control the length of actin filaments. The role of nebulin and other proteins associated with thin filaments in actin dynamics will be discussed at the end of this chapter.

Tropomyosin (Tm) and Troponin (Tn) are key elements in the interaction between thin and thick filaments and thus the generation of force. Tm forms homodimers and heterodimers to produce two chained parallel coils that extend the length of both sides of the actin thin filament (Perry, 2001). In resting muscle Tm blocks the myosin head from binding to the actin filament. Tn is a trimer composed of three subunits C, I and T. Upon activation of muscle contraction calcium binds to TnC, altering its confirmation and thus the interaction between TnC and TnI

(McKay et al., 1997). As a result Tm shifts its position and therefore a binding site becomes available for the myosin head to dock to the actin filament. Once the myosin head has bound to actin, myosin ATPase is activated and causes further movement of Tm along the rest of the thin filament, thereby allowing myosin to 'walk' along the entire length of the filament and generate force (Craig and Lehman, 2001). Tm is also thought to function in stabilizing the thin filaments as it increases the stiffness of the actin polymer and inhibits fragmentation of the filament (Wegner, 1982). It is also able to affect polymerization and depolymerization at the pointed ends due to its interaction with the N-terminus of Tmod (Broschat, 1990; Kostyukova and Hitchcock-DeGregori, 2004). The interaction of Tmod with Tm increases the binding affinity between Tmod and the pointed ends of the actin filament, and in the absence of Tm it has been shown that Tmod caps the pointed end much more weakly (Babcock and Fowler, 1994).

1.4.1.2 The myosin thick filament and its associated proteins

Myosin is the second most abundant protein in striated muscle after actin and is regarded as a molecular motor that drives muscle contraction. Different muscle types generate forces at different strengths. This is achieved by having many different classes of heavy and light chain myosin isoforms that have varying activity rates and are tightly regulated in terms of their expression. Indeed, 15 classes of myosin heavy and light chain isoforms have been identified (reviewed in Sellers, 2000). The thick filament within striated muscle is composed of members of the myosin II family. Each member of this family is comprised of a long rod like tail domain and two head domains. The rod domain is composed of two identical heavy chains that are twisted into a coiled coil at their C-terminal regions. The head domain is composed of the N-terminal regions of each heavy chain from the rod domain and two light chains. Each head domain has ATPase and motor activity and binds to actin (forming a cross-bridge, reviewed Milligan, 1996),

as well as containing binding sites for nucleotides (Rayment et al., 1993). The rod enables two myosin filaments to join in a bipolar orientation (Fig. 1.8, light green golf shaped rods), so that the thick filament is able to move groups of oppositely oriented actin filaments past each other and induce muscle contraction. Briefly, muscle contraction involves changes to the conformation of the myosin head derived from ATP binding and hydrolysis. Attachment of ATP to the myosin head changes the conformation of the actin binding site, thus reducing the affinity of the myosin head for the actin filament. Moreover, ATP binding allows the myosin head to move along the actin filament. ADP and inorganic phosphate (Pi) remain attached to the myosin head after ATP hydrolysis.At this stage the myosin head binds weakly to a new site on the actin filament, however, release of the Pi results in tighter binding and induces the head to undergo a large angular rotation (the power stroke). Following rotation, ADP dissociates and the actomyosin complex returns to the relaxed state.

Titin is the largest protein identified to date (Maruyama et al., 1977; Wang et al., 1979). Two titin molecules are associated with each thick filament and span the entire sarcomere (Fig. 1.8, orange line). The C-terminal end of each titin molecule overlaps at the M-line, and at the Z-line the N-termini of titin from adjacent sarcomeres overlap. Titin appears to have a number of roles in sarcomeric function and assembly. Firstly, the portion of titin spanning the I band has elastic properties and therefore it has been labeled as a molecular spring and is thought to maintain the position of the thick filaments during contraction and resting phases. Secondly, it is a primary candidate for acting as the template for sarcomere assembly. Indeed, ablation of titin in rat cardiomyocytes disrupted myosin incorporation into myofibrils (Person et al., 2000) and similar results were obtained in a myofibroblast cell line lacking titin (van der Ven et al., 2000). Therefore it has been hypothesized that titin is required for thick filament incorporation into the sarcomere. Titin may also play a role in assembly of the Z-lines. The N-terminus of titin is

capped and anchored to the Z-line by telethonin (Tcap) (Gregorio et al., 1998; Mues et al., 1998). In addition to this anchorage point the N-terminal region of titin also contains a number of repeats (Z-repeats) that interact with α-actinin, the predominant scaffolding element of the Z-line. Intriguingly, the number of titin Z-repeats varies between muscle types that differ in Z-line width. The current hypothesis is that titin can influence the width of the Z-line by regulating the number of cross-links generated between anti-parallel titin Z-repeats and α-actinin dimers (Ohtsuka et al., 1997; Sorimachi et al., 1997). Finally, it has been suggested that titin is also involved in signaling pathways as the C-terminus contains a serine/threonine kinase domain.

Myosin binding proteins C and H (MyBP-C and MyBP-H) bind to myosin at the bare zone of the thick filament in a series of transverse stripes. MyBP-H is also found outside this zone (Bahler et al., 1985; Bennett and Bagshaw, 1986; Craig and Offer, 1976). To date only MyBP-C has been found to contain a titin binding site (Gilbert et al., 1996; Gruen et al., 1999) and it has therefore been speculated that this protein links titin to the myosin filament and aligns the thick filaments within the A-band. It has also been reported that both these proteins are important in aiding the assembly of the myosin polymer to the correct length, as myosin filaments polymerized in the absence of MyBP-C are shorter and less uniform (Davis, 1988; Gregorio et al., 1998; Koretz, 1979; Seiler et al., 1996). They may also be involved in regulating muscle contraction (for review see Winegrad, 1999).

1.4.1.3 Z-line

The boundaries of each sarcomere are defined by Z-lines that are precisely aligned within and between myofibrils. This structure is thought to act like a scaffold and anchors all the major components of the sarcomere including actin thin filaments, titin and nebulin. An increasing

number of novel proteins associated with the Z-line have also been discovered such as myotilin, cypher, MuRF1 and myopalladin (Frank et al., 2006). For many of these novel proteins their function at the Z-line is still unknown, however, a few key proteins will be discussed below. In addition to integrating the sarcomeric components, the Z-line is also laterally associated with intermediate filament proteins such as desmin. These associated proteins are thought to link the peripheral myofibrils to costameres at the sarcolemma, and also to mitochondria and the nuclear membrane. The Z-line has been likened to a biomechanical sensor that can respond to changes in tension in the sarcolemma. Indeed, Z-lines are responsible for transmitting tension generated by individual sarcomeres along the length of the myofibril, allowing for efficient contractile activity (Squire, 1997). Due to the multiple functions of the Z-line it is not surprising that many different proteins associate with it and assist in maintaining its structural stability and signalling properties. Deciphering the molecular interactions of the proteins involved in the formation and maintenance of Z-lines will be pivotal for understanding the regulation of myofibril assembly, sarcomeric organization and the mechanical properties of striated muscle.

The major component of the Z-line is the actin thin filament cross linking protein α-actinin (reviewed Blanchard et al., 1989). The rod domains of actinin monomers interact to form anti-parallel dimers which cross link actin and titin from adjacent sarcomeres. Moreover, they are capable of transmitting and distributing the force generated by the sliding filaments (Vigoreaux, 1994). Intriguingly, in invertebrates α-actinin is not essential for proper assembly of the sarcomere (Fyrberg et al., 1998). In *Drosophila* the muscle still forms in the absence of α-actinin and although there are defects in Z-line organization and muscle attachment to the tendon matrix, the muscle is still able to contract albeit poorly. α-Actinin therefore appears to be required for sarcomere stability once contraction begins. Many other Z-line proteins are able to bind to α-actinin and therefore it is understandable that even in its absence a Z-line can still form. The

modular nature of α-actinin enables it to bind to many proteins simultaneously. In addition to actin, α-actinin interacts with muscle LIM proteins (MLPs), α-actinin associated LIM proteins (ALPs), FATZ-1 (also known as calsarcin-2/myozenin) and myopalladin.

MLPs are members of the cysteine rich protein (CRP) family and localize to the periphery of the Z-line and the intercalated disc in cardiomyocytes (Ehler et al., 2001). In addition to binding to α-actinin, MLPs can also bind to zyxin and nebulin related anchoring protein (NRAP) (Ehler et al., 2001). The multiple binding properties of this protein reinforce the hypothesis that MLPs act as scaffold or linker proteins. Loss of this protein in cardiac muscle results in disorganization of the myofibrils suggesting that its primary role is in stabilizing the Z-line (Arber et al., 1997). It may also link the Z-line to the membrane via costameres through its interaction with NRAP. In *Drosophila*, MLPs are localized to the nucleus and in vertebrates over expression in cultured myocytes enhanced muscle differentiation (Arber et al., 1994). Moreover, MLPs have been shown to bind to MyoD *in vitro* (Kong et al., 1997), therefore they may also play a role in directly regulating transcription of muscle components.

Several members of the enigma protein family are expressed in muscle and localize to the Z-line including enigma, ALP and cypher. All these proteins bind to α-actinin and enigma is also able to bind to Tm. One of the functions of the enigma protein may be to serve as a docking site for other signaling molecules at the Z-line. For example enigma and cypher bind to protein kinase C. Moreover, mouse knock outs of *cypher* and *ALP* indicate that they stabilize the muscle cytoskeleton (Pashmforoush et al., 2001; Zhou et al., 2001).

Filamin, α-actinin and telethonin binding protein of the Z-disc-1 (FATZ-1), as its name suggests, binds to α-actinin, telethonin and filamin and is exclusively located at the Z-line

(Faulkner et al., 2000; Takada et al., 2001). FATZ-1 is part of a novel family of proteins named calsarcins. They are able to interact with calcineurin, a calcium/calmodulin dependent phosphatase which is involved in the regulation of genes affecting muscle differentiation and the formation of different fibre types (Delling et al., 2000). FATZ-1 has been proposed to anchor calcineurin to the Z-line and may regulate its activity.

Myopalladin tethers together the C-terminal domain of nebulin to α-actinin at the Z-line (Bang et al., 2001b). The N-terminal region of myopalladin also specifically binds to cardiac ankyrin repeat protein (CARP). CARP is a nuclear protein involved in control of muscle gene expression and has been shown to negatively regulate the expression of cardiac genes. Myopalladin may link the regulatory mechanisms involved in Z-line structure (i.e. α-actinin and nebulin) to those involved in muscle gene expression (Bang et al., 2001b).

1.4.1.4 M-line components

The formation of the M-line or M-band is proposed to be the final step in myofibril assembly (Markwald, 1973). It is thought to arrange and anchor thick filaments within the sarcomere (Agarkova and Perriard, 2005; Knappeis and Carlsen, 1968; Luther and Squire, 1978). Indeed, myosin filaments are crosslinked at the M-line by M-bridges (Van Der Ven et al., 1996). As yet it has still not been confirmed what these M-bridges are made of, however, the two primary candidates are myomesin and M-protein. Myomesin is arranged in an anti-parallel staggered fashion at the M-line (Obermann et al., 1996) and is able to bind to titin (Obermann et al., 1997) and myosin. Due to these properties myomesin has been proposed to integrate the thick filament into the sarcomere (Ehler 1999). M-protein has only been found at the M-line of fast muscle fibre types and cardiac muscle (Grove et al., 1984; Noguchi and Tanaka, 1982; Obermann

et al., 1997). Like myomesin it is also able to bind to titin and myosin (Masaki and Takaiti, 1974; Nave et al., 1989), however, its function remains unclear. It is possible that it may interact with myomesin and MyBP-C to anchor thick filaments to titin in fast skeletal and cardiac muscle (Clark et al., 2002).

Three members of the Muscle specific RING finger protein family (MuRFs) have been identified (Centner et al., 2001; Dai and Liew, 2001). MuRF1 is the only member that directly binds to titin at the M-line (Centner et al., 2001). Recent studies have implicated MuRF-1 in regulating muscle protein degradation (Bodine et al., 2001). Intriguingly, this protein has also been associated with the nucleus and interacts with transcription factors as well as other nuclear components. Therefore there is speculation that this protein is in fact dynamic and is involved in regulating myofibril signaling pathways.

1.4.2 The Sarcolemma

The sarcolemma is the plasma membrane of the muscle cell. It is connected to the underlying myofibrils and organelles by a cytoskeletal network that is essential for stabilizing the muscle fibre and transducing the force across each cell. Intermediate filaments and microtubules are the main cytoskeletal elements that link the sarcomere to anchorage points associated with the sarcolemma (e.g. the costameric network and myotendinous junction in skeletal muscle and the intercalated disc in cardiac muscle (Fig. 1.9)).

1.4.2.1 Intermediate filaments and microtubules

The intermediate filament cytoskeleton of mature muscle is composed predominantly of desmin (Lazarides, 1980; Lazarides, 1982). It binds to a number of intermediate filament proteins such as skelemin, desmuslin and syncoilin (Bilak et al., 1998; Granger and Lazarides, 1980; Newey et al., 2001). In addition, it also interacts with sarcomeric proteins such as α-actinin and nebulin (Bang et al., 2002) and is thought to link individual myofibrils laterally via the Z-lines (Fig. 1.9). Moreover, it has been shown to connect the sarcomeres with the mitochondria, nucleus, sarcolemma, microtubules and is also concentrated at myotendinous junctions of skeletal muscle. Knock out mice studies indicate that although desmin is not essential for muscle function it contributes to maintaining the integrity and alignment of the mature and regenerating myofibrils (Carlsson et al., 1999; Li et al., 1997). Less is known about other intermediate filament proteins such as vimentin, nestin, synemin and paranemin, however, it is thought that they may be important in the assembly of the muscle cytoarchitecture and may link contractile apparatus to costameres or adjacent myofibrils (reviewed in Clark et al., 2002). Additional intermediate filament proteins such as cytokeratins are thought to cooperate with desmin and its associated molecules in organizing and stabilizing the sarcolemma (O'Neill et al., 2002). Unexpectedly, nuclear lamins also appear to be involved in contributing to muscle cytoarchitecture and function. Moreover, mutations in a number of *lamins* are the cause of several types of muscular dystrophy (Morris, 2001).

Microtubules are polymers of α and β tubulin and are involved in numerous cell processes such as mitosis, cell motility and intracellular transport. Relatively little is known about their role in striated muscle, however, mounting evidence is emerging that microtubules are involved in muscle differentiation, morphology and contractile activity. In skeletal muscle microtubules are

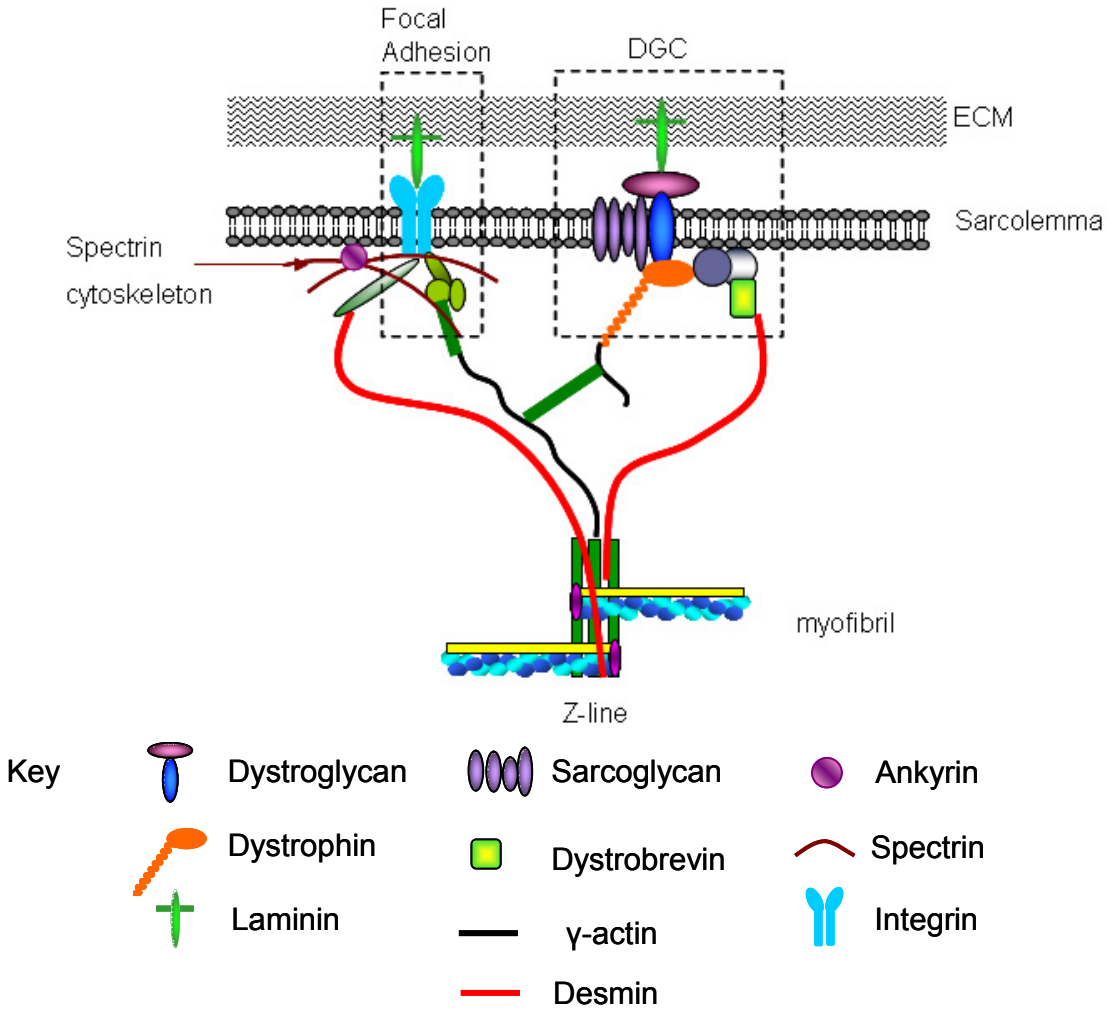

Fig. 1.9. Illustration of the costameric network and the components that link the myofibrils to the sarcolemma. The focal adhesion / integrin kinase complex and the dystrophin glycoprotein complex (DGC) are boxed. The spectrin cytoskeleton (brown lines) is anchored to the sarcolemma via ankyrin (purple circle). Desmin (red lines) and γ-actin (black lines) link the costameric network to the myofibrils by attaching to Z-lines. Most intermediate filament proteins, including desmin associate with the costamere through dystrophin and dystrobrevin.

positioned between myofibrils and are also associated with the sarcolemma, the golgi complex and nuclei. When microtubule dynamics is disrupted in skeletal myocytes, myoblast fusion and differentiation are disrupted (Antin et al., 1981; Saitoh et al., 1988). Moreover, the loss of microtubules in heart muscle affects contractile function (reviewed in Hein et al., 2000).

1.4.2.2 The Costameric network

Costameres are subsarcolemmal protein assemblies that surround and align with each Z-line and M-line of the peripheral myofibrils and anchor the sarcomere to the sarcolemma (Craig and Pardo, 1983; Danowski et al., 1992; Pardo et al., 1983; Porter et al., 1992). Costameres are composed of at least three structures: integrins /focal adhesion complexes; the dystrophin glycoprotein complex (DGC) and the spectrin based cytoskeleton (Fig. 1.9). All these elements work together to promote the stability of the muscle fibre and to efficiently transduce the force from the Z-line to the membrane, where the force is transmitted laterally to the muscle termini (Danowski et al., 1992).

Integrins are transmembrane proteins that mediate attachment of the actin cytoskeleton to the ECM (Adams and Watt, 1993). Over 20 distinct integrin isoforms have been identified so far and each possesses unique functional properties (Bouvard et al., 2001). β1 Integrin is enriched within costameres and studies indicate that it plays a critical role in maintaining the organization of sarcomeres in cardiomyocytes (Fassler et al., 1996). In addition to playing a structural role within striated muscle, integrins are also important signaling molecules and are able to sense mechanical stress and activate signaling pathways to induce changes in gene transcription and cytoskeletal reorganization (reviewed in Shyy and Chien, 1997). Their prominent location makes them ideal candidates for biomechanical sensors that respond to changes in force.

The DGC functions to anchor the sarcolemma to the costameres and stabilize the sarcolemma against the physical forces transduced through costameres during muscle contraction. Defects in a number of molecules that make up this complex such as dystrophin, dystroglycan, laminin 2 and sarcoglycans result in human muscular dystrophies (reviewed in Davies and Nowak, 2006). Dystrophin is the core component of this complex and mediates the critical connection between the ECM, the muscle membrane and the costameric network by linking β dystroglycan to costameric actin. Indeed, as previously described in section 1.1.2, mutations in *dystrophin* result in DMD, the most common form of human muscular dystrophy. Moreover, dystrophin is also important in the organization of other components of the costameric network such as vinculin and spectrin (Williams and Bloch, 1999).

The involvement of spectrins in the costameric network is just beginning to be elucidated. Spectrin is primarily known for organizing the membrane cytoskeleton of erythrocytes and in conjunction with ankyrin, also plays a prominent role in anchoring integral membrane proteins to the membrane cytoskeleton (reviewed in Thomas, 2001). In striated muscle α/β spectrin heterodimers are found in the costameric network surrounding the Z-line, whereas β homodimers are found at the M-line (Porter et al., 1997). All populations of spectrin are linked to ankyrin, which limits the spectrin cytoskeleton to the sarcolemma (Williams et al., 2001).

1.4.2.3 Myotendinous junction

The myotendinous junction (MTJ) is the structure in skeletal muscle where the myofibrils terminate and is equivalent to the vertical myoseptum in zebrafish. The MTJ is especially

reinforced as it is the main structure that bears the brunt of the force transmitted during muscle contraction. The thin filaments terminate at a dense subplasmalemmal layer that appears to mediate thin filament attachment to each other and to the muscle membrane (reviewed in Tidball, 1991). Focal adhesion-like adhesion plaques containing integrins, vinculin and talin are found at the MTJ along with the DGC, and implicates these structures in connecting the terminal thin filaments to the muscle membrane.

1.5 Myofibrillogenesis

Formation of myofibrils requires the assembly of thin and thick filaments, Z and M-lines and the association of many other components that are all arranged into a highly organized structure to form the sarcomere. Due to the complexity of the sarcomeric structure deciphering the mechanisms that lead to its assembly have proved to be challenging, however, a number of models have been proposed.

1.5.1 Models for sarcomere assembly

It is generally agreed that myofibrillogenesis occurs in a stepwise process and initially occurs in association with the sarcolemma. One of the first models described was the template model (Dlugosz et al., 1984). In this model thin filaments, thick filaments and Z-band proteins are recruited to stress fibre-like structures (temporary bundles of actin) in the developing muscle cell. These structures serve as a template for assembly of the sarcomeres. This model has since been disregarded as the stress fibre-like structures are composed of sarcomeric proteins such as α-actinin, tropomyosin, troponins and tropomodulin (Almenar-Queralt et al., 1999; Rhee et al., 1994). Thus it has been concluded that the stress fibre-like structures are in fact the newly formed myofibrils themselves. It has also been observed that Z-bodies containing α-actinin fuse to form mature Z-lines in myofibrils of muscle cells (Dabiri et al., 1997; McKenna et al., 1986). This finding is inconsistent with the template model, where it would be expected that no fusion would occur as the stress fibre-like structures should already act as a template to position all the components of the sarcomere.

The independent subunit assembly model (the stitching model) proposes that I-Z-I bodies (dense bodies of Z-band proteins associated with thin filament) and thick filaments assemble randomly throughout the muscle cell (Holtzer et al., 1997). Titin then joins the I-Z-I bodies and thick filaments together to form sarcomeres. This model was based on reports where myosin was not detected between the I-Z-I bodies (Schultheiss et al., 1990). Moreover, it was supported by studies of *Drosophila* mutants that lacked muscle myosin, where the I-Z-I brushes in flight muscles were still able to align (Beall et al., 1989). The caveat of this model is that it omits evidence for the presence of non-muscle myosin II, detected in differentiating cardiomyocytes (Dlugosz et al., 1984; Fallon and Nachmias, 1980). However, the third model (the premyofibril model) does explain the presence of non-muscle myosin II in myofibrillogenesis.

The premyofibril model incorporates aspects of the two previously described models. In this model premyofibrils containing 'mini sarcomeres' (I-Z-I bodies which are distributed throughout the myofibril) interdigitate with non-muscle myosin II in the absence of titin. Premyofibrils then become nascent myofibrils, where non-muscle myosin II is replaced by myosin and titin. Moreover, the thick filaments become fairly well aligned between adjacent clusters of Z-bodies, which begin to align and cluster into groups and often form irregular Z-lines. Actin and titin may contribute to aligning the thick filaments (that have been assembled separately) into the sarcomere. At this stage the M-line becomes apparent, however, the I-bands are still of a variable length. These nascent myofibrils then become mature myofibrils by further addition of myosin, titin, MyBP-C, and other elements that localize to the M and Z-lines. Finally, the thin filaments within the myofibrils mature and grow in length resulting in complete alignment of all sarcomeric components (Rhee et al., 1994).

One of the main controversies of this current model is the function and presence of non-muscle myosin IIb. It has been demonstrated that non-muscle myosin IIb is present in association with I-Z-I bodies in cardiomyocytes (Rhee et al., 1994), and it has been proposed that the function of this protein would be to interdigitate and organize the mini-sarcomeres prior to the incorporation of muscle myosin and titin. Indeed, inhibition of phosphorylation activity of non-muscle myosin results in the loss of premyofibrils and nascent myofibrils in cardiomyocytes (Du et al., 2003; Ferrari et al., 1998). However, sarcomeres are still formed in the mouse knock out of non-muscle myosin IIb (Tullio et al., 1997). It is also unclear how non-muscle myosin is replaced by muscle myosin.

The caveat of all the models proposed is that they are based on observations and experiments performed in cultured cells, which may not truly reflect what occurs *in vivo*. Cultured muscle cell extracts may already have some mature myofibrils at the time of isolation, therefore it cannot be excluded that what is observed is not *de novo* myofibril assembly. The *in vitro* two dimensional environment might favour specific structures to form which aren't found *in vivo*. Indeed, several *in vivo* studies do not support many aspects of the premyofibril model. Costa and colleagues (2002) reported no intermediate premyofibril stages in zebrafish. Ehler and colleagues (1999) were also not able to detect any premyofibril like elements in developing chicken hearts, and although non-muscle myosin IIb was expressed in the heart it did not arrange between Z-bodies as was observed in cardiomyocytes. It is possible that premyofibrils are not detected as this event occurs much more quickly *in vivo* compared to within a cultured muscle cell. It is clear that although studies of myofibrillogenesis in cultured cells have been important in unraveling aspects of sarcomere assembly, to gain a more realistic understanding of events these processes need to be examined *in vivo*.

All the models proposed so far do not elaborate on how the final length of the thin filament is determined. However, two different proposals have been documented, the variable length model and the fixed length model. In the variable length model, which supports the Sanger premyofibril model, nascent thin filaments that are attached to the Z-bodies are either shorter or longer than their final mature length and in the final stages of maturation they grow to the correct size by polymerization from the barbed or pointed ends (Rhee et al., 1994). In the fixed length model proposed by Fowler and colleagues (1999) the thin filaments are pre-assembled to defined lengths by nebulin, the capping proteins are then integrated into non-striated premyofibrils (I-Z-I bands) and the thin filament is subsequently rearranged and aligned to form the proper length. The fixed length model proposes that the thick and thin filaments are organized into striated myofibrils by a process of filament sliding, where interactions with titin, nebulin, M-line and Z-line proteins align the barbed and pointed ends of the thin filament at the Z-line and central bare zone. Titin is one of the main candidates for aligning the filaments and has been proposed to act as a template to organize the thin and thick filaments into mature sarcomeres based on its size, its interacting partners and the presence of different isoforms i.e. different templates.

The length of the thin filament is likely to be defined by the dynamics of actin polymerization, which is regulated by nebulin and the capping proteins capZ and Tmod. Significantly, the C-terminus of nebulin and capZ are detected in discontinuous punctuate patterns in non-striated actin filament bundles at the tips of skeletal myotubes (Holtzer et al., 1997; Schafer et al., 1993). One could therefore speculate that nebulin acts as a template for the formation of actin filaments in the premyofibril with capZ and Tmod. This aspect of sarcomere assembly has still not been addressed fully in any of the models proposed to date, however, it is an integral part of myofibrillogenesis and investigation of this field may reveal new insights into sarcomere assembly.

1.5.2 Actin thin filament dynamics and assembly

Actin dynamics are crucial in not only assembly of the actin filament but maintaining the structure and length of each filament. Actin filaments differ in length between different cell types, however within each cell type the length is precisely controlled. A number of different components are required to maintain the length of the actin filament in the sarcomere, including the template protein (nebulin), capping proteins (Tmod and capZ) and severing proteins (e.g. gelsolin and severin), in addition to molecules that sequester monomeric actin or promote polymerization/depolymerization (Cooper and Schafer, 2000).

In most cells actin filaments are always in a continuous state of assembly and disassembly. Elongation of the actin filaments can occur from either the pointed or the barbed end. The predominant site of actin monomer incorporation in non-muscle actin occurs at the barbed ends of the actin filament (Dome et al., 1988; McKenna et al., 1985; Shimada et al., 1997) and disassociation occurs predominantly at the pointed ends. In striated muscle the dynamics of actin polymerization are quite different. Studies by Littlefield and colleagues in 2001 indicated the pointed ends were the major sites of actin monomer incorporation, and the dynamics of Tmod capping maintained and determined the length of the actin filament. Moreover, Tmod dynamics is regulated by tropomyosin and is able to exist in low and high affinity binding states (Fowler et al., 2003). While capZ only exists in a high affinity state, as the levels of exogenous CapZ in muscle cells are such that the barbed end is rapidly and securely capped (Schafer et al., 1996; Wear et al., 2003).

Nebulin has long been classified as the template that defines the length of the actin thin filament within sarcomeres. However, there has been much debate on exactly how this process

occurs (Fowler, 1997). The ruler mechanism is currently the most widely accepted theory for how actin filament length is defined. In this model the actin filament periodically binds to nebulin and extends along the length of the nebulin filament. Once the actin filament has reached each end of the nebulin filament it is capped by the capping proteins (capZ and Tmod), which prevent further monomer addition or loss and securely tether the ruler to the actin filament. In light of the recent findings that Tmod is integral to actin dynamics, the cap locator model has been proposed (Fowler et al., 2006). In this model the nebulin N-terminus is important in localizing Tmod to the desired length of the actin filament, and as nebulin interacts with Tmod at the N-terminus this end could create a localized concentration of Tmod. This model is consistent with findings that thin filament length is dependent on Tmod concentrations (Littlefield et al., 2001; Sussman et al., 1998), however, further experiments will be required to resolve which of the two models occurs *in vivo*.

The mechanisms involved in actin thin filament length regulation are complex and involve multiple sarcomeric components. Determining the molecular roles of each length determining factor will be important in defining how this process occurs. Moreover, it may provide further insight into how the actin filament is assembled into sarcomeres during myofibrillogenesis.

1.6 Objectives and outcomes of this thesis

The aim of this PhD project was to positionally clone and characterize the zebrafish muscle motility mutant *schnecke* (*sne*). I identified a mutation at the *sne* locus in *capzα1*, a subunit of the actin capping protein, CapZ. Analysis of the *sne* mutant and MO knockdown of other CapZ subunits suggests that CapZ is essential for the myofibril and sarcomeric integrity within zebrafish skeletal muscle. Additional double knockdown studies with associated components of the actin thin filament (Nebulin and Tmod) indicate that CapZ is required for maintenance of the Z-line and thin filament formation. Moreover, localization of the intermediate filament protein Desmin is altered in *sne* mutants, thus CapZ may be involved in linking the myofibrils with the costameric network. Finally, motoneuron development is affected in capZα1 MO injected embryos. This raises the possibility that CapZ may be directly involved in movements that facilitate motoneuron formation.

The results presented in this thesis provide new evidence for an additional role of CapZ in maintaining the stability of the myofibril within skeletal muscle. The phenotype produced from the mutation in *capzα1* illustrates the importance of sarcomeric proteins in maintaining muscle integrity, and although the loss of this protein does not completely abolish sarcomere formation, the architecture and integrity of the muscle is disrupted. The progressive degeneration of the muscle structure in the *sne* mutants is characteristic of human muscular dystrophies, therefore dysfunctional CapZ could potentially be a novel candidate for this type of myopathy. Further analysis of *sne* mutant will benefit our understanding of the complex interactions within the myofibre and will ultimately assist in our knowledge of many aspects of muscle function and development, which will enable us to design new methods in treating myogenic disorders.

Chapter 2

Materials and Methods

Chapter 2: Materials and Methods

2.1 Embryo collection

Male and female zebrafish (*Brachydanio rerio*) pairs were set up in breeding boxes the evening before embryos were required. The following morning, upon light cycle activation (at 8.30am), the female is stimulated to release her eggs, which are subsequently fertilized by the male. Both the male and female zebrafish are separated from the embryos by a mesh divider to prevent them from eating their offspring. To obtain precise staging of the embryos, the male and female can be separated overnight within the same breeding box (by the mesh divider), and then the following morning put together. Embryos were collected and raised in either Egg Water (0.18g/l sea salt, 2mg/l methylene blue) or 0.3 X Danieaus (17.4mM NaCl, 0.21mM KCl, 0.12mM $MgSO_4$, 0.18mM $Ca(NO_3)_2$, 1.5mM HEPES (4-(2-hydroxyethyl)-1-piperazineethanesulfonic acid)) at 28^{o}C. Embryos were staged according to their morphology as outlined by(Kimmel et al., 1995).

2.2 Morpholino oligonucleotide design and injection

Antisense morpholino oligonucleotides (MOs) were used to block translation at the start or splice site of a given gene. All MOs used were 24-25 oligomers of approximately 50% GC content and were generated and designed by Gene Tools LLC, see Table 2.1 for MO sequences. All ordered MOs were checked for by performing a BLAST (Basic Local Alignment Search Tool) search of the Ensembl zebrafish genome to ensure that each MO specifically matched the target sequence.

Table 2.1 Sequence of MOs used in this thesis.

MO	Sequence 5′-3′	N° of bases identical to capZα1	N° of bases identical to capZα2
CapZa1 ATG	GCTCGTGACCATAATAGGGCAAAAC		0/25
CapZa1 splice 1	AATGCTTTATTTTTACCTTCTCCTC		16/25
CapZa1 splice 2	GCTTGTAGCTCTTACCTGATAATCG		13/25
CapZa2 ATG	AAGCTGTTCCTCAAAGTCCGCCATC	21/25	
CapZa2 splice	AGATTACTCACCTGATCTTCACTTC	13/25	
CapZb ATG	CCAACTGCTGCTCATTCATGTCTGC		
CapZb splice	GGGCTGGCTACTCACAGGTCTCTG		
Desmin ATG	TTGGGTTTGTACGCTGTGTGAATGC		
Desmin splice	ATAAAGTACATACAGCTCTGAAAGC		
SK Tmod4 ATG	TCTCTGGGATCACTCTTAGACATAC		

All MOs received were diluted in 100µl of Milli-Q (MQ) H_2O. The concentration of each MO in mg/ml was subsequently determined by measuring the MO (diluted 1 in 800 in 0.1M HCL) at 265nm with a spectrophotometer (Amersham Biosciences Ultrospec 1100 *pro*), and then using this reading in the following formula:

$$\text{Absorbance at 265nm} \times \text{Dilution factor} \times \frac{\text{Molecular Weight}}{\text{Molar Absorbance}}$$

The molecular weight and molar absorbance were stated in the Gene Tools LLC data sheet accompanying each requested MO. The MO was subsequently diluted in morpholino buffer (5mg/ml phenol red, 4mM HEPES (pH7.2), 160mM KCl) or MQ H_2O to produce final concentrations ranging between 3-10ng/1.4nl. Needles for injecting MO into embryos were made by a needle puller (David Kopf Instruments, Model 720) using F-type capillaries (Kwik-Fil TM borosilicate glass capillaries with filament). 1.5µl of MO was loaded per needle, once in the holder (World Precision Instruments), which is controlled by a three axis micromanipulator (Narishige), the tip of the needle was cut open with a blade. The amount of MO ejected from the needle was controlled by a compressed air flow control panel (World Precision Instruments

Pneumatic Pico Pump PV820), and measured using a graticule (0.05mm striations). Each needle was calibrated by producing a droplet with a diameter of 0.3mm (14nl) from ten pulses, therefore each single pulse ejected 1.4nl. The MO was then injected into the yolk of 1-2 cell stage embryos aligned along the edge of a slide placed in a petri dish.

2.3 General molecular biology techniques

2.3.1 Purification of DNA using phenol chloroform

The volume (vol) of each DNA sample was firstly made up to 100µl with MQ H_2O and then phenol:chloroform:isoamyl alcohol (25:24:1) was added. The solution was vortexed for 30 s and centrifuged (14645 xg) for 5 min at 4^{o}C. The aqueous top layer was placed in a new tube and vortexed for 30 s with an additional 100µl of chloroform:isoamyl alcohol (24:1). The solution was then centrifuged again for 5 min at 4^{o}C. The top layer was pipetted into a new tube and 0.1 vol of 3M sodium acetate and 3 vols of 100% ethanol were added. The solution was left at -20^{o}C for 1 hr then centrifuged (16168 xg) for 30 min. The pellet was subsequently washed in 70% ethanol and resuspended in 20µl of MQ H_2O.

2.3.2 DNA extraction from agarose gels

DNA bands were observed under UV light (365 nm) and cut out of a 2% agarose gel. A Qiagen gel extraction kit was then used to extract the DNA from the gel according to the manufacturer's protocol. Three vols of buffer QB was added to each gel piece and the gel dissolved by incubation at 55^{o}C for 10 min. The solution was then transferred to a column and centrifuged for 1 min (16168 xg), the column was then washed with PE buffer and the DNA was eluted in 30µl of MQ H_2O.

2.3.3 Restriction digestions

All digests were performed according to enzyme manufacturer's instructions (Promega or New England Biosciences (NEB), using appropriate buffers at the recommended temperature (temp), for 2 hrs in a total vol between 20-40µl.

2.3.4 Ligation

The NEB Quick Ligation™ kit was used ligate digested PCR products into the appropriate vector according to the manufacturer's protocol. Linearized vector (50ng) was mixed with a three fold molar excess of insert in a final vol of 10µl. Then 10µl of 2 X Ligation buffer and 1µl of T4 DNA ligase was added to each sample and incubated for 5 min at room temp. The ligated vector was then transformed into chemically competent cells by heat shock as described in the following section.

2.3.5 Ligation using TOPO TA® and TOPO Blunt II® vectors

PCR product (2-4µl) was mixed with 0.5µl of TOPO® vector (0.5ng), 1µl of NaCl (1.2 µmol) and made up to a vol of 6µl with MQ H_2O. The solution was incubated for 30 min at room temp. The ligated plasmids were then transformed into Invitrogen TOP10 chemically competent cells by incubating 2µl of ligation mix with 25µl of competent cells for 30 min on ice. Cells were heat shocked for 1 min at 42^{o}C and then recovered in ice for 5 min. SOC (2% Tryptone, 0.5% yeast extract, 8.55mM NaCl, 20mM $MgSO_4$ $7H_20$, 20mM dextrose monohydrate) (250µl) was then added to the cells and the sample was shaken at 200 rpm at 37^{o}C for 1 hr, before being plated onto Kanamycin (50µg/ml) (TOPO® Blunt II vector) or Ampicillin LB agar plates (100µg/ml) (TOPO® TA vector). If the cloning was successful single colonies formed on the plates after they had been incubated at 37^{o}C overnight.

2.3.6 Colony PCR

Each single colony was mixed with 0.2mM dNTPs, 0.4µM of forward and reverse primer, 1 X REDTaq PCR reaction buffer and REDTaq® polymerase (0.06U/µl). PCR conditions were as follows: 94 ^{o}C for 2 min followed by 35 cycles of 94 ^{o}C for 30 s, 60^{o}C for 1 min, 72 ^{o}C for 2 min, and finally 72 ^{o}C for 3 min.

2.3.7 Extraction and purification of plasmids

Individual colonies were picked and grown in 2ml of 2 x YT (1.6% tryptone, 1% yeast extract, 85.5mM NaCl) and the appropriate antibiotic (Kanamycin 50µg/ml and Ampicillin 100µg/ml), shaking at 200 rpm overnight at 37^{o}C. Cultures were spun down and plasmids were extracted using the QIAprep® miniprep kit. Cells were resuspended in 250µl of solution 1 containing RNase A (1mg/ml), then 250µl of solution 2 was added, samples mixed gently and finally 350µl of solution 3 was added, the samples were mixed again and then centrifuged (16168 xg) for 10 min. The supernatant was then transferred to a QIAprep spin column and centrifuged for 1 min (16168 xg). The column was washed with PE buffer (1 min at 16168 xg) and then the plasmid DNA was eluted with 50µl of MQ H_2O. Plasmid concentrations were quantified on a Nano Drop®-1000 spectrophotometer at 260nm. An OD of 1 at 260nm equates to 50µg/ml of double stranded DNA.

2.4 DNA sequencing of PCR products and plasmids

DNA sequencing was performed by the Sanger Centre Small Sequencing Facility using the ABI PRISM big dye terminator cycle sequencing ready reaction kit according to the manufacturer's instructions, in an ABI 3730x1 automatic sequencer. 100ng of plasmid or 15-25ng of PCR product and 0.4pmols of primer were provided for each sequencing reaction.

2.5 Bioinformatics

DNA sequence was analyzed and manipulated using the Lasergene software package. Determining the genotype of adult fish and embryos by sequencing was performed by aligning sequences in GAP4 and identifying nucleotide changes. Orthologous alignments and phylogenetic trees were made in MegAlign using the Clustal W method. The Ensembl search engine was used to find zebrafish sequence, and NCBI and Ensembl were used to find orthologous sequences.

2.6 RNA extraction and RNA *in vitro* synthesis

2.6.1 RNA extraction from zebrafish embryos

Total RNA was isolated at various stages by homogenizing 30-50 dechorionated embryos in 500µl of TRIzol® reagent (Invitrogen). The homogenized tissue was then incubated for 5 min at 30^{o}C. Chloroform (0.1ml) was subsequently added to each sample and shaken vigorously for 15 s, then incubated for a further 3 min at 30^{o}C. The solution was centrifuged for 15 min (13362 xg) at 4^{o}C and the upper aqueous phase was removed to a fresh tube before the RNA precipitated by adding 0.25ml of isopropanol. Samples were then incubated for 10 min at 30^{o}C, centrifuged for 10 min (16168 xg) at 4^{o}C, the supernatant was removed and pellet washed once in 75% ethanol and centrifuged for 5 min (5220 xg). The pellet was then air dried for 5-10 min at room temp and the RNA finally dissolved in RNase free water by incubation for 10 min at 55^{o}C.

2.6.2 Capped RNA synthesis

DNA (2µg) was incubated with 1X transcription buffer (Promega), 9.26mM DTT (dithiothreitol), 0.926mM CAP structure, 60U of RNA Polymerase, 100U of RNAse inhibitor 0.926mM ATP, UTP, CTP and 92.6µM GTP, for 20 min at 37^{o}C. More GTP was then added to give a final GTP concentration of 0.74mM and the solution was incubated for a further hour. Roche DNAse I (30U) was added and the solution incubated for 45 min at 37^{o}C, then the RNA was purified in a BD Biosciences CHROMA SPIN™ column. The column was first prepared by centrifuging it for 5 min at 1258 xg, flow through was discarded and the column re-centrifuged again under the same conditions, prior to the addition of the RNA sample to the column. The RNA was eluted from the column by centrifugation at 1811 xg for 5 min. The RNA concentration was subsequently determined by measuring the absorbance at 260nm on the Nano Drop®-1000 spectrophotometer. An OD of 1 at 260nm equates to 40µg/ml of RNA.

2.6.3 Anti-sense RNA probe synthesis for whole-mount *in situ* hybridizations

Each RNA probe was synthesized from 0.4µg of linearized plasmid, 1 X Transcription buffer, 0.01M DTT, 1 X DIG (Digoxigenin) RNA labeling Mix (Roche), 52.5U of RNase Inhibitor and 20U of RNA Polymerase in a total vol of 20µl. The solution was incubated at 37^{o}C for 2 hrs, and then the volume was increased to 50µl with MQ H_2O. DNase I (20U) was also added to digest the plasmid template. The sample was incubated for a further 30 min at 37^{o}C before the RNA was recovered in a CHROMA SPIN™ column as outlined in the previous section. After measuring the RNA concentration on the Nano Drop®-1000 spectrophotometer the RNA was diluted to 10 X working concentration (10µg/ml) in RNA *in situ* hybridization (ISH) buffer. The probes generated and the plasmids they were derived from are shown in Table 2.2.

Table 2.2 *In situ* probes generated to detect the expression of the zebrafish *capz* subunits. The primers used to generate each insert are shown in the appendix, Table 3.

Probe	size	Vector	Enzyme used to linearize plasmid	Polymerase used to transcribe RNA
capzα1	599 bp	pCR®-blunt II-TOPO®	Spe I	T7
capzα2	480 bp	pCR®-blunt II-TOPO®	BamHI	T7
capzβ	596 bp	pCR®-blunt II-TOPO®	XhoI	Sp6

2.7 Whole-mount mRNA *in situ* hybridizations

Whole-mount mRNA ISHs were performed as described in (Thisse et al., 1993). Embryos at various stages were fixed in 4% PFA in PBS overnight at 4°C before being stored in 100% methanol at -20°C prior to use in whole-mount ISHs. Embryos stored in methanol were initially rehydrated by washing for 5 min in decreasing concentrations of methanol (75%, 50%, 25%) diluted in PBT (1 X PBS / 0.1% Tween 20). They were then washed four times in PBT for 5 min each. Embryos over 24 hpf were permeabilized with Proteinase K (10µg/ml) for 15 min. All embryos were re-fixed in 4% PFA for 20 min then washed in PBT five times for 5 min each. Embryos were subsequently pre-hybridized in 800µl of hybridization buffer (50% formamide, 5 X SSC, 0.1% Tween 20, 50µg/ml Heparin, 500 µg/ml Torula RNA) for 2 hrs at 68°C prior to hybridization with 200µl of RNA anti-sense probe diluted in hybridization buffer (final concentration 1µg/ml) overnight at 68°C. The next day the embryos were washed briefly in hybridization wash buffer (does not contain Heparin and Torula RNA) followed by 75% hybridization wash buffer (HWB)/2XSSC at 68°C for 15 min, 50% HWB /2XSSC at 68°C for 15 min, 25% HWB/2XSSC at 68°C for 15 min, 2XSSC at 68°C for 15 min, two washes in 0.2XSSC/50% formamide for 30 min each at 68°C. All subsequent washes were done at room temp starting with 75% 0.2XSSC/PBT for 10 min, 50% 0.2XSSC/PBT for 10 min, 25% 0.2XSSC/PBT for 10 min and finally PBT for 10 min. The embryos were then blocked in 2%

sheep serum / 2mg/ml BSA / PBT at room temp for several hours. The Anti-DIG alkaline phosphatase conjugated fab fragment antibody (1:2500, Roche) was then added and left overnight at 4°C. The following day embryos were washed with PBT at room temp six times for 15 min each, before being washed three times for 5 min each in staining buffer (100mM Tris-HCL pH 9.5, 50mM $MgCl_2$, 100mM NaCl, 0.1% Tween 20). Embryos were then placed in glass staining dishes and the colour developed with a 100 mg/ml NBT (Nitro blue tetrazolium) /50 mg/ml BCIP (5-Bromo-4-chloro-3-indolyl phosphate dipotassium salt) solution. The colour reaction was stopped by washing embryos in stop solution (1 XPBS pH 5.5, 2mM EDTA) for 3 min and re-fixing in 4% PFA for 20 min.

2.8 Extraction of genomic DNA from embryos and adult zebrafish

2.8.1 Extraction of DNA from 5 dpf embryos

Embryos were fixed overnight in 100% methanol at 4°C, then individual embryos were placed in PCR tubes and the excess methanol was evaporated by placing the tubes at 42°C for 5 min. 50µl of lysis buffer (10mM Tris-HCL pH8, 1mM EDTA, 0.3% Tween 20, 0.3% Igepal CA-630) was then added to each well and embryos were incubated for 10 min at 98 °C, prior to digestion with Proteinase K (1mg/ml) at 55°C overnight. The Proteinase K was inactivated by incubation at 98°C for 10 min. and the DNA was subsequently diluted (1: 25) before use in PCR reactions.

2.8.2 Extraction of DNA from adult zebrafish

Adult zebrafish were anaesthetized in 0.02% 3-amino benzoic acidethylester (tricaine), approximately 0.5cm of the tip of the tail fin was cut and the tissue was digested in 400µg/ml of Proteinase K/TE(10mM Tris-HCL pH8, 1mM EDTA) at 55°C overnight. The Proteinase K was

inactivated by incubation of the sample at 98^{o}C for 10 min. A 1 in 50 dilution of each DNA sample was used in subsequent PCR reactions.

2.9 Primer design and PCR

2.9.1 Primer design

All primers were created by Primer 3 (http://frodo.wi.mit.edu/cgi-bin/primer3/primer3_www.cgi) using sequence obtained from the Ensembl zebrafish genome browser (Zv4, Zv5 and Zv6) (Hubbard et al., 2007). Indel primers were generated from indel regions annotated onto the Ensembl Zv5 DAS (distributed annotation system) track. Indels are regions of insertions or deletions in the genome that are polymorphic between two individual Tübingen zebrafish.

2.9.2 Genomic DNA PCR for genotyping of adult fish by sequencing

Nested PCR was performed to amplify the region containing the mutation for sequencing. The second set of inside primers were extended with M13F and M13R sequence for sequencing purposes. Each PCR was performed in a total vol of 10µl and contained 5µl of genomic DNA (diluted 1 in 50), 0.6µM forward and reverse primers, 1 X genotyping PCR buffer (10mM Tris-HCL pH8.5, 50mM KCL, 2mM $MgCl_2$, 0.01% Tween 20), 0.6mM dNTPS, 0.4U Taq polymerase. The PCR conditions were as follows. 94^{o}C for 3 min, 35 cycles of 94^{o}C for 45 s, 64^{o}C for 45 s, 72^{o}C for 90 s and finally 72^{o}C for 10 min. The second PCR had the same conditions as the first PCR, however, the genomic DNA was replaced with 180nl of the first PCR product (transferred by a Matrix QRep 96 pin replicator).

Prior to sequencing excess nucleotides were removed from the PCR product by addition of EXOSAP (0.5U of Shrimp alkaline phosphatase, 1U of Exonuclease I, and 1 X SAP buffer (20mM Tris-HCL-pH8, 10mM $MgCl_2$), samples were incubated at 37^{o}C for 1 hr followed by 80^{o}C for 15 min. The amount of PCR product was quantified using the Invitrogen Quant iT™ PicoGreen® dsDNA kit. PicoGreen® reagent (200nl) and TE buffer (10mM Tris-HCL pH7.5, 1mM EDTA) (100µl) was added to PCR product (2µl) and provided DNA standards, and the luminescence was detected in a fluorescence microplate reader (Perkin Elmer Fusion™) at 480nm. The concentration of DNA was calculated from the graph of the standards.

2.9.3 SSLP PCR from embryos

Simple sequence length polymorphisms (SSLPs) were detected by performing the PCR in a total vol of 15µl with 1µl of genomic 5 days post fertilization (dpf) embryonic DNA, 1 X PCR buffer (2mM $MgCl_2$, 13.6mM Tris-HCL, 68mM KCL, 0.00126% gelatin, 136.36µg/ml of BSA, 200µM of dNTPs), 0.3 µM of forward and reverse primers, and 0.4U of Taq polymerase. PCR conditions were as follows: 94^{o}C for 2 min, 35 cycles of 94^{o}C for 30 s, 60^{o}C for 30 s, 73^{o}C for 30 s and finally 73^{o}C for 5min. PCR products were run on a 2.5-3% agarose gel (with 0.75 µg/ml of ethidium bromide) in a Maxi-Plus horizontal electrophoresis unit (Sigma-Aldrich) at 200-250 V for 90 min, and visualized on a BIO RAD UV imager.

2.9.4 RT-PCR

cDNA was synthesized from 2µg of total RNA using the SuperScript™First-Strand Synthesis System (Invitrogen). RNA was mixed with random primers (0.25µg/µl) and incubated for 10 min at 70^{o}C. Then 1 X First Strand buffer, 0.5mM DTT and 10mM dNTPs were added to the RNA and incubated for 2 min at 42^{o}C, prior to the addition of the SuperScript reverse

transcriptase (10U/µl). The sample was subsequently incubated at 42°C for 1 hr, 70°C for 15 min then placed on ice for 10 min. The resulting cDNA was diluted 1 in 10 and 2 µl was used in a 20µl KOD polymerase PCR.

2.9.5 KOD Polymerase PCR

Blunt ended high fidelity PCR products were generated using Novagen® KOD Hot Start polymerase according to the manufacturer's protocol. The PCR was performed in a total vol of 20µl using 2µl of cDNA diluted 1 in 10, 1 X PCR buffer, 1mM $MgSO_4$, 2mM of dNTPs, 2µM of forward and reverse primer and 0.75U of KOD Hot Start polymerase. PCR conditions were as follows: 94°C for 2 min, 35 cycles of 94°C for 15 s, 60°C for 1 min, 72°C for 90 s and finally 72°C for 10 min. PCR products were run on a 1-2% agarose gel (with 0.75 µg/ml of ethidium bromide) and visualized using the BioRad UV imager.

2.10 Construction of the capZα1-GFP expression plasmid

The capZ α1-GFP pCS2+ construct was designed with GFP attached to the C-terminus of capZα1 by a 4 amino acid glycine linker (see appendix, Fig.1). Restriction sites and the sequence of the glycine linker were incorporated into the primers to facilitate the formation of the fusion construct and insertion into pCS2+. The open reading frame of capZα1 was amplified from cDNA (derived from 24 hpf wild type embryos) by KOD polymerase PCR using the CapZORFF and GFPR1 primers (Table 2.3). The GFP open reading frame was also amplified by KOD polymerase PCR (from an eGFP-pCS2+ plasmid) using GFPF2 and GFPR2 primers (Table 2.3). The capZα1-GFP fusion product was subsequently generated by an additional KOD polymerase PCR using the individually amplified capZα1 and GFP products (3ng) and capZORFF and GFPR2 primers. The fusion product was digested with BamHI and Xho I prior to ligation with

linearised pCS2+ (linearised with the same enzymes). The sequence of each clone was checked before RNA injection into the embryo.

Table 2.3. Table of primers used in generation of the capZ α1-GFP fusion construct. The BamHI and XhoI restriction sites are incorporated into the capZORFF and GFPR2 primers respectively. The sequence for the glycine linker is incorporated into the GFPR1 primer.

Primer name	Sequence 5′-3′
capZORFF	TCGAGTGGATCCATGACCGACTTTGAGGAGCCG
GFPR1	CTCCTCGCCCTTGCTCACGCCACCTCCGCCAGCGTTTTGCATCTCTTTACC
GFPF2	GTGAGCAAGGGCGAGGAGCTGTTCACCG
GFPR2	CCAGGCCTCGAGTTACTTGTACAGCTCGTCCAT

2.11 Immunohistochemistry

2.11.1 Phalloidin staining

Embryos at 1, 2, 3 and 5 dpf were fixed in 4% paraformaldehyde (PFA) for 2 hrs, permeabilized in 2% TritonX-100/1X PBS for 2 hrs, then incubated in Alexa Fluor® 488 phalloidin (Molecular Probes, 2.5 U/ml) overnight at 4^{o}C. The following day the embryos were washed three times for 10 min each in PBST (1 X PBS, 0.2% BSA, 0.1% TritonX-100), re-fixed for 20 min in PFA and washed again in PBST three times for 10 min each, before being mounted for visualization under the confocal microscope.

2.11.2 α-Actinin antibody staining

Embryos at various stages were fixed in 4% PFA for 2 hrs, washed twice in PBST and subsequently re-fixed at -20^{o}C in acetone for 20 min. They were then permeabilized in Proteinase K (5µg/ml), blocked in PBDT (1 X PBS, 1% BSA, 1% DMSO, 0.5% TritonX-100) and incubated with the primary antibody, mouse monoclonal anti-alpha-actinin 1:200 (Sigma A7811)

overnight at 4°C. After washing in PBDT several times the embryos were incubated in Fluorescein Isothiocyanate (FITC) conjugated, donkey anti-mouse antibody (1:400) overnight at 4°C. Embryos were washed in PBST and the staining pattern was subsequently observed by confocal microscopy.

2.11.3 CapZα1 antibody staining

Embryos were fixed in 100% methanol overnight at -20°C, they were then rehydrated into PBT with 5 min washes in 75% methanol/ PBST, 50% methanol /PBST, 25% methanol /PBST and finally 100%PBST for 30 min. Embryos were then permeabilized for 8 min in Proteinase K (10μg/ml). After three x 5 min washes in PBST they were then blocked for 2 hrs in 10% goat serum / PBST. The chicken CapZα1 primary antibody (1:200, Abcam) was left on overnight at 4°C. On the second day embryos were washed with PBST for 6 x 15 min, and blocked in the 10% goat serum/PBST for an hour before the secondary antibody was left on overnight (donkey anti-chicken conjugated to FITC, 1:200). On the third day the embryos were washed again with three 10 min washes in PBST, before being mounted onto slides and visualized by confocal microscopy.

2.11.4 Desmin antibody staining

Embryos were fixed on day 5 in 4%PFA for 1 hr at room temp, they were then washed in 0.5% Triton X-100/PBS three times for 5 min each. The primary antibody (1:100 dilution of rabbit anti-desmin antibody, Sigma D8281) was left overnight at 4°C. The following day the embryos were washed again in 0.5% Triton X-100/PBS three times for 5 min each before being incubated in the secondary antibody (1:200, anti-rabbit conjugated to FITC) for 1 hr at room

temp. The embryos were then washed in PBST, before they were mounted on slides and the immunostaining observed with the confocal microscope.

2.12 Image capture of live and fixed embryos

Images of live embryos and whole mount *in situ* hybridized specimens were taken with a Leica MZ16 FA dissecting scope or a Zeiss AXIO imager M1 compound microscope using a Zeiss Axiocam digital camera. The live embryos were initially anaesthetized in 0.02% tricaine and mounted in 2% methyl cellulose. The fixed and stained embryos were washed in increasing concentrations of glycerol (25%, 50% and 75%) before images were taken of embryos mounted in 100% glycerol. Confocal images of immunostained skeletal muscle were taken using a BioRad Radiance 2100 system with a Nikon E800 Eclipse microscope. The head and yolk of each embryo was removed before being mounted in VECTA SHIELD®.

2.13 Protein extraction from embryos

Chorions were removed from embryos of various stages, before embryos were added to lysis buffer (50mM Tris-HCL pH7.5, 150mM NaCl, 1mM EDTA, 1% Triton-X 100, 0.1% SDS, 2.5% Igepal CA-630) and 1 X Complete protease inhibitor (Roche). The embryos were then macerated in an eppendorf with a pestle. The homogenized tissues were centrifuged (16168 xg) for 10 min at 4^{o}C and the supernatant was recovered and snap frozen on dry ice prior to storage at -80^{o}C.

2.14 Western blotting

Each protein sample was mixed with 1 X NuPAGE®LDS sample buffer (Invitrogen) and 50mM DTT before being heated to 70^{o}C for 10 min, loaded onto a NuPAGE® Novex 4-12% Bis-Tris gel in 1 X MOPS SDS running buffer and run at 200 V for 1 hr. The protein on the gel was then transferred to a PVDF (polyvinylidene difluoride) membrane (Hybond™-P, Amersham Biosciences) in transfer buffer (20% methanol, 0.192M glycine, 0.025M Trizma base pH 8.3), using the Invitrogen Xcell II™ Blot Module for 90 min at 30 V. The membrane was then blocked in blocking buffer (5% Marvel skim milk in 0.05%Tween/PBS) for 2-3 hrs at room temp. The primary antibody (mouse IgG, anti-human CapZα, BD biosciences) was diluted (1:200) in antibody blocking buffer (2% Marvel in 0.05% Tween/PBS) and left to incubate with the membrane overnight at 4^{o}C. The membrane was then washed three times for 10 min with 0.05% Tween/PBS prior to incubation with the secondary antibody (1:2000 dilution of goat anti-mouse, IgG (H + L) HRP conjugated, diluted in blocking buffer) for 1 hr at room temp. The membrane was washed again in 0.05% Tween/PBS three times for 10 min. The secondary antibody was subsequently detected by chemiluminescence using the Amersham ECL plus Western Blot Detection System according to the manufacturer's protocol. Solution A (8 ml) was mixed with 200µl of Solution B. This mixture was then poured onto the membrane and incubated in the dark for 5 min before the membrane was transferred to a cassette, exposed to film (Amersham Hyperfilm™ ECL) and the image on the film detected on the developer (Compact X4, Xograph Imaging systems).

2.15 Transmission electron microscopy

Transmission electron microscopy (TEM) was performed by David Goulding. Embryos were dissected under fix at 4°C, separating the tails by transverse section just before the yolk sac. Primary fixation with 2.5% gluteraldehyde and 2% PFA in PBS (0.01M at pH7.2) was continued for a total of 2 hrs and followed by three rinses in PBS and two rinses in sodium cacodylate buffer (0.1M at pH 7.42) for 5 minutes each, all at 4°C. All further steps were conducted at room temp. Secondary fixation in cacodylate buffered 1% osmium tetroxide for 1 hr was followed by a brief rinse in the same buffer, immersion in buffered 1% tannic acid for 30 min and 1% aqueous sodium sulphate for 10 min. Specimens were dehydrated in an increasing series of alcohols and propylene oxide (staining *en bloc* at the 20% ethanol stage with 2% uranyl acetate for 20 min), infiltrated with Epon overnight (TAAB Laboratories) and then cured at 60°C for 24 hrs. Longitudinal 70nm ultrathin sections along the embryo tail were cut on a Leica EM UC6 ultramicrotome, mounted onto 200 mesh copper support grids and contrasted with uranyl acetate and lead citrate. Imaging was performed on a Tecnai Spirit Biotwin TEM at 120kV using a Tietz F4.15 CCD camera.

Chapter 3

Positional cloning of *schnecke*

Chapter 3: Positional cloning of *schnecke*

3.1 Summary

In this chapter I have described the positional cloning of the muscle mutant, *schnecke* (*sne*). Using simple sequence length polymorphism (SSLP) and insertion-deletion (indel) markers the location of the *sne* mutant locus was initially defined to a 1 centimorgan (cM) interval on chromosome 8. Subsequent sequencing of one of the candidate genes within this region revealed a point mutation at a splice site of *capzα1*. Unexpectedly, the splice site mutation induces the transcription of three mis-spliced transcripts in the *sne* mutant.

3.2 Introduction

3.2.1 ENU mutagenesis screens

Forward mutagenesis screens using the mutagen *N*-ethyl-*N*-nitrosurea (ENU) were first performed in *Drosophila* (Nusslein-Volhard, 1994; Nusslein-Volhard and Wieschaus, 1980) and many genes involved in embryonic patterning were successfully identified such as *wingless* (*wg*), *decapentaplegic* (*dpp*) and *hedgehog* (*hh*). In vertebrates, zebrafish have proved to be an ideal model organism for use in mutagenesis screens to identify genes important in development. Zebrafish have a short generation time (2-4 months) and hundreds of progeny are produced from each mating, therefore many mutant phenotypes can be scored and mutant lines can be established quickly. Additionally, very early developmental phenotypes can be detected as the embryos are transparent and develop externally from the first cell division.

In the mid 1990s two landmark zebrafish ENU mutagenesis screens were performed and almost 2000 mutations affecting approximately 600 genes were identified (Driever et al., 1996; Haffter et al., 1996). Over the past decade the study of these developmental mutants has dramatically assisted in extending our knowledge of vertebrate development, however, many mutants still remain uncharacterized. The *sne* mutant is one of more than 50 muscle mutants generated in the Tübingen screen (Granato et al., 1996; Haffter et al., 1996). In this screen single base mutations were induced into the premeiotic germ cells of Tübingen male zebrafish by incubating the male in a solution of ENU for 1 hour. The treatment was repeated up to six times at weekly intervals. The male was then outcrossed with a Tübingen longfin (TL) wild type female zebrafish, resulting in heterozygote F1 progeny. Sibling F1s were then incrossed in single pair matings, so that half of the subsequent F2 progeny were heterozygous for a specific mutation carried by either of the F1 parents. The F2 progeny were then intercrossed and the embryos analyzed for a phenotype (Fig. 3.1). If both F2 parents were heterozygous for a specific recessive mutation then a quarter of their progeny would have a mutant phenotype that could be scored. In this type of screen only mutations in genes that have unique and partially non-redundant functions and that produce a scorable phenotype will be detected. Once a mutant line has been established the mutation is identified by positional cloning.

3.2.2 Positional cloning

Positional cloning is currently the most common method used to identify mutated loci in ENU generated mutants and can be divided into three main steps. Firstly, the location of the mutation is mapped to a genomic interval on a particular chromosome via linkage analysis. Secondly, candidate genes within the chromosomal region are selected, and finally the mutation within a candidate gene is identified by sequencing.

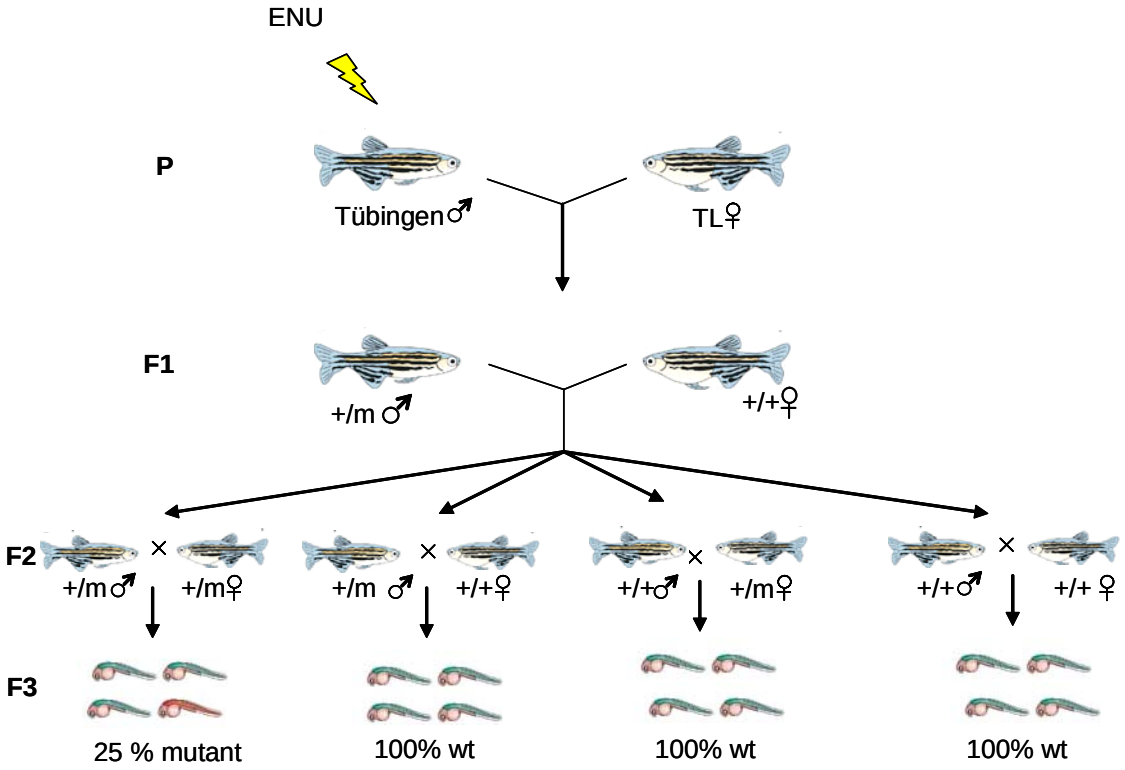

Fig. 3.1. Generation of a zebrafish ENU mutant library. The ENU mutagenized founder male is outcrossed to a wild type female of a different strain (P). The subsequent progeny (F1) are intercrossed in single pair matings and produce an F2 generation where half the offspring are heterozygous for a particular mutation. In a quarter of the F2 intercrosses both the male and female will be heterozygotes, therefore 25% of their progeny will be homozygous for a mutation which can be phenotyped. This figure was adapted from Lieschke and Currie, 2007.

A number of PCR based mapping technologies such as RAPDs (random amplified polymorphic DNAs), AFLPS (amplified fragment length polymorphisms) and SSLPs have been utilized to create genetic maps that enable the locus of a mutation to be assigned to a particular region on a chromosome by linkage (Johnson et al., 1994; Knapik et al., 1998; Postlethwait et al., 1994; Vos et al., 1995). The premise behind all these different mapping techniques is to detect polymorphisms between strains that can be linked to the mutant locus. SSLP mapping is by far the simplest positional cloning technique compared to RAPD or AFLP mapping. The amplification of SSLP markers is generally consistent, and as fewer amplified products are generated it is much easier to score the linkage of a particular marker. Moreover, as the SSLP markers tend to be co-dominant, heterozygous and homozygous genotypes can be distinguished, thus diploid embryos can be used for mapping. For these reasons, SSLP markers are now routinely used to identify mutations in ENU mutagenized zebrafish.

SSLPs (also known as microsatellites) were originally identified in the zebrafish genome by cloning and sequencing of hundreds of CA repeat regions from genomic DNA (Goff et al., 1992; Knapik et al., 1996; Knapik et al., 1998). These regions are highly polymorphic between strains. Therefore, PCR amplification of the microsatellites enables linkage to be established between a marker and the mutant locus. Linked SSLP markers that are closer to the mutation will have a lower recombination rate than markers further away from the mutant locus. By determining the recombination frequency of each linked SSLP, the distance (in cM) of the marker from the mutation can be estimated (see Fig 3.2 as an example). The recombination frequency at a particular SSLP marker is determined by identifying the recombinations that have occurred at this locus in many individual mutant embryos. The distance in cM is calculated by dividing the number of recombinations observed by the total number of meioses (total number of mutant embryos scored x 2) then multiplying this ratio by a 100. The accuracy of this distance

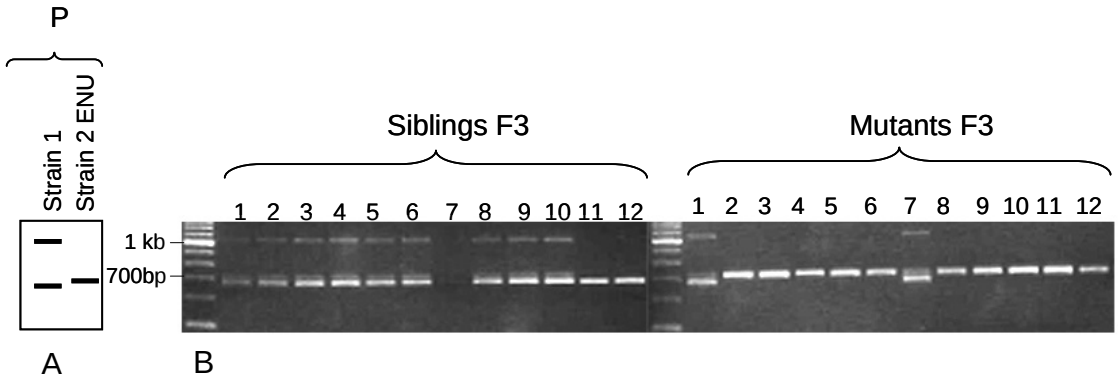

Fig. 3.2. Example of how the recombination frequency of a linked SSLP polymorphic marker is determined by PCR. A) The SSLP marker produces 3 products at 680bp, 710bp, and 1050bp. The 680bp and 1050bp product are linked to parental strain 1 and the 710bp product is specific for strain 2 (which has been mutagenized). B) PCR products generated from individual F3 sibling and mutant embryos using the linked SSLP marker. Most of the F3 siblings amplified all 3 products (1-6 and 8-10) or only the 680bp product (11 and 12) (PCR 7 failed). In the mutant embryos the 710bp product (specific to strain 2) was amplified in most individuals. However, due to recombinations in two of the mutants (1 and 7), products from the unmutagenized strain (strain 1) were also amplified. The number of mutants which have a banding pattern corresponding to the unmutagenized strain can therefore be used to determine the recombination frequency and subsequently the distance of the marker from the mutant locus.

measurement improves as greater numbers of mutant embryos are scored for recombination events.

There are several methods available to pinpoint the affected gene once the genomic interval that contains the mutation has been established. Usually the candidate gene approach is taken, whereby likely candidate genes within the defined region are selected and sequenced. Antisense morpholino oligonucleotides (MOs) can also be designed to knockdown the candidate gene, to determine whether the mutant phenotype can be copied. Unfortunately, this approach is limited by the number of genes that have been fully sequenced in the region and the size of the interval.

3.3 Positional cloning of *sne*

The mutation in the *sne* mutant was originally roughly mapped to linkage group 8 using a subset of SSLP markers derived from the Massachusetts General Hospital (MGH) marker map (Knapik et al., 1998; Shimoda et al., 1999) http://zebrafish.mgh.harvard.edu/). 384 SSLP markers from the G4 and H2 marker set (Geisler 2007) were tested for linkage, and the *sne* locus was mapped to a 10.7 cM region between markers Z21483 and Z21115 on chromosome 8 by Dr. E. Busch-Nentwich (Fig. 3.3). Recently a mutant mapping screen was published that also roughly mapped the *sne* locus between SSLP markers Z14312 and Z21115 (Geisler et al., 2007).

The region containing the *sne* locus was subsequently refined by initially testing whether 24 of the markers within this region were polymorphic by PCR, on pooled mutant and sibling genomic DNA. Seven markers were found to be polymorphic (Fig. 3.3) and the recombination frequency was determined at these loci by scoring individual mutant embryos. A discrepancy between the position of three of the markers (Z21315, Z10456 and Z60737) on the MGH map

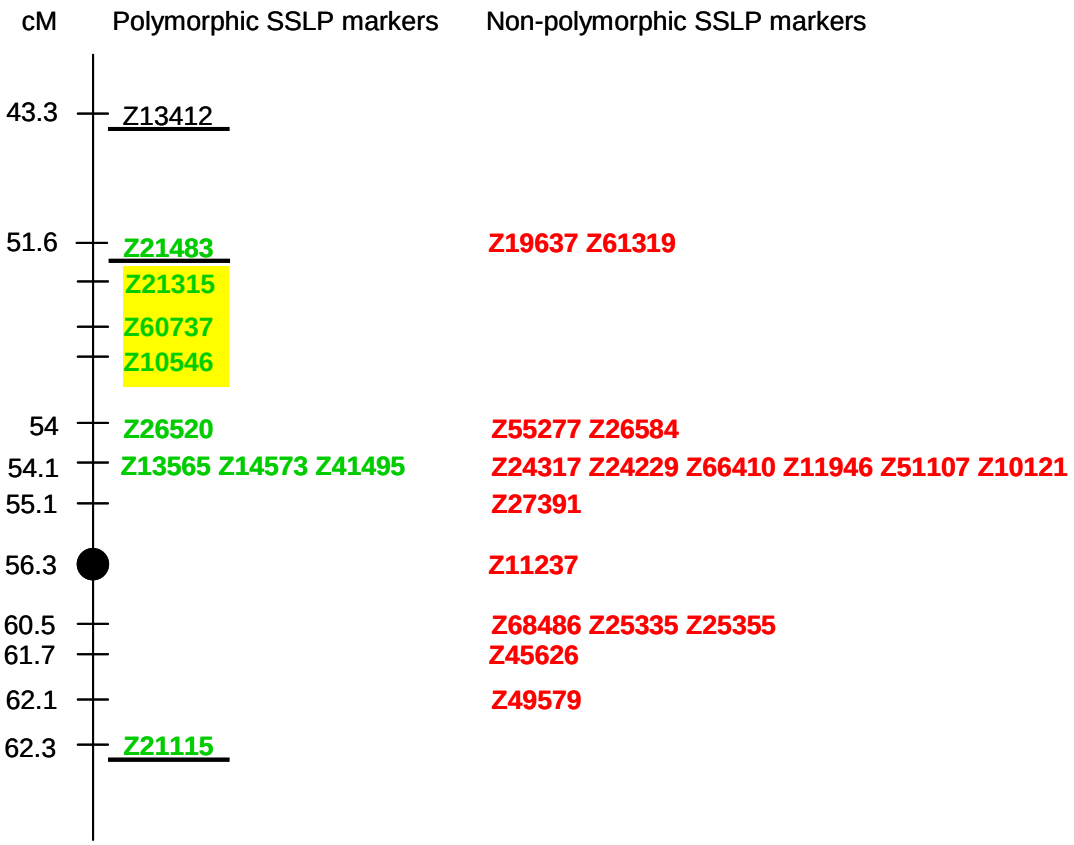

Fig. 3.3. SSLP marker map of chromosome 8 between 43.3 and 62.3cM. Markers identified as non-polymorphic are in red, polymorphic markers are in green and were tested on individual mutant embryos to determine recombination frequencies. The linked markers determined by E. Busch-Nentwich and Geisler et al., 2007 are underlined. Markers that were in a position on the MGH map that were inconsistent with the recombination frequencies I obtained have been re-positioned and are highlighted in yellow. On the published MGH map Z21315 and Z10456 are located at 54.1cM and Z60737 is at 56.5cM. The black dot indicates the centromeric region of the chromosome.

compared to the recombination frequencies I calculated was observed, therefore they have been repositioned on the map shown in Fig. 3.3.

Due to the relatively low number of polymorphic SSLP markers in the region containing the *sne* mutation, indels were also used as markers to more accurately pinpoint the *sne* mutant locus. Indels are polymorphic insertions or deletions that were identified from the initial sequencing of the zebrafish genome, when DNA from ~ 1000 individual Tübingen zebrafish were pooled and used as the template for whole genome shotgun sequencing. They are usually found in repeat regions, are greater than 4bp and have been mapped to the zebrafish genome assembly (shown on a DAS (distributed annotation system) track in Zv5).

Prior to selection of the indel markers, the existing SSLP markers that encompassed the *sne* locus had to be mapped directly to the zebrafish Ensembl genome assembly. Unfortunately, when this was performed the assembly (Zv5) was still rudimentary. Many contigs were not joined and a number of markers mapped to more than one chromosome, reducing the efficiency of finding closely linked markers. Nevertheless, the markers that were identified ultimately proved to be useful in determining the site of the mutation.

To ensure that any polymorphic indel size differences could be detected on agarose gels, primers were designed to amplify indels that were either repetitive sequences or were greater than 20bp in length (see appendix, Table 1). Out of 79 indel markers identified, seven were found to be polymorphic between the Tübingen and TL strains (Fig. 3.4). Six indel markers were used to assist in the mapping process along with seven SSLP markers. PCR amplification of these markers was performed on a maximum of 741 mutant embryos and the recombination frequency

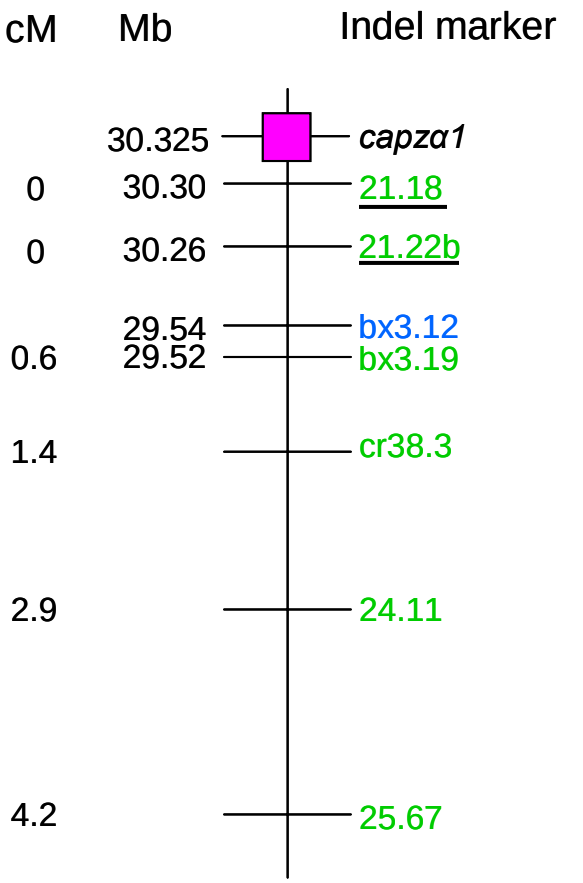

Fig. 3.4. Map of indel markers on chromosome 8. Indel markers were mapped according to their location established from the Ensembl genome assembly (Zv6). All markers except bx3.12 (labelled in blue) were tested on individual mutant embryos. No recombination events were identified at markers 21.18 and 21.22b (underlined). I was unable to determine the location of cr38.3, 24.11 and 25.67 due to discrepancies between the assembly and my analysis.

determined (Table 3.1). No recombination events were detected at indel markers 21.22b and 21.18 in all the mutant embryos tested. The two nearest SSLP markers that flanked the indel markers (Z13565 and Z26520) spanned a region of 1 cM (Z14573 was omitted as not all mutant embryos had been tested for recombination events at this marker). Mapping of Z13565 and Z26520 onto the Ensembl genome assembly revealed that this 1 cM interval corresponded to 0.7Mb.

Having mapped the *sne* mutation to as small an interval as possible, a candidate gene approach was taken to identify which of the three genes present in this region carried the causative mutation: *wnt2bb*, *capzα1*, and a hypothetical gene (orthologous to *cortactin-binding protein 2 N-terminal-like protein* (*cttnbp2*) in mouse and human) (Fig. 3.5). The most likely candidate for the *sne* locus appeared to be *capzα1*. This gene encodes an important muscle component and both the closest indel markers (21.22b and 21.18) were positioned within the intronic region. For this reason, *capzα1* was sequenced first.

3.4 The sne locus is *capzα1*

The coding region of *capzα1* was initially cloned from RT-PCR products derived from pooled mutant and sibling cDNA. The cDNA was amplified by two overlapping sets of primers and covered the 5′ and 3′ regions of the gene (Fig. 3.6, see appendix, Table 2 for primer sequence). Surprisingly, from *sne* mutant pooled cDNA, two PCR products were amplified from the 3′ region of *capzα1*. This indicated that a mutation in this region may be producing aberrant splice transcripts (Fig. 3.7). The PCR was repeated using cDNA from individual wild-type sibling and mutant 5 day old embryos (Fig. 3.8A). Three PCR products were amplified from

Table 3.1. Table of polymorphic SSLP and indel markers used to define the region of the *sne* locus. The distance of each marker locus from the mutation locus was calculated by dividing the number of recombinations that have occurred by the number of meioses and the multiplying this fraction by100.

Markers	*Z21115*	*25.67*	*24.11*	*cr38.3*	*bx3.19*	*Z13565*	*Z14573*	*21.22b*	*21.18*	*Z26520*	*Z10546*	*Z60737*	*Z21315*
Mutant embryos with recombinant markers	47	12	32	3	6	7	0	0	0	7	3	7	11
Total number of mutant fish tested	185	142	545	104	474	738	193	687	715	741	285	473	283
Distance from mutation in cM	12.7	4.2	2.9	1.4	0.6	0.5	0.0	0.0	0.0	0.5	0.5	0.7	1.9

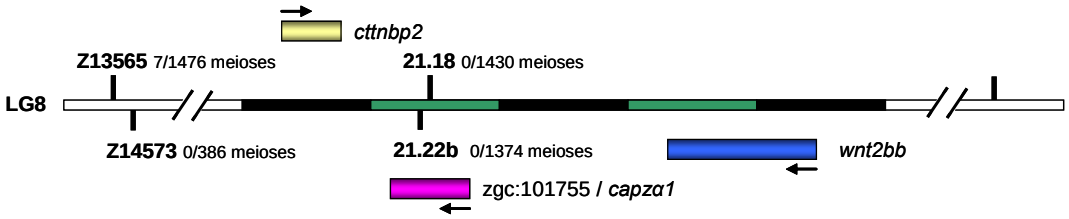

Fig. 3.5. Schematic diagram of the genomic region on chromosome 8 containing the three candidate genes for the *sne* locus. Each green or black bar represents 0.02Mb. Arrows indicate the orientation of the genes with respect to transcription.

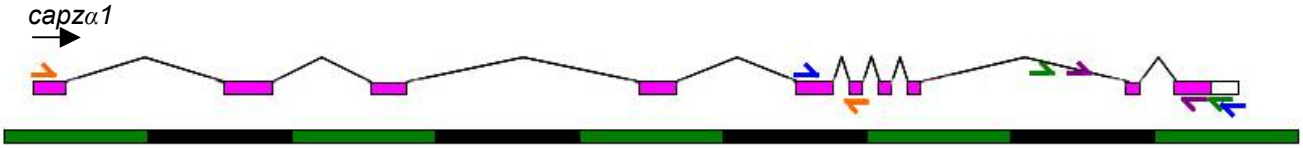

Fig. 3.6. Coding region of *capzα1* exons illustrating the position of the primer binding sites used to amplify this gene. Primers that amplified *capzα1* cDNA are represented by orange arrows (primer pair 2) and blue arrows (primer pair 4). Nested primers that amplified genomic DNA for sequencing are represented in green (fact3) and purple (fact2).The 3′ untranslated region is illustrated in white. Each green or black bar represents 2kb.

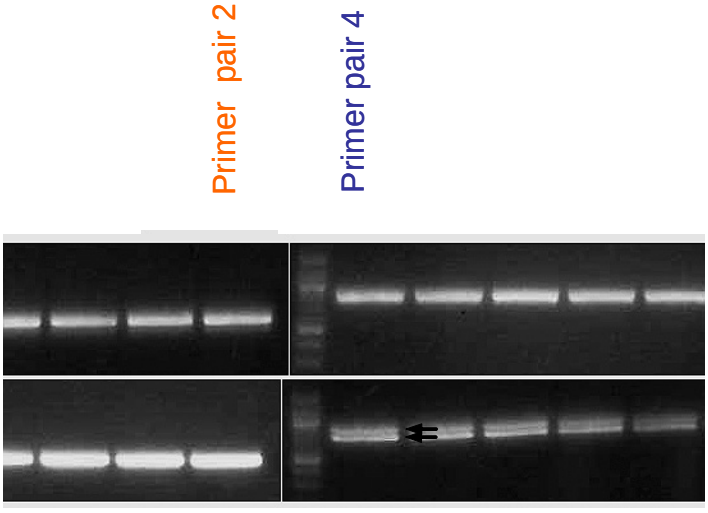

Fig. 3.7. Gel of RT-PCR products from pooled *sne* sibling and mutant cDNA, using primers that amplified the 5′ and 3′ prime regions of *capzα1*. Arrows indicate the two PCR products amplified from *sne* mutant cDNA. See Fig. 3.6 for position of the primers and the appendix, Table 2 for primer sequence.

mutant embryos, but not wild-type siblings. All three products were cloned into TOPO blunt II® vectors and sequenced. This revealed that three aberrant splice transcripts were expressed in the mutant (Fig 3.8B). In the 750bp product exon 9 had been skipped. In the 900bp and 950bp product, 24bp and 46bp of intron 9 (respectively) were retained in the mRNA. *In silico* translation of these products indicated that the 950bp product would produce a frame shift, which would result in a premature stop codon 19 amino acids into the translation of the intronic region and the first part of exon 10. Translation of the 750bp and 900bp product would result in a 21 amino acid deletion (loss of exon 9) and an 8 amino acid insertion from residue 240 (between exon 9 and 10) respectively (see appendix, Fig. 2. for the predicted protein sequence of all aberrant splice transcripts). Therefore, both these aberrant splice transcripts would still produce in-frame protein products and exon 10 would be translated.

The aberrant splice transcripts detected in the mutant indicated that there was a point mutation at the donor splice site of exon 9. This was confirmed by sequencing of the exon/intron boundary using nested primers that flanked exon 9 and 10 (Fig. 3.6). A single G-A base pair change was found at the exon 9 donor splice site (Fig 3.8C). RNA splicing depends on the recognition of pairs of splice junctions that flank each intron. The generic consensus at the 5′ donor splice site is GU, and at the 3′ acceptor splice site is AG. As the mutation in *capzα1* disrupts the 5′ donor splice site consensus sequence, it is highly likely that the splice site becomes unrecognizable to the splicing machinery, thus alternative donor splice sites are used. Indeed, two potential generic donor splice sites were detected 23bp and 47bp into intron 9 and correlate with the aberrant splice transcripts detected in the mutant (Fig. 3.9).

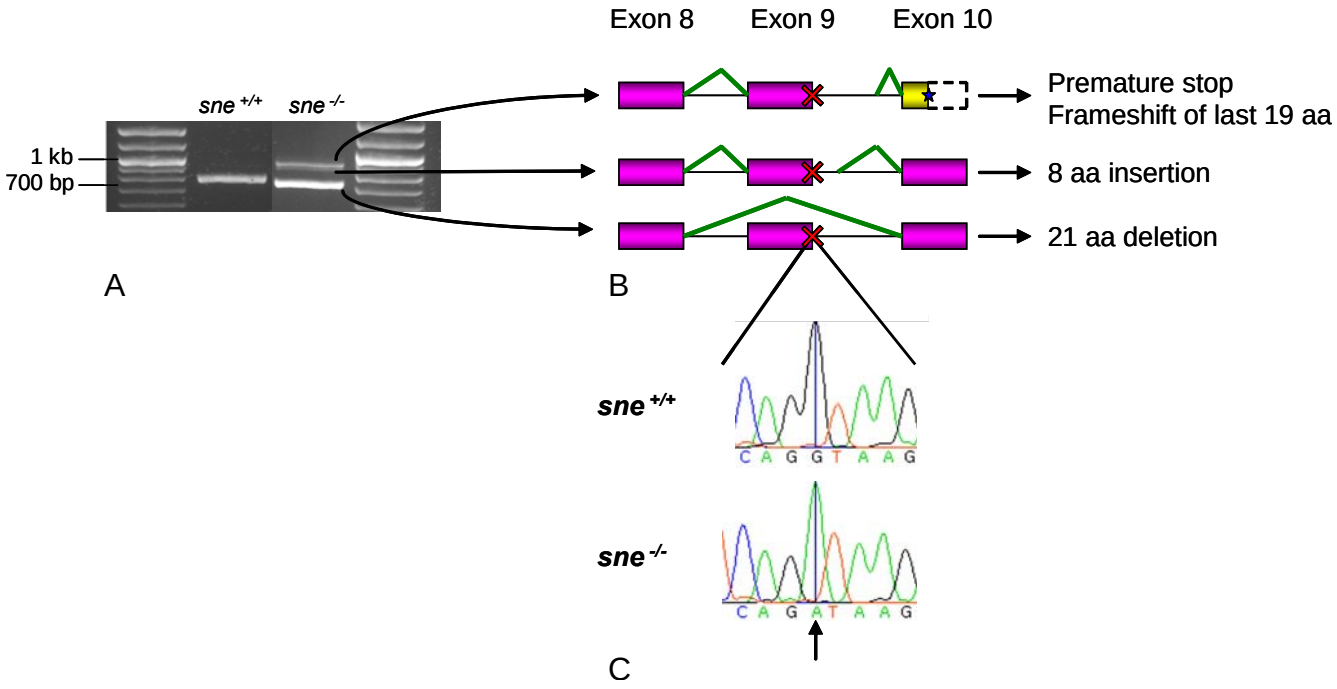

Fig. 3.8. Identification of the mutation in *capzα1* of the *sne* mutant. A) Gel of RT-PCR products from *capzα1* cDNA of individual *sne* mutant and wild-type sibling embryos. The three RT-PCR products that were amplified from *sne* mutant cDNA were cloned into TOPO Blunt II® vectors and sequenced. B) A schematic diagram illustrating the exons and introns at the 3′ end of *capzα1* that are aberrantly spliced in the *sne* mutant. The red crosses indicate the site of the mutation, the partially filled yellow exon indicates that it was translated out of frame and the blue star indicates a stop codon. C) Sequence traces of the exon 9 donor splice site revealed the base change in the mutant from a G to A (arrow).

Fig. 3.9. Position of alternative donor splice sites in intron 9 of *capzα1*. Two alternative donor splice sites were identified (underlined in blue) at positions that correspond to the aberrant splice transcripts expressed in the *sne* mutant (dashed line represents intronic sequences that are transcribed in the *sne* mutant). The normal splice site is highlighted in green and matches the vertebrate donor splice site consensus (5′-AGGUAAGU-3′). In both alternative splice sites the general donor splice site consensus is present (GU).

3.5 Discussion

The ENU muscle motility mutant *sne* was positionally cloned to a 1cM region using SSLP and indel markers. SSLPs are advantageous in mapping because they are co-dominant markers i.e. both alleles are equally detectable in heterozygotes, they are also abundant and widely distributed throughout the genome. Moreover, they can be assayed relatively easily by PCR and, coupled with the generation of the MGH SSLP marker map, it is possible to perform high throughput positional cloning and roughly map mutants derived from ENU screens with relatively ease (Geisler et al., 2007). The efficiency of SSLP mapping is limited, however, by a number of factors. Firstly, SSLP markers have to be polymorphic between the two strains used in the ENU screen. There is still a significant amount of allele sharing between strains (Knapik et al., 1998) so not all SSLP markers will be polymorphic. Secondly, two closely positioned markers that flank the mutation locus are ideally required. Thirdly, these markers need to be accurately positioned onto the genetic map i.e. the zebrafish genome assembly.

Within the large region that the *sne* locus was previously mapped to on linkage group 8 (51.6-62.3cM), nine SSLP markers were polymorphic (37.5%). Out of the nine linked markers, six were genetically mapped to the genome assembly and correctly corresponded to the positions that I had obtained from the recombination data. As it was very difficult to accurately define the region containing the mutation using only SSLP markers, indel markers were also selected to assist in postional cloning of the *sne* mutant. Although less than 10% of the indel markers were polymorphic, they were crucial to placing the SSLP markers on to the genome assembly and in determining the likely candidate gene to contain the mutation. The low polymorphic differences of the indel markers I tested may be due to the fact that the indels in Ensembl were derived from

differences between individual Tübingen fish, which is one of the strains that was used to generate the *sne* mutant.

A mutation at the exon 9 donor splice site of the primary candidate gene, *capzα1*, was identified by sequencing. RT-PCR of *capzα1* cDNA products from *sne* mutants indicated that the mutation induces mis-splicing of the *capzα1* transcript. The aberrant splicing produces three *capzα1* transcripts: 1) exon 9 is completely spliced out of the transcript, 2) 24bp of intron 9 is included in the transcript, 3) 46bp of intron 9 is included in the transcript. This finding indicates that the mutation disrupts the exon 9 donor splice site causing the use of alternative donor splice sites within intron 9, resulting in the production of three different transcripts. *In silico* analysis of two of the transcripts predicted partial translation of the intron, however, only one of these transcripts encoded a premature stop. It remains to be determined whether all the aberrantly spliced transcripts are equally abundant, and whether any of the transcripts are translated. Quantitative RT-PCR or Northern blotting may be useful in determining the ratio of expression levels between the mis-spliced *capzα1* transcripts. If the three transcripts are translated they may be detectable by Western blotting, however, due to the small differences in the predicted sizes and isoelectric points of the protein products, (exon 9 deletion: 30.3kDa, p I5.5, 24bp insert: 33.6kDa, pI 5.4 and 46bp insert: 29.5 kDa, pI 4.2) it may be difficult to separate them, even on a two dimensional gel.

Chapter 4

Comparison of CapZ Subunits and Analysis of the *sne* Phenotype

Chapter 4: Comparison of CapZ subunits and analysis of the *sne* phenotype

4.1 Summary

In the previous chapter the positional cloning of the *sne* locus to *capzα1* was described. In the first part of this chapter I primarily focus on comparing the homology of the known zebrafish CapZ subunits (CapZα1, CapZα2 and CapZβ) to other species. These homology comparisons confirm that the site of the mutation is indeed in *capzα1*. Moreover, they illustrate how extremely well conserved the CapZ subunits are across vertebrates. Analysis of the temporal and spatial expression pattern of the CapZ subunits reveals that all subunits are maternally expressed and are ubiquitous in the early stages of zebrafish development. However, by 24 hpf the *capzα2* expression pattern differs to that of *capzα1* and *capzβ*. These findings could reflect a situation in which the α subunits are partially redundant during early development, but take on specific/unique roles during muscle differentiation. The final section of this chapter describes the *sne* mutant phenotype. In *sne* mutants wavy skeletal myofibres and reduced motility are observed from 4 days post fertilization (dpf). Intriguingly, the expression of *capzα1* itself is not affected in the mutants, and immunostaining of CapZα1 reveals that mutant forms of CapZα1 are translated, albeit with an altered cellular localization. In wild type skeletal muscle, CapZα1 is detected at the Z-line, however in *sne* mutant embryos aggregates of protein are observed adjacent to the myoseptum boundaries. Further immunostaining of sarcomeric components and transmission electron microscopy (TEM) analysis indicate that although the main elements that define the sarcomere are still preserved, the mutation in *capzα1* disrupts myofibrillar organization and sarcomeric integrity. Indeed, the muscle phenotype worsens over time in *sne* mutant embryos and when the movements of mutant embryos are restricted, the skeletal muscle phenotype is partially

rescued. These findings provide further support for the prediction that the mutation in *capzα1* destabilizes skeletal muscle architecture following the commencement of contraction.

4.2 Introduction

CapZ is a heterodimeric capping protein that consists of α and β subunits that dimerize to form a fully functional protein, which caps the barbed end of actin filaments. Expression studies performed in yeast, *Dictyostelium* and in cultured vertebrate muscle cells indicate that CapZ is only stable as a heterodimer, and that the individual subunits are highly unstable and have little or no function *in vivo* or *in vitro* (Amatruda et al., 1992; Hug et al., 1995; Hug et al., 1992; Schafer et al., 1992). Invertebrates such as *C. elegans* or *D. melanogaster* express only one of each of the CapZ α and β subunits, however, up to three different α and β isoforms have been found in vertebrates. The production of distinct isoforms is achieved in different ways; the α subunits are encoded on separate genes, while the β subunits are produced from alternative splicing of one transcript. Two isoforms of CapZ α (CapZα1 and CapZα2) and β (CapZβ1 and CapZβ2) exist in chicken, mouse and human (Hart et al., 1997b). In mammals, a third isoform of the α and β subunits (*capZα3* and *capZβ3*) have also been found and are only expressed in male germ cells (Hart et al., 1997a; Schafer et al., 1994; von Bulow et al., 1997).

To date, research on CapZ has focused on how it controls actin dynamics *in vitro* and relatively little is known about potential alternate roles of CapZ in vertebrate development. Indeed, the high homology shared between the CapZ subunits of different species and their early expression during development suggest that they are essential components for vertebrate development and function.

4.3 Comparison of CapZ subunit sequences between species

4.3.1 CapZα1 and CapZα2

In zebrafish only two isoforms of *capZα* (*capZα1* and *capZα2*) were identified and they are located on chromosomes 8 and 6 respectively. CapZα1 and CapZα2 are highly conserved between species and over 80% amino acid sequence identity was observed when zebrafish CapZα1 and CapZα2 were aligned with chicken, mouse, and human orthologues (Fig. 4.1 and Fig. 4.2). Intriguingly, not only are both these proteins the same length (286 residues) but they also share 86 % sequence identity in zebrafish. A similar percentage was also observed between CapZα1 and CapZα2 in the other vertebrates that were compared (Fig. 4.3). CapZα1 and CapZα2 are so highly conserved within vertebrates that the regions between 23 -58 amino acids and 239-286 amino acids are invariant between zebrafish, chicken, mouse and human. The C-terminal region (239-286 amino acids) is thought to be important for actin binding (Casella and Torres, 1994; Hug et al., 1992; Sizonenko et al., 1996). Notably, the mutation identified at the splice junction in *sne* affects translation of the C-terminal region.

One of the major discrepancies caused by the high similarity between *capzα1* and *capzα2* became apparent in Ensembl. In the latest version of the zebrafish genome assembly (Zv6) the *capzα* gene on chromosome 6 is assigned *capzα1* while the *capzα* gene on chromosome 8 (*sne* locus) is assigned as an 'unknown' gene. As described below, I have used different sequence comparison tools to analyze orthologues of the different CapZ subunits, to verify that the gene on chromosome 8 is in fact *capzα1*, and the gene on chromosome 6 is *capzα2*. For the remainder of this thesis zebrafish *capzα1* will always refer to the gene encoded on chromosome 8 and *capzα2* will refer to the gene on chromosome 6.

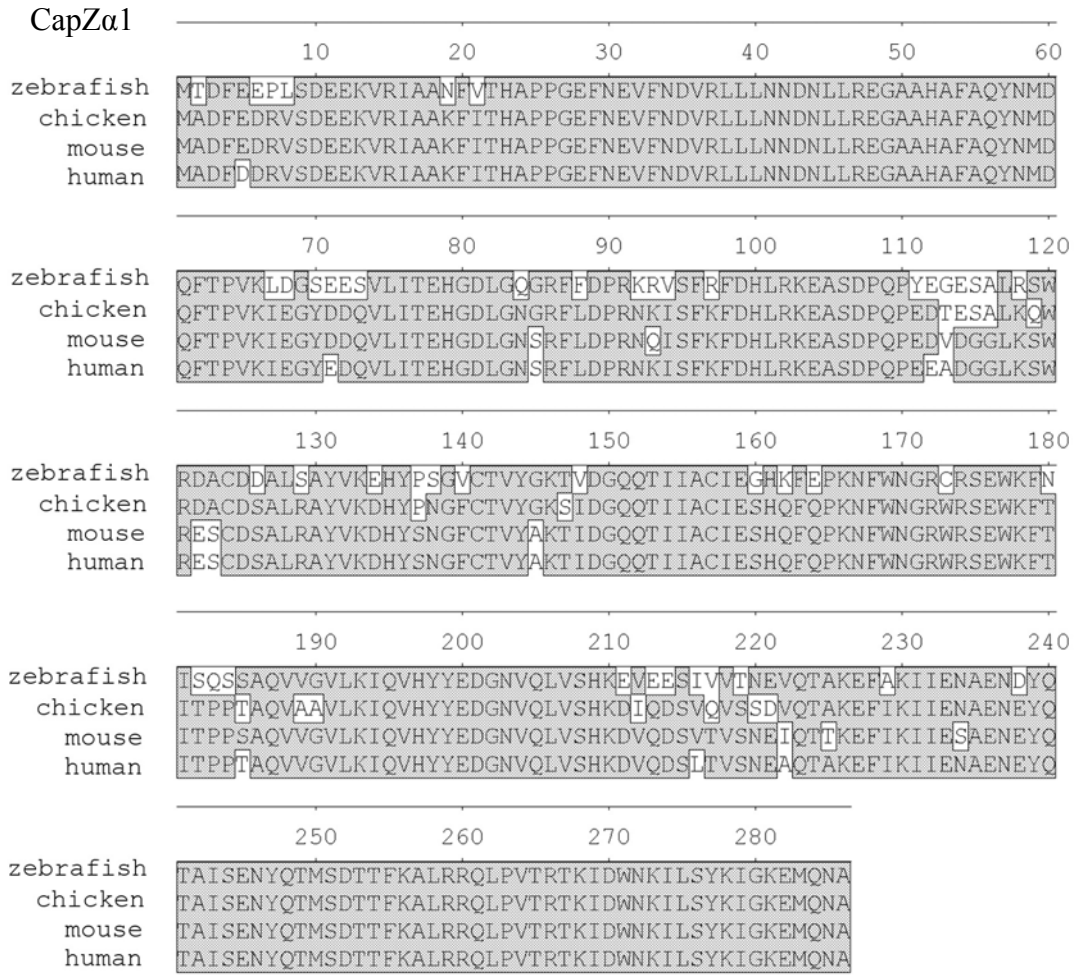

Fig. 4.1. Alignment of zebrafish, chicken, mouse and human CapZα1 protein sequence.

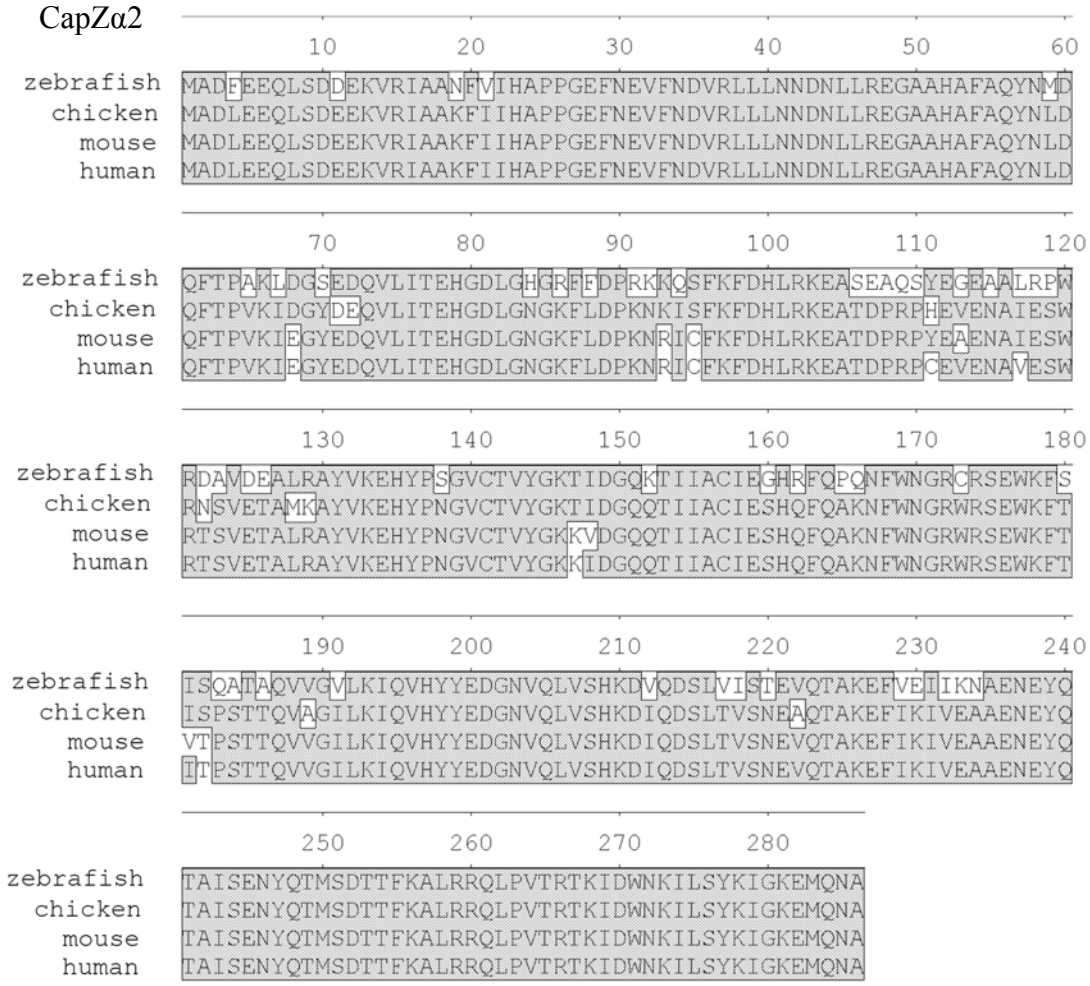

Fig. 4.2. Alignment of zebrafish, chicken, mouse and human CapZα2 protein sequence.

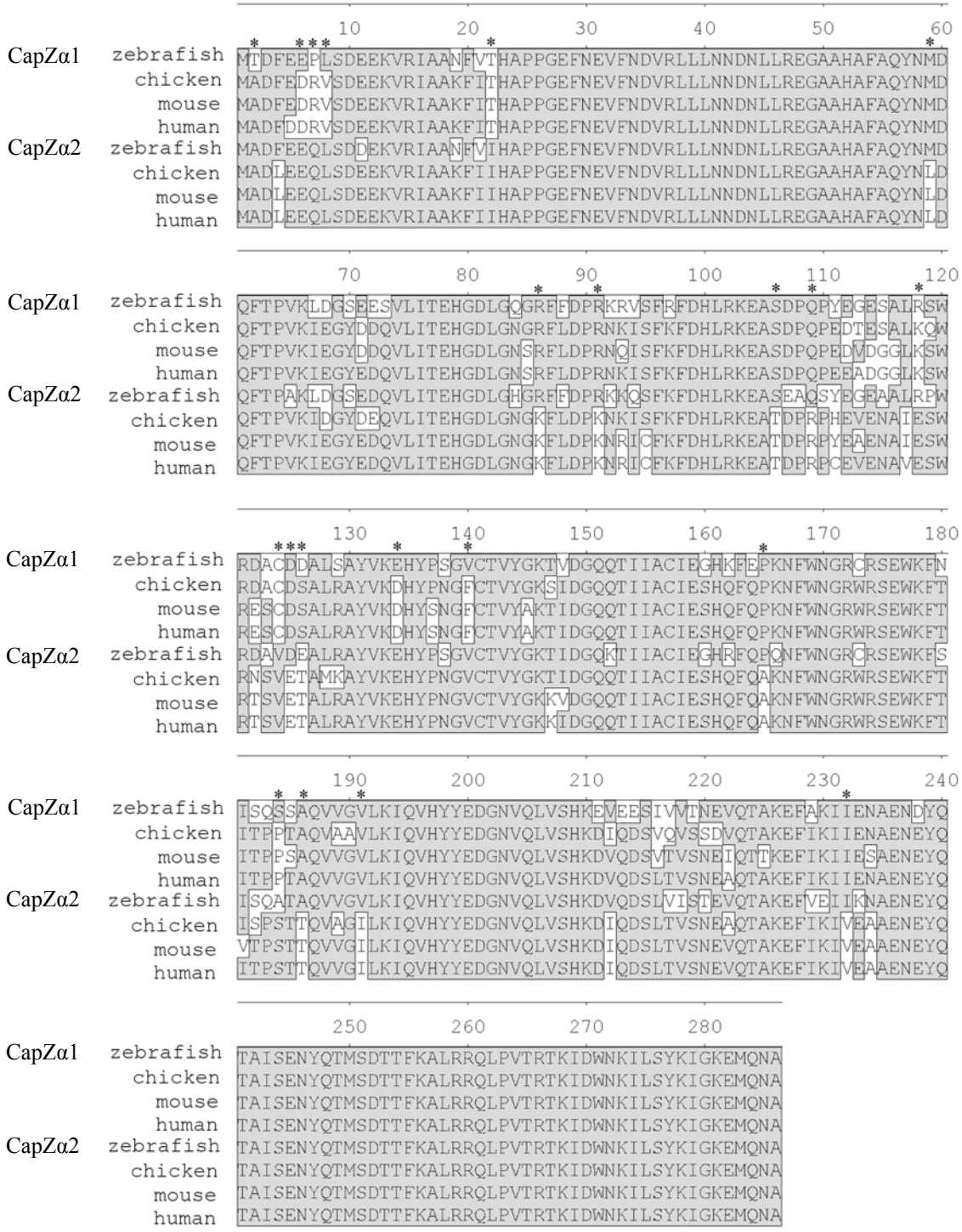

Fig. 4.3. Alignment of CapZα1 and CapZα2 protein sequence from zebrafish, chicken, mouse and human. Amino acids that are identical between the majority of orthologues are shaded. Asterisks indicate residues that are distinctive between CapZα1 and CapZα2 in chicken, mouse and human as determined by Hart et al. 1997b. The percentage identities shared between CapZα1 and CapZα2 of zebrafish, chicken, mouse and human are 86%, 85%, 84% and 86% respectively.

A phylogenetic tree was initially generated using CapZα1 and CapZα2 protein sequences, aligned by Clustal W, to determine whether the two zebrafish isoforms clustered with CapZα1 and CapZα2 sequence of the higher vertebrates (Fig. 4.4A). The tree groups the CapZα1 and CapZα2 sequences of mouse, chicken and human separately, however, zebrafish CapZα1 and CapZα2 were clustered with the CapZα1subunits of other fish species. It is therefore impossible to ascertain whether zebrafish CapZα1 is orthologous to CapZα1 or CapZα2 in the higher vertebrates using these alignment parameters. Interestingly, both medaka and stickleback have two CapZα1 subunits. Moreover, the α2 subunits from these species clustered with the α2 subunits of higher vertebrates. It could be speculated that zebrafish CapZα1 may in fact be CapZα1b, however, no other gene of the CapZα family has been identified in the zebrafish genome. As DNA sequence is generally not as well conserved as protein sequence another phylogenetic tree was generated using *capzα1* and *capzα2* cDNA sequence (Fig. 4.5). Strikingly, similar clusters were observed as in the protein phylogenetic tree, emphasizing the high level of α subunit conservation across species.

A comparison study of the CapZα1 and CapZα2 isoforms performed by Hart and colleagues (1997b) claimed to identify key amino acid differences between CapZα1 and CapZα2. They identified 21 residues that demonstrated isoform specificity when the two isoforms of chicken, mouse and human were aligned (asterisks in Fig. 4.3). To determine whether this isoform specificity was also conserved in zebrafish and could be used to distinguish the two α subunits, these key residues were examined. Unfortunately in zebrafish, only two out of the 21 residues were isoform specific for CapZα1 and CapZα2, and also matched the amino acid residues in the respective orthologues (amino acid 22 and amino acid 124). The majority of the key residues were identical between CapZα1 and CapZα2 in zebrafish (16/21). The remaining three key residues differed between the two zebrafish isoforms, however, did not match the

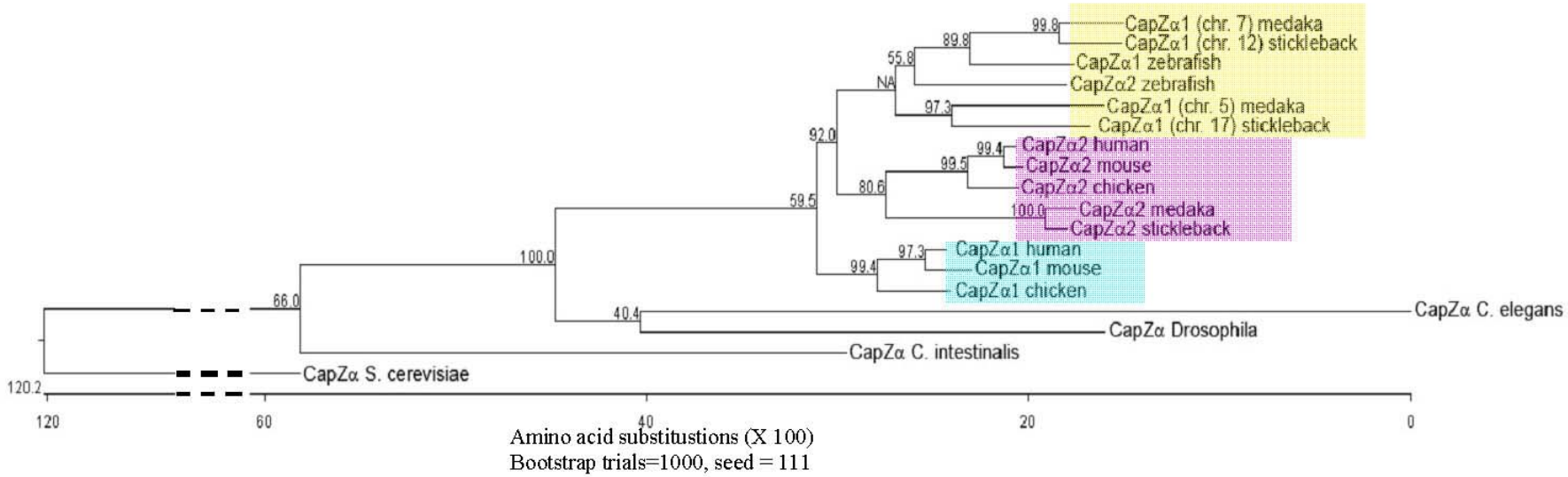

Fig.4.4A. Phylogenetic tree of CapZα subunits from various species. The Clustal W program was used to align amino acid sequences from yeast (*S. cerevisiae*), worm (*C. elegans*), *Drosophila*, *C. intestinalis*, zebrafish, medaka, stickleback, chicken, mouse and human. The yellow box highlights the clustering of the medaka and stickleback CapZα1 subunits. The pink box highlights the clustering of the CapZα2 subunits. The blue box highlights the separate clustering of the CapZα1 subunits of higher vertebrates. Units at the bottom of the tree indicate the number of substitution events. Boostrap values (an estimate of the reliability of each branch point) were calculated based upon a 1000 bootstrap trials (i.e. the displayed tree was compared 1000 times to random tree constructs) and a random seed of 111 (the default setting). The random seed is a number used to initialize the pseudorandom generator and makes bootstrapping consistent with the Clustal interface.

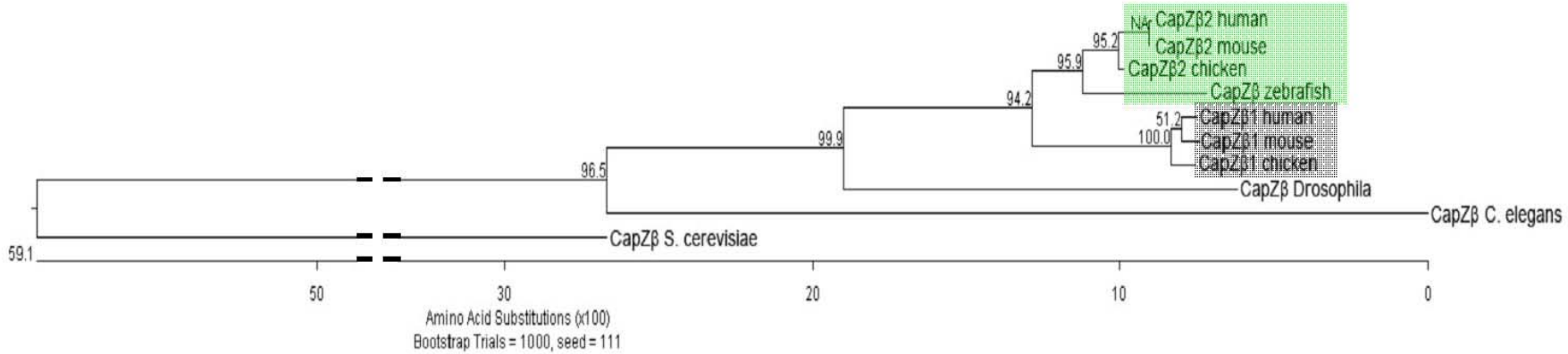

Fig.4.4B. Phylogenetic tree of CapZβ subunits from various species. The Clustal W program was used to align amino acid sequences from yeast (*S. cerevisiae*), worm (*C.elegans*), *Drosophila*, zebrafish, chicken, mouse and human. The green box highlights the clustering of the CapZβ2 subunits and the grey box highlights the clustering of the CapZβ1 subunits. Units at the bottom of the tree indicate the number of substitution events. Boostrap values were calculated based upon a 1000 boot strap trials and a random seed of 111.

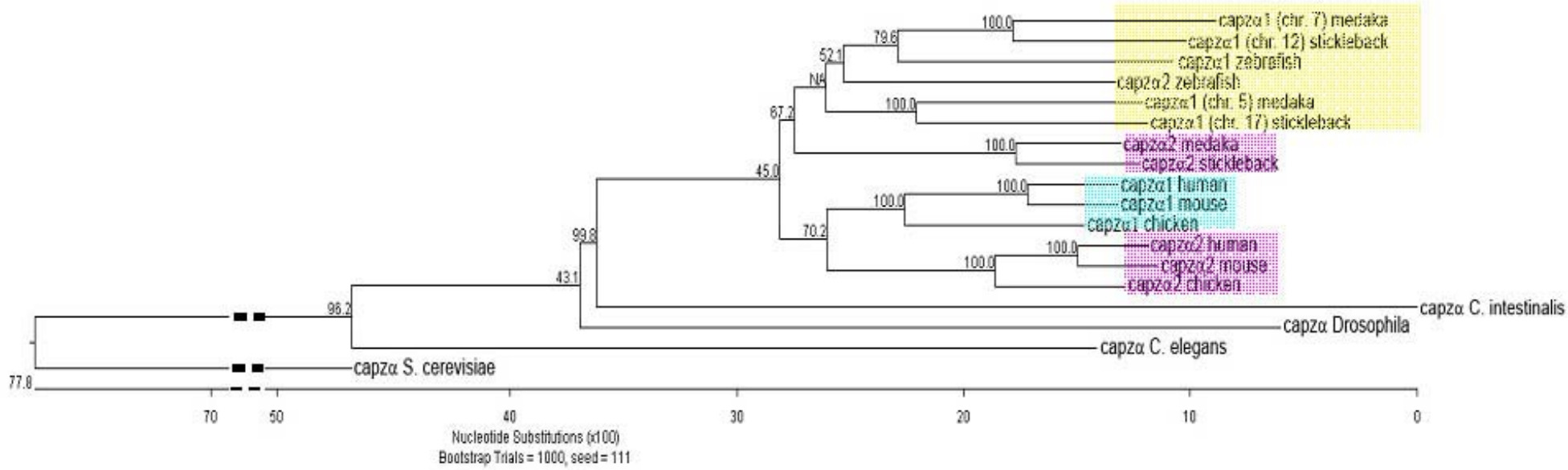

Fig.4.5. Phylogenetic tree using DNA sequence of the α subunits of *capz* from various species. The Clustal W program was used to align DNA sequences from yeast (*S. cerevisiae*), worm (*C. elegans*), *Drosophila*, zebrafish, chicken, mouse and human. Pink and yellow boxes highlight the clustering of the *capzα2* and *capzα1* subunits respectively. The blue box highlights the separate clustering of the capzα1 subunits of higher vertebrates.Units at the bottom of the tree indicate the number of substitution events. Boostrap values were calculated based upon a 1000 bootstrap trials and a random seed of 111.

residues in the corresponding orthologues. It is therefore debatable as to whether these key regions truly signify the difference between the α1 and α2 subunits as the data was based on comparison of only higher vertebrate sequences.

Hart and colleagues (1997b) also compared the 3′ UTR of *capzα1* and *capzα2*, and found that there is approximately 60% and 70% identity for α1 and α2 respectively between chicken, mouse and human. However, when comparing the similarity between the 3′ UTR of α1 and α2, only 32% identity was observed. In zebrafish, the UTR is far less conserved when compared to the other species, and *capzα1* only shares approximately 36% identity with the higher vertebrates (Table 4.1). This finding was also apparent with the 3′ UTR of *capzα2*, and only 35% DNA sequence identity was observed. Therefore, by comparing the 3′ UTR I was still unable to verify that zebrafish *capzα1* is located on chromosome 8.

Another approach commonly used to give an indication of gene orthology between species is to investigate its synteny. Syntenic regions are genetic loci that lie in the same order on a chromosome in different species, indicating that they derive from a common ancestral chromosome. Zebrafish *capzα1* was found to share greater synteny with the regions surrounding *capzα1* in other species (Fig. 4.6). Four common genes were located near *capzα1* in mouse, human and zebrafish: *rho2*, *wnt2bb*, a putative helicase *mov10* and *cttnbp2*. The region surrounding zebrafish *capzα2* only shared *suppressor of tumorigenicity 7* (*st7*) with the mouse and human *capzα2* equivalent region. BLAST comparison of zebrafish *st7* against mouse *st7* and *st7-like isoform 3* (syntenic with *capzα1* in mouse and human) was performed to verify that zebrafish *st7* had been annotated correctly. Zebrafish *st7* shares 81% amino acid identity to mouse *st7* and 69% amino acid identity to mouse *st7-like isoform* 3 indicating that *st7* is indeed syntenic with *capzα2*. Zebrafish *capzα2* therefore does not share any synteny with the region

surrounding *capzα1* in mouse and human and vice versa. The synteny of *capzα1* provides the strongest evidence that zebrafish *capzα1* is located on chromosome 8 and *capzα2* is located on chromosome 6.

Table 4.1. Percentage of DNA sequence identities of zebrafish *capzα1* and *capzα2* 3′ UTRs (700bp) against chicken, mouse and human *capzα1* and *capzα2* 3′ UTRs.

	Chicken	Mouse	Human
capzα1 zebrafish	34.6%	38%	37.1%
capzα2 zebrafish	35.5%	36.1%	35.8%

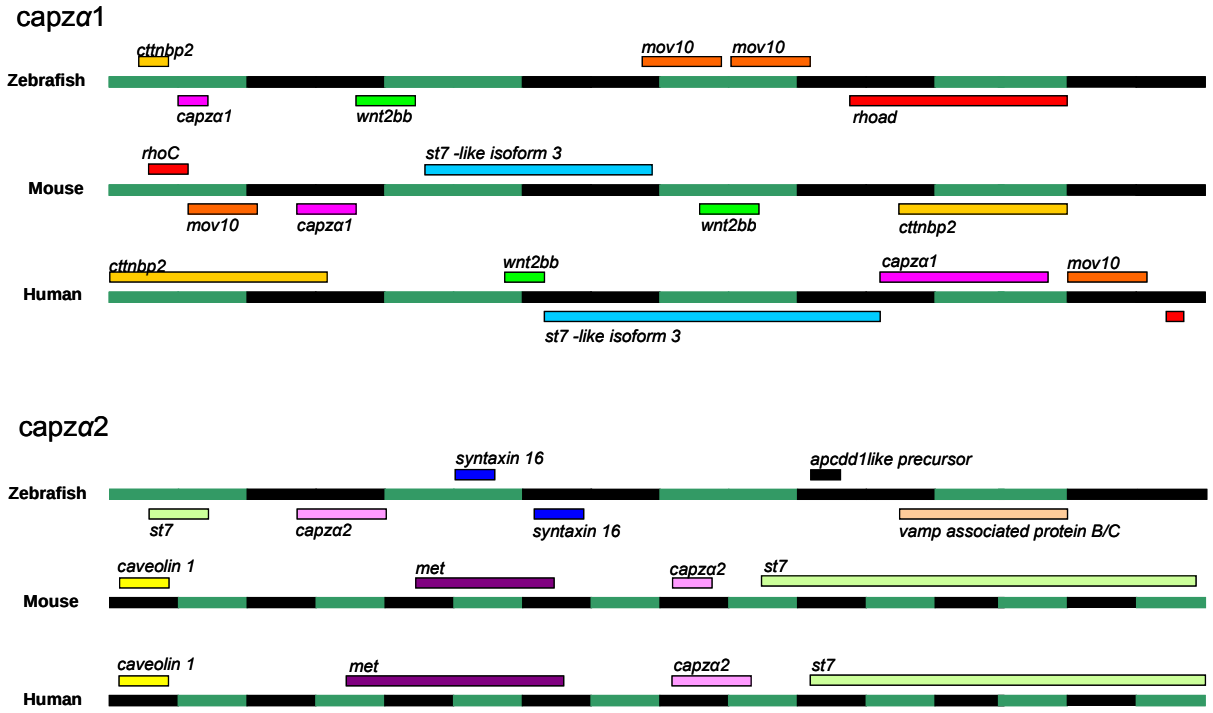

Fig. 4.6. Syntenic regions surrounding *capzα1* and *capzα2* in zebrafish, mouse and human. *mov10* is a putative helicase (moloney leukemia virus), *cttnbp2* is cortactin binding protein 2 N-terminal-like gene, *met* is a proto-oncogene, *apcdd1-like precursor* is adenomatosis polyposis coli down- regulated 1–like protein, *vamp* is vesicle-associated membrane protein and *st7* is suppressor of tumorigenicity-7. Green and black bars represent represent 0.04 Mb.

4.3.2 CapZβ

Isoforms 1 and 2 of CapZβ in chicken, mouse and human differ only in the last 27-31 amino acids and arise from alternative splicing of the last exon (Fig.4.7). Unexpectedly, only one *capzβ* isoform has thus far been identified in zebrafish. Alignments of the zebrafish CapZβ sequence (derived from cDNA sequence Amsterdam et al., 2003) along with the β1 and β2 orthologous isoforms from other species indicate that zebrafish CapZβ is the β2 isoform (Fig. 4.8). Zebrafish CapZβ shares approximately 89% amino acid identity with the orthologous β1 isoforms and approximately 94% identity with the β2 isoforms. Additionally, in zebrafish CapZβ, 20 amino acids out of the last 26 amino acids are identical with the β2 orthologous isoforms, however, only 8 amino acids out of 26 amino acids are identical with the β1 orthologous isoforms. A phylogenetic tree of the alignments also shows that the zebrafish CapZβ sequence clusters with the CapZβ2 orthologues (Fig. 4.4B) and therefore indicates that the annotated zebrafish *capzβ* is in fact *capzβ2*.

In an attempt to detect expression of the *capzβ1* isoform in zebrafish, RT-PCR was performed using primers that amplified the 3′ region of *capzβ* from 18 somite cDNA. Two products that differed in size by 100bp were amplified (Fig. 4.9), which coincided with the size difference between the cDNA of the chicken β1 and β2 isoforms (Schafer et al., 1994), however, cloning and sequencing of the products revealed that only one of these cDNAs encoded the previously identified *capzβ* isoform 2. The other product matched another region of the genome (an rRNA gene on chromosome 4) and may have arisen from a lack of primer specificity. Due to the poor genomic annotation of zebrafish *capzβ*, I was unable to establish whether the exon characteristic of the β1 isoform was encoded in the 3′ region of the gene.

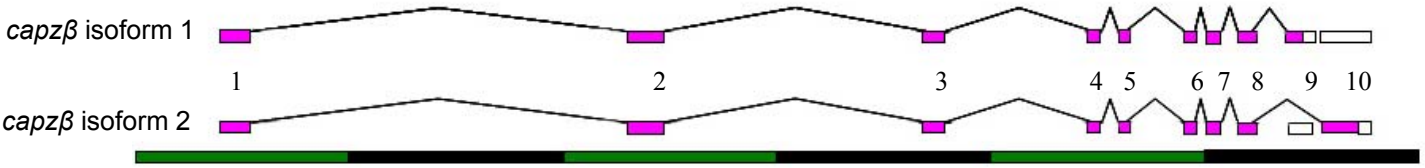

Fig. 4.7. Illustration of *capzβ* exons spliced to form isoforms 1 and 2. Each bar represents 0.04Mb. Isoform 2 skips exon 9 and splices into exon 10 which is encoded in the 3′ UTR of what is transcribed in isoform 1.

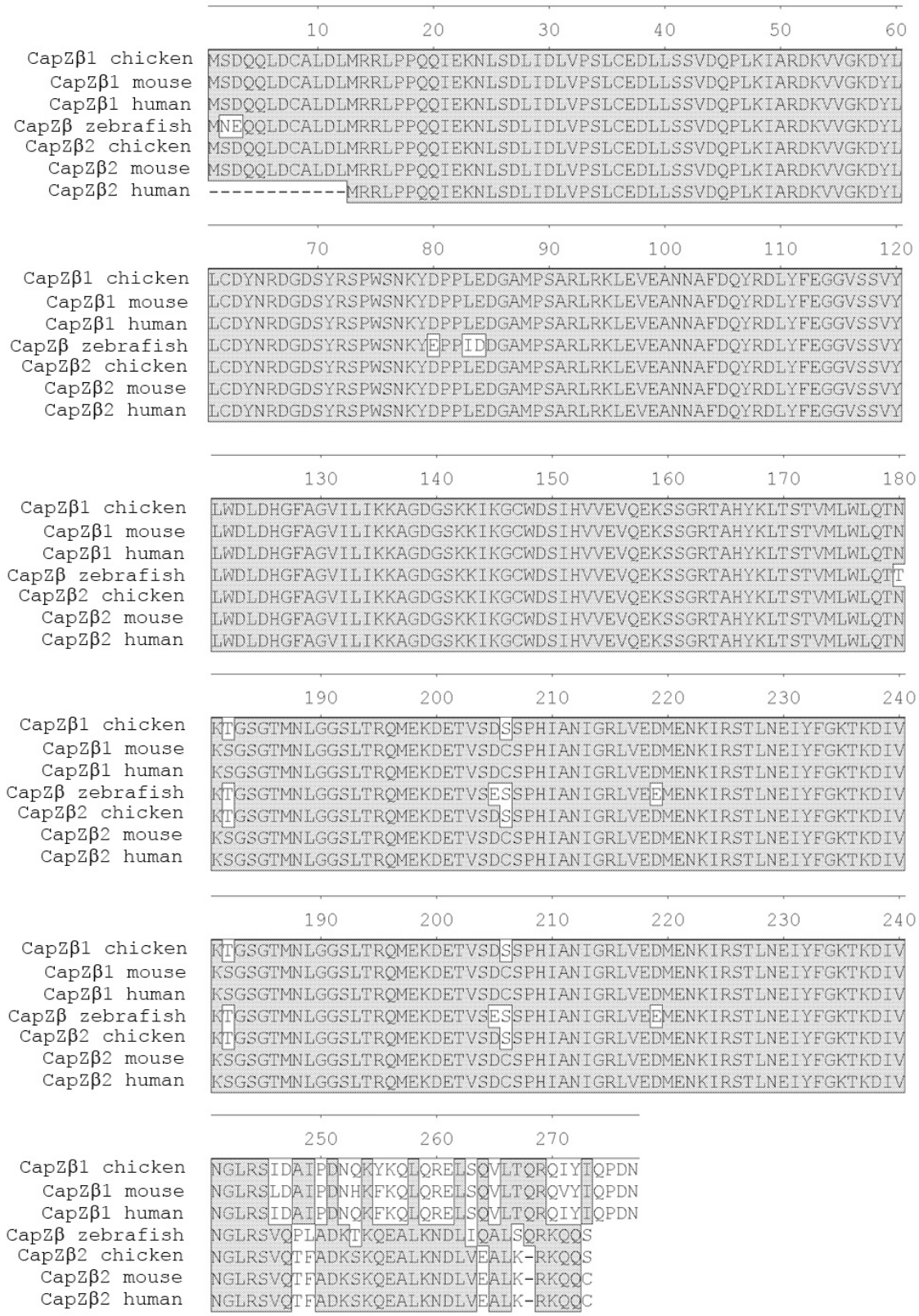

Fig. 4.8. Multiple alignments of CapZβ isoforms 1 and 2 of chicken, mouse and human with the zebrafish CapZβ protein sequence. Amino acids that are identical between the majority of orthologues are shaded.

4.4

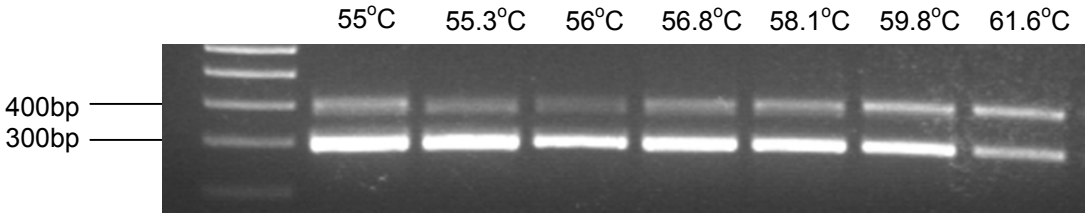

Fig. 4.9. Gel of *capzβ* products from a gradient RT-PCR using 18 somite cDNA.

RNA expression patterns of the *capz* subunits

4.4.1 Probe design

To examine the RNA expression profile of the *capz* subunits during zebrafish embryonic development, labeled antisense RNA probes for *capzα1*, *capzα2* and *capzβ* were constructed. Due to the high sequence similarity between the coding regions of *capzα1* and *capzα2* (80% DNA sequence identity), the probes for these genes were designed to bind predominantly to the more divergent 3′ UTR (Fig. 4.10). The *capzα1* probe targeted just the 3′ UTR of *capzα1* (599bp), and the *capzα2* probe targeted the last 266bp of the coding sequence and 214bp of the 3′ UTR. The region that overlapped between the two probes had low sequence similarity (40 %), therefore the likelihood that the probes would be cross reactive was extremely low. The *capzβ* antisense RNA labeled probe (595bp) was designed to bind to the 5′ region of the coding sequence, beginning at the start site.

4.4.2 The *capzα1* expression pattern

Expression of *capzα1* RNA is first observed very early in development, and is present by the 16-cell stage (Fig. 4.11A), demonstrating that *capzα1* is expressed maternally. At 90% epiboly and 13-15 somites there is ubiquitous expression (Fig. 4.11C-F), however, by 24 hpf stronger expression is detected within the somites, midbrain, hindbrain and the eye (Fig. 4.11G). This expression pattern is also apparent at 48 hpf (Fig. 4.11H), and heart-specific expression is also observed at this stage (Fig. 4.11I).

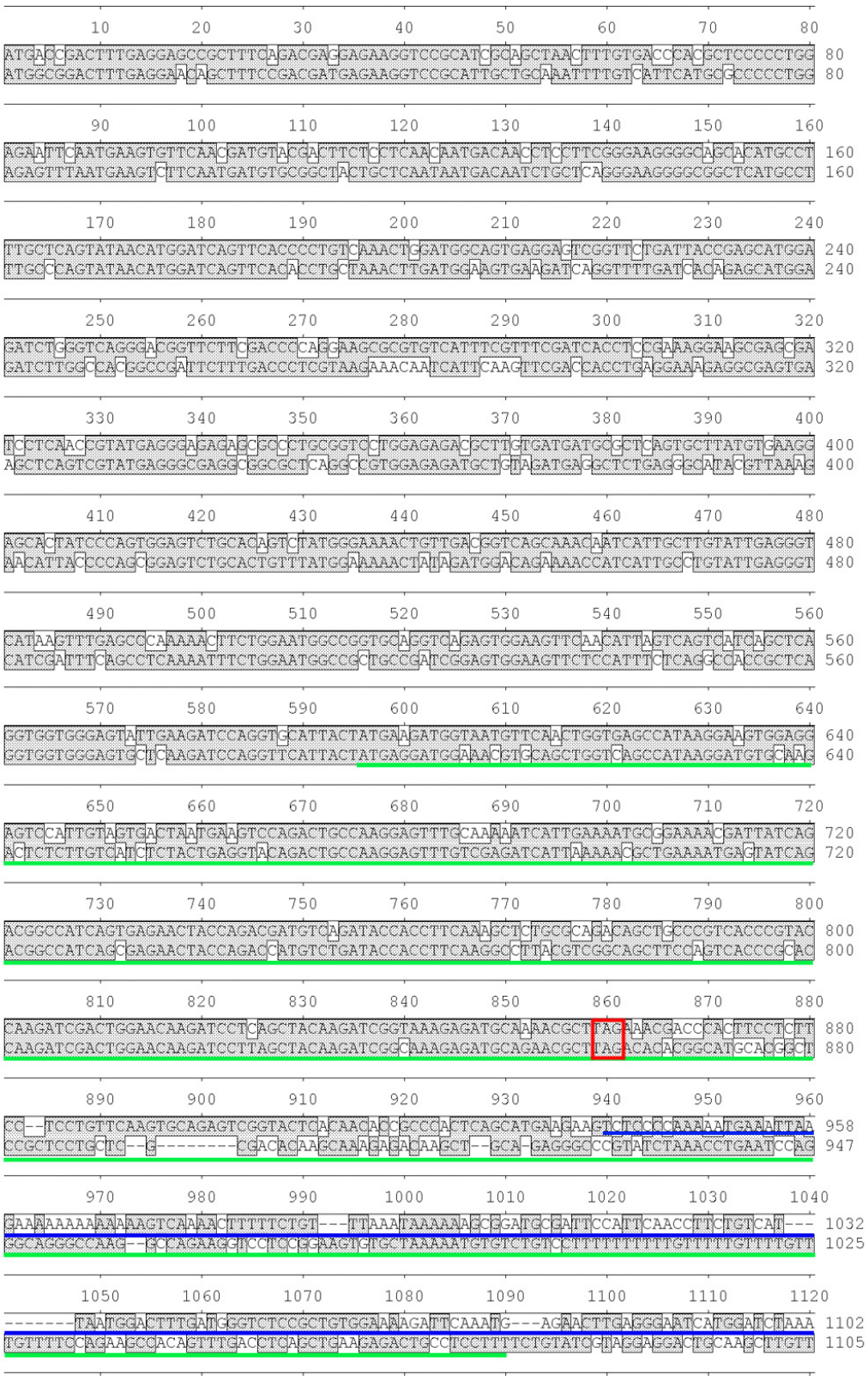

Fig. 4.10. Legend overleaf.

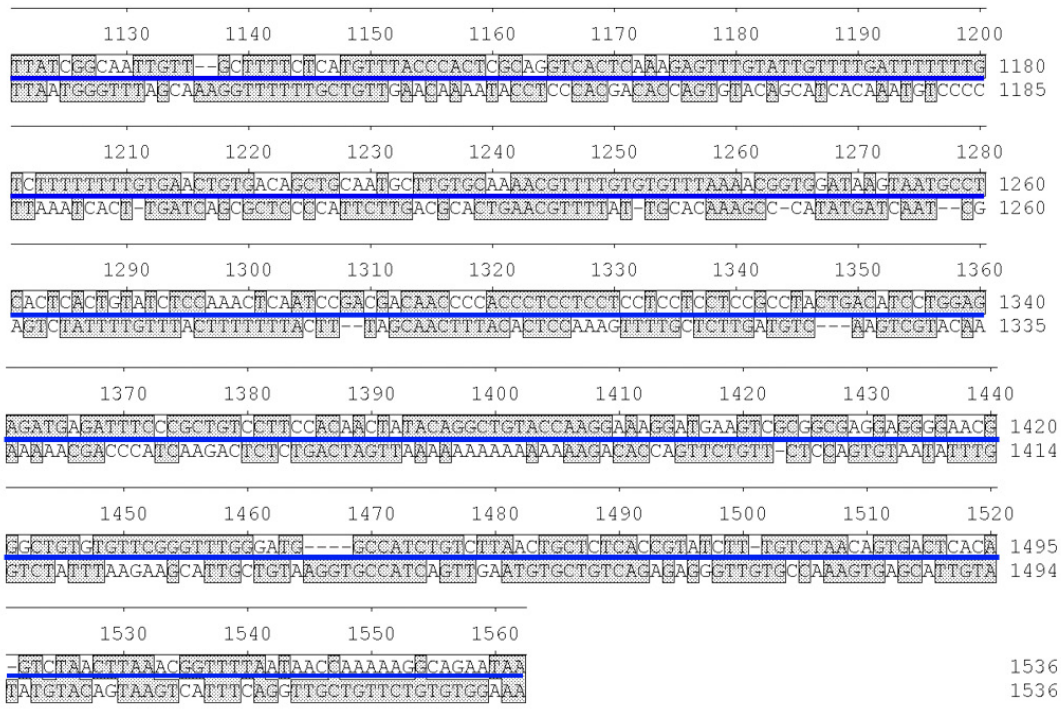

Fig. 4.10. Alignment of *capzα1* and *capzα2* zebrafish cDNA sequence. The *capzα1* RNA *in situ* probe targets the region underlined in blue and the *capzα2 in situ* probe targets the region underlined in green. The *capzα1* RNA *in situ* probe shares 43% sequence identity with *capzα2* and the *capzα2 in situ* probe shares 67% sequence identity with *capzα1*. The stop codon is boxed in red.

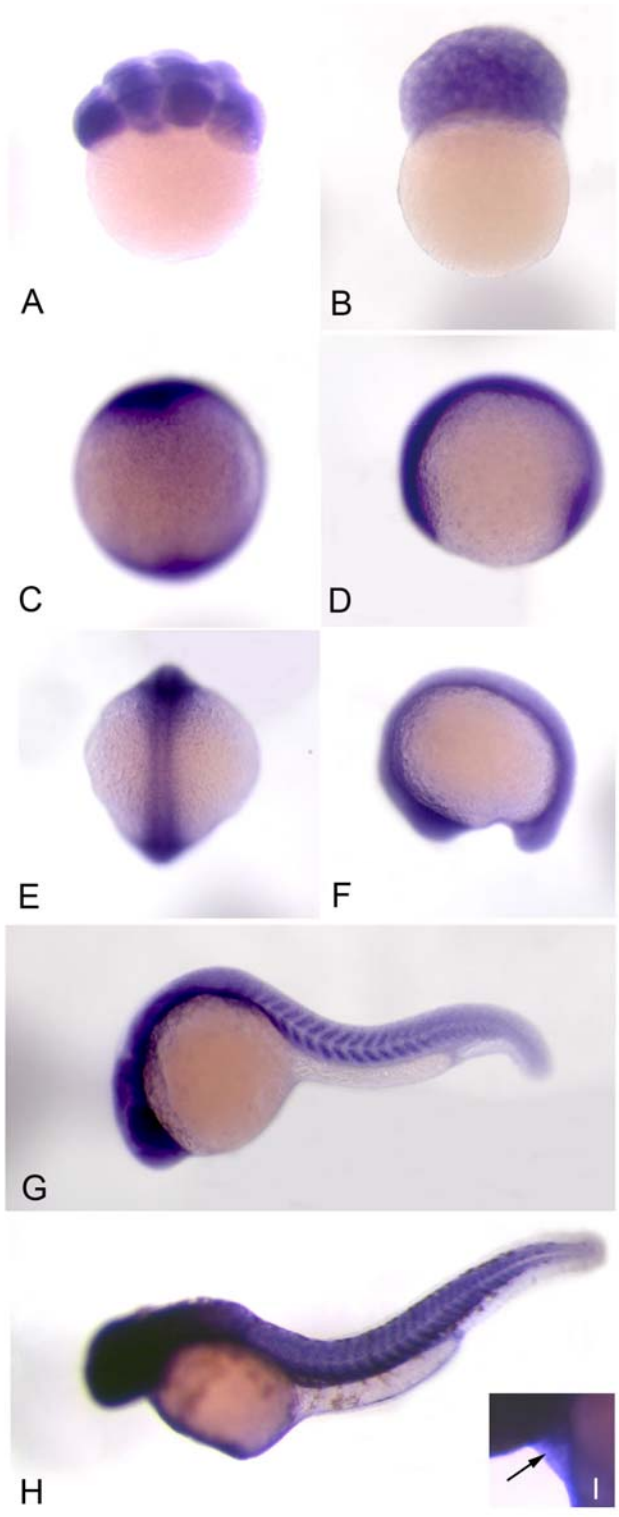

Fig. 4.11. *capzα1* RNA *in situ* expression pattern at different stages of zebrafish embryonic development. A) 16 cell, B) 128 cell, C and D) 90% epiboly, E and F) 13 -15 somites, G) 24 hpf and H) 48 hpf. I) Close up of the heart at 48 hpf. Arrow points to expression in the heart.

4.4.3 The *capzα2* expression pattern

A low level of ubiquitous *capzα2* RNA expression is detected at all the stages of development tested. Like *capzα1*, expression of *capzα2* is first observed at the 16 cell stage (Fig. 4.12A) indicating that *capzα2* is also expressed maternally. Expression is ubiquitous at 90% epiboly and 13-15 somites (Fig. 4.12C-F), and by 24 hpf stronger expression in the midbrain, hindbrain and the eye is detected, however, in the trunk of the embryo expression is ubiquitous but greatly reduced (Fig. 4.12G). This is distinct from the stronger blocks of expression that were observed in the somites with the *capzα1* probe. By 48 hpf the expression pattern remained similar to the 24 hpf embryo (Fig 4.12H) with the addition of clearly detectable staining in the heart (Fig. 4.12I).

4.4.4 The *capzβ* expression pattern

The expression pattern of *capzβ* is very similar to *capzα1*. As with the α subunits *capzβ* RNA is also first expressed maternally and is detected at the 16 cell stage (Fig. 4.13A). At 90% epiboly and 13-15 somites ubiquitous expression is observed (Fig. 4.13C-F), however, by 24 hpf stronger expression is localized to the somites, midbrain, hindbrain and the eye (Fig. 4.13G). This expression pattern continues at 48 hpf (Fig. 4.13H), and expression of *capzβ* is also seen in the heart (Fig. 4.13I).

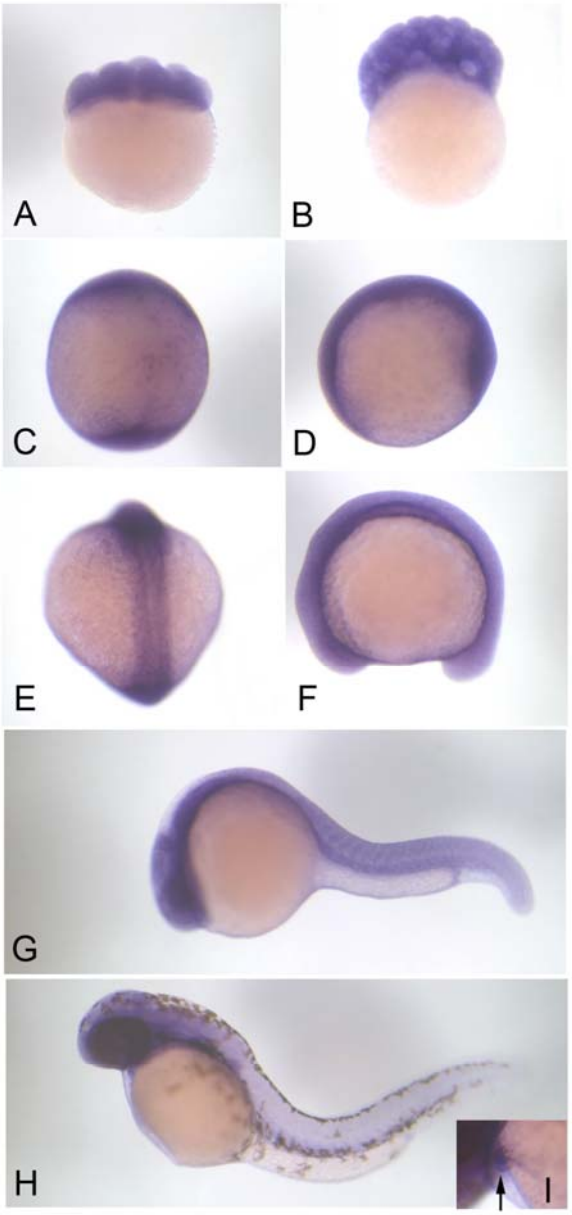

Fig. 4.12. *capzα2* RNA *in situ* expression pattern at different stages of zebrafish development. A) 16 cell, B) 128 cell, C and D) 90% epiboly, E and F) 13 -15 somites, G) 24 hpf and H) 48 hpf. I) Close up of the heart of 48 hpf. Arrow points to expression in the heart.

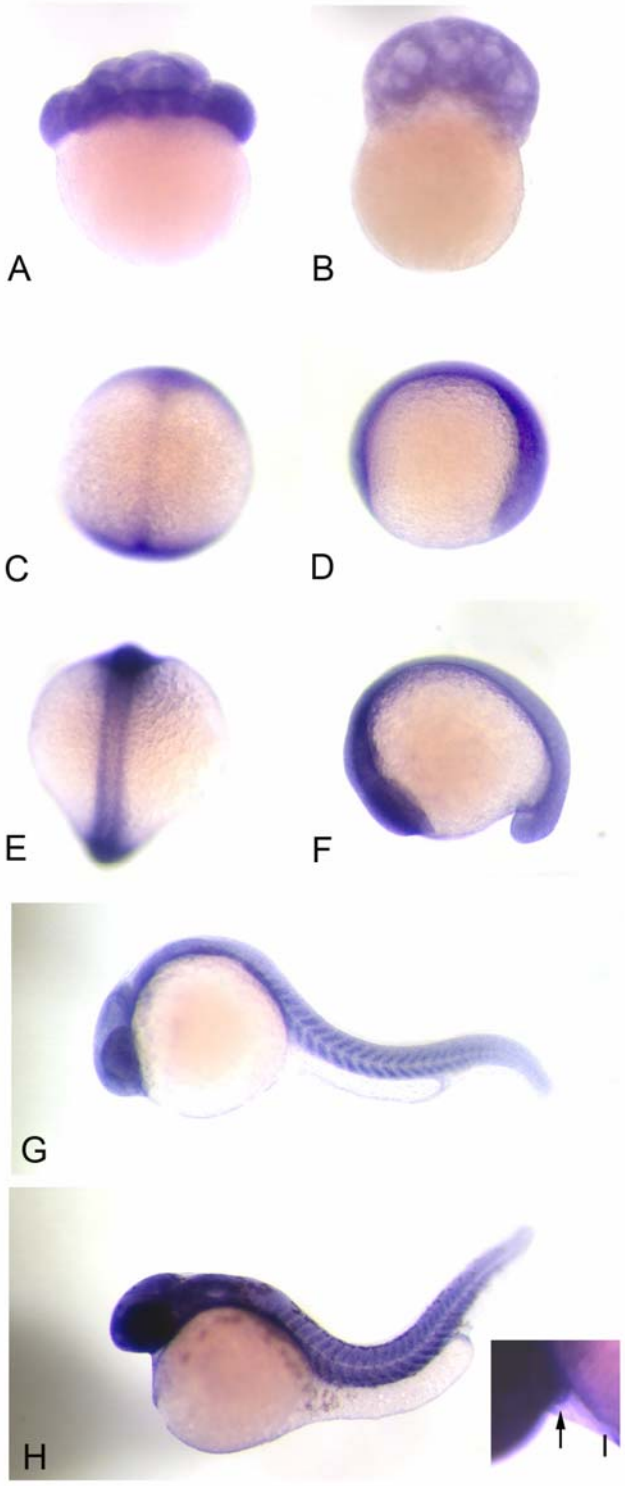

Fig. 4.13. *capz*β RNA *in situ* expression pattern at different stages of zebrafish development. A) 16 cell, B) 128 cell, C and D) 90% epiboly, E and F) 13-15 somites, G) 24 hpf and H) 48hpf. I) Close up of the heart at 48 hpf. Arrow indicates expression in the heart.

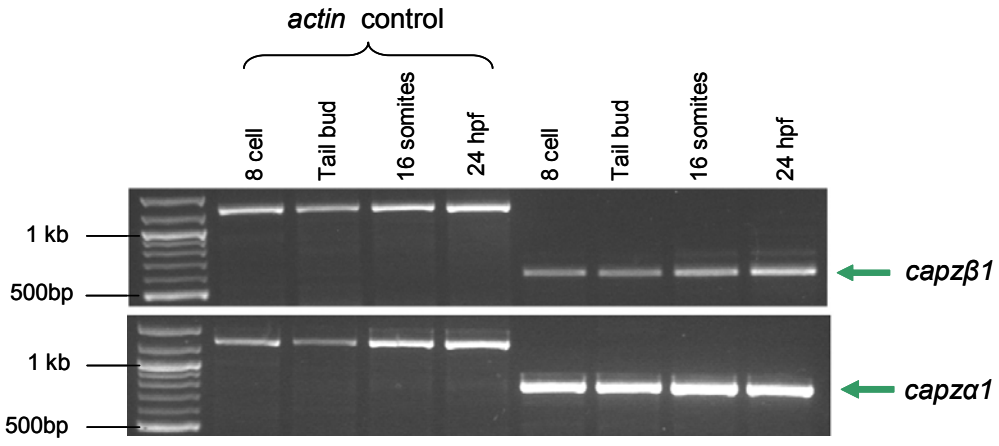

Fig. 4.14. Gel of *capzα1* and *capzβ* RT-PCR products amplified from cDNA of 8 cell, tail bud, 16 somites and 24 hpf embryos. Actin was also amplified as a control. Primers are shown in Table 2 of the appendix.

4.4.5 Expression of *capzα1* and *capzβ* detected by RT-PCR

To confirm that *capzα1* and *capzβ* are expressed throughout the early stages of development RT-PCR was performed on RNA extracted from 8 cell, tail bud, 16 somites and 24 hpf embryos (Fig. 4.14). RT-PCR products were amplified from both genes at all stages, confirming the early expression of *capzα1* and *capzβ* indicated by *in situ* hybridizations.

4.5 Morphology of the *sne* mutant

To investigate how the mutation in *capzα1* affects muscle structure and function, the morphology of *sne* mutant skeletal muscle was examined. This following section describes the skeletal muscle phenotype of *sne* mutants by using light microscopy, immunostaining and TEM techniques.

4.5.1 Gross morphology observed by light microscopy

The motility defect in the *sne* mutant is apparent by 4 dpf, as embryos are unable to respond to a stimulus as quickly as wild type embryos. Additionally, the swim bladder fails to inflate and wavy muscle fibres can be detected by differential interference contrast (DIC) microscopy in the mutants (Fig. 4.15). Mutant embryos die soon after transfer to the fish facility, most likely as a result of being unable to find food, due to their inability to swim properly. In the original description of this mutation reduced birefringence was seen in the muscle of *sne* mutants (Granato et al., 1996). Birefringence is the ability of muscle to rotate polarized light due to its highly ordered structure and is used to identify any defects in muscle organization.

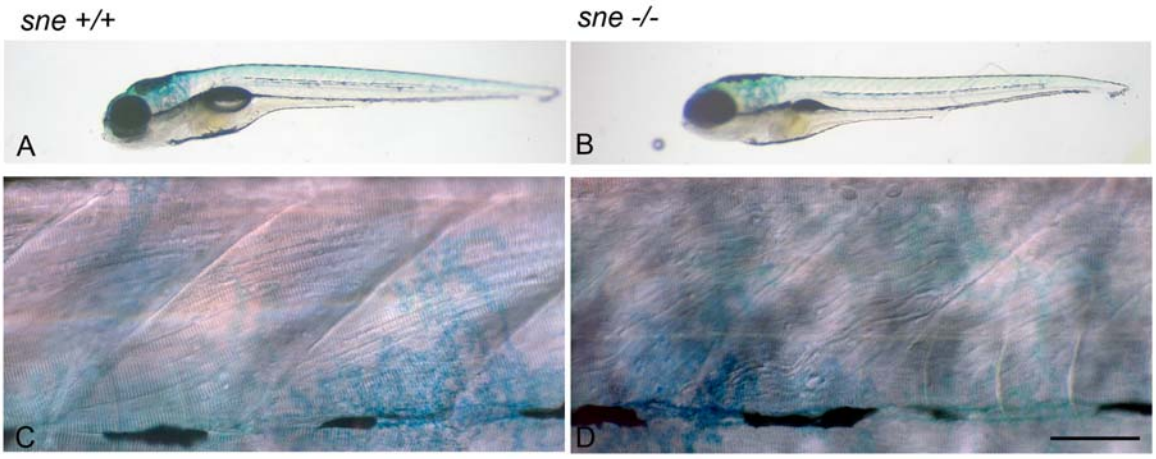

Fig.4.15. Live images of *sne* mutant and wild-type sibling 5 dpf embryos. Wild-type sibling (A and C) and *sne* mutant (B and D) images of the whole embryo (A and B) and the skeletal muscle under DIC microscopy (Cand D). The scale bar for C and D =100μm.

4.5.2 Immunostaining of F-actin and α-actinin in *sne* mutants

Closer inspection of the skeletal muscle was achieved by staining of the actin filaments and Z-lines. Phalloidin conjugated to FITC was used to detect the actin filaments. Phalloidin (a toxin that was originally isolated from the *Amanita phalloides* mushroom) binds filamentous actin (F-actin) at the junction between each monomeric actin subunit (Barden et al., 1987; Faulstich et al., 1993; Steinmetz et al., 1998). In the *sne* mutants both slow and fast F-actin are detected, however, fewer muscle fibres are observed in mutant embryos than in their wild-type siblings. Moreover, the fibres are wavy and accumulations of actin filament are observed at myoseptum boundaries (Fig. 4.16A and B). α-Actinin staining reveals that Z-lines are formed in *sne* mutant embryos, however, the Z-lines are not aligned laterally between myofibrils and the fibrils appear to be detached from the myoseptum (Fig. 4.16C and D). α-Actinin also accumulates at the myoseptum boundaries.

At 2 dpf Mendelian ratios of mutants were observed by scoring the morphology of the actin filament using phalloidin staining. Three out of ten embryos derived from a heterozygous cross had detectably abnormal 'wavy' myofibre organization (Fig. 4.17). Although this phenotype is less pronounced than at 5 dpf, it suggests that the muscle defect in the *sne* mutants worsens over time. However, greater numbers and genotyping of fixed embryos would be necessary to verify this result fully.

4.5.3 The expression levels of *capzα1* and *capzβ* are not reduced in the *sne* mutant

It has been speculated that the α and β CapZ subunits regulate each other's expression, therefore RNA levels of *capzα1* and *capzβ* were examined in 24 hpf *sne* mutant and wild-type sibling embryos by performing RNA *in situ* hybridizations. Mutants and wild-type siblings are

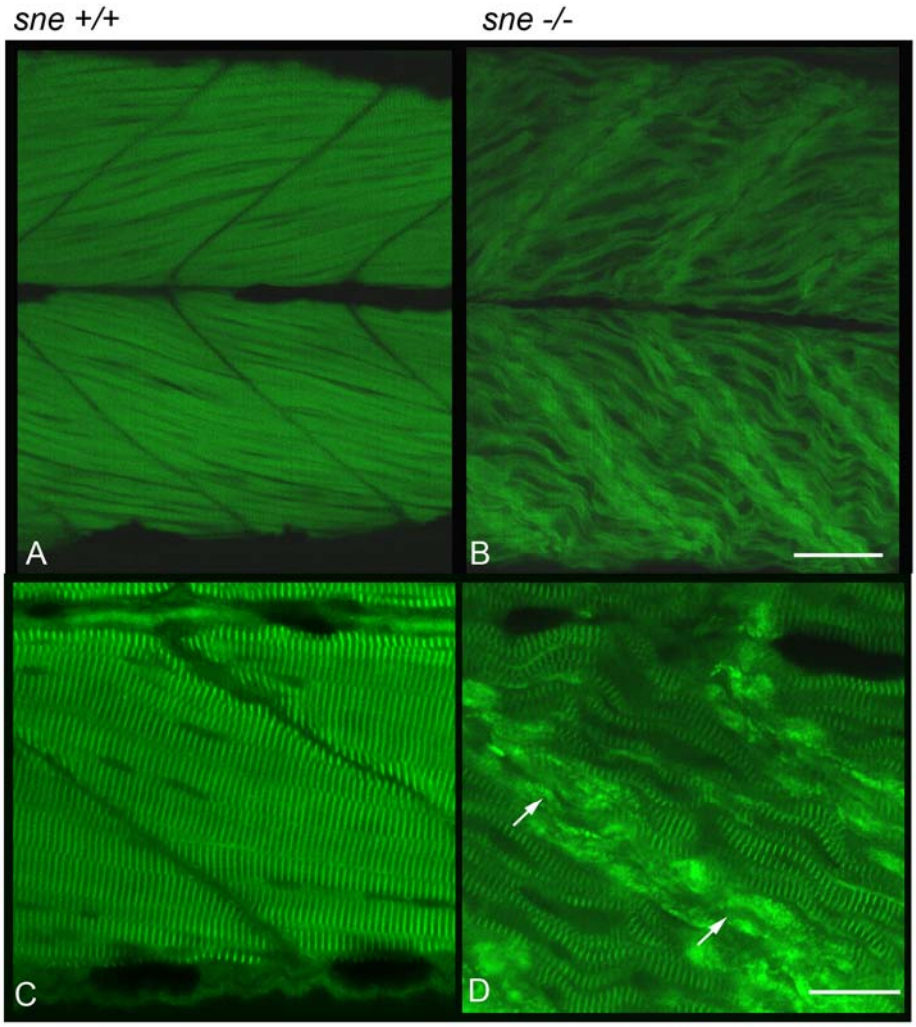

Fig. 4.16. Phalloidin (A and B) and α-actinin staining (C and D) of *sne* wild-type sibling (A and C) and mutant (B and D) at 5 dpf. Arrows indicate accumulations of α-actinin adjacent to the myoseptum. The scale bar for A and B = 44.36μm and for C and D =22.18μm.

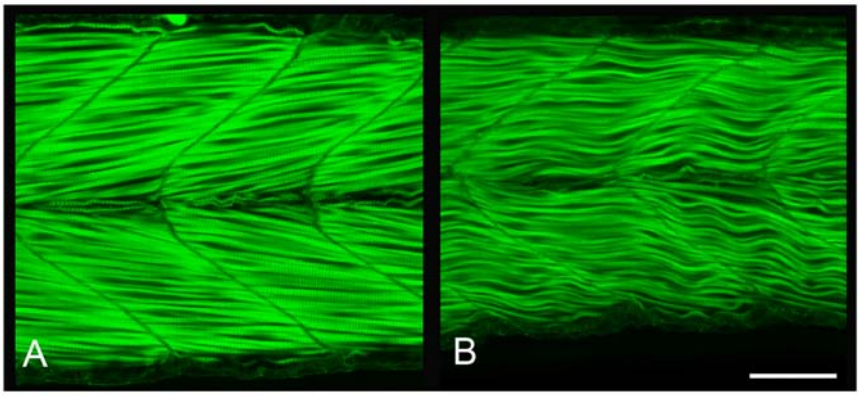

Fig. 4.17. Phallodin staining of 2 dpf *sne* wild-type sibling and mutant embryos. A) Wild-type sibling, B) possible mutant embryo, note the slightly wavy myofibres.Scale bar = 44.36μm.

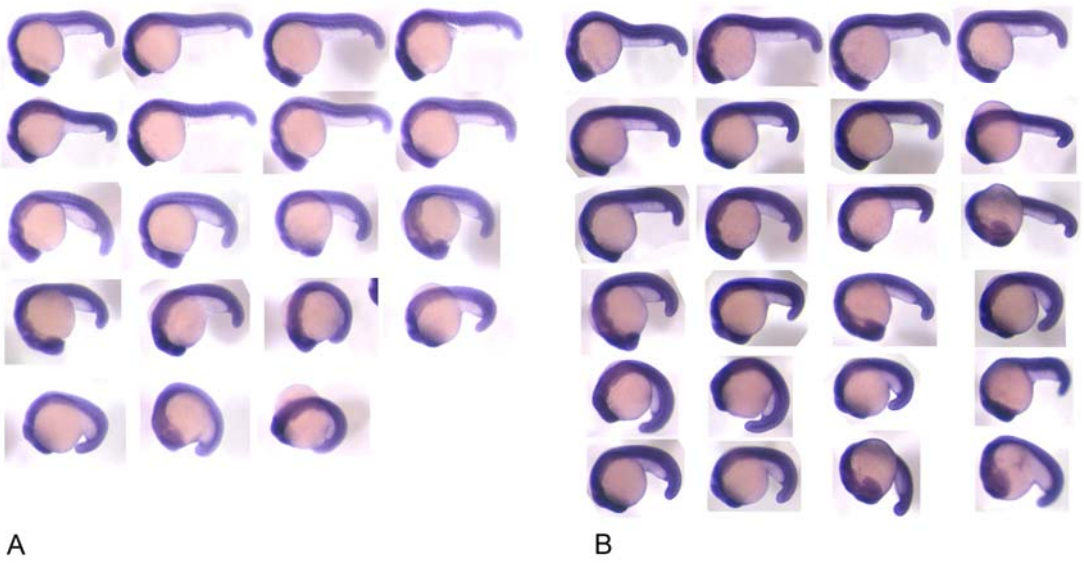

Fig. 4.18. RNA *in situ* expression pattern of A) *capzα1*and B) *capz*β in 24hpf *sne* mutant and wild-type sibling embryos.

not distinguishable at this stage, so 19 and 25 embryos from a heterozygous cross were hybridized with *capzα1* and *capzβ* RNA probes respectively. Differences in levels of *capzα1* and *capzβ* RNA expression were not detected in any of the embryos tested (Fig. 4.18) and therefore indicate that RNA levels of each gene are not affected in this mutant. As *capzα1* RNA appears to be expressed at normal levels in the mutant it also suggests that the mutation does not affect transcription levels of *capzα1*, nor induces RNA degradation of the transcript. However, as this experiment is only semi-quantitative, real time RT-PCR will be required to verify this finding.

4.5.4 Immunostaining of CapZα1 in *sne* mutants

To determine whether mutant *capzα1* transcript (observed from the *in situ* hybridization experiments and the RT-PCR in chapter 3) is translated, *sne* mutant and wild-type sibling embryos were immunostained with a polyclonal antibody raised in chicken against recombinant human CapZα1 (Abcam). In the skeletal muscle of day 5 wild type zebrafish embryos CapZα1 localizes to Z-lines, as determined by co-immunostaining with α-actinin (Fig. 4.19A-C). Additionally, CapZα1 is also localized to the myoseptum. In the mutants CapZα1 is detected, however it is mis-localized and accumulates adjacent to the myoseptum. Intriguingly, this mis-localization largely associates with the aberrant accumulation of α–actinin at the myoseptum (Fig. 4.19D-F).

4.5.5 Transmission Electron Microscopy (TEM)

TEM of *sne* mutant skeletal muscle (performed by David Goulding) show that thick and thin filaments incorporate into the sarcomere (Fig. 4.20). Distinct M-bands, I-bands and A-bands are still observed in most sarcomeres, however, the I-bands appear larger than in the wild type embryos and the thin filaments seem to be splayed at the Z-line within this region (Fig. 4.20B). In

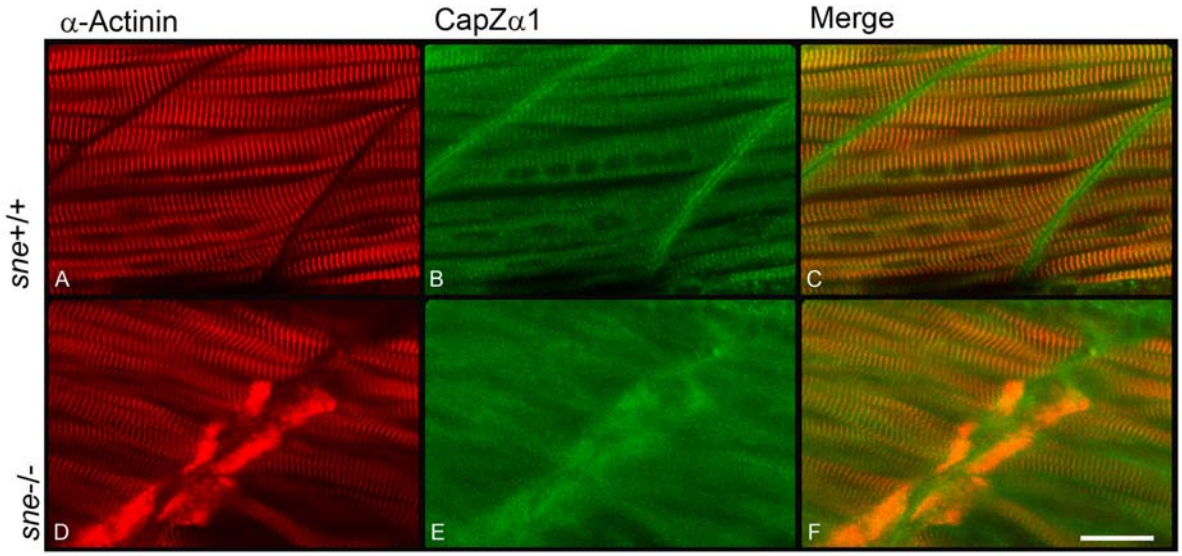

Fig. 4.19. Co-immunostaining of CapZα1 and α-actinin. *sne* wild-type sibling (A-C) and mutant (D-F) 5dpf embryos stained with the α-actinin (A and D) and CapZα1 antibody (B and E). The merge of both these stainings is shown in C and F. Scale bar = 22.18μm.

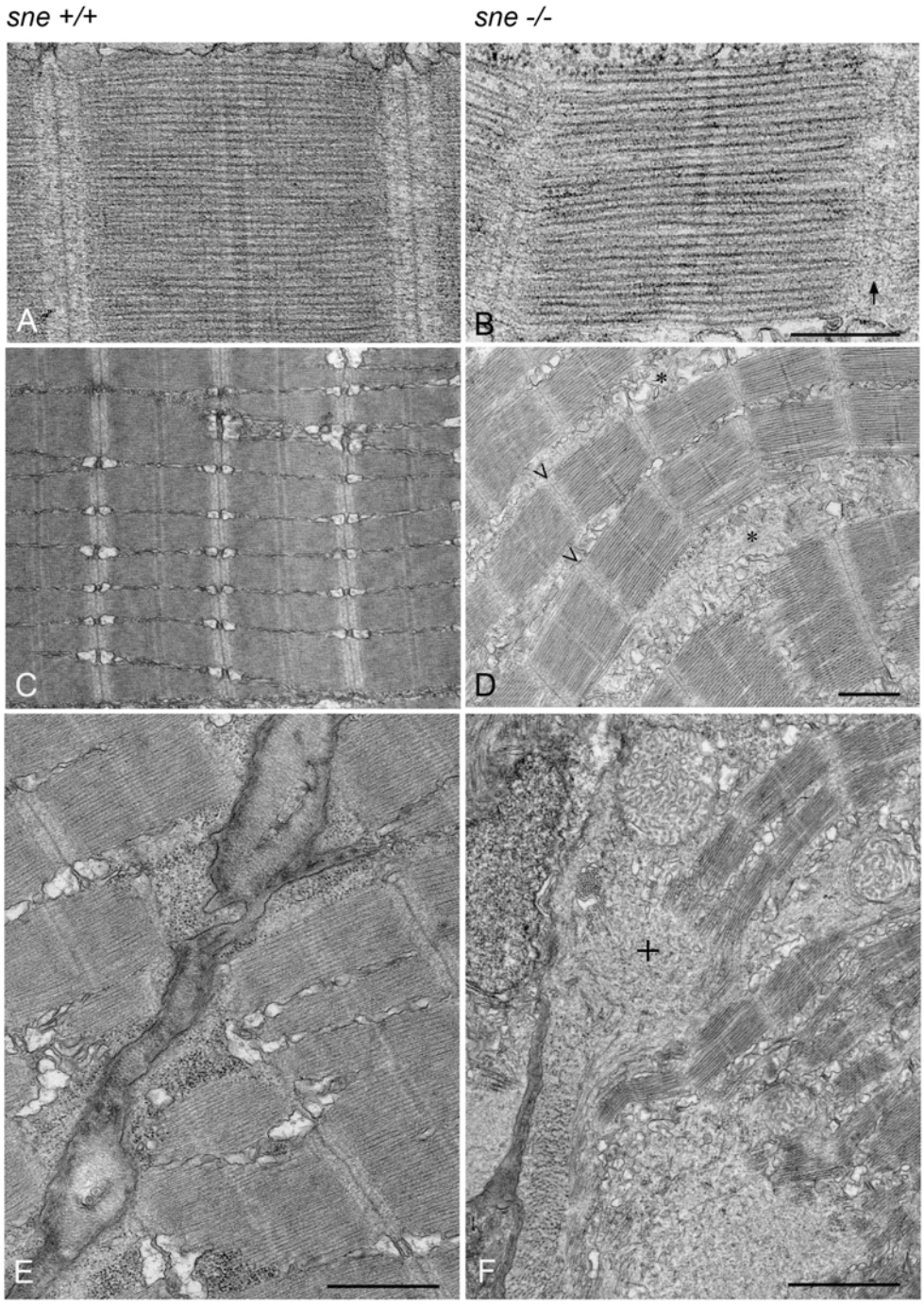

Fig.4.20. TEM of skeletal muscle in *sne* wild-type sibling (A, C and E) and mutant (B, D and F) 5 dpf embryos. Arrow in B indicates the remnants of Z-line in the mutant. Arrowheads in D point to the misalignment of Z-lines between myofibrils and asterisks indicate the accumulation of sarcoplasmic reticulum. Cross in F indicates the accumulations of protein adjacent to the myoseptum boundary. Scale bar for A and B=660nm, C and D=1364nm, E=1480nm and F=2960nm.

many sarcomeres the Z-line is not well defined compared to wild-type embryos and appears much more diffuse. Additionally, in some sarcomeres the Z-lines have partially disintegrated. In some regions the Z-lines are not aligned between myofibrils and sarcoplasmic reticulum has accumulated between myofibrils (Fig. 4.20D). The wavy myofibrils that were observed by immunostaining are also detected by TEM and these images suggest that the myofibrils are separating from each other and breaking apart. The myosepta in the *sne* mutant are also less distinct than the wild-type embryos and sarcomeres that had attached directly to the myoseptum were not observed. Instead, un-incorporated protein aggregates, most likely to be F-actin and/or α-actinin (which were observed in the immunostaining) accumulate adjacent to the myoseptum (Fig. 4.20F).

To determine whether sarcomere size is affected in the *sne* mutants, the length of each sarcomere was measured and compared to wild-type sarcomere length. The sarcomeres were measured from the TEM images using Zeiss Axiovision Rel. 4.5 software. Sixty nine and seventy sarcomeres from one wild-type sibling and one mutant 5 dpf embryo were measured respectively. Surprisingly, the *sne* mutants have significantly shorter sarcomeres compared to their wild-type siblings, and the confidence interval (99%) calculated for wild-type (2738nm +/- 178nm) and mutant (1747 nm +/- 180.6nm) sarcomere lengths were not overlapping. The box and whisker plot shown in Fig. 4.21 indicates that the range of sarcomere length in both the mutant and the wild-type is actually very small (wild-type: 2640.6nm - 2902.2 nm, mutant: 1614.4nm - 1887.9nm). However, additional measurements of sarcomere widths from a greater number of samples will need to be performed to substantiate this finding.

The TEM analysis on the *sne* mutants has revealed that although the main components of the sarcomere are present there remain significant defects in muscle ultrastructure; in particular in

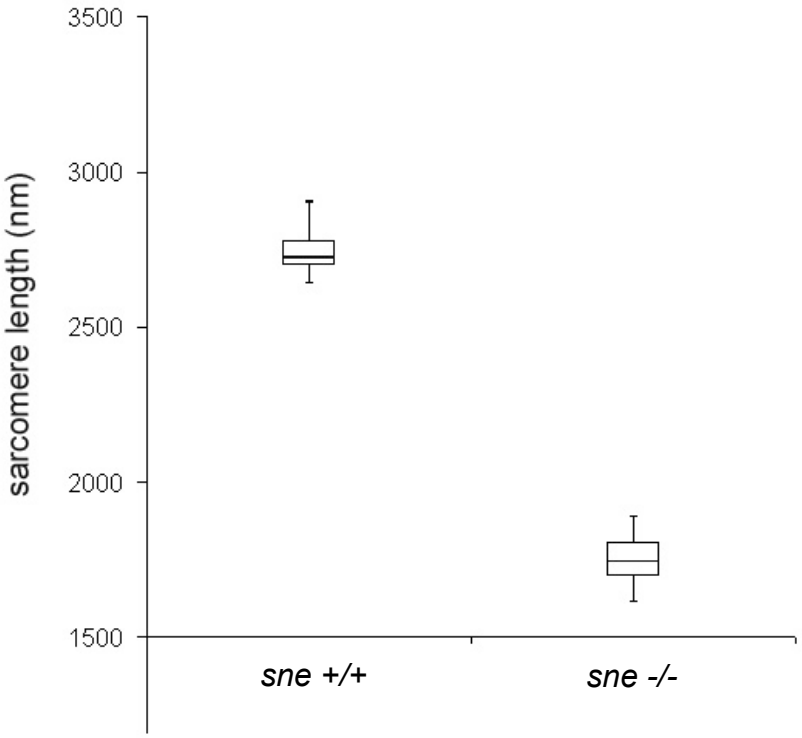

Fig. 4.21. Box and whisker plot of 5 dpf *sne* wild-type sibling and mutant sarcomere lengths. The median is indicated as the line through the centre of each box.

sarcomere length, Z-line integrity, proper myofibrillar organization, attachment and tethering to the myoseptum.

4.6 The *sne* phenotype is ameliorated by decreased muscle usage

To determine whether the *sne* mutant phenotype was enhanced by excessive muscle use, 2 day old sibling and mutant embryos (40) were grown in either just Egg water, Egg water with 0.005% tricaine or Egg water with 0.6% methyl cellulose for 3 days. Tricaine (an anesthetic) inhibits the embryos from freely swimming in the dish, however, they still twitch slightly when touched. The methyl cellulose increases the viscosity of the Egg water, thereby requiring the embryos to place greater strain on their muscles when swimming. At 5 dpf, mutant embryos in methyl cellulose are discernible from wild-type siblings. Conversely, for the embryos that were exposed to tricaine, it was difficult to distinguish mutants from wild-type siblings. Therefore mutants had to be scored using DIC microscopy to visualize the wavy myofibre phenotype. Follow-up phalloidin staining of the identified mutants, shows that the mutant embryos exposed to tricaine have straighter fibres compared to those embryos left in methyl cellulose or in normal media (Fig. 4.22). The methyl cellulose treatment did not enhance the wavy phenotype, which suggests that normal movement in water will produce the wavy myofibres. These experiments demonstrate that the *sne* phenotype is exacerbated by muscle use and they also indicate that CapZ plays an important role in maintaining the integrity of the myofibrillar architecture.

4.7 Discussion

Two *capzα* isoforms were found in the zebrafish genome that share high homology and identity in their DNA and protein sequences. Various comparison tools were utilized to examine

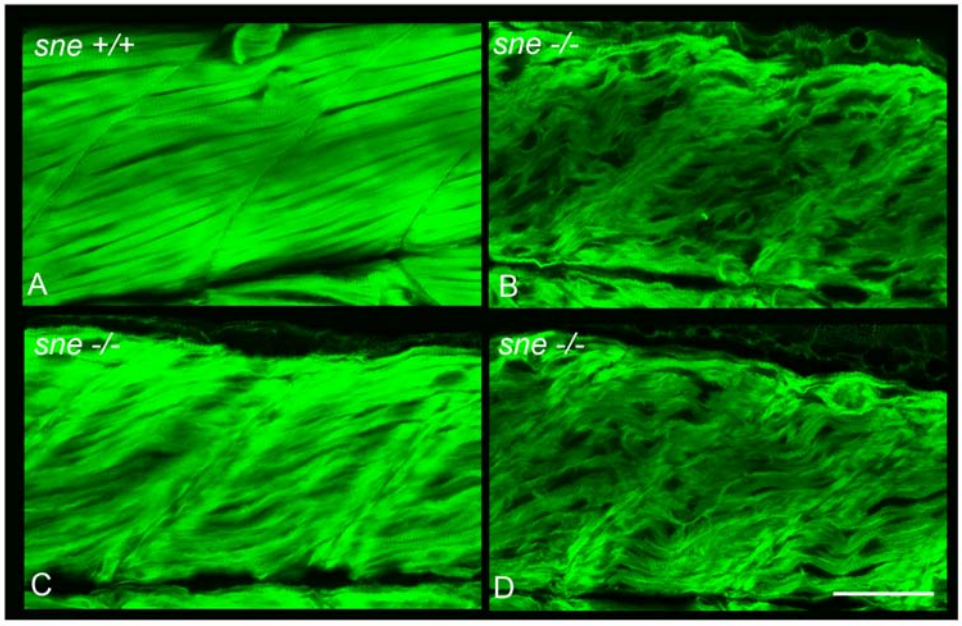

Fig. 4.22. Phalloidin staining of 5dpf *sne* wild-type sibling and mutant embryos grown in Egg water with the addition of methyl cellulose (0.6%) or tricaine (0.005%) from day 2 to day 5 of development. A) Wild-type sibling embryo grown in tricaine B) *sne* mutant embryo grown in Egg water only, C) *sne* mutant embryo grown in tricaine and D) *sne* mutant embryo grown in methyl cellulose. Scale bar= 44.36μm.

homology between zebrafish *capzα* subunits and those of other species to establish conclusively the nomenclature of the isoforms in zebrafish. Synteny proved to be the major deciding element in identifying that *capzα1* in zebrafish was indeed located on chromosome 8; the site of the *sne* locus.

The high amino acid sequence identity shared between the two α isoforms raises the possibility that these proteins may be partially redundant in zebrafish. Indeed, the RNA *in situ* expression pattern of *capzα1* and *capzα2* is ubiquitous until 24 hpf, and thus supports the hypothesis that the α subunits may have overlapping functions in the early stages of development. However, by 24 hpf the *capzα1* and *capzβ* expression patterns become stronger in the somites, while the expression pattern for *capzα2* becomes weaker throughout the trunk of the embryo. The differences in staining pattern between the α subunits in the later stages of development could therefore suggest that the α1 subunit predominantly functions in skeletal muscle while the α2 subunit functions in non-muscle cells. Studies performed by Shafer and colleagues in 1994 found that the β subunits are differentially localized in cardiomyocytes and striated muscle cells (the β1 subunit localized to Z-lines and the β2 subunit localized to the intercalated disc and cell-cell junctions), and are therefore thought to have distinct functions *in vivo* (Hart and Cooper, 1999). This feature may also be shared by the α subunits and localization studies of CapZα1 and CapZα2 will no doubt assist in determining whether the α subunits also have non-redundant functions in muscle tissues. As yet it is unclear whether each α subunit is able to bind to more than one β subunit *in vivo*. If this can be proved then one could speculate that the dimerization of different subunit combinations enables CapZ to take on different functions. It is evident that further in-depth analysis is required to fully determine the function of the α subunits and their interactions with the CapZβ isoforms.

A fully functional CapZ protein requires the dimerization of the α subunit with the β subunit. In chicken, mouse and human at least two isoforms of *capzβ* exist, however, in zebrafish only one *capzβ* isoform has been identified. Comparison of the zebrafish CapZβ with its orthologues indicates that it has greater similarity to the β2 isoform than the β1 isoform. RT-PCR was unsuccessful in establishing whether the capzβ1 isoform is also expressed in zebrafish embryos, however, it seems likely that a β1 isoform would exist in zebrafish as two α1 isoforms have been identified. Additionally, the β1 isoform has been reported to be the predominant isoform expressed in muscle, while the β2 isoform is predominantly expressed in non-muscle tissues (Hart et al., 1997b; Schafer et al., 1994). Further investigation into whether a β1 isoform is expressed in zebrafish by genomic re-sequencing of *capzβ* is required to determine whether a second subunit is also encoded in the zebrafish genome.

The most striking morphological feature of the *sne* mutants are the undulating wavy muscle fibres, which are clearly visible following immunostaining of actin filaments and Z-lines. These initial results reveal that F-actin and α-actinin are partly able to localize to the correct regions within skeletal muscle, however, unincorporated accumulations of both these elements were observed adjacent to the myoseptum. TEM images of skeletal muscle in *sne* mutants also reveal that although most of the sarcomeric components are formed, the Z-lines appear to be disintegrating and the highly ordered architecture of the myofibrils and their attachment to the myosepta are lost. The length of each sarcomere in mutants was also shorter than in wild-type siblings. Additionally, inhibition of movement of mutant embryos by anaesthetizing them in tricaine partially rescued the wavy muscle phenotype observed in the *sne* mutant. The phenotypic analysis of this mutant therefore strongly suggests that the mutation in *capZα1* results in the loss of muscle stability and integrity.

No discernible differences in the RNA expression levels of *capzα1* were observed between 24 hpf *sne* sibling and mutant embryos, which suggests that the mutation does not result in RNA degradation of the mis-spliced *capzα1* products, although it is noted that *in situ* hybridizations only give a semi-quantitative view of expression levels. Notably, wholemount antibody staining with a CapZα1 polyclonal antibody supported the RNA *in situ* hybridization results, and revealed that a mutant form of CapZα1 was translated in the *sne* mutants. However, the striated staining pattern in skeletal muscle, characteristic of localization to the Z-line was not observed. Instead, CapZα1 was mis-localized and had aggregated in clumps adjacent to the myoseptum. Intriguingly, the aberrantly localized CapZα1 co-localized with accumulations of α-actinin, also found adjacent to the myoseptum in the mutants. This result suggests that although the mis-spliced transcripts of *capzα1* are translated they are unable to localize to the Z-line, therefore in terms of participating in capping the barbed end of the thin filament within the sarcomere, they are likely to be non-functional. The main questions arising from these experiments are: 1) To what extent is the function of the mis-spliced CapZα1 isoforms deteriorated? E.g. can they still bind to the β subunit? 2) Which mis-spliced transcripts are translated? 3) Is the α2 subunit capable of compensating for the lack of a fully functional CapZα1? In the following chapter I attempt to address these questions by MO and Western analysis.

The overall findings of the examination of the *sne* mutant phenotype are consistent with a model where muscle differentiation and sarcomere assembly does take place in these mutants, however, the loss of functional CapZ destabilizes the link between the actin filament and the Z-line, and as the muscle starts to function the connection is no longer strong enough to endure the continual force placed on the sarcomere by the sliding of the filaments during muscle contraction. Thus the sarcomeric structure gradually disintegrates and induces destabilization of the myofibrillar structure, resulting in wavy myofibres and misaligned Z-lines observed in the *sne*

mutant. These results suggest that CapZ is important in the maintenance of myofibrillar organization, enabling sarcomeres to withstand the pressure applied during muscle contraction.

The subunits of CapZ are highly conserved in vertebrates and undoubtedly play important roles in development. The phenotypic analysis of the *sne* mutant indicates that CapZ is integral to the maintenance of skeletal muscle structure.

Chapter 5

MO Knockdown of CapZ Subunits and Confirmation of *sne* Positional Cloning

Chapter 5: MO Knockdown of CapZ Subunits and confirmation of *sne* positional cloning

5.1 Summary

In this chapter antisense morpholino oligonucleotides (MOs) were used to: 1) examine the functions of the various CapZ subunits, 2) determine the extent of CapZα1 function in the *sne* mutant and 3) confirm that the mutation in *capzα1* is the cause of the *sne* mutant phenotype. Unfortunately, MO analysis of CapZα2 function was inconclusive in determining whether it was partially redundant to CapZα1. Interestingly, severe developmental defects, much worse than the *sne* mutant phenotype, were observed from complete ablation of CapZ (either by injection of high doses of capZβ MO or knockdown of both α subunits). These findings indicate that the mutation in *sne* does not completely ablate CapZ function, and suggests that the *sne* mutant is hypomorphic. Western analysis performed to conclusively determine which different transcripts were translated in the *sne* mutant was unsuccessful. Finally, the morphants (that is MO injected embryos) generated from the knockdown of the various CapZ subunits confirm that the *sne* phenotype is caused by a mutation in *capzα1*. Moreover, the CapZα1 morphant phenotype is partially rescued by over expression of *capzα1*-GFP.

5.2 Introduction

Very little is known about the role of CapZ in vertebrate development and only a handful of studies have looked at CapZ in an *in vivo* context. CapZ is able to cap the barbed end of actin filaments that are localized in all cell types. Indeed, actin filaments are involved in many different processes including cell motility, cytokinesis and are integral to the cellular cytoskeleton. It is therefore likely that CapZ plays an important role in controlling actin dynamics early in development, where gastrulation cell movements are critical to embryogenesis. In order to gain a

greater understanding of how CapZ is involved in development, MO knockdowns on one or more of the CapZ subunits were performed. The MOs were also used to investigate the extent of function of the mis-spliced forms of CapZα1 in the *sne* mutants, as well as to determine whether the *sne* mutant phenotype could be replicated by knockdown of CapZα1. Western blotting was performed to identify which transcripts were translated in the mutant and to verify the effectiveness of each MO. Finally, a *capzα1*-GFP fusion construct was generated to confirm the localization of CapZα1 *in vivo* and to rescue a capZα1 morphant with exogenous CapZα1.

5.3 MO knockdown of the CapZ subunits

In the previous chapter antibody staining revealed that the mis-spliced forms of CapZα1 were translated in the mutants. MOs against all the CapZ subunits were therefore used to determine firstly, whether the mutant forms of CapZα1 were functional. Secondly, to confirm that the *sne* phenotype was indeed a result of the mutation in *capzα1*, and finally to ascertain whether CapZα2 could compensate for the loss of CapZα1. MOs that targeted the start site and splice sites of each subunit (*capzα1*, *capzα2* and *capzβ*) were designed to look at the effect of knocking down the zygotic contribution (splice MO) versus the maternal and zygotic contribution (ATG MO). The sequences of all MOs used are listed in Table 1, Chapter 2, and the target sites for the MOs are illustrated in Fig. 5.1. See appendix, Table 4 for the number of experiments performed with each MO.

5.3.1 MO knockdown of CapZα1

Initially, CapZα1 was completely knocked down with an ATG or splice 1 MO to determine whether the *sne* phenotype could be replicated. However, as suspected, the morphant embryos had a more severe phenotype than the *sne* mutant. Injection of capZα1 ATG MO (5ng) resulted in embryos that were developmentally delayed, had smaller brains and eyes, less

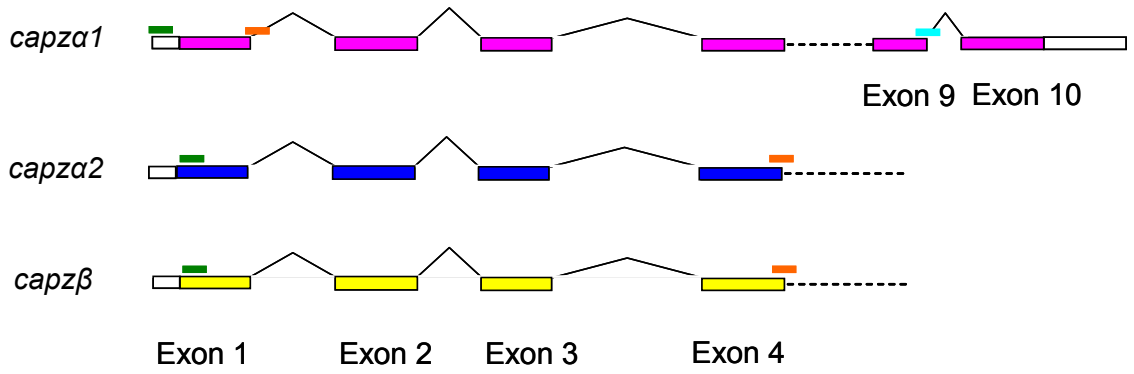

Fig. 5.1. Schematic diagram of MO target sites for *capzα1*, *capα2* and *capzβ*. The green bars represent the target sites for the ATG MOs, the orange bars represent the target site for the splice 1 MOs and the blue bar represents the target site for the MO that phenocopies the mutation in the *sne* mutant (capZα1 splice 2). Blocks that are not coloured are UTRs.

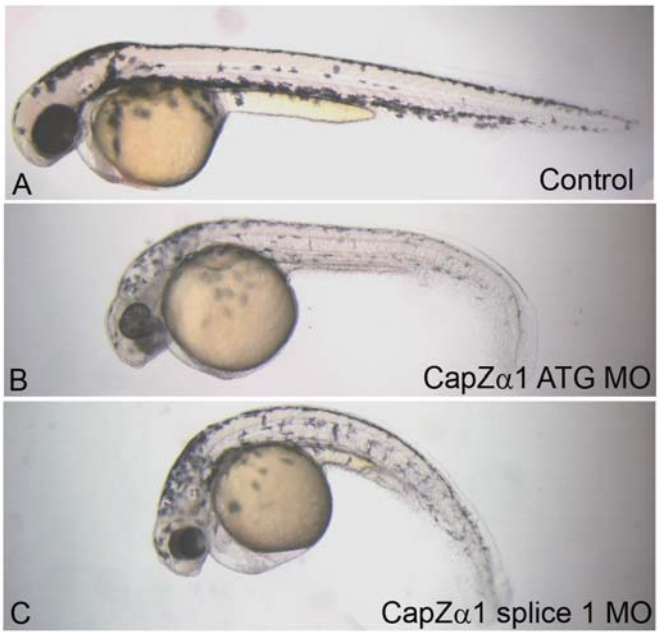

Fig. 5.2. 48 hpf embryos injected with a capZα1 ATG and splice 1 MO. A) Buffer injected control, B) 5ng of capZα1 ATG MO, C) 4ng of capZα1 splice 1 MO.

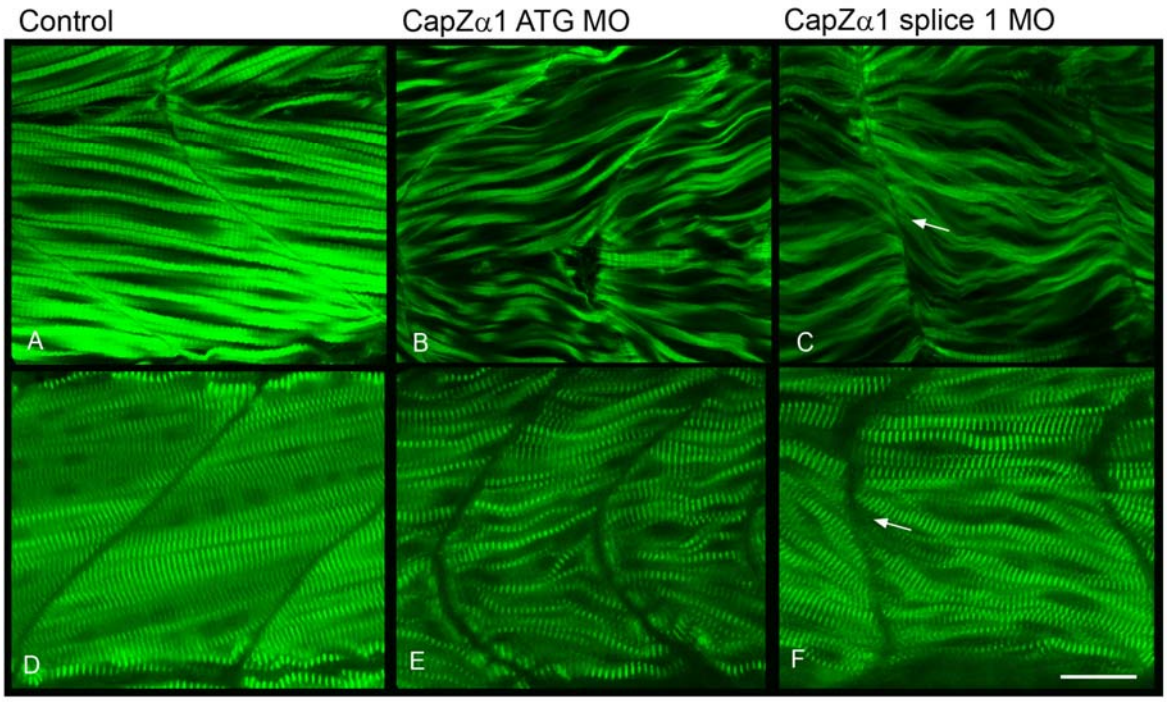

Fig. 5.3. Phalloidin and α-actinin immunostaining of 48 hpf embryos injected with capZα1 ATG and splice 1 MO. A-C) Phalloidin staining, D-F) α-actinin staining. A and D) Buffer injected control, B and E) 5ng of capZα1 ATG MO, C and F) 4ng of capZα1 splice 1 MO. Arrows in C and F indicate the U-shaped myoseptum. Scale bar = 22.18μm.

pigment, and shorter axes compared to buffer injected control embryos by 48 hpf (Fig. 5.2A and B). The somites and notochord had formed, however, the morphants were much slower to respond when prodded. The capZα1 splice 1 MO (4ng, targeted against the exon 1 donor splice site) produced a similar phenotype to the ATG MO. The splice morphants also had smaller brains and eyes, less pigment and shorter axes at 48 hpf, however, their tails were substantially more curved than the ATG morphants. Moreover, the splice morphants had acquired heart edemas (Fig. 5.2C).

Closer inspection of the skeletal muscle by phalloidin staining revealed that although F-actin had assembled within the myofibres, the filaments were wavy in both ATG and splice 1 morphants compared to the buffer injected controls at 48 hpf (Fig. 5.3A-C). The myosepta of the capZα1 splice 1 morphants also appeared u-shaped compared to the ATG morphants or the controls. α-Actinin antibody staining on both these morphants indicated that Z-lines had formed and α-actinin had localized correctly to the Z-line (Fig. 5.3D-F). This staining pattern also highlighted the presence of wavy myofibres in the morphants.

By day 5 the capZα1 splice 1 morphants were more severely affected compared to the ATG morphants. The splice 1 morphants were immotile and severely truncated with curved tails, very small brains and large heart edemas. Conversely, the ATG morphants had recovered from the effects of the MO and were comparable to controls, however, their swim bladders had not inflated and they did not respond as quickly to touch (Fig. 5.4). Phalloidin and α-actinin antibody staining of the skeletal muscle at this stage indicated that the wavy myofibres were still present. Interestingly, unlike the *sne* mutants, accumulations of mis-localized α-actinin were not observed at the myosepta (Fig. 5.5).

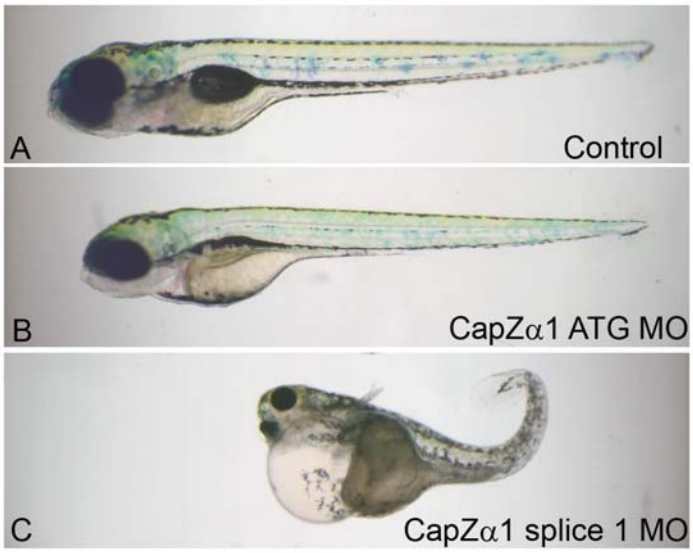

Fig. 5.4. Live images of 5 dpf embryos injected with capZα1 ATG and splice 1 MO. A) Buffer injected control, B) 5ng of capZα1 ATG MO, C) 4ng of capZα1 splice 1 MO.

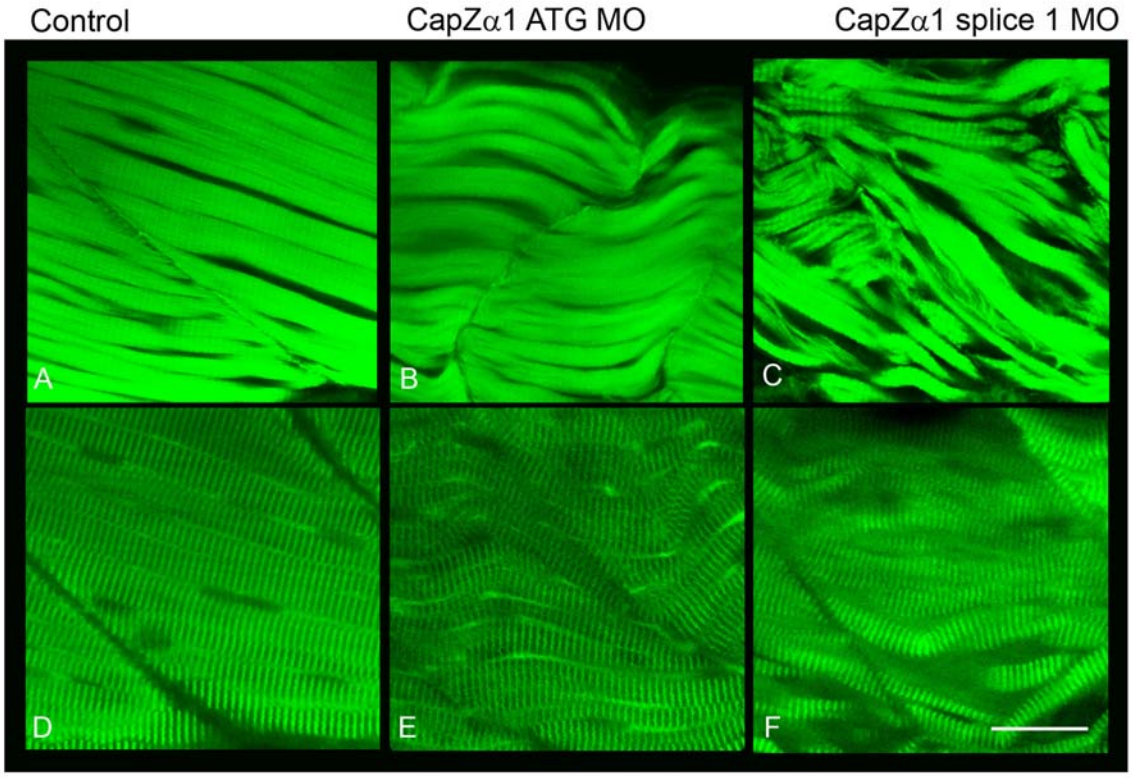

Fig. 5.5. Phalloidin and α-actinin staining of 5 dpf embryos injected with capZα1 ATG and splice 1 MO. A-C) Phalloidin staining, D-F) α-actinin staining. A and D) Buffer injected control, B and E) 5ng of capZα1 ATG MO, C and F) 4ng of capZα1 splice 1 MO. Scale bar = 22.18 μm.

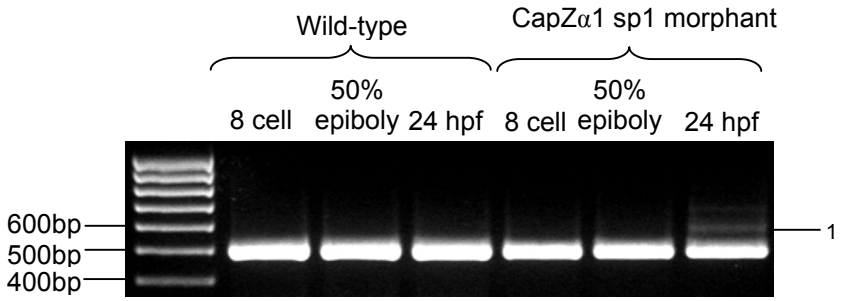

A

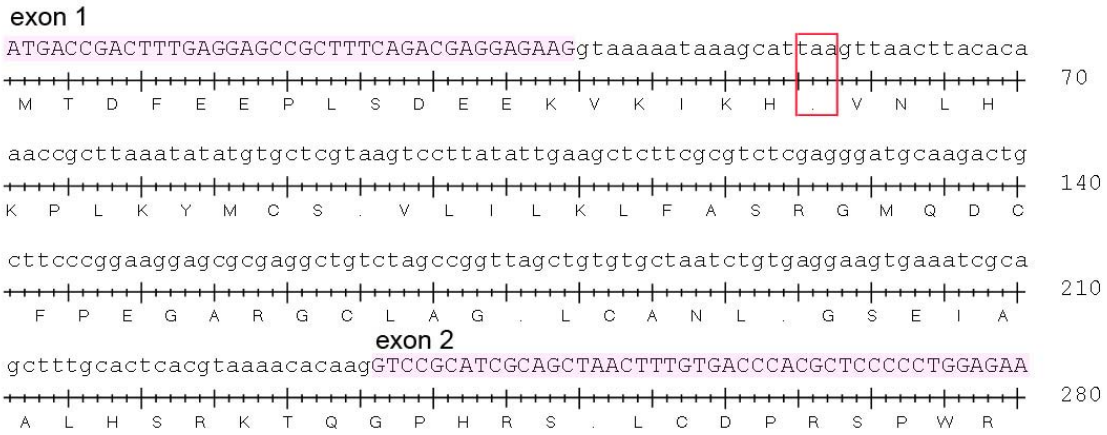

B

Fig. 5.6.A) Gel of *capzα1* RT-PCR products from cDNA of capZα1 splice 1 morphants taken at 8 cell, 50% epiboly and 24 hpf. The aberrant splice transcript (1) was observed in the 24 hpf sample only. B) DNA sequence and predicted translated protein product of the aberrant transcript cloned from the RT-PCR product (1) shown in A. The capZα1 splice 1 MO induces a mis-splicing event to occur within intron 1 and therefore the resulting protein product encodes a stop after 18 amino acids (indicated by the red box).

To verify the effectiveness of the capZα1 splice 1 MO, RT-PCR on RNA extracted from splice 1 morphants at different stages was performed, and confirmed that the splice 1 MO produces an aberrant splice transcript (Fig. 5.6A). Sequencing of this product revealed that the MO blocked splicing at the exon 1 donor splice site and induced splicing at an alternative splice site within intron 1, therefore resulting in aberrant transcription of 196bp of the intron (Fig. 5.6B). The predicted protein product from this transcript contains a termination codon 4 amino acids after translation of the transcribed intronic region, producing a truncated product of 18 aa that is unlikely to be functional.

To precisely replicate the effect of the mutation in the *sne* mutant a capZα1 splice 2 MO was designed to target the exon 9 donor splice site. Injection of 10ng of this MO produced morphants with a very similar phenotype to the *sne* mutant. On day 2, embryos appeared grossly normal compared to buffer injected controls, however, phalloidin and α-actinin staining of skeletal muscle tissue revealed that the myofibres were wavy (Fig. 5.7). At 5 dpf a similar phenotype was observed, where the MO injected embryos appeared grossly normal compared to buffer injected controls, however, lacked a swim bladder. The wavy actin filaments were also apparent by phalloidin and α-actinin staining (Fig. 5.8). Moreover, although α-actinin had localized to the Z-lines, it had also accumulated in large clumps adjacent to the myoseptum in the capZα1 splice 2 morphants.

RT-PCR was performed on cDNA from capZα1 splice 2 morphants to confirm that the MO blocked splicing at the exon 9 donor splice site (Fig. 5.9). Sequencing of the cloned RT-PCR products identified that two out of the three mis-spliced transcript isoforms expressed in the mutant were also observed in the capZα1 splice 2 morphant; the deletion of exon 9 and the addition of 46bp of intron 9. The capZα1 splice 2 morphant phenotype and the RT-PCR results

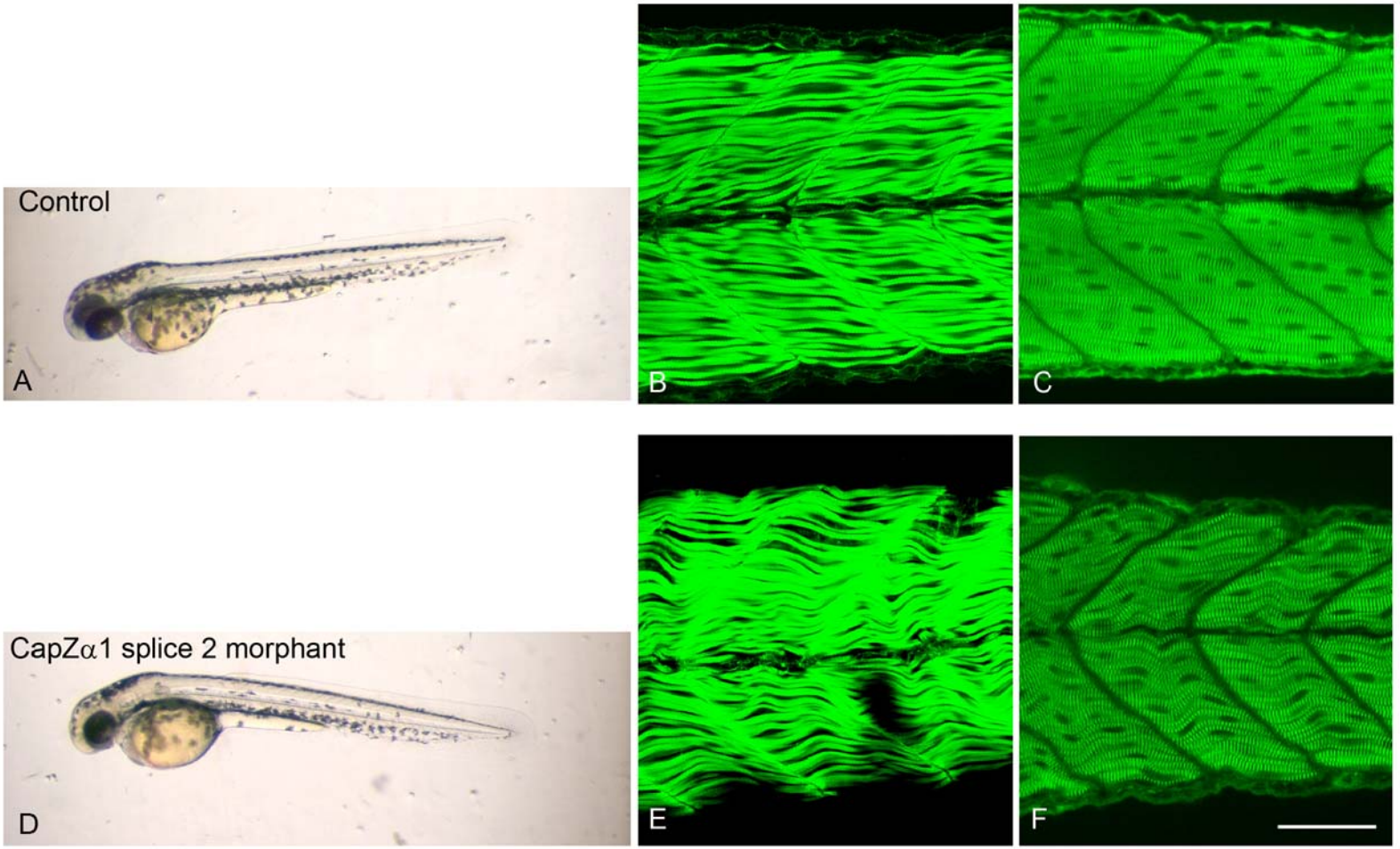

Fig. 5.7. Morphology of 2 dpf capZα1 splice 2 morphants. A-C) Buffer injected control, D-F) 10ng of capZα1 splice 2 MO, A and D) live images, B and E) phalloidin staining, C and F) α-actinin staining. Scale bar = 44.36 μm.

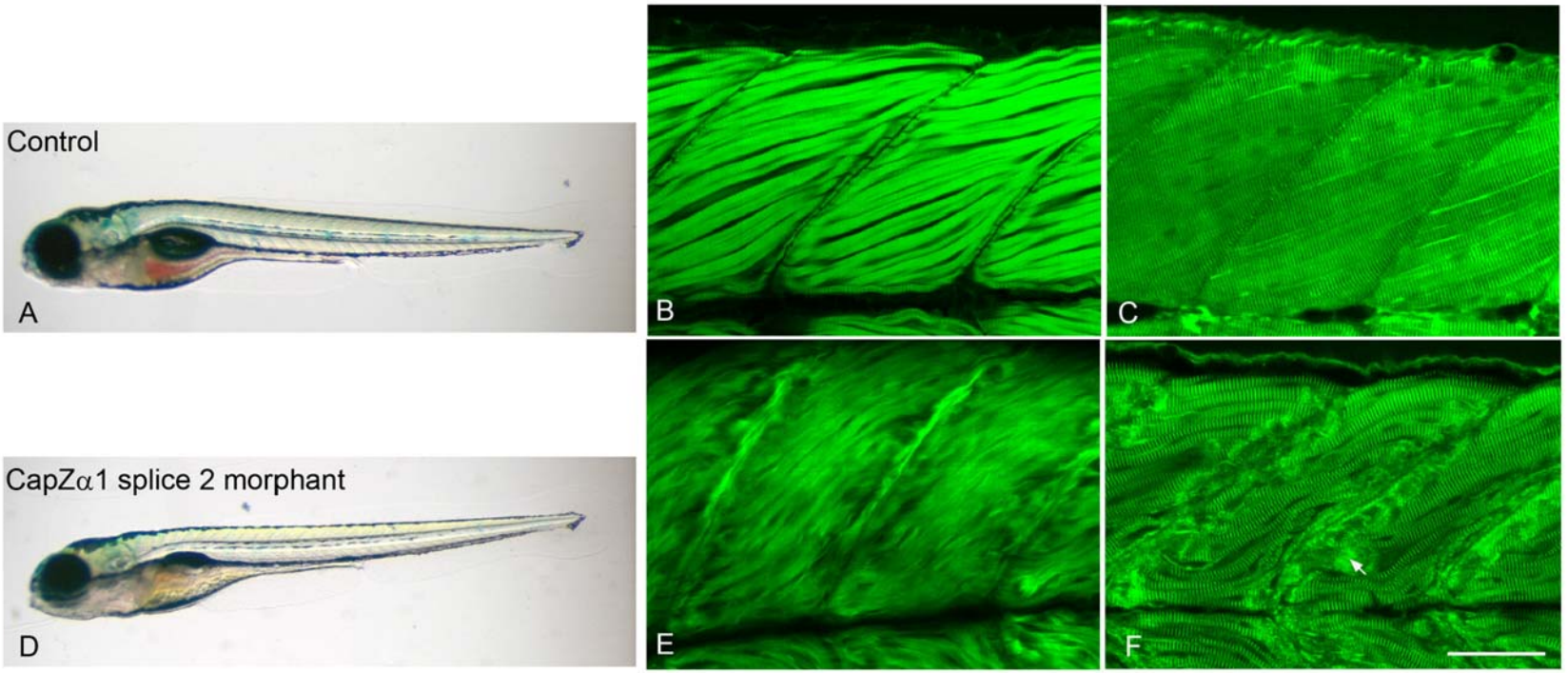

Fig. 5.8. Morphology of a 5 dpf capZα1 splice 2 morphant. A-C) Buffer injected control, D-F) 10ng of capZα1 splice 2 MO, A and D) live images, B and E) phalloidin staining, Cand F) α-actinin staining. Scale bar = 44.36μm. Arrow in F indicates the ectopic accumulation of α-actinin adjacent to the myoseptum.

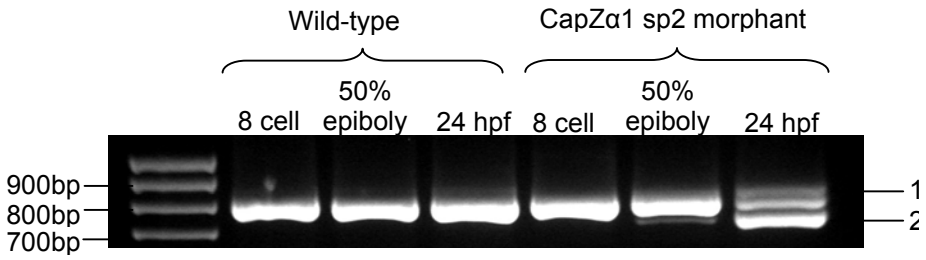

Fig. 5.9. Gel of *capzα1* RT-PCR products from cDNA of capZα1 splice 2 morphants taken at 8 cell, 50% epiboly and 24 hpf. The aberrant splice transcripts were observed in the 50% epiboly (2) and 24 hpf samples (1 and 2).

therefore confirmed that the mutation at the exon 9 donor splice site does indeed produce the *sne* mutant phenotype.

To confirm that the CapZα1 ATG and splice 1 MOs were effective in dramatically reducing CapZα1 protein levels, and also that the splice 2 MO would induce mis-localization of CapZα1, CapZα1 antibody staining on all morphants was performed. At 5 dpf there was a reduction in the localization of CapZα1 at the Z-line in all morphants (Fig. 5.10). Accumulation of CapZα1 at the myosepta was particularly prevalent in the splice 2 morphants. Unfortunately, CapZα1 antibody staining was not successful at earlier stages, therefore I was unable to observe the full effect of the MOs on CapZα1 expression and localization earlier in development. By day 5 MOs tend to be less effective, and as a result normal localization of CapZα1 was observed at the Z-line in some myofibrils of the morphants. Moreover, as the CapZα1 antibody is polyclonal, very high background levels were detected, making confocal imaging and interpreting the levels of protein difficult. Nevertheless, staining of the morphants at this stage provided circumstantial evidence that the MOs used were effective at reducing the levels of CapZα1.

Knockdown of CapZα1 using different MOs has provided some preliminary clues as to the nature of the *sne* phenotype. It was speculated that the *sne* mutant may have a milder phenotype due to the maternal contribution of CapZ, however, this is clearly not the case as the early splice MO (splice 1, which does not knockdown the maternal contribution) gives the same phenotype as the ATG MO (which knockdowns maternal contribution). As the early splice morphant also produces a more severe phenotype than late splice (splice 2), this also indicates that the aberrant protein product that is produced in the mutant and has some partial function.

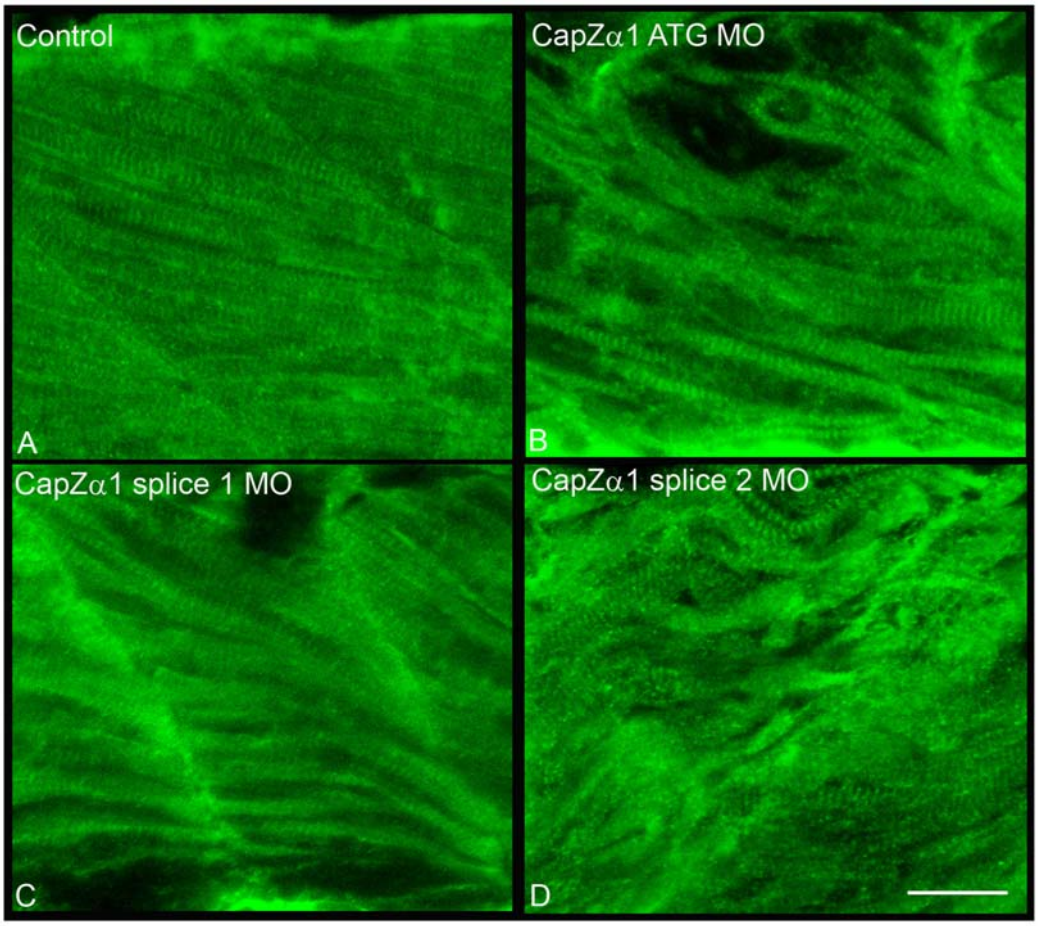

Fig. 5.10. CapZα1 antibody staining of capZα1 morphants at 5 dpf. A) Buffer injected control, B) 5ng of capZα1 ATG MO, C) 4ng of capZα1 splice 1 MO, D)10ng of capZα1 splice 2 MO. Scale bar = 22.18μm.

5.3.2 MO knockdown of CapZα2

To determine whether CapZα2 also plays a role in compensating for a lack of completely functional CapZα1 in the *sne* mutant, an ATG and splice MO were designed to knockdown the α2 subunit. Intriguingly, the capZα2 ATG and splice MOs produced quite variable phenotypes. Injection of only 1.5ng of the capZα2 ATG MO caused severe developmental defects. By 24 hpf the embryos were severely delayed and had a smaller brain and eyes, as well as u-shaped somites, however, side to side movement of the tail was still observed. By 48 hpf the ATG morphants had a shortened axes, smaller brains, curved tails, heart edemas and less pigment compared to controls (Fig. 5.11A and C), and by day 5 most of the morphants had not survived. Unexpectedly, injection of 6ng of the capZα2 splice MO did not affect the morphology of injected embryos. At 48 hpf they swam normally and had very straight axes, although their brains were slightly smaller and reduced pigmentation levels were observed compared to controls (Fig. 5.11B). On day 5 the splice morphants still had a similar morphology to buffer injected embryos (Fig. 5.11D and E).

Phalloidin and α-actinin staining of these morphants revealed that actin filaments and Z-lines had formed in the ATG morphant, however, the actin filaments were not as straight as the wt equivalents on day 2 (Fig 5.12C and F). As expected from its gross morphology, the staining pattern of the splice morphant was indistinguishable from the wt on both day 2 (Fig. 5.12B and E) and day 5 (Fig. 5.13A-D). CapZα1 antibody staining also indicated that CapZα1 was normally localized to the Z-line on day 5 in the splice morphant (Fig. 5.13E and F).

5.3.2.1 The CapZα2 ATG MO knocks down CapZα1

The capZα2 ATG MO sequence only differs by 4bp to the coding region surrounding the ATG of *capzα1*. According to the MO manufacturer this difference should be sufficient to ensure

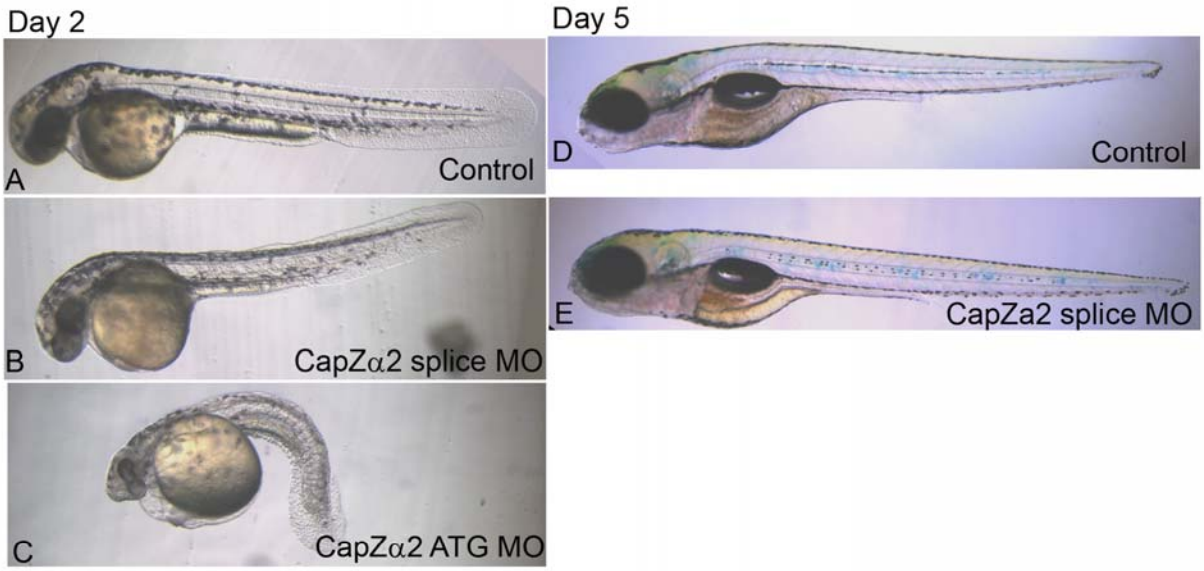

Fig. 5.11. Day 2 (A-C) and day 5 (D-E) live images of capZα2 ATG and splice morphants. A and D) buffer injected control, B and E) 6ng of capZα2 splice MO and C) 1.5ng of capZα2 ATG MO.

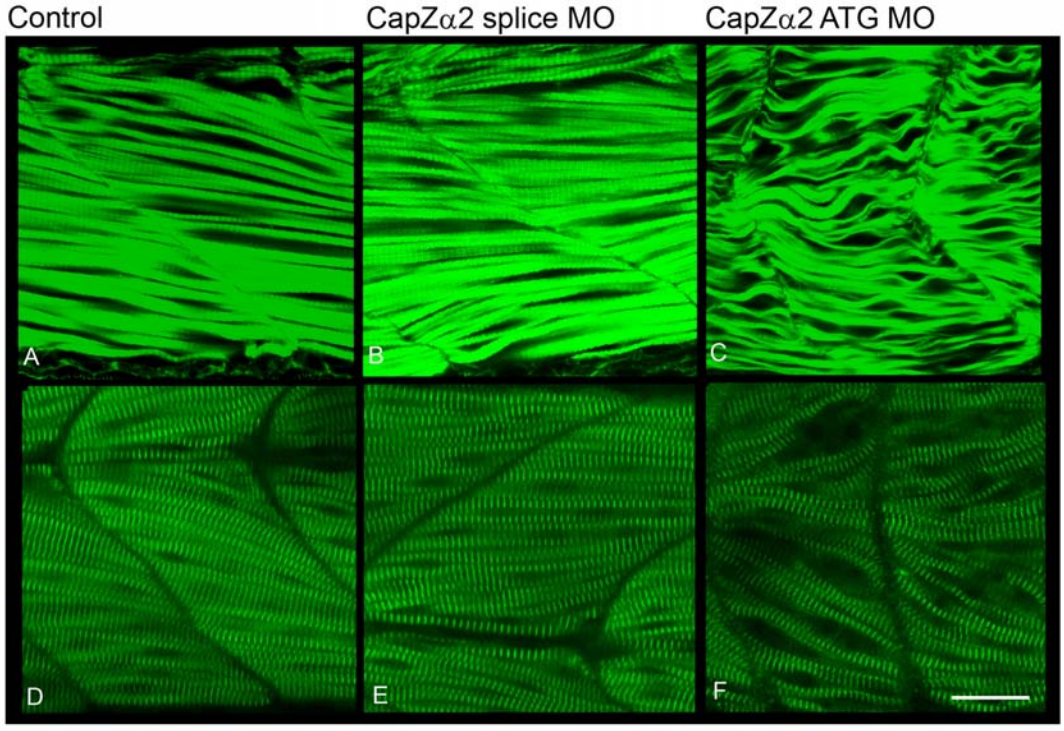

Fig. 5.12. Phalloidin (A-C) and α-actinin staining (D-F) of day 2 capZα2 ATG and splice morphants. A and D) buffer injected control, B and E) 6ng of capZα2 splice MO, C and F) 1.5ng of capZα2 ATG morphant. Scale bar = 22.18 μm

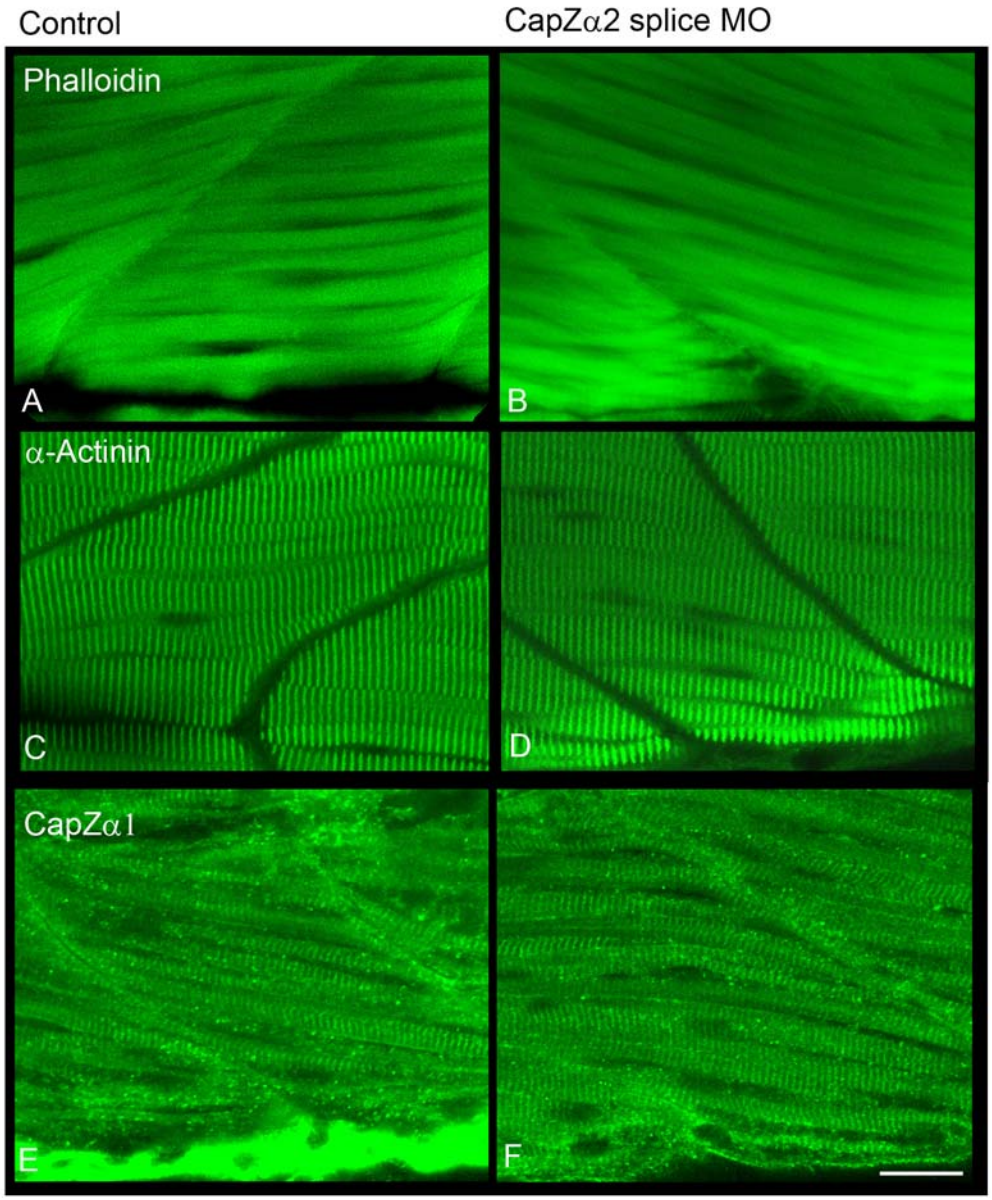

Fig. 5.13. Phalloidin A and B), α-actinin C and D) and CapZα1 staining E and F) on 5 dpf capZα2 splice morphants.A, C and E) buffer injected control, B, D and F) 6ng of capZα2 splice MO. Scale bar = 22.18 μm.

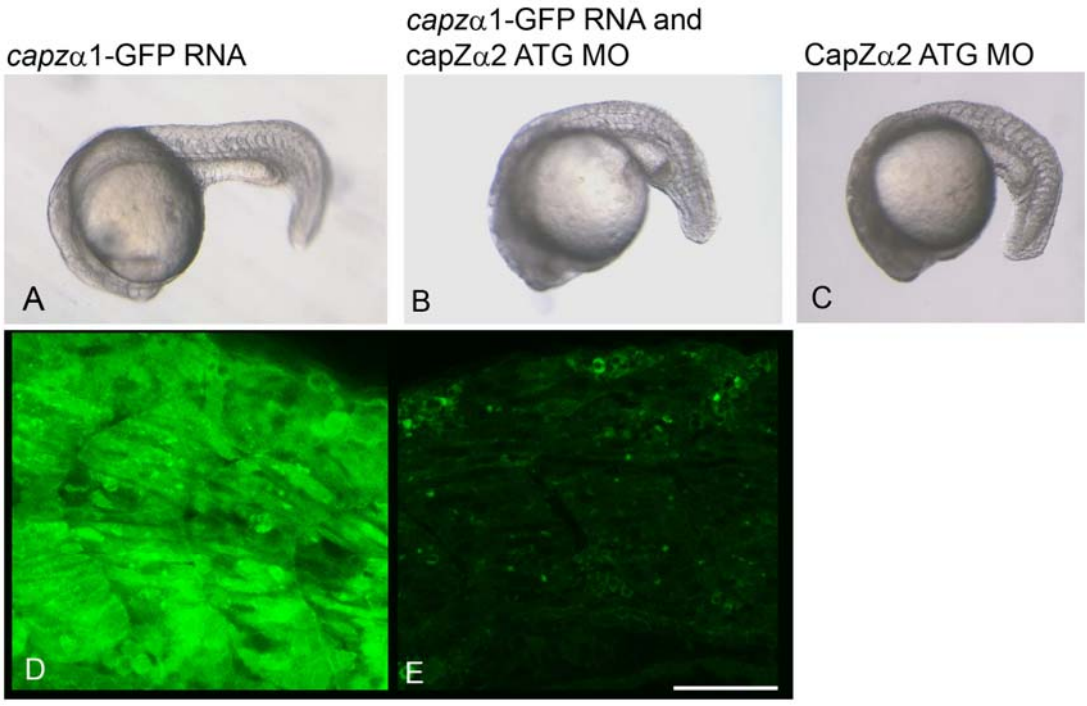

Fig. 5.14. Twenty hpf embryos that were co-injected with *capzα1*-GFP RNA and capZα2 splice MO at the 1-2 cell stage. A, B and C) live images, D and E) confocal images of embryos expressing CapZα1-GFP. A and D) Embryo injected with 150pg of *capzα1*-GFP RNA only, B and E) embryo injected with 150pg of *capzα1*-GFP RNA and 1.5ng of capZα2 ATG MO. C) Embryo injected with 1.5ng of capZα2 ATG MO only. Scale bar = 44.36 μm.

that the MO binds to a specific site. However, due to the severity of the capZα2 ATG morphant, I suspected that this MO was able to bind to the start site of both *capzα1* and *capzα2* RNA and block translation. To test this hypothesis, I co-injected *capzα1*-GFP RNA (150pg) (described in further detail in section 5.4) and capZα2 ATG MO (1.5ng) into 1-2 cell stage embryos, and after 20 hpf observed the GFP expression. Confocal imaging of the co-injected embryos indicated that addition of capZα2 MO severely reduced the translation of CapZα1-GFP (Fig. 5.14), and therefore demonstrates that the capZα2 ATG MO is also able to knockdown CapZα1.

5.3.3 MO knockdown of CapZβ

Two isoforms of *capzβ* are expressed in all tissues of higher vertebrates and are transcribed from one gene. Unfortunately, I was only able to detect the *capzβ2* isoform in zebrafish, however, it seems likely that two isoforms also exist in this species. Presuming that a *capzβ1* and *capzβ2* isoform are expressed in zebrafish, both the ATG and splice MOs designed against this gene should target each isoform, which only differ in their C-terminal region. Injection of 6ng of ATG MO did not affect the outward appearance of the injected embryo on day 2 (Fig. 5.15), however, injection of 3ng of the splice MO produced embryos with smaller brains, shorter axes, and fewer pigmented cells than the wt controls. Both the ATG and the splice morphants reassuringly produced a similar muscle phenotype to the capZα1 morphants at 48 hpf. Phalloidin and α-actinin staining at this stage revealed that in both morphants actin filaments and Z-lines had formed and the myofibrils were wavy, however, the ATG morphant myofibrils were not as wavy as the splice morphant (Fig. 5.16).

On day 5 the jaw of the splice morphants had not formed properly and the swim bladder had not inflated, but embryos moved normally (Fig. 5.17). The ATG morphants also had a

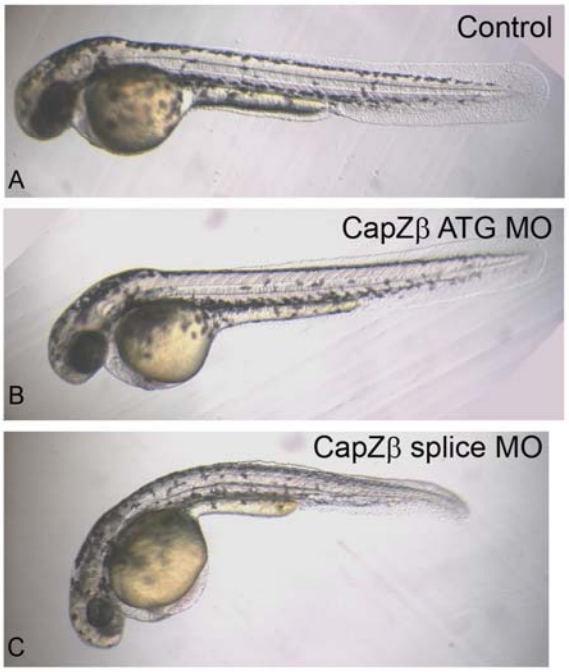

Fig. 5.15. CapZβ ATG and splice morphants at 2 dpf. A) Buffer injected control, B) 6ng of capZβ ATG MO, C) 3ng of capZβ splice MO.

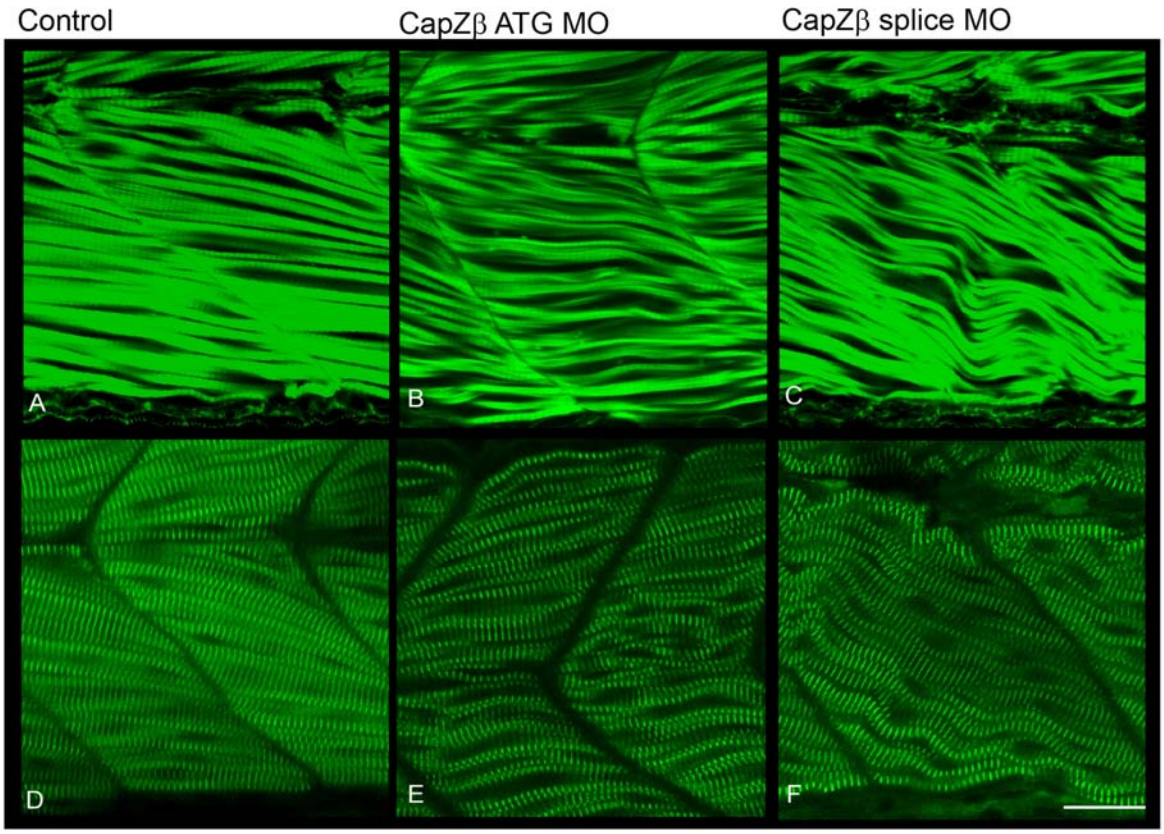

Fig. 5.16. Phalloidin (A-C) and α-actinin staining (D-F) of capZβ ATG and splice morphants at 2 dpf. A and D) Buffer injected control, B and E) 6ng of capZβ ATG MO, C and F) 3ng of capZβ splice MO. Scale bar = 22.18 μm.

deformed jaw and uninflated swim bladder. Additionally, the edges of both the dorsal and ventral fins were ragged (Fig. 5.17B arrow), which was not observed in the splice morphants. Interestingly, the ragged fin phenotype has previously been observed in a retroviral insertional *capzβ* mutant (capzβ^{hi1858bTg}) by Amsterdam et al., 2003 (Fig. 5.17D). The phalloidin and α-actinin staining pattern of the morphants on day 5 was very similar to day 2, however, the ATG morphants had much wavier myofibrils at this stage (Fig. 5.18A-F). Intriguingly, accumulations of mis-localized α-actinin at the myosepta were detected in the splice morphants and resembled the *sne* mutant phenotype.

CapZα1 antibody staining of the CapZβ ATG and splice morphants on day 5 revealed that CapZα1 was not localized to Z-line in either of the morphants and had accumulated at the myosepta (Fig. 5.18G-I). In addition to the accumulation of α-actinin at the myosepta and the wavy myofibrils, this result indicates that in the absence of CapZβ, CapZα1 is unable to localize to the Z-line. As the loss of CapZβ partially phenocopies the morphology of the *sne* mutant, it could be proposed that in the mutant, defective CapZα1 is unable to bind to CapZβ and therefore becomes mis-localized.

Higher doses of capZβ MO did induce a more severe phenotype that was similar to the double knockdown of the α subunits using the capZα2 ATG MO. Injection of 8ng of capZβ ATG MO produced embryos that were developmentally delayed with gross morphological defects. By day 5 both the capZβ and capZα2 ATG morphants suffered from heart edemas, severely truncated axes, small brains and eyes, and were immotile (Fig. 5.19). These phenotypes confirm that CapZ is non-functional if either α or β subunits are lost.

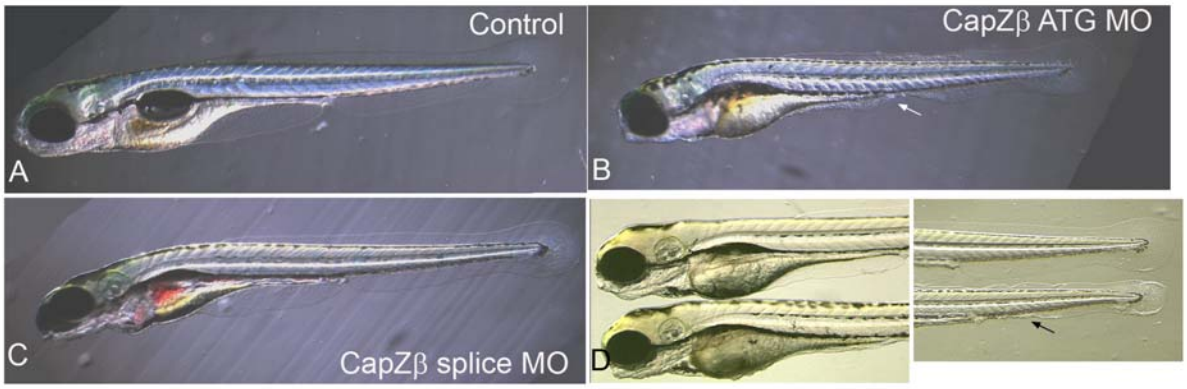

Fig. 5.17. CapZβ ATG and splice morphants at 5 dpf. A) Buffer injected control, B) 6ng of capZβ ATG MO, C) 3ng of capZβ splice MO, D) 5 dpf *capz*β retroviral mutant generated in Nancy Hopkins laboratory (image taken from Amsterdam et al., 2003). The embryo on top is wild-type and on the bottom is a mutant. Note the frayed ventral fins in the ATG morphant and the retroviral mutant (arrows).

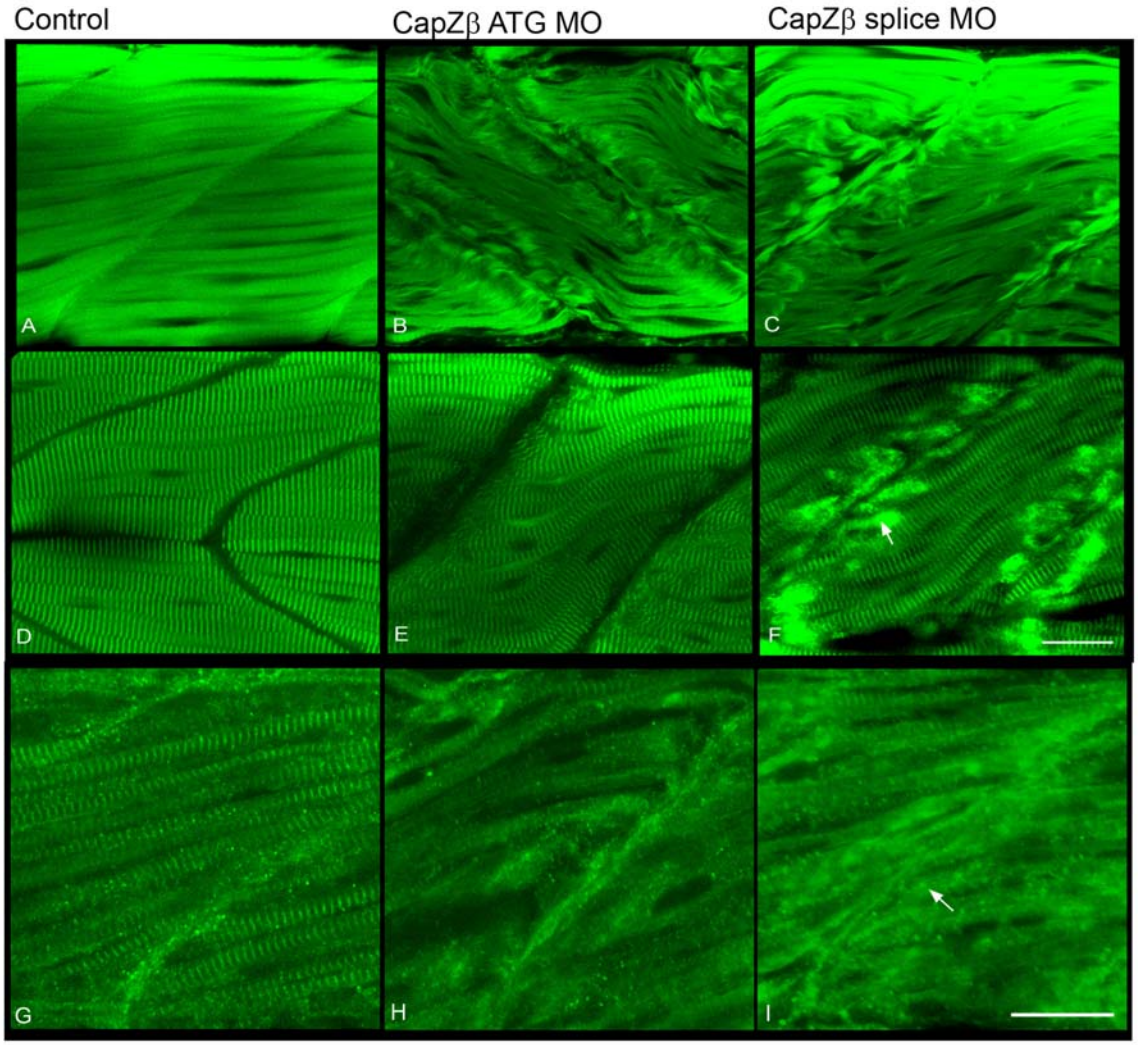

Fig. 5.18. Phalloidin (A-C), α-actinin (D-F) and CapZα1 staining (G-I) of capZβ ATG and splice morphants at 5 dpf. A, D and G) Buffer injected control, B, E and H) 6ng of capZβ ATG MO, C, F and I) 3ng of capZβ splice MO. Scale bar = 22.18 μm for images A-F and G-I.Arrows in F and I indicate accumulations of α-actinin and CapZα1 respectively.

Fig. 5.19. Live images at 5 dpf of A) a capZα2 ATG morphant (1.5ng) and B) a capZβ ATG morphant (8ng).

5.3.4 Detection of CapZα1 in mutant and morphants by Western blotting

Western blotting was performed to conclusively determine if any CapZα1 was translated in the mutant, and as an additional measure to determine the effectiveness of the MOs. As the chicken polyclonal CapZα1 antibody used in whole mount staining was not specific in the Western, a monoclonal IgG mouse CapZα antibody (BD Life sciences), targeted against the N-terminal region (1-108 amino acids) of human CapZα was used. Using this monoclonal antibody I was able to detect a single band from wild type and mutant protein extracts (Fig. 5.20A), however, the band was not of the expected size (should be ~37 kDa). It is possible that this size discrepancy is due to differences in post translational modifications between species.

Due to the similarity of CapZα1 with CapZα2 it was speculated that the antibody is able to bind to both subunits. However, as both α isoforms are of a similar size (32.73 and 32.77kDa respectively) it is unlikely that I would be able to discern differences in CapZα1 levels in a Western from a one dimensional gel. I therefore repeated the Western on protein extracted from embryos injected with either the capZα1 and/or capZα2 ATG MO: Firstly, to decipher whether the antibody bound to both α subunits and secondly, to confirm that the antibody did indeed bind to CapZ subunits. If the antibody recognized both α subunits, I would expect a reduction in the band intensity of the embryos co-injected with capZα1 and capZα2 MO. If the antibody only bound to capZα1 then there should be a reduction in the band intensity of protein extracted from the capZα1 MO injected embryo and the double knockdown. Unfortunately, no discernable differences in the levels of the band intensity were detected (Fig. 5.20B). This suggests that this antibody is not binding to CapZα at all. An alternative explanation is that as the embryos were taken at shield stage, excess maternal protein is detected and is masking the knockdown effect of

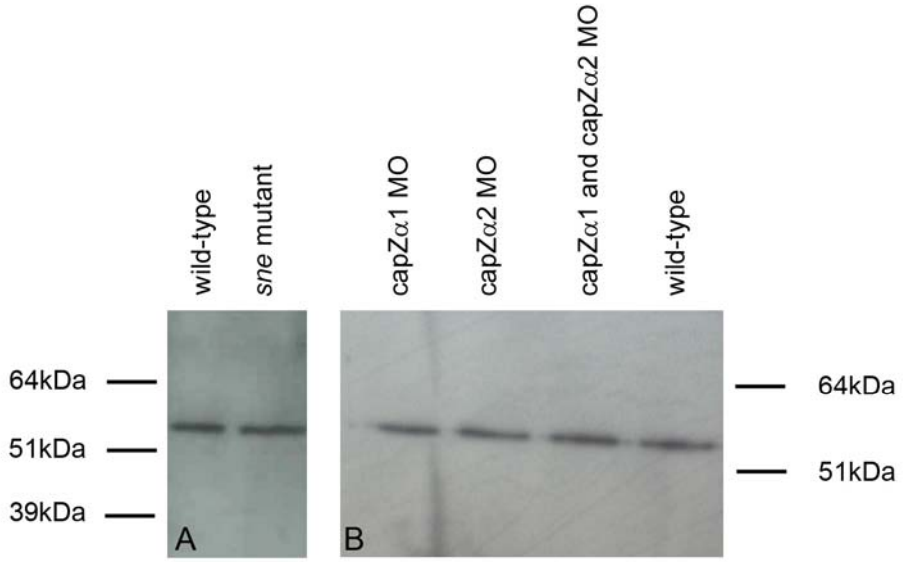

Fig. 5.20. Western blots on protein isolated from *sne* mutant and capZ morphants using the mouse monoclonal CapZα antibody. A) Western blot using wild-type protein extracted from 24 hpf embryos. Mutant protein was isolated from a 5 dpf indivudual *sne* mutant embryo. B) Western blot using equivalent amounts of protein extracted from 50% epiboly stage embryos injected with capZα1 MO (8ng),capZα2 MO (6ng), co- injected with capZα1 MO (8ng) and capZα2 MO (6ng), and wild-type controls.

the MOs. Therefore, using this approach I was not able conclusively establish whether any CapZα1 was produced in mutants.

5.4 Rescue of the capZα1 morphant using *capzα1*-GFP RNA

To confirm the localization of CapZα1 within the muscle and to determine whether exogenous CapZα1 could rescue the morphant phenotype, a CapZα1-GFP construct was generated. The GFP sequence was ligated to the 3′ end of *capzα1* via an 18bp linker, to ensure the GFP was able to fold correctly once translated. The whole construct was ligated into a pCS2+ vector and the capped RNA transcribed *in vitro* using an SP6 polymerase. Injection of up to 200pg of *capzα1*-GFP RNA had no effect on muscle development or the morphology of the muscle, and *capzα1*-GFP RNA was expressed and localized to the Z-line and myoseptum (as confirmed by double staining with α-actinin) (Fig. 5.22B-D). This finding supports the CapZα1 antibody staining pattern and verified that CapZα1-GFP can still dimerize with the β subunit to form functional CapZ.

capzα1-GFP RNA (150ng) was co-injected into 1-2 cell stage embryos with 4ng of capZα1 ATG MO, to determine whether exogenous CapZα1 could rescue the morphant phenotype. The ATG MO was used rather than splice 2 MO or the *sne* mutant because the defect is seen much earlier and therefore any amelioration of the phenotype would be much easier to score. By 48 hpf rescued embryos looked slightly better than MO only injected embryos. Although they had a smaller axes and brains in addition to reduced pigment, there was slightly more pigment in the RNA and MO injected embryos than in MO only injected embryos (Fig. 5.21). The skeletal muscle was then stained with α-actinin and the myofibrillar structure examined. Rescued embryos had straighter myofibrils than those embryos that were not injected

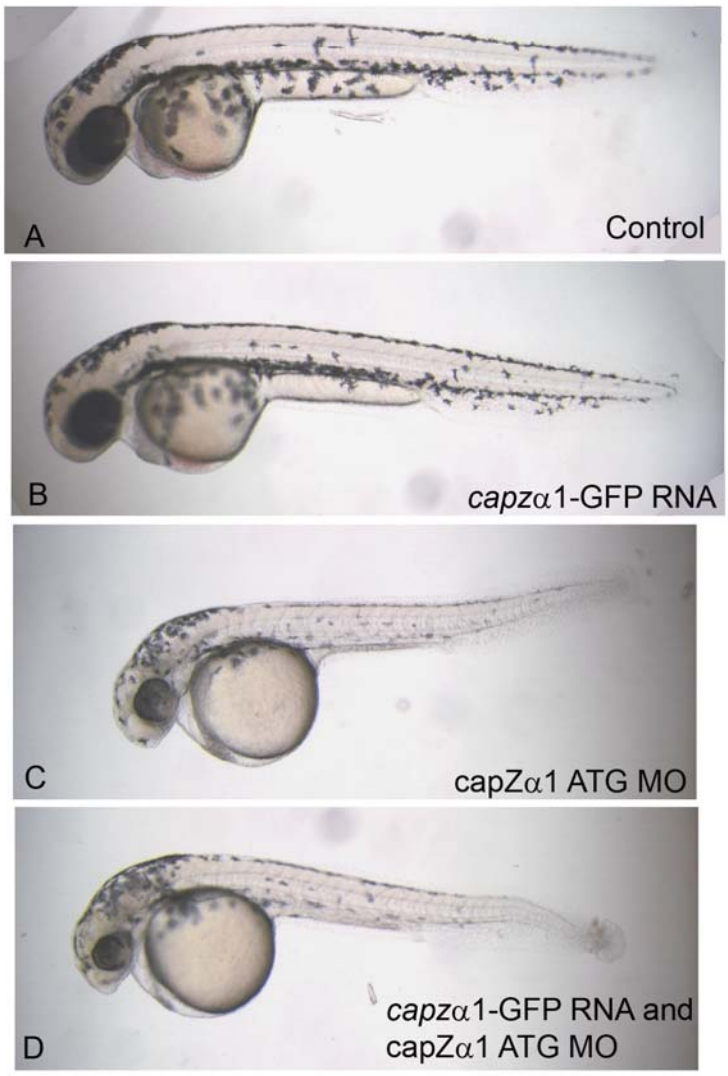

Fig. 5.21. Live images of embryos co-injected with capZα1 ATG MO and *capzα1*-GFP RNA. A) Buffer injected control, B) 150pg of *capzα1*-GFP RNA only, C) 4ng of capZα1 ATG MO only and D)150pg of *capzα1*-GFP RNA and 4ng of capZα1 ATG MO.

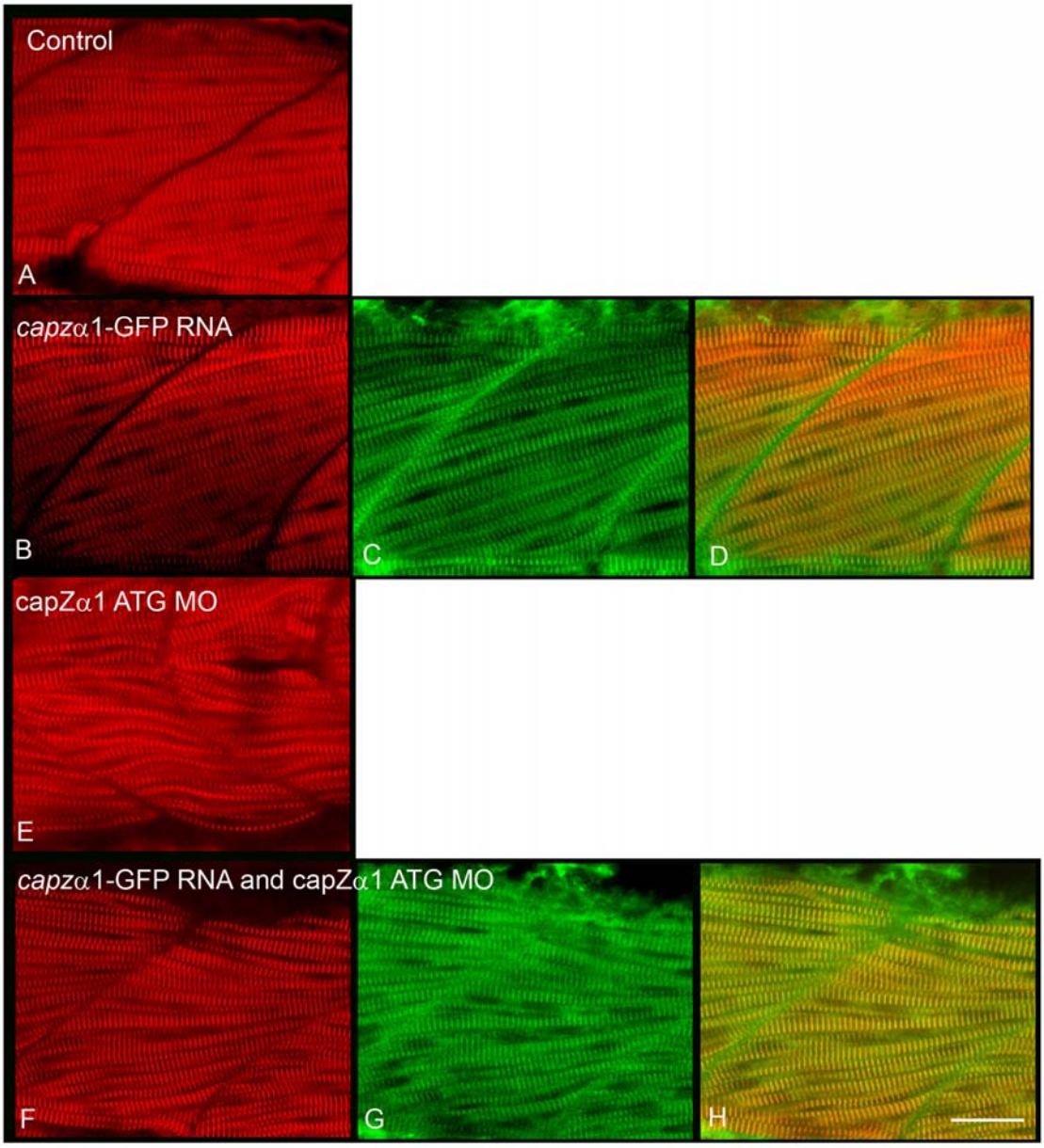

Fig. 5.22. Skeletal muscle confocal images of capZα1 ATG morphants rescued with *capzα1*-GFP RNA. A, B, E and H) α-Actinin staining (red), C and G) CapZα1-GFP expression (green), and D and H) merge of α-actinin and CapZα1-GFP images. A) Buffer injected control, B-D)150pg of *capzα1*-GFP RNA only, E) 4ng of capZα1 ATG MO only and F-H) 150pg of *capzα1*-GFP RNA and 4ng of capZα1 ATG MO. Scale bar = 22.18 μm.

with *capzα1*GFP RNA, and CapZα1-GFP had incorporated into the Z-lines and the myoseptum (Fig.5.22).

5.5 Discussion

The use of an ATG and two different splice MOs to knockdown CapZα1 has shed new light on the nature of the *sne* mutant and the role of CapZα1 in other aspects of embryonic development. Firstly, the *sne* mutant could be phenocopied by injecting embryos with a MO (splice 2) designed against the exon 9 donor splice site of *capzα1*. This strongly confirmed the site of the mutation in the *sne* mutant. Moreover, co-injection of *capzα1*-GFP RNA with the capZα1 ATG MO partially rescued the capZα1 ATG morphant phenotype. Secondly, injection of the ATG or splice 1 MO (which targets the exon 1 donor splice site) produced a more severe phenotype than the mutant or the splice 2 morphant. This indicated that the CapZα1 mis-spliced products present in the capZα1 splice 2 morphant (and therefore the *sne* mutant) must be partially functional. However, as all three morphants displayed wavy skeletal muscle fibres, this suggests that CapZα1 function in the muscle is severely affected in all capZα1 morphants. Indeed, CapZα1 antibody staining on day 5, suggests that in all three capZα1 morphants, CapZα1 is non-functional in skeletal muscle, either as a result of complete depletion of the protein or mis-localization. In this respect all morphants replicated the *sne* mutant phenotype.

The maternal contribution of *capzα1* could be an important factor in reducing the severity of the *sne* mutant phenotype compared to the ATG morphant. However, the splice 1 morphant has a similar phenotype to the ATG morphant suggesting that the maternal contribution has no bearing on the *sne* mutant phenotype. Rather, the more severely affected ATG and splice 1 morphants indicate that CapZα1 may be required much earlier in development. The mis-spliced

products that are translated in the *sne* mutant may be sufficient to carry out functions early in development, resulting in a milder phenotype compared to the ATG and splice 1 morphant where no CapZα1 is expressed. However, at the later stages of development, when CapZα1 is required in skeletal muscle, the mutant forms are unable to function in this tissue and the muscle specific phenotype is observed.

Knockdown of CapZα2 was also performed to determine whether CapZα2 could compensate for the loss of CapZα1. The ATG capZα2 MO produced a very severe phenotype at low doses, and co-injection with *capzα1*-GFP RNA established that this was because the ATG MO is able to knockdown expression of both the α1 and α2 transcripts. Unexpectedly, injection of the capZα2 splice MO did not produce a phenotype at all. This indicates that either the MO is not effective or the α1 subunit is able to rescue the phenotype in the absence of the α2 subunit. The latter theory is plausible as the RNA *in situ* hybridization expression patterns (shown in chapter 4) revealed that at 24 hpf there were higher levels of *capZα1* expression compared to *capZα2* in the muscle. However, further analysis is required to establish whether the CapZα2 splice MO is actually knocking down CapZα2.

In higher vertebrates the *capzβ1* and *capzβ2* isoforms are transcribed from one gene and only differ in their C-terminal regions. In zebrafish only one isoform has been identified, however, MOs against CapZβ were designed to knockdown both isoforms (if they do indeed exist). Functional CapZ requires the dimerization of α and β subunits, therefore loss of CapZβ would be predicted to produce a similar phenotype to the loss of the α subunits. As expected, both the capZβ ATG and splice MO produced a similar wavy myofibre phenotype to the capZα1 morphants, however, the ATG morphant phenotype was not as severe as the splice morphant. Generally, an ATG MO will produce a more severe phenotype than the splice as it knocks down

the maternal transcript as well as the embryonic transcript, which starts to be expressed at around the 1000 cell stage. It is possible that in this case the splice MO may be more efficient at knocking down the CapZβ subunit and therefore produce a more severe overall phenotype than the ATG MO. In any case RT-PCR experiments on capZβ splice morphants at different stages are required to confirm that the splice MO is knocking down translation of the transcript. However, due to the very specific phenotype that correlates with the *sne* phenotype it is more than likely that the MO is functioning correctly.

High doses of the CapZβ ATG MO replicated the severe defects observed in the capZα2 ATG morphant (which knocks down both α subunits). These findings therefore corroborate previous studies where the loss of either the α or β subunit prevents the formation of CapZ (Amatruda et al., 1992; Hug et al., 1995; Hug et al., 1992; Schafer et al., 1992), resulting in the same phenotypic defect being observed when either subunit is depleted. However, it cannot be ruled out that these phenotypes are not due to a general toxic effect of the MO (Robu et al., 2007). Co-injection with a p53 MO may assist in proving whether this phenotype is genuine. Additional Western analysis may also be beneficial in showing the effectiveness of each MO.

Antibody staining of CapZα1 on capZβ morphants revealed that CapZα1 had accumulated at the myoseptum. This particular phenotype is identical to what is observed in the *sne* mutant and supports the hypothesis that in the mutant an aberrant form of the CapZα1 protein is produced but is unable to dimerize with the β subunit, and therefore mutant CapZα1 accumulates at the myoseptum. Conversely, in the capZβ1 morphant, as the α1 subunit is unable to dimerize to form CapZ due to a lack of the β subunit, CapZα1 aggregates are also observed adjacent to the myoseptum.

The aberrant staining pattern of mis-localized α-actinin aggregates at the myoseptum is observed in the *sne* mutant as well as in the CapZβ morphant, however, is absent in the capZα1 ATG and splice 1 morphants. The differences in α-actinin accumulation indicate that this phenomenon is an artefact of the accumulation of the unincorporated mutant form of CapZα1, which is still able to bind to α-actinin. This theory is supported by the fact that the capZβ morphant produces the same phenotype and in these embryos normal CapZα1 protein would be produced. Unusually, the accumulations were not seen earlier than day 5, which suggests that over time sarcomeric components start to disassemble from a lack of functional CapZ, and eventually accumulate ectopically. The notion that the α1 subunit alone is able to bind to α-actinin contradicts a study done by Papa and colleagues in 1999, which identified that only the CapZ heterodimer was able to bind to α-actinin. As these studies were done *in vitro* it is quite possible that *in vivo* the α1 subunit is able to bind to α-actinin. Further experiments will be required to determine conclusively whether α-actinin or CapZβ can still bind to the mis-spliced CapZα1 product produced in the mutant.

Interestingly the capZβ ATG morphant produces a slightly different gross morphology to the splice morphant. Although both morphants produce a wavy myofibre phenotype, the ATG morphant also has ragged dorsal and ventral fins that become visible by 5 dpf, which are not observed in the splice morphant. As this phenotype was also seen in the *capZβ* retroviral mutant (capZβ^{hi1858bTg}) (Amsterdam et al., 2004) it verifies that the MO is effectively knocking down *capZβ*.

The MO analysis on the different subunits of CapZ has provided further insight to the nature of the *sne* mutant. It is likely that the mutation in *sne* results in the translation of mis-spliced forms of CapZα1, which are unable to dimerize with the β subunit or localize to Z-lines,

due to an inability to bind to the β subunit. Although the whole mount antibody staining provided evidence that CapZα1 protein is expressed in the *sne* mutants, Western blotting is still necessary to determine the number, type and abundance of mis-spliced transcripts that are translated. This experiment was performed but was unsuccessful as I was unable to establish whether the antibody specifically bound to CapZα1. Specific monoclonal antibodies against the α1 and α2 subunits have been generated (Hart et al., 1997b; Schafer et al., 1996), and may be more useful in detecting the presence of any protein product in the mutant. It has also been shown that the α1 and α2 subunits can be separated on a two dimensional (2D) gel (Hart et al., 1997b). In future, Western blotting experiments should incorporate 2D gels to separate the mutant α1 subunits and they should be detected using unique antibodies. This type of experiment will be more informative in determining conclusively which forms of mis-spliced transcripts are translated. Once the predominant mis-spliced CapZα1 product has been identified it will be easier to investigate precisely how the truncated product induces the phenotype. For example, its exact location within the cells during development could be determined by generating a GFP fusion construct, and the extent of its function and binding capability with other sarcomeric proteins could also be tested.

It is clear that CapZ is involved in many aspects of cell development, not just in skeletal muscle function. The different subunits are likely to have diverse roles in the cell and may be important in early developmental processes. Further research is required to fully understand the functions of the individual subunits and how they affect the role of CapZ during development.

Chapter 6

The Additional Roles of CapZ in Thin Filament assembly, Myofibril Organization and Motoneuron Patterning

Chapter 6: The additional roles of CapZ in thin filament assembly, myofibril organization and motoneuron patterning

6.1 Summary

In this chapter the role of CapZ in thin filament assembly was investigated. Combined loss of function of CapZ with skeletal fast muscle Tropomodulin 4 (Tmod4) or Nebulin (both regulators of actin thin filament formation) produced severe defects in skeletal muscle development. These results indicate firstly, that either CapZ or Nebulin are required for Z-line integrity. Secondly, CapZ is involved in the formation of nemaline rods that are observed in both the zebrafish Nebulin mutant *buzz off* (*buf*) and the Tmod4 morphant. Finally, Tmod4 rather than CapZ is predominantly responsible for nucleation of actin filaments in zebrafish skeletal muscle. The potential interaction of CapZ with the intermediate filament protein Desmin was also explored. MO knockdown of Desmin in zebrafish embryos produced misaligned and wavy myofibrils, similar to the loss of CapZ in skeletal muscle of the *sne* mutant. Additionally, Desmin was severely reduced in the myofibrils of *sne* mutants. These findings suggest that both proteins have overlapping functions in myofibril stability and organization. In the last section of this chapter the axonal projections of motoneurons are shown to be affected in embryos lacking CapZ, thus CapZ may be involved in motoneuron development.

6.2 Introduction

It has been well established that CapZ is an important factor in actin assembly due to its ability to dynamically cap the barbed end of F-actin (Littlefield et al., 2001; Schafer et al., 1996). Actin dynamics is crucial in maintaining thin filament length in muscle cells cultured *in vitro* (Littlefield et al., 2001). In skeletal muscle, CapZ, Nebulin and Tmod have been proposed to be key elements in regulating actin filament formation and ensuring that each actin filament is the

right length. To determine how CapZ is involved in thin filament formation and integrity *in vivo*, knockdown of CapZα1 in *buf* mutants, or double MO knockdowns of Tmod4 and CapZα1 were performed. All double loss of function experiments were performed in collaboration with Dr Elisabeth Busch-Nentwich.

To establish how loss of CapZ caused lateral misalignment of myofibrils in the *sne* mutant, the potential for this protein to link the Z-line to costameric network was investigated. As highlighted in chapter 1, Desmin has been implicated in maintaining the structural and regulatory organization of the myofibrils, therefore this protein was selected as a candidate for potentially interacting with CapZ. Additionally, the Desmin targeted mouse knock out has a strikingly similar phenotype to the *sne* mutant (Li et al., 1997).

A novel protein involved in neural development, V-1, was recently found to interact with CapZ (Taoka et al., 2003). It was suggested that V-1 regulates dynamics of actin polymerization by its interaction with CapZ. Moreover, it has been proposed that V-1 could also play a role in actin driven cell movement and motility during neuronal development (Fujigasaki et al., 1996; Taoka et al., 1994; Taoka et al., 1992). To investigate the possibility that CapZ may affect neuronal development, motoneurons were examined in Islet-1 GFP transgenic embryos injected with capZα1 MOs.

6.3 Combined loss of function studies of thin filament associated proteins

6.3.1 Loss of Nebulin affects myofibrillar structure and produces nemaline rods

The *buf* mutant was first identified in the ENU mutagenesis screen performed in Tübingen (Granato et al., 1996; Haffter et al., 1996) Dr Elisabeth Busch-Nentwich positionally cloned and analyzed the *buf* mutant, and established that the mutant completely lacked expression of the giant thin filament protein Nebulin. The phenotype of this mutant becomes visible at 2-3 dpf, when the embryos fail to emerge out of their chorions. The mutants have a reduced response when touched and are not as motile as wild-type sibling embryos. By 5 dpf the mutant embryos are thinner and have longer axes (Fig. 6.1A and B).

Phalloidin staining indicated that sarcomeric F-actin had formed and assembled into fibrils in the *buf* mutants, however, accumulations of filament at the myoseptum were observed at 3 dpf and 5 dpf (Fig.6.3B and Fig. 6.2B respectively). Immunostaining of α-actinin did not reveal any major defects in the Z-line of 5 dpf mutants, apart from small accumulations of ectopic α-actinin in the myoseptum (Fig. 6.2F). TEM on skeletal muscle sections of 5 dpf mutant embryos indicated that in many places the sarcomeric architecture was still preserved and M-lines, Z-lines, A and I-bands were observed, although the Z-lines were wider than wild-type siblings (Fig. 6.2M and N inset). The ultrastructural analysis also revealed the presence of nemaline rods and large accumulations of ectopic filament (it was not clear whether this was myosin or actin filament) (Fig. 6.2J and N). This phenotype is similar to human patients with nemaline myopathy that have defects in the nebulin gene (Pelin et al., 1999). At 3 dpf fewer nemaline rods were observed by TEM in the *buf* mutants (Dr Elisabeth Busch-Nentwich, personal communication), which suggests that the muscle phenotype is progressive. The phenotypic analysis of the *buf* mutant

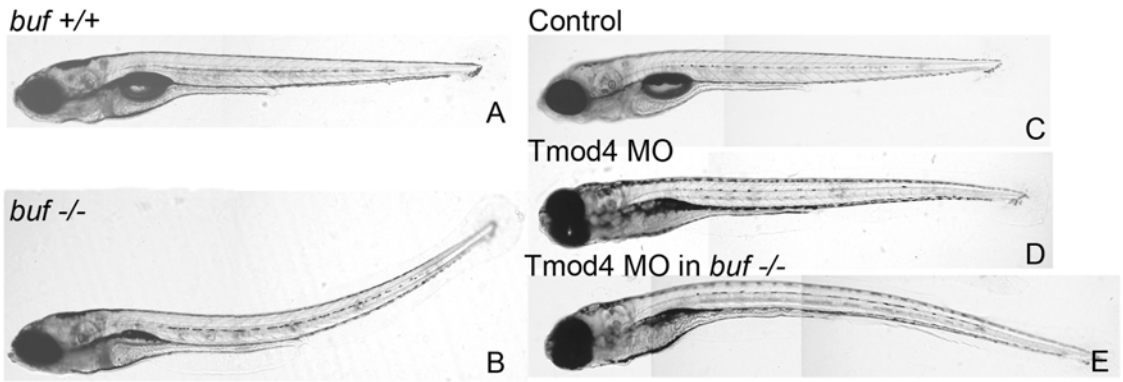

Fig. 6.1. Live images of 5 dpf *buf* and Tmod4 MO injected embryos. A) wild-type sibling, B) *buf* mutant, C) buffer injected control, D) embryo injected with 3ng of Tmod4 MO, E) *buf* mutant injected with 3ng of Tmod4 MO.

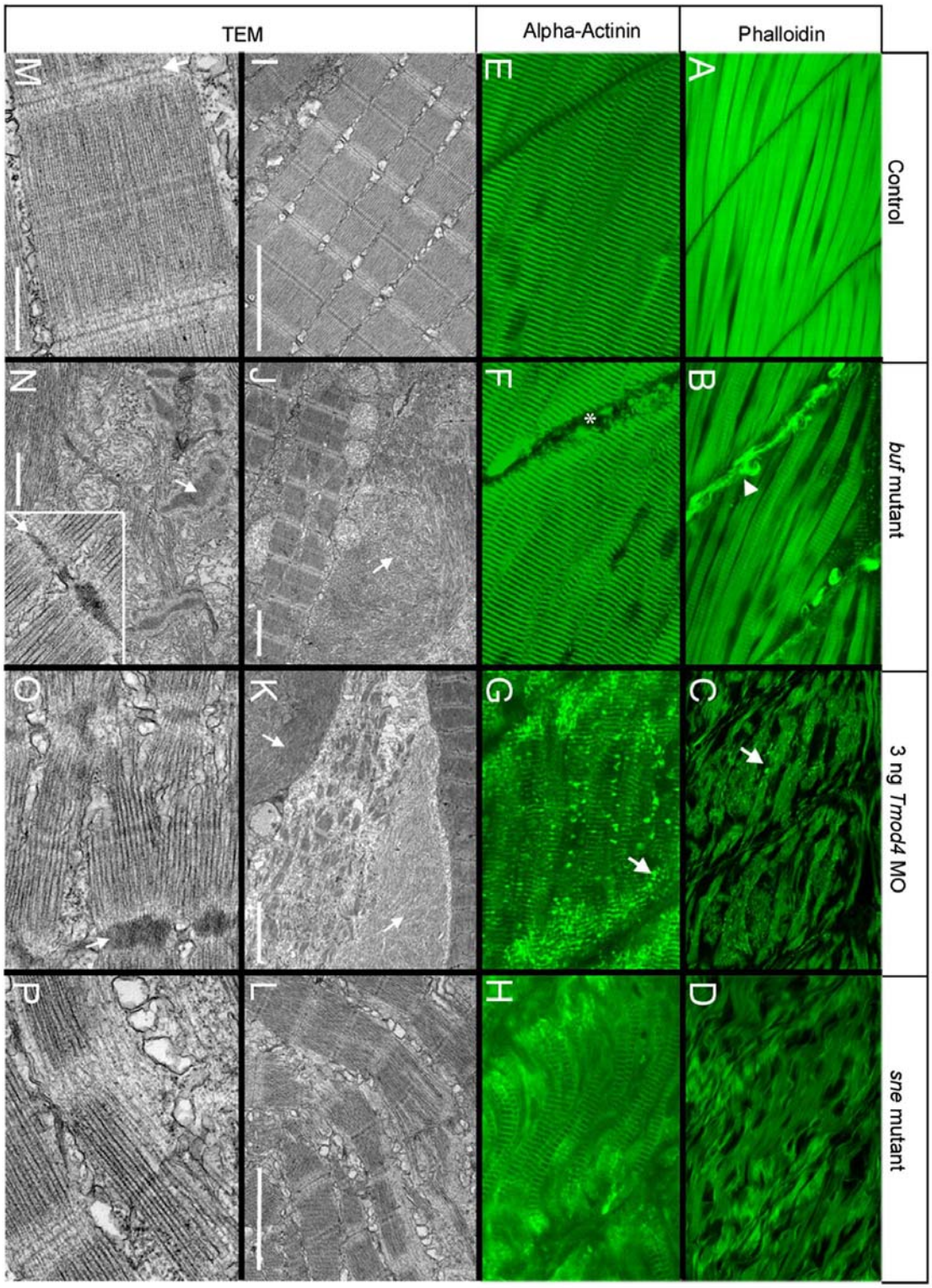
Phalloidin
Alpha-Actinin
TEM
Control
buf mutant
3 ng Tmod4 MO
sne mutant
A
B
C
D
E
F
G
H
I
J
K
L
M
N
O
P

Fig. 6. 2

Fig. 6.2. Phalloidin and α-actinin immunostaining of skeletal muscle in addition to TEM images of day 5 *buf* mutant, *sne* mutant and Tmod4 morphant embryos. A, E, I and M) control, B, F, J and N) *buf* mutant, C,G, K and O) embryo injected with 3ng of Tmod4 MO, D, H, L and P) *sne* mutant. A-D) Phalloidin staining, E-H) α -actinin staining, I-P) TEM images. Scale bar = 2μm for I, J and L, 4μm for K, 500nm for M, inset in N, and P and 1μm for N. Arrowhead in B points to accumulations of actin filament at the myoseptum. Arrow in C points to fragmented actin filaments. Asterisk in F indicates aggregates of α -actinin at the myoseptum. Arrow in G points to punctuate accumulations of α -actinin adjacent to the myoseptum. Arrows in J and K point to ectopic swirls of filament. Arrows in M and N inset point to the Z-line and arrow in N and O indicates the nemaline bodies.

therefore indicates that Nebulin is not essential for initial sarcomere assembly, however, is likely to play a role in maintaining the integrity of the sarcomere structure.

6.3.2 Knock down of Tmod4 produces a similar phenotype to the *buf* mutant

Tmod4 has a similar function to CapZ in that it caps the actin filament, however, it does so at the pointed end, close to the M-line. Littlefield and colleagues (2001) have shown that E-Tmod (Tmod-1) is the primary site for actin filament nucleation, rather than CapZ in cultured chicken cardiomyocytes. Therefore it was not surprising that loss of fast muscle Tmod4 using 3ng of MO targeted to the ATG produced pronounced muscular defects in injected embryos (analysis of the Tmod4 morphant was performed by Dr Elisabeth Busch-Nentwich). At 48 hpf morphants had reduced motility and had failed to come out of their chorions by day 3. On day 5, Tmod4 morphant embryos had longer axes than control embryos and their swim bladders had not inflated (Fig. 6.1D).

Phalloidin staining of day 5 Tmod4 morphant embryos indicated that F-actin was greatly reduced and very few fibrils spanned across each somite (Fig. 6.2C). Immunostaining of α-actinin indicated that Z-lines had formed, however, additional punctate accumulations of α-actinin were also observed that were especially prevalent at regions close to the myoseptum (Fig. 6.2G). TEM images of day 5 muscle sections showed that in many regions the sarcomere structure had collapsed in the Tmod4 morphants (Fig. 6.2K), however, there were still some areas where the sarcomere structure was preserved to some extent, and M-line, Z-line, A-band and I-bands were visible (Fig. 6.2O). Intriguingly, as in the *buf* mutant, nemaline rods and swirls of thick and thin filament (Fig. 6.2K arrows) were also observed.

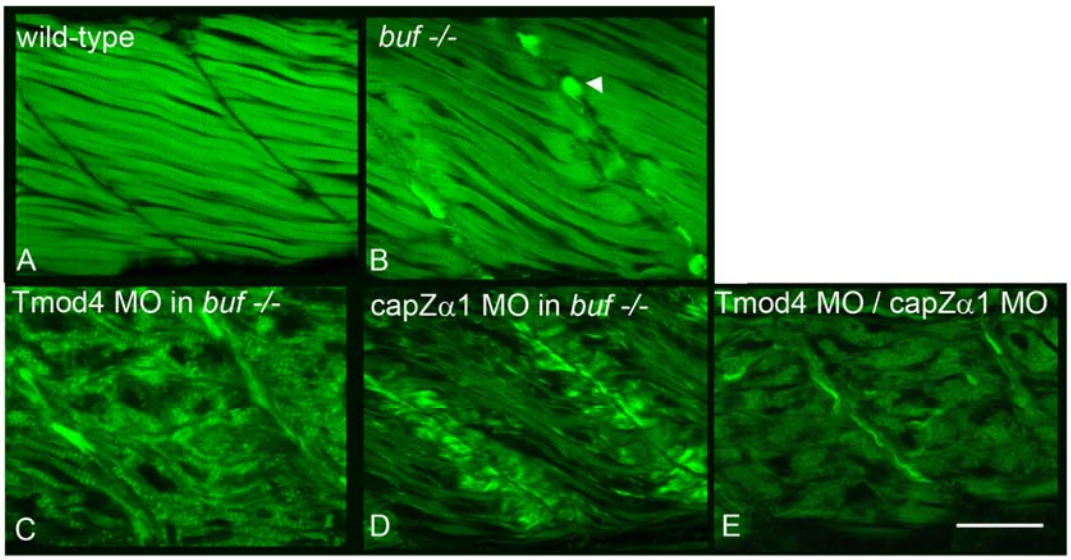

Fig. 6.3. Phalloidin staining of 3 dpf double loss of function embryos. A) wild-type sibling, B) *buf* mutant, arrowhead indicates accumulation of actin filament at the myoseptum C) *buf* mutant injected with 3ng of Tmod4 MO, D) *buf* mutant injected with 10ng of capZα1 splice 2 MO, E) embryo co-injected with 3ng of Tmod4 MO and 10ng of capZα1 splice 2 MO. Scale bar = 44.36 μm.

6.3.3 Loss of CapZ (by MO knockdown) and Nebulin results in loss of the Z-line and thin filament

CapZ, Nebulin and Tmod are thought to be integral in thin filament formation and maintenance. Although the loss of each of these proteins clearly affects muscle function, sarcomere assembly is not completely inhibited as Z-lines and some components of the sarcomere are still visible by day 5. This would suggest that alone each of these proteins are not essential for sarcomere formation, but are required for maintaining the stability and integrity of the muscle tissue as it contracts. However, it is still not known whether *in vivo* the combination of these proteins would be required to establish and maintain thin filaments within the sarcomere.

To observe the effect of loss of Nebulin and CapZ during zebrafish development, 10ng of the capZα1 splice 2 MO was injected into *buf* embryos and the muscle phenotype of these embryos was assessed. On day 3 the motility of the *buf* /CapZα1 double loss of function embryos was severely diminished and they were only able to move the posterior end of their tails when a flight stimulus was provoked. Phalloidin staining at both 3 and 5 dpf showed that actin filaments were severely reduced and there also appeared to be accumulations of actin filament at the myoseptum boundaries (Fig. 6.3D and 6.4D). Moreover, staining with the α-actinin antibody revealed an almost complete loss of α-actinin localization at the Z-line at 5 dpf, however, α-actinin had accumulated ectopically near the myosepta (Fig. 6.4H). TEM images at this stage also confirmed the complete loss of Z-lines (Fig.6.4P arrow) in the *buf* /CapZα1 double loss of function embryos. Surprisingly, the arrangement and localization of thick filament was not affected in what was left of the sarcomere and nemaline bodies were not observed. However, the swirls of ectopic filament as seen in the *buf* only mutants were still present. The absence of Nebulin and CapZ therefore results in loss of thin filaments and Z-lines within sarcomeres.

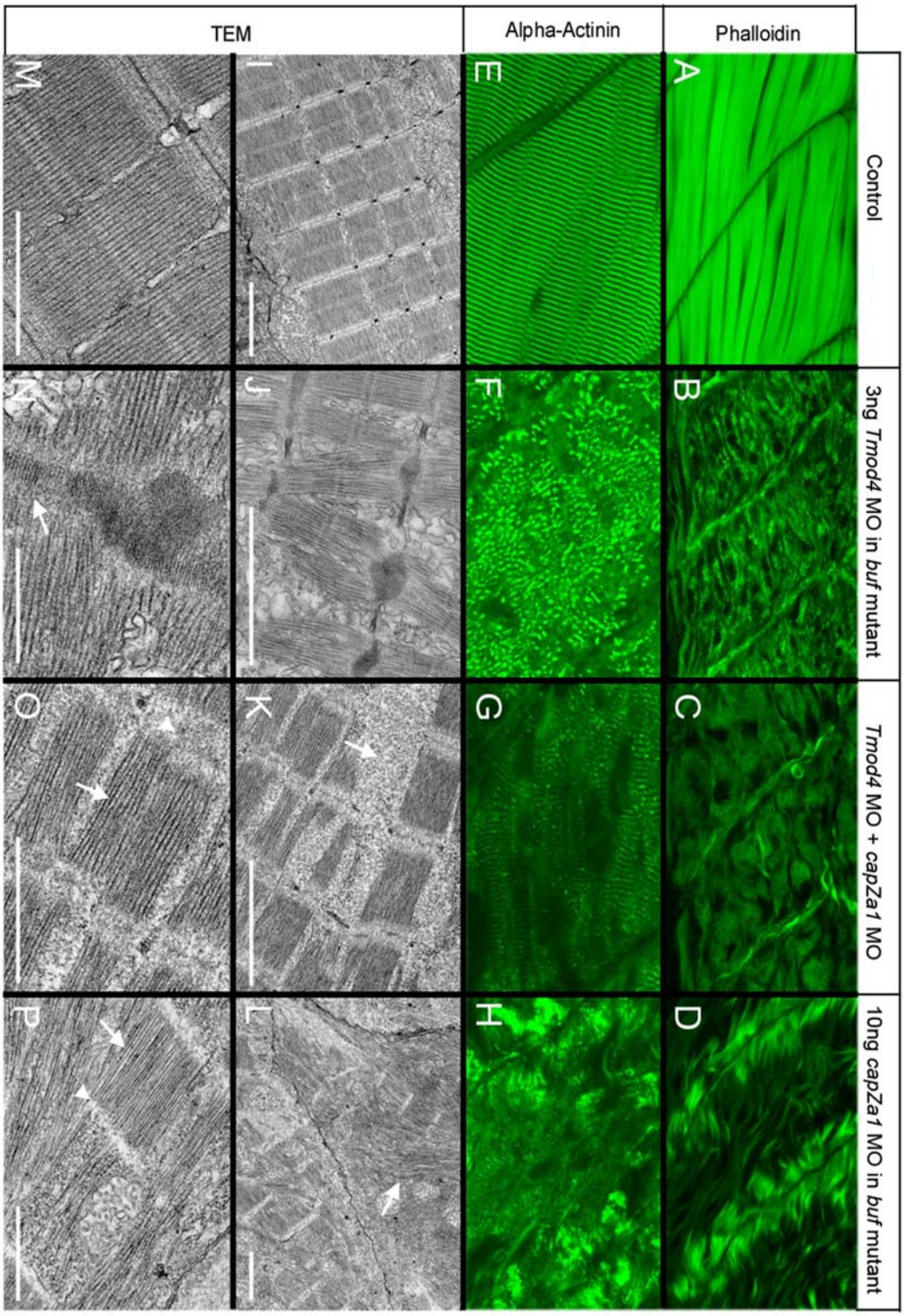
Phalloidin
Alpha-Actinin
TEM
Control
3ng Tmod4 MO in buf mutant
Tmod4 MO + capZa1 MO
10ng capZa1 MO in buf mutant
A
B
C
D
E
F
G
H
I
J
K
L
M
N
O
P

Fig. 6.4

Fig. 6.4. Phalloidin and α-actinin immunostaining of skeletal muscle, in addition to TEM images of day 5 *buf* /capZα1 double loss of function embryos. A, E, I and M) control, B, F, J and N) *buf* mutant injected with 3ng of Tmod4 MO, C,G, K and O) embryo co-injected with 3ng of Tmod4 MO and 10ng of capZα1 splice 2 MO, D, H, I and P) *buf* mutant injected with 10ng of capZα1 splice 2 MO. A-D) Phalloidin staining, E-H) α-actinin staining, I-P) TEM images. Scale bar = 2μm for I, J, K and L, 1μm for M, O, and P, 500nm for N. Arrow in K indicates the absence of a sarcomere. Arrow in L points to swirls of ectopic filament. Arrow in N indicates the nemaline bodies. Arrows in O and P point to the lack of M-line and arrowheads point to the lack of Z-line

6.3.4 *sne/buf* double mutants phenocopy the mutant/morphant knockdown

To confirm the *buf* /CapZα1 double loss of function phenotype, *sne* and *buf* heterozygotes were crossed. The F1s were genotyped for an allelic mutation in *capZα1* and subsequently incrossed to identify carriers that were heterozygous for the *sne* and *buf* mutations. The double mutant embryos phenocopied the *buf* /CapZα1 double loss of function embryos and were virtually immotile by 3 dpf. At 5 dpf the double mutants had shorter axes compared to the *buf* mutants, however, they were still longer than the *sne* mutants or the wild-type siblings (Fig.6.5). α-Actinin antibody staining of day 5 double mutant embryos revealed that very few Z-lines were present and α-actinin had accumulated adjacent to the myoseptum. Phalloidin staining also indicated that virtually no actin filaments had assembled within the myofibres (Fig.6.6A and D). The generation of the *sne*/*buf* mutants therefore supports the results of the double loss of function experiments. However, ideally, TEM analysis will be necessary to completely verify that the double mutants replicate the *buf* /CapZα1 double loss of function phenotype.

The *buf* only mutants produced from the *sne*/*buf* heterozygote cross can be readily distinguished by their gross morphology (Fig. 6.5C). However, when the skeletal muscle of these mutants was stained with phalloidin, wavy actin filaments were detected. Moreover, large clumps of F-actin had accumulated at the myoseptum (Fig. 6.6C). This phenotype differs from the phalloidin immunostaining images of the originally characterized *buf* mutants (Fig. 6.2B) and is more similar to the *sne* mutant phenotype. The unique morphology of these *buf* mutants raises the possibility that in addition to the loss of Nebulin, they are also heterozygous at the *sne* locus. Therefore, perhaps lower amounts of CapZ and a complete lack of Nebulin in these mutants exacerbates the skeletal muscle phenotype. Genotyping will be required to verify this

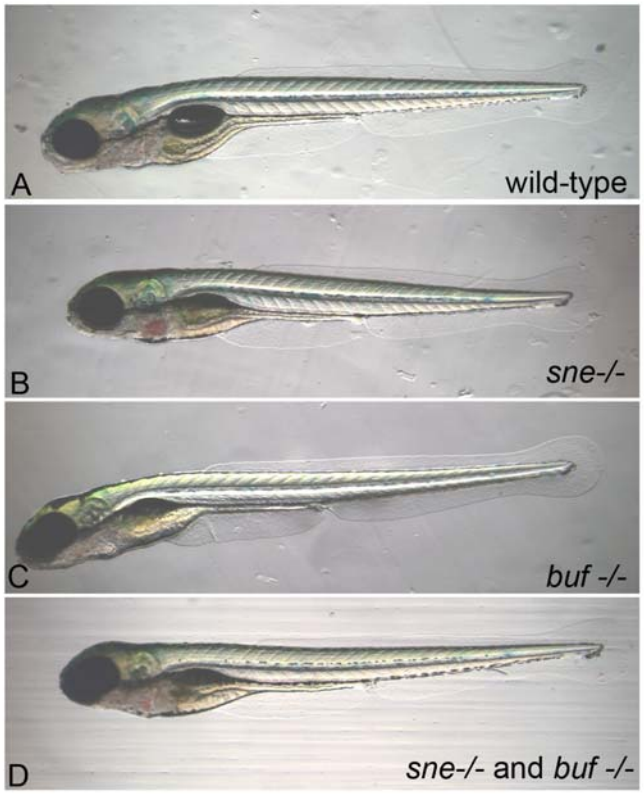

Fig. 6.5. Live images of 5 dpf *sne/buf* mutant embryos. A) wild-type sibling, B) *sne* mutant, C) *buf* mutant, D) *sne/buf* mutant.

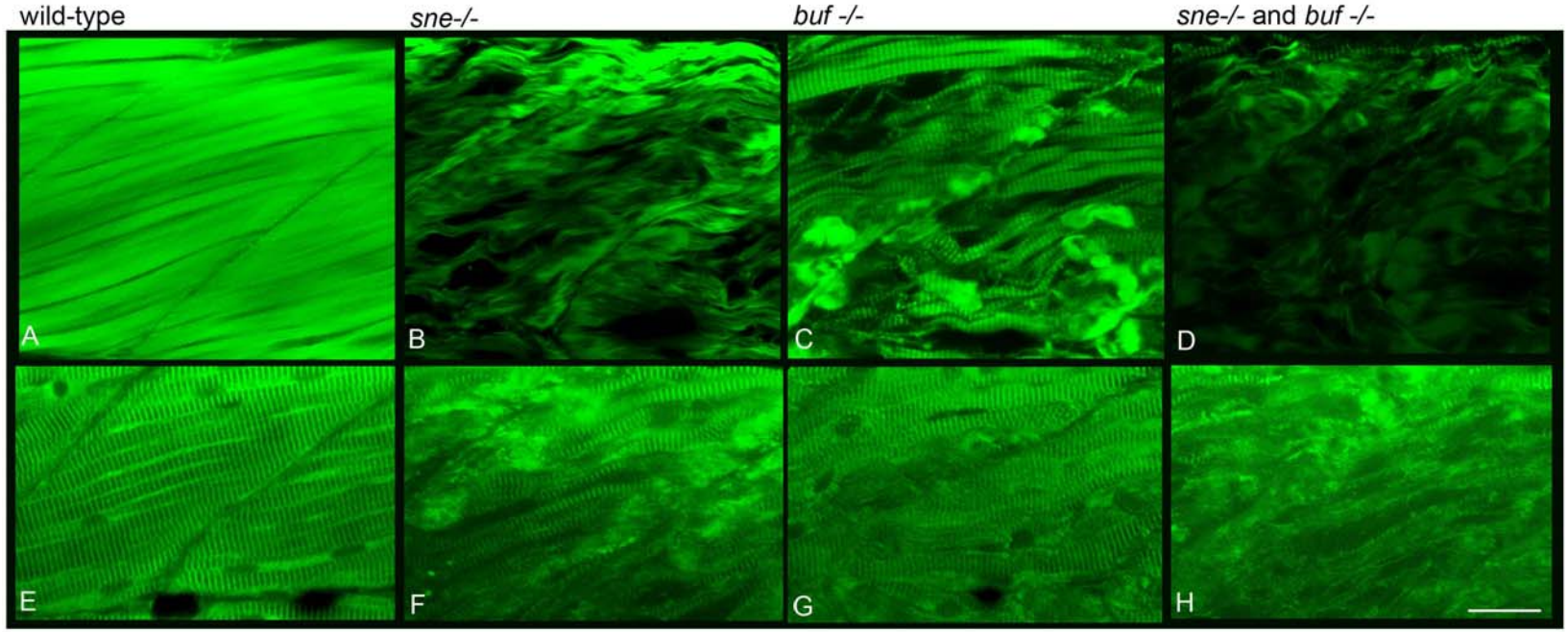

Fig. 6.6. Phalloidin and α-actinin staining of 5 dpf *sne*/*buf* mutant embryos. A-D) Phalloidin staining, E-H) α-actinin staining. A and E) wild-type sibling, B and F) *sne* mutant, C and G) *buf* mutant, D and H) *sne*/*buf* mutant.

interpretation, however, it suggests that levels of CapZ and Nebulin may play an important role in maintenance of the myofibril.

6.3.5 Double MO knockdown of CapZ and Tmod4 completely ablates actin filament and Z-lines

MO injection of 1-2 cell stage embryos with 10ng of capZα1 splice 2 MO and 3ng of ATG Tmod4 MO caused severe muscular defects. On day 3 the double morphants did not move very well and had not emerged from their chorions. Phalloidin staining at this stage revealed that actin filaments were abolished (Fig. 6.3E) and by day 5 they were still not detected (Fig. 6.4C). Although striated Z-lines were visible on day 5, α-actinin levels were dramatically reduced, indicating that many Z-lines had either not assembled or had disintegrated (Fig. 6.4G). TEM analysis of the double loss of function embryos on day 5 confirmed the immunofluorescent stainings. There were very few Z-lines and those that were observed were wider and more diffuse. The sarcomere structure had been partially lost and there was a lack of thin filament, however, thick filament was still observed in ordered blocks even though the Z-line and the thin filament were absent (Fig. 6.4K and O). Unincorporated G-actin also appeared randomly within the myofibril (Fig. 6.4K arrow). Intriguingly, as with the *buf* /CapZα1 double loss of function embryos nemaline rods were not found, however, swirls of ectopic thick filament were still apparent, as seen in the Tmod4 only morphant. These results therefore indicate that *in vivo*, loss of Tmod4 and CapZ completely ablates formation of thin filament and causes Z-line disintegration.

6.3.6 Loss of Tmod4 in *buf* mutants increases the formation of nemaline bodies

Injection of the ATG Tmod4 MO into *buf* embryos produced acute muscle deficiencies that were more severe than loss of Tmod or Nebulin alone. At 3 dpf many of the *buf*/Tmod4

double loss of function embryos had not emerged from their chorions and were almost immotile, and by day 5 had very long axes (Fig. 6.1E). Phalloidin staining on day 3 indicated that virtually no actin filaments had formed within the myofibrils in orderly arrays. Instead, they appeared to accumulate in clumps within the somite (Fig 6.3E), which was also apparent on day 5 (Fig. 6.4B). α-Actinin antibody staining on day 5 identified regions of the somite full of punctuate accumulations of the Z-line protein (Fig. 6.4F). Closer inspection by TEM confirmed that these accumulations were nemaline bodies (Fig. 6.4J and N). Thick filament was also observed between the condensed Z-lines, however, the sarcomeres were randomly orientated and fragmented. Incorporation of thin filament into the distorted sarcomere was also detected and appeared to attach to the nemaline bodies (Fig. 6.4 N). Loss of Tmod4 and Nebulin therefore induces the formation of nemaline bodies from Z-lines, which are likely to result in the complete distortion and fragmentation of the sarcomeric architecture.

6.4 Desmin

Desmin is an intermediate filament costameric protein found in all types of muscle and endothelial cells. Very little is known about the various functions of Desmin in zebrafish development, however, its RNA expression pattern has been characterized (Loh et al., 2000). Whole mount *in situ* hybridization has revealed that *desmin* is expressed in a very similar stage and specific manner to *capZα1*. It is maternally expressed and as development progresses it becomes restricted to the somites, and by 24 hpf it is predominantly expressed in skeletal muscle. The mouse Desmin knockout also produces a strikingly similar phenotype to the *sne* mutant (Li et al., 1997). The muscle myofibres of the soleus and diaphragm became disorganized through progressive muscle use, the myofibrils were wavy and the Z-lines were also not aligned between

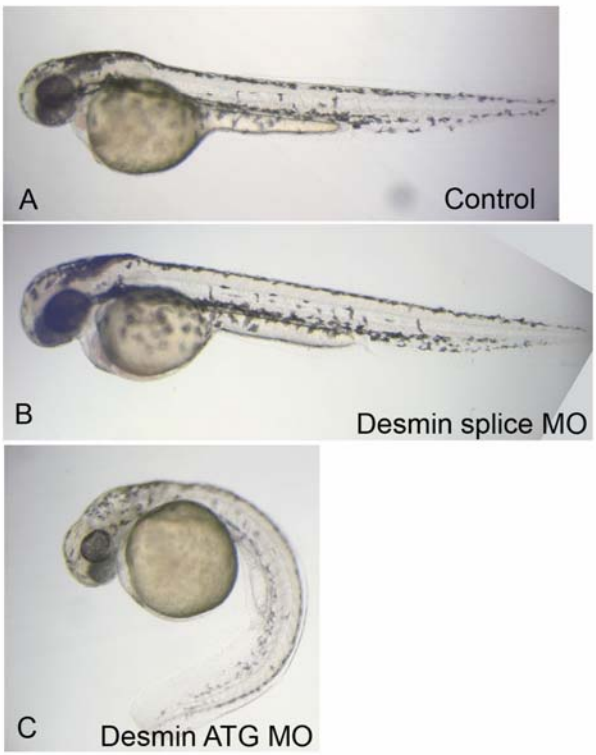

Fig. 6.7. Live images of 2 dpf desmin morphants. A) Buffer injected control, B) embryo injected with 6ng of desmin splice MO, C) embryo injected with 3ng of desmin ATG MO.

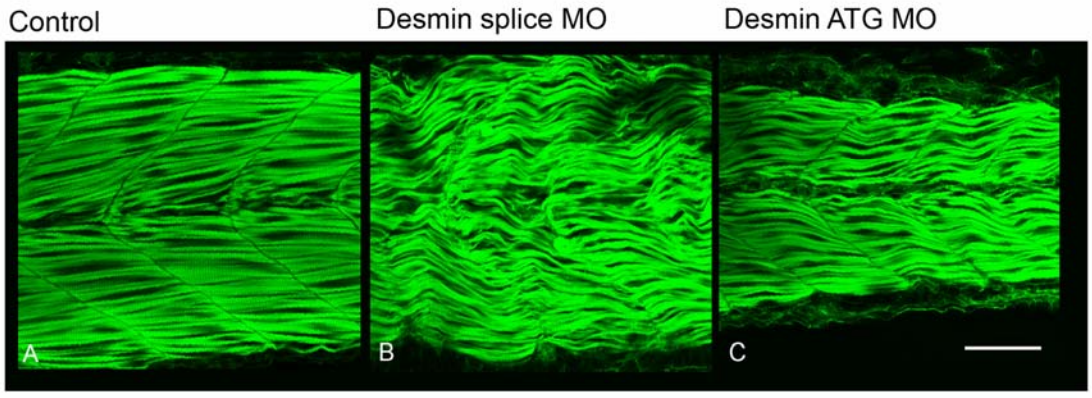

Fig. 6.8. Phalloidin staining of 2 dpf desmin morphants. A) Buffer injected control, B) embryo injected with 6ng of desmin splice MO, C) embryo injected with 3ng of desmin ATG MO.

myofibrils. Other defects included focal degeneration, mitochondrial disorganization and also loss of anchorage of the myofibrils to the plasma membrane at the costamere. Due to the remarkable similarities between the *sne* mutant and the desmin mouse mutant a few experiments were performed to determine whether Desmin and CapZ share functional roles.

6.4.1 Knockdown of Desmin in zebrafish produces wavy myofibres

To examine whether loss of Desmin produced the same phenotype in zebrafish as it did in mice, 6ng of desmin splice MO (targeted against the exon 3 donor splice site) and 3ng of desmin ATG MO were injected into 1-2 cell embryos. By day 2 the splice morphants looked very similar to the wild type controls, however, the ATG morphants were severely affected. The ATG morphant embryos had curved tails, smaller brains, less pigment, and did not respond well to prodding by a mechanical stimulus (Fig.6.7). By day 5, the swim bladders had not inflated in the ATG morphants. Moreover, most injected embryos had shortened axes, heart edemas, smaller brains, and bent tails. The splice MO at this stage was comparable to wild type buffer injected control embryos, the swim bladder had inflated and embryos were swimming normally. Intriguingly, phalloidin staining of day 2 morphants illustrated that wavy myofibres were produced in both the splice and the ATG MO injected embryos (Fig. 6.8). This phenotype is very similar to the phenotype observed with the knock down of CapZα1, and is also similar to what is observed in the Desmin mouse mutant.

6.4.2 Loss of CapZ and Desmin does not enhance myofibrillar disorganization

To determine whether loss of both CapZα1 and Desmin are directly involved in the same mechanism for maintaining myofibrillar integrity, double MO injections were performed to determine whether loss of both these proteins enhanced the wavy phenotype. Both MOs were injected at low doses so that individually each MO only produced a mild phenotype. Embryos

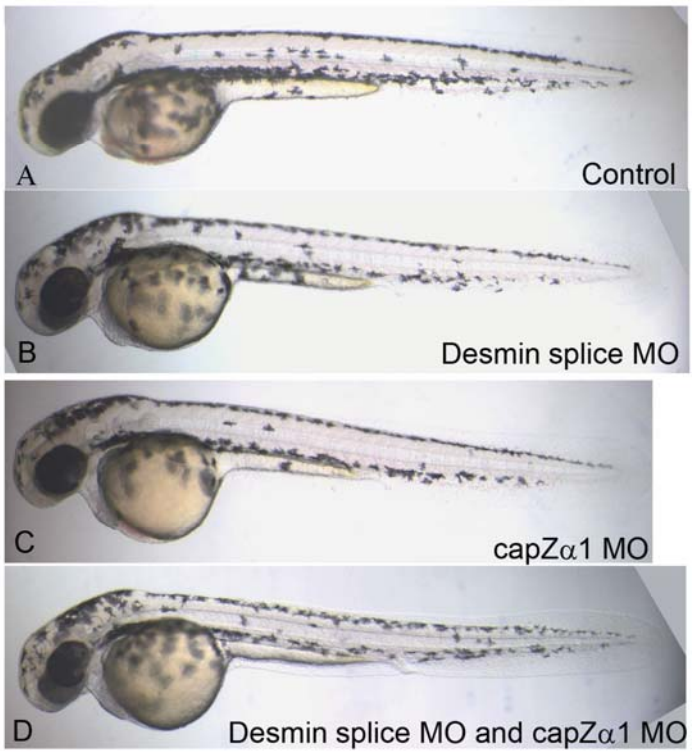

Fig. 6.9. Live images of 2 dpf embryos co-injected with desmin and capZα1MO. A) Buffer injected control, B) embryo injected with 8ng of desmin splice MO,C) embryo injected with 10ng of capZα1 splice 2 MO,D) embryo co-injected with 8ng of desmin splice MO and10ng of capZα1 splice 2 MO.

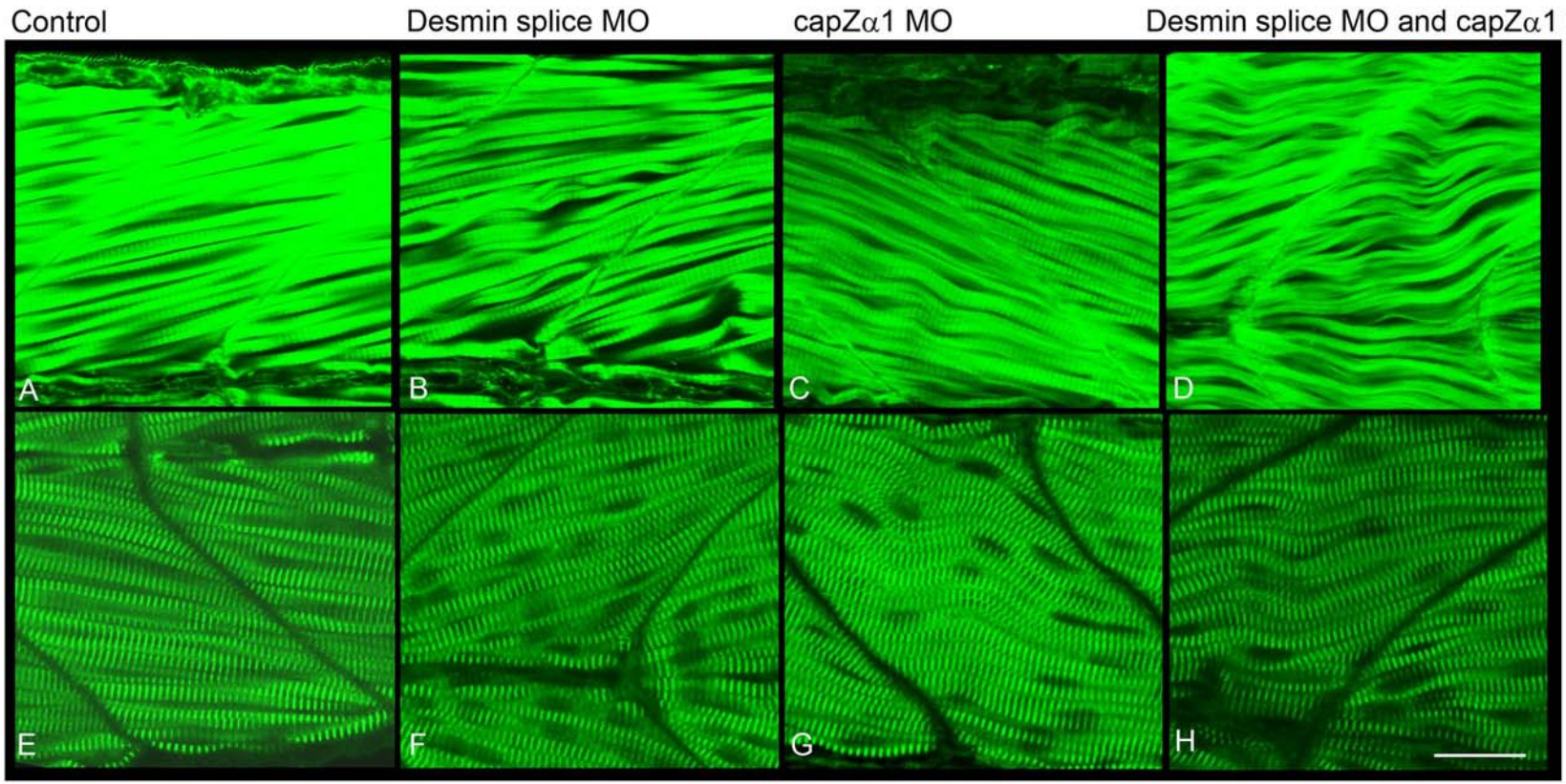

Fig. 6.10. Phalloidin and a-actinin immunostaining of embryos co-injected with desmin and capZa1 MO.A-D) phalloidin, E-H) a-actinin. A and E) Buffer injected control, B and F) embryo injected with 8ng of desmin splice MO,C and G) embryo injected with 10ng of capZa1splice 2 MO, D and H) embryo co-injected with 8ng of desmin splice MO and10ng of capZa1 splice 2 MO. Scale bar = 22.18 mm.

were visualized on day 2, as the effect of the MO tends to decline after three days. 8ng of desmin splice MO and 10ng of capZα1 splice 2 MO were injected separately and co-injected into 1-2 cell stage embryos. On day 2, both individually injected embryos were comparable to the wild type control (Fig. 6.9A, B and C). The overall morphology of the double morphants was very subtle, they had a slightly smaller brain and eyes, however, the tail had extended properly and somites and notochord had formed normally (Fig. 6.9D). Phalloidin staining revealed that the double morphants had slightly wavier fibrils compared to the single morphants, however, no significant difference was observed with α-actinin staining (Fig. 6.10). These results suggest that loss of both Desmin and CapZ does not disrupt the myofibrillar organization in zebrafish embryonic muscle any more than loss of either alone.

6.4.3 Desmin is mis-localized in the myofibrils of *sne* mutants

To determine whether Desmin was affected by loss of CapZ, a polyclonal antibody was used to detect Desmin in the skeletal muscle of 5 dpf *sne* mutant and wild-type sibling embryos. In wild-type sibling embryos Desmin clearly localized to the myoseptum and also appeared to surround each muscle fibre (Fig.6.11). Moreover, within each confocal section a few fibres possessed a distinct striated staining pattern (Fig.6.11A inset). It is possible that this staining pattern is only observed when the confocal scans across a section of tissue that cuts through the edge of the fibril. Alternatively, as this particular staining pattern is not observed uniformly throughout the muscle tissue, the antibody may not be able to penetrate the muscle tissue effectively. Despite the discrepancies in the staining pattern, the control (secondary antibody only) produced virtually no signal. This confirms that the Desmin antibody is specific and the positive staining observed in the myosepta is not an artifact of the accumulation of secondary

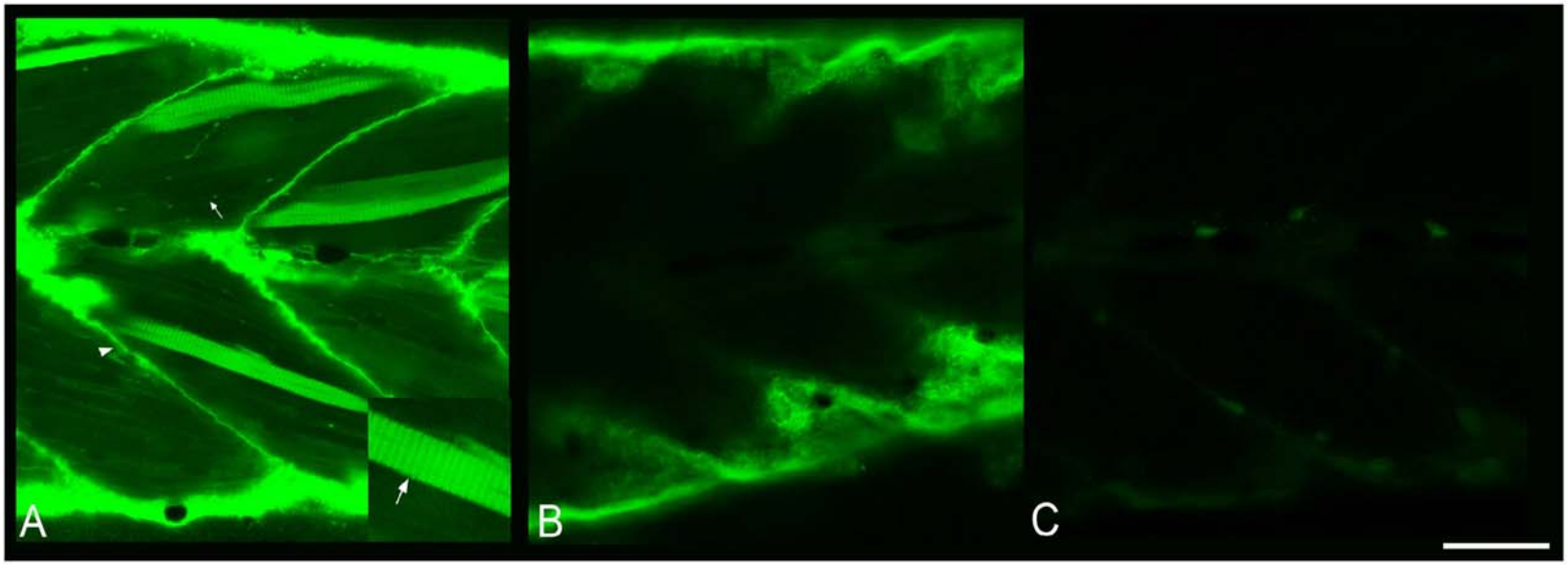

Fig. 6.11. Desmin antibody staining of 5 dpf *sne* mutant and wild-type sibling embryos. A) Wild-type sibling, arrowhead indicates staining in the myoseptum and arrow points to staining around each myofibril. The inset in A is a magnification of the myofibril, illustrating the striated staining pattern (arrow). B) *sne* mutant, C) control (secondary antibody only) on wild-type sibling embryo. Scale bar = 44.36 μm.

antibody. Surprisingly, in the *sne* mutant, staining was absent at the myoseptum. Moreover, Desmin was not detected surrounding the myofibrils or in the characteristic striated pattern that was observed in some of the myofibrils within the wild-type sibling muscle tissue. However, Desmin was still localized to the epithelial layer surrounding the skeletal muscle. These findings suggest that Desmin localization within the muscle is severely affected by lack of CapZ.

6.5 Loss of CapZ affects secondary motoneuronal axon growth

The role of CapZ in neuronal development was initially investigated using transgenic Islet-1 GFP embryos. Islet-1 is a member of the LIM/ homeobox gene family and is expressed in all postmitotic motoneurons early in their development (Appel et al., 1995; Ericson et al., 1992). Transgenic zebrafish expressing an *islet-1* promoter/ enhancer linked to GFP has enabled visualization of cell bodies, main axons, and peripheral branches of motoneurons within cranial and muscle tissues (Higashijima et al., 2000). CapZα1MOs were therefore injected into transgenic Islet-1 GFP embryos to observe the effect of loss of CapZα1on motoneuron development.

Both the ATG (5ng) and splice 2 capZα1 MOs were injected into1-2 cell stage Islet GFP embryos. On day 3, motoneurons were visualized under a fluorescence dissecting microscope. As mentioned in previous chapters, the capZα1 ATG morphants were delayed in development and therefore had smaller brains and eyes compared to the capZα1 splice 2 morphants and the controls, however, no major differences were observed in the cranial motoneurons (Fig. 6.12A and B). There were a reduced number of Islet-1 positive motoneurons along the body axes of ATG morphants on day 3, however, this defect was not observed on day 4 (Fig. 6.13C and D). This observation was probably due to a general delay in development of the ATG morphants. The

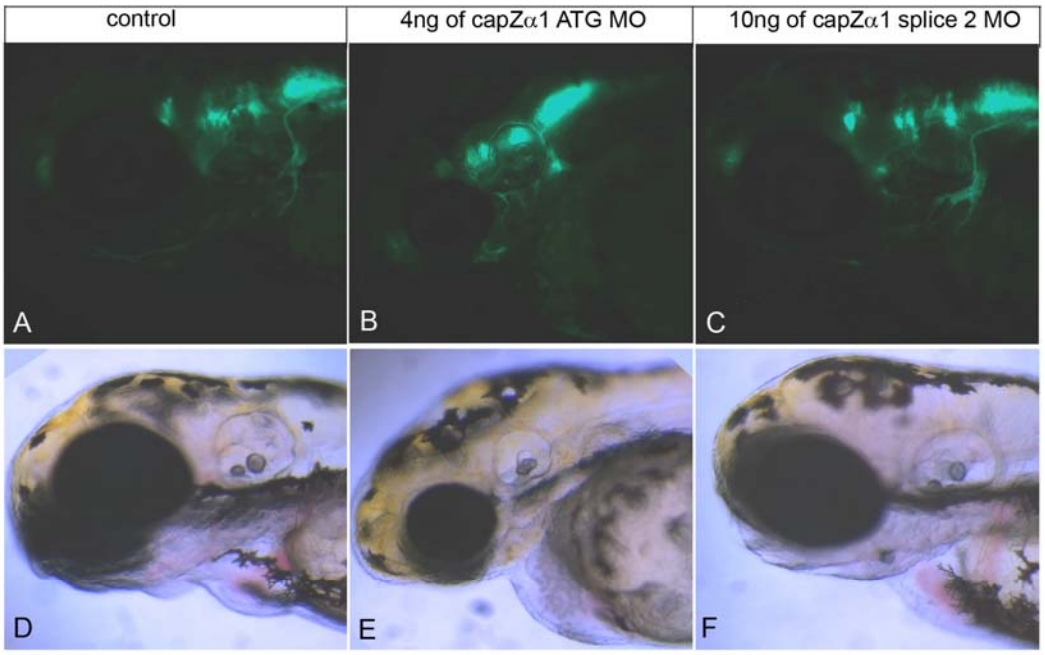

Fig. 6.12. 3 dpf live images of the cranial region of Islet-1 GFP embryos injected with capZα1 ATG or splice 2 MO. A-C) fluorescent images, D-F) bright field images. A and D) Islet-1 GFP control embryo, B and E) Islet-1 GFP embryo injected with 4ng of capZα1 ATG MO, C and F) Islet-1 GFP embryo injected with 10ng of capZα1 splice 2 MO.

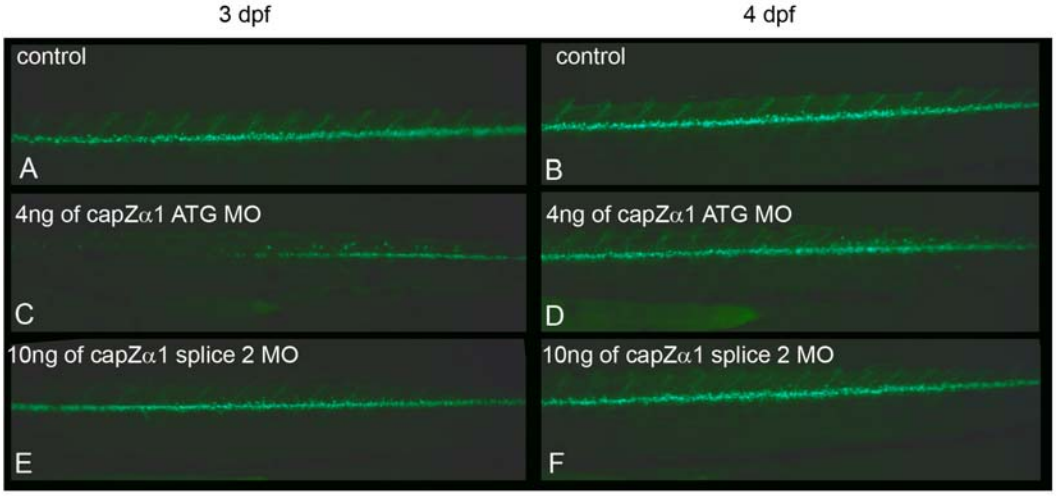

Fig. 6.13.Fluorescent live images of the tail region of Islet-1 GFP embryos injected with capZα1 ATG or splice 1 MO at 3 dpf and 4 dpf. A, C and E) 3 dpf, B, D and F) 4 dpf. A and B) Islet-1 GFP control embryo, C and D) Islet-1 GFP embryo injected with 4ng of capZα1 ATG MO, E and F) Islet-1 GFP embryo injected with 10ng of capZα1 splice 2 MO.

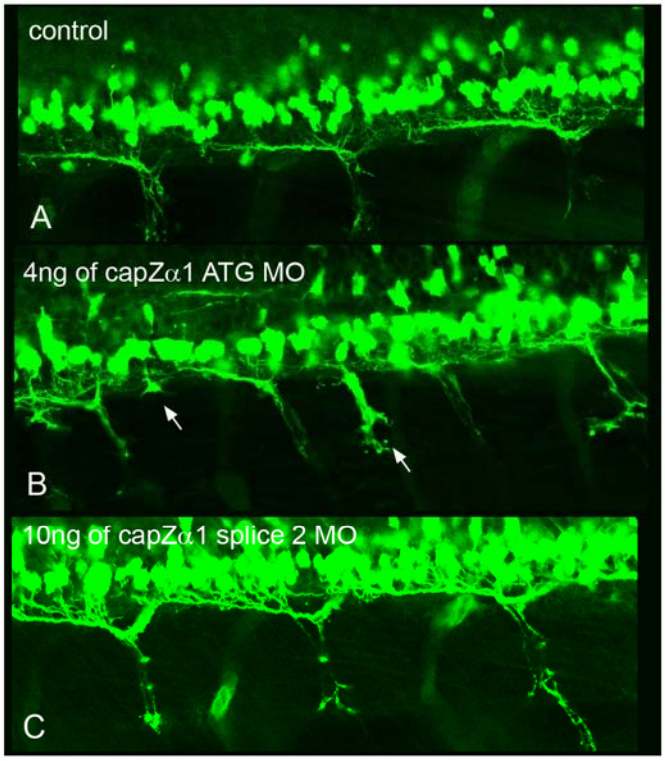

Fig. 6.14. Confocal images of motorneurons from Islet-1 GFP embryos injected with with CapZα1 ATG or splice 1 MO at 5 dpf. A) Islet-1 GFP control embryo, B) Islet-1 GFP embryo injected with 4ng of capZα1 ATG MO, Arrows indicate aberrant axonal projections. C) Islet-1 GFP embryo injected with 10ng of capZα1 splice 2 MO.

formation of motoneurons in the splice 2 morphant was also not defective in the brain or along the spinal cord on day 3 or 4 (Fig. 6.12C and Fig. 6.13E and F). To look in more detail at the axonal projections of the motoneurons within the muscle, confocal imaging of 4 dpf embryos fixed for 2 hrs in 4% PFA was performed (Fig. 6.14). Although the axons had branched and extended into the muscle in the ATG morphants, additional axonal exit points were observed along the spinal cord compared to the control. Moreover, the exit points were also not evenly spaced along the spinal cord (Fig. 6.14B arrows). Aberrant exit points were not observed in the capZα1 splice 2 morphants and therefore indicate that this phenotype is not a non-specific MO effect. Secondary motoneuronal axon projections follow the path of the axons derived from primary motoneurons. Thus it remains to be determined whether the aberrant motoneuron patterning in the ATG capZα1 morphant is due to an initial defect in primary motoneuron axonal growth.

6.6 Discussion

Loss of function of CapZ, in conjunction with other thin filament proteins has indicated that this capping protein clearly plays a major role in maintaining myofibrillar and sarcomeric organization. In this chapter it has been demonstrated that either CapZ or Nebulin are required for maintenance of the Z-lines within the sarcomere. Loss of each of these proteins alone did not affect Z-line stability, however, when both proteins were depleted the Z-lines disassembled. A very small number of intact Z-lines were visualized with α-actinin staining in the *sne*/*buf* double mutants and therefore suggests that in these mutants the Z-line integrity is affected, rather than the initial assembly of the Z-line. Moreover, combined loss of CapZ and Nebulin results in the loss of thin filament. Residual actin filaments were observed by phalloidin staining in day 5 *buf* /CapZα1 double loss of function and double mutant embryos. This observation implies that CapZ and Nebulin are required for stabilizing the actin filament and maintaining it as a polymer.

As expected, loss of both capping proteins completely ablates formation of thin filament. However, the single knockdown of Tmod4 produces a more severe effect in terms of actin filament formation than loss of CapZ, and supports the finding by Littlefield and colleagues (2001) that Tmod is able to nucleate more filaments than CapZ. It is surprising to note that loss of Tmod alone can also affect the morphology of the Z-line, as nemaline bodies very similar to those observed in the *buf* mutant were detected. Tmod could therefore be a novel candidate for causing nemaline myopathies in humans. Intriguingly, CapZ appears to be integral to the formation of nemaline bodies, as knock down of CapZ in both the *buf* mutant and Tmod4 morphants results in loss of nemaline bodies.

In zebrafish, loss of Desmin by MO knockdown induces the formation of wavy myofibres which was very similar to the myofibre phenotype observed in the *sne* mutant. Double knockdowns of Desmin and CapZα1 were performed to determine whether myofibrillar organization was exacerbated by loss of both proteins, however, no obvious effects were observed. In the *sne* mutant, Desmin localization at the sarcolemma and at the myosepta is completely ablated. This suggests that CapZ plays an important role in anchoring Desmin to the Z-line and the myosepta. Moreover, this finding substantiates the CapZα1 /Desmin double knockdown results. As the loss of CapZ alone appears to affect Desmin localization, it is foreseeable that additional loss of Desmin would have no effect on enhancing the existing CapZα1 loss of function phenotype. It will be interesting to determine if CapZ and Desmin directly interact and whether CapZ plays a molecular role in upregulation of Desmin expression. Desmin is an important factor in aligning of the Z-lines between myofibrils and producing a very ordered myofibrillar structure, therefore loss of this protein in *sne* mutants may have a large impact on the phenotype.

In 2003 Taoka and colleagues identified an interaction between CapZ and the neuronally expressed protein V-1 by tandem affinity purification, followed by mass spectrometry. V-1 is expressed in the cerebellum of mice, particularly in the early stages of postnatal development, in the regions where synaptic formation and neuronal migration occur actively during neurogenesis. V-1 inhibited CapZ regulated actin polymerization *in vitro* in a dose dependent manner. In light of this finding the effect of loss of CapZ on neuronal development was investigated.

Motoneurons of transgenic Islet-1 GFP embryos injected with capZα1 MO indicated that the loss of CapZ affected the patterning of axonal exit points from the spinal cord. In wild type embryos only one exit point forms per spinal cord hemisegment, however, in the capZα1 ATG morphants at least two exit points were detected per hemisegment. Spinal motoneurons develop in two waves: The first wave generates three main types of primary motoneurons per hemisegment (CaP, MiP and RoP) and each motoneuron projects axons which leave through a central exit point per hemisegment to innervate the somites. As development proceeds a second wave of motoneurons develop (secondary motoneurons) and extend their axons along the same path as primary axons (For review see (Beattie, 2000)). As the motoneuron defect in the capZα1 morphants was detected on day 4, further experiments will be required to determine whether the loss of CapZ affects primary axonal projections earlier in development. If the primary motoneurons are affected it will be interesting to determine which types of primary motoneuron are forming aberrant axonal projections. Investigation of CapZ's role in motoneuronal development may therefore provide further insight into the mechanisms behind axon growth and intraspinal guidance.

Chapter 7

General Discussion

Chapter 7: General Discussion

A vast amount of research has been performed to date towards understanding the complex processes that underlie muscle formation and function in vertebrates. However, further research will be required to fully comprehend how the muscle develops, especially *in vivo*. In this thesis I have described the positional cloning of the zebrafish muscle mutant *sne* to *capzα1* and determined that CapZ, in conjunction with other sarcomeric proteins, is crucial for maintaining the integrity and architecture of striated skeletal muscle.

7.1 The *sne* locus is *capzα1*

SSLP and indel markers were used to map the *sne* locus to a 0.7Mb region on chromosome 8. The primary candidate within this region was *capzα1* and sequencing of this gene identified a G-A mutation at the donor splice site of exon 9. The mutation affected splicing of the 3′ region of *capzα1* and three mis-spliced transcripts were identified in the *sne* mutant (Fig. 3.8). The mutant was phenocopied using a MO that targeted the exon 9 donor splice site (Fig. 5.8) and the phenotype of the capZα1 ATG morphant was also rescued by expression of exogenous *capzα1*-GFP (Fig. 5.22). These experiments provided conclusive evidence that the *sne* mutant phenotype is due to a mutation in *capzα1*.

7.2 The mutation in *capzα1* affects the sarcomere and myofibrillar structure of skeletal muscle

The *sne* mutant has a distinctive muscle phenotype that affects embryonic motility as well as the morphology of skeletal muscle. The motility defect is first apparent at 4 dpf and mutant embryos do not survive to adulthood, presumably as they are unable to swim effectively and therefore cannot independently source food. Immunostaining of *sne* mutant skeletal muscle

revealed that the myofibres were wavy, CapZα1 was not localized to the Z-lines and the Z-lines were misaligned between myofibrils. Moreover, the myofibrils did not appear to attach cleanly to the myoseptum (Fig. 4.16 and 4.19). Closer inspection of striated muscle architecture by TEM also indicated that, although all the sarcomeric components were present, the structure of the sarcomere was disrupted; thin filaments were splayed near the Z-line and the Z-lines were more diffuse compared to the sibling controls (Fig. 4.20).

It is evident from the morphology of the *sne* mutant that the mutation in *capzα1* does not affect the assembly of the sarcomere *per se*, but rather its integrity is lost. It is tempting to speculate that in the absence of CapZ the thin filament is not tethered securely to the Z-line. Once the sarcomere starts to contract, the link between the thin filament and the Z-line is not strong enough to withstand the forces generated and subsequently the thin filament starts to dissociate from the Z-line. Moreover, as the barbed end of the actin filament is not capped by CapZ polymerization is likely to continue, resulting in the extension of thin filament across the Z-line which in turn leads to the splayed thin filaments and diffuse, wider Z-lines that are observed in the TEM images of mutant muscle.

The C-terminus of nebulin has been shown to interact with the actin thin filament, capZ and the Z-line protein α-actinin (Chen et al., 1993; Gonsior et al., 1998; Papa et al., 1999; Witt et al., 2006). It is likely that in the absence of capZ, nebulin may act as a stabilizer for the thin filament and partially tether the thin filament to the Z-line. Therefore it may be possible that more extreme phenotypes such as complete loss or massive elongation of the thin filament are not observed in *sne* mutants due to the compensatory roles of nebulin. If thin filaments were extended due to the lack of capZ then it would be expected that the width of each sarcomere would be longer.

Surprisingly, measurements of the sarcomere width from TEM images indicated that the sarcomeres were shorter in the mutants (Fig. 4.21). This puzzling result may be due to the interaction of capZ with other components that are involved in aligning the myofibrils and linking them to the sarcolemma. One could speculate that in the *sne* mutants the smaller sarcomeres are generated as the Z-lines are unable to return to their original position within the myofibril after contraction. This in turn contributes to the myofibrillar disorganization and misaligned Z-lines which are characteristic of the *capzα1* mutant.

The misalignment of myofibrils and Z-lines has also been observed in the skeletal muscle of the obscurin zebrafish morphant (Raeker et al., 2006). Obscurin is a giant sarcomere associated protein that localizes to the Z-line and M-lines. Knock down of this protein in zebrafish produces disarrayed myofibrils as well as somite segmentation defects. This finding indicates that sarcomeric proteins are important not only in facilitating contraction but are also essential for organization of myofibrils within muscle cells. Indeed, Raeker and colleagues suggest that obscurin links myofibrils to the ECM and disruption of this linkage affects the stability and organization of the myofibril architecture and myosepta.

To demonstrate that the smaller sarcomeres are due to muscle contraction in the *sne* mutants one would need to show that the sarcomere width is normal at earlier developmental stages, prior to muscle contraction. It seems likely that muscle contraction does contribute to the *sne* muscle phenotype as inhibition of muscle use with an anesthetic (tricaine) was able to partially rescue the mutant phenotype. The actin dynamics in *sne* mutants could also be examined to determine whether actin polymerizes from the barbed end in the absence of functional capZ.

This could be performed by photobleaching of Actin-GFP expressed in *sne* mutants, in a similar fashion to the experiments that were performed in cultured muscle cells (Littlefield et al., 2001).

Characterization of the *sne* mutant phenotype has shown that CapZα1 and thus CapZ is important in maintaining the myofibrillar and sarcomeric structure of striated skeletal muscle. To date *sne* is the only vertebrate mutant of *capzα1*, therefore in depth analysis and manipulation of this mutant will no doubt provide further insight into the complex interactions that occur within striated skeletal muscle.

7.3 The *sne* allele is hypomorphic

Of vital importance to an informed analysis of *sne* has been defining whether the mutant is a complete null (i.e. where none of the aberrant transcripts are translated and the function of CapZα1 is completely abolished) or a hypomorph. CapZα1 immunostaining and MO knockdown of the various CapZ subunits has provided substantial evidence to suggest that the *sne* mutant is a hypomorph, and the aberrant CapZα1 protein product that is produced in the mutant is non-functional in its capacity to cap actin filaments at sarcomeric Z-lines.

7.3.1 The *capzα1* mis-spliced transcripts are translated in the *sne* mutant

By using a polyclonal CapZα1 antibody to detect CapZα1 in wholemount embryos I was able to establish that a mis-spliced form of CapZα1 was translated in the mutants (Fig. 4.19). However, the distinctive striated pattern seen in normal muscle tissue was absent and positive staining was instead observed in aggregations adjacent to the myoseptum . This result indicated that the mutant form of CapZα1 is unable to localize to the Z-line and cap the barbed end of the actin filament in skeletal muscle. There are a number of possible explanations for this finding:

Firstly, the mutant isoform may not be able to dimerize with the β subunit, therefore no functional CapZ is produced and no capping takes place. Secondly, CapZα1 is still able to dimerize with the β subunit but cannot bind to actin. Thirdly, CapZ dimerizes with the β subunit and is able to bind to the barbed end of actin, however, it is unable to localize to the Z-line and therefore cannot cap the barbed end of the actin filament in skeletal muscle. In light of the MO analysis discussed below the first possibility appears to be the most feasible.

7.3.2 Knockdown of CapZ subunits suggests that the *sne* mutant protein is functional in non-muscle cells

Complete ablation of CapZα1 expression by injection of the capZα1 ATG and splice 1 MOs into 1-2 cell stage embryos resulted in a more severe defect than was observed in the *sne* mutant (Fig. 5.2-5.5). This finding implies that the mutant form of CapZα1 has some function, particularly in the early stages of development prior to muscle differentiation. It would also suggest that the aberrantly spliced CapZα1 must be able to dimerize with a β subunit and cap the actin filaments in non-muscle cells. If this is indeed the case then why does the mutant form of CapZα1 only affect skeletal muscle tissues? One explanation for the different phenotypes observed between the *capzα1* mutant and morphant is perhaps that CapZα1 is able to bind to more than one β subunit. Therefore, this may result in the formation of CapZ isoforms that localize to unique sub-cellular locations within different tissues. In cardiomyocytes of other vertebrates the β subunits are differentially localized. The β1 subunit is located at Z-lines and the β2 subunit is localized to the intercalated disc and cell to cell junctions (Hart and Cooper, 1999; Schafer et al., 1994). Due to their different locations within the cardiomyocytes the two isoforms of CapZβ are thought to have distinct functions *in vivo*. If more than one β subunit exists in zebrafish and they are differentially localized, one could speculate that the CapZα1 mutant

isoforms are able to bind to the β2 subunit and function early in development. However, are unable to dimerize with the β1 subunit located at the Z-line in striated muscle, resulting in the muscle specific defects observed in the *sne* mutant. This theory is supported by studies that recombinantly generated a capping protein comprised of the mouse α1 and β2 subunit, and showed that this isoform can bind to Twinfilin and CARMIL (Palmgren et al., 2001; Yang et al., 2005). Both these proteins are thought to be important in regulating non-sarcomeric actin filament dynamics. This finding supports the hypothesis the different α and β subunits can dimerize to form capping proteins that have distinct functions within muscle and non-muscle cells.

Different levels of CapZβ knock down also suggest that more than one isoform of CapZ exists in zebrafish. Additionally, they indicate that the *sne* mutant forms of CapZα1 are unable to bind to the β subunit expressed in skeletal muscle. Low doses of both the capZβ splice and ATG MOs produce morphants that have a very similar phenotype to the *sne* mutant (Fig. 5.17 and 5.18). Moreover, wholemount CapZα1 antibody staining revealed that CapZα1 was mis-localized to the myoseptum in these morphants. These results illustrate that CapZβ is required for the correct localization of these capping proteins; in the absence of CapZβ, although functional CapZα1 is produced, it is unable to dimerize with the β subunit to form CapZ, and therefore it cannot localize to the Z-line and cap the barbed end of the actin filaments.

Complete knock down of the CapZβ subunit using high doses of the capZβ ATG MO (which would be able to knock down the CapZβ1 isoform if it exists) produced a severe phenotype similar to the knock down of both the α subunits with the capZα2 ATG MO (Fig. 5.19). This phenotype supports the previous findings that the *sne* mutant must produce some form

of functional CapZ and confirms that severe defects are induced in the complete absence of CapZ, either by knockdown of all α or β subunits. It also verifies the importance of CapZ in the early stages of development, long before sarcomere assembly. Indeed, similar findings were observed in a *Drosophila capzβ* mutant (Hopmann et al., 1996), where the generation of a complete null resulted in lethality in the early larval period, indicating that CapZ is essential in the early stages of development.

7.3.3 The crystal structure of CapZ indicates that the C-terminal region of CapZα1 is important in actin binding and dimerization to the β subunit

The crystal structure of chicken CapZ (α1 and β1) has been published (Yamashita et al., 2003) and provides further support for the proposal that the CapZα1 mis-spliced products may not able to dimerize with CapZβ and cap the end of actin filaments. Analysis of the crystal structure indicated that the C-terminal region of CapZα1 is critical for actin binding and dimerization with the β subunit. Additionally, Yamashita and colleagues have also suggested that the C-termini of the CapZα1 and CapZβ1 subunits are mobile and this enables the C- terminal region to dock to the end of the actin filament. I*n vitro* studies have subsequently confirmed that the capping protein caps the barbed end using the mobile C-termini of the α1 and β1 subunits (Wear et al., 2003). Moreover, the C- terminal of the α1 subunit was found to contribute more to capping affinity and kinetics than the C- terminal of the β subunit. *In vivo* studies performed in yeast also indicate that the C-terminal region of CapZα (residues 259-286) is crucially required for actin binding (Casella and Torres, 1994; Hug et al., 1992; Sizonenko et al., 1996).

By comparing the surface area that is exposed between each subunit, the crystal structure of CapZ also revealed that interactions between the α1 and β1 subunit occur mainly between C-terminal domains. 74% of the regions that come into contact between the subunits are buried between the C-terminal domains and only 19% are buried between the N-terminal regions. The interactions between the C-termini are likely to be very important in dimerization of the α and β subunits.

In silico translation of all mis-spliced transcripts expressed in the *sne* mutants revealed that the C-terminal domain of CapZα1 would be disrupted (residues 240-286). Out of the three mis-spliced transcripts observed in the mutant, only one would be unable to translate the critical C-terminal domain. The other two transcripts were predicted to still produce the C-terminal domain, however, it is entirely feasible that the deletion and insertion of amino acids in these mis-spliced products could affect the stoichiometry of this region. As shown in chapter 4 the C-terminal region is highly conserved between vertebrates (Fig. 4.1) and therefore it is possible that even a slight change in the C- terminal domain may affect the ability for the α1 subunit to dimerize to the β subunit.

Although the MO knockdowns and immunostaining analyses have provided the initial evidence that the *sne* allele is hypomorphic, further experiments are required to confirm the functional capability of the mis-spliced CapZα1 isoforms translated in the mutant. Firstly, the predominant mis-spliced CapZα1 isoform that is translated in the mutant needs to be established and its function in terms of its ability to bind to the β subunits needs to be determined. Secondly, the existence, function and localization of a CapZβ1 subunit in zebrafish need to be verified. Finally, experiments would need to be performed that show that the α and β subunits could

combine in different ways to produce isoforms of CapZ that have different functions. Identifying how the mutation in *capzα1* induces the *sne* mutant phenotype on a molecular level will be invaluable in discerning the functions of the different CapZ subunits, and will no doubt contribute to defining the exact role of CapZ isoforms in early vertebrate development.

7.4 Potential roles for the α2 and β subunits of CapZ

7.4.1 CapZα2

MOs were designed against the α2 subunit of CapZ to determine if there was any redundancy between the two α subunits. Due to their high homology, the capZα2 ATG MO knocks down both the α1 and α2 isoforms (Fig. 5.14). Despite this, injection of this MO still produced an informative phenotype. Very small doses of capZα2 ATG MO severely delayed embryonic development and by 24 hpf many embryos had truncated axes, U-shaped somites and smaller brains (Fig. 5.11 and 5.12). As this phenotype is more severe than knock down of CapZα1 alone, it would suggest that complete ablation of CapZ severely affects development of the embryo and the α2 subunit may play a more important role in earlier stages of development than the α1 subunit. Indeed, the *capzα2* RNA *in situ* expression pattern is equivalent to the *capzα1* expression pattern until the 13-15 somite stage. However, by 24 hpf *capzα2* expression is more widespread and diffuse throughout the embryo than *capzα1*, which is strongly expressed in the somites (Fig. 4.11 and 4.12). Intriguingly, in adult mouse skeletal tissue the RNA and protein levels of the α2 subunit are much greater than the α1 subunit (Hart et al., 1997b). This finding contradicts the expression pattern I observed, however, adult tissues may have different levels of the α subunits compared to embryos.

In zebrafish, the expression pattern and double knockdown of the CapZα subunits indicate that CapZα1 has a more prevalent role in capping actin filaments within the sarcomeres of the skeletal muscle, while CapZα2 may be more important in capping actin filaments that play other essential roles within all cells. Surprisingly, no phenotypic defects were observed in the capZα2 splice morphant, therefore, assuming that the splice MO is actually knocking down CapZα2, this finding may suggest that the α1 subunit is also able to compensate for the lack of the α2 subunit throughout development. Of course there is still the possibility that the splice MO is not effective and confirmation of its function by RT-PCR is necessary.

Further characterization of the α2 subunit is required to determine its exact function in development. A MO specifically designed against a unique site of the *capzα2* 5′ UTR will be useful in determining whether loss of CapZα2 alone produces a severe defect, as is seen in the double knock down of the α subunits, or whether there is some redundancy shared with the α1 subunit. Defining the *in vivo* localization of the α2 subunit will also assist in unraveling its function in zebrafish development and this could be achieved by making a GFP fusion construct. The fusion constructs for both the subunits could subsequently be co-injected with different α1 and α2 MOs to determine whether exogenous CapZα2 can rescue the phenotype of the capZα1 morphant or vice versa.

7.4.2 CapZβ

The other key element in the function of CapZ is the β subunit. Without α and β subunit dimerization CapZ is not produced. As mentioned previously, the β1 and β2 isoforms display tissue specific expression and localization: the β1 isoform localizes to the Z lines and the β2 subunit localizes to the intercalated disc and cell to cell junctions in chicken cardiac muscle and

striated muscle cells (Schafer et al., 1994). Over expression of the β subunits in the cardiomyocytes of transgenic mice indicated that each subunit is distinctly localized *in vivo* and each isoform is unable to compensate for the other (Hart and Cooper, 1999). RNAse protection assays found that in skeletal muscle there was a much higher expression of the β1 isoform than the β2 isoform (Schafer et al., 1994) and this was also verified by 2-D immunoblots (Hart et al., 1997b). In zebrafish I was only able to identify the *β2* isoform, however, due to the unique function of each the β subunits observed in other vertebrates it seems likely that an alternate isoform of *capzβ* is expressed in zebrafish. Genomic sequencing of the intronic region encoding the exon that makes the *β1* isoform unique will be required to establish whether zebrafish do indeed express more than one *capzβ* subunit.

Low doses of capZβ ATG or splice MO produce morphants with similar phenotypes to the *sne* mutant (Fig. 5.17 and 5.18). It could be speculated that only the muscle phenotype is observed in these morphants as the MO does not completely knock down all CapZβ. Therefore in the early stages of development there is enough CapZβ for CapZ to function normally, however, upon muscle differentiation these levels are not sufficient and subsequently gives rise to a phenotype similar to the *sne* mutant.

Intriguingly, in addition to the muscle defect, the edges of the caudal fin were frayed in 5 dpf capZβ ATG morphants (Fig. 5.17). It is uncertain as to why this phenotype is only observed in the ATG morphant and not in the splice morphant but may be due to differences in effectiveness of each MO. Zebrafish embryos possess two types of fin, the caudal fin and the pectoral fins, that are composed of epithelial and mesenchymal cells. Very little is known about the development of the caudal fin, however, DiI labeling was used to show that early caudal fin

bud mesenchyme is derived from trunk neural crest cells (Smith et al., 1994). Neural crest cells are precursors to a wide variety of cell types and develop from the edge of the neural ectoderm before migrating to various regions within the embryo. In addition to the caudal fin these cells give rise to most of the neurons and glia of the peripheral nervous system, craniofacial cartilage and bone, pigment and smooth muscle (Christiansen et al., 2000; LaBonne and Bronner-Fraser, 1999; Le Dourain and Kalcheim, 1999). It could be speculated that the loss of CapZβ disrupts the migration of neural crest cells. This hypothesis is supported by the fact that defects the jaw, another neural crest derivative, is observed in capZβ morphants. Actin dynamics is essential for the formation of filopodia and thus cell movement, therefore it is possible that a depletion of CapZ may affect the movement of neural crest cells. In future experiments it may be worth exploring whether defective neural crest migration does indeed give rise to the caudal fin and jaw phenotype in these morphants.

Interestingly, the defective caudal fin phenotype was also observed in the *capzβ* retroviral insertion mutant (Amsterdam et al., 2004). The insertion in this mutant is located immediately after the start site and correlates with the capZβ ATG MO target site. No muscle phenotype was described in the *capzβ* mutant, however, close inspection of the muscle may have been overlooked as the images provided do suggest that their may be a defect in the muscle. Acquisition of this mutant line will assist in the further analysis of CapZ in zebrafish muscle and caudal fin development.

7.5 CapZ regulates thin filament assembly and integrity with nebulin and tropomodulin

One of the major mysteries in sarcomere assembly has been how the actin thin filament is able to precisely polymerize into uniform lengths within the sarcomere. For a number of years a model in which nebulin acts as a ruler for defining thin filament length has been widely accepted. Additionally, the capping proteins capZ and Tmod are also thought to be involved in maintaining the length of the actin filament. However, the exact mechanisms and interactions between these three components that results in the formation of uniform actin polymers is still not completely understood.

In collaboration with Elisabeth Busch-Nentwich the effect of loss of one or more of these components on thin filament formation and stability was examined during zebrafish muscle development. The results indicate firstly that loss of CapZ or Nebulin alone does not affect Z-line integrity or formation, however, loss of function of both these proteins destabilizes the Z-line and therefore suggests that at least CapZ and Nebulin are required for maintenance of Z-line integrity. Moreover, in the absence of CapZ and Nebulin thin filament does not form in skeletal muscle indicating that CapZ and Nebulin are required for actin filament stability (Fig. 6.4 and 6.6). Secondly, double knock down of CapZ and Tmod4 results in loss of Z-lines and almost completely ablates thin filament formation (Fig. 6.4). This indicates that both proteins are required for nucleation of sarcomeric actin filament. Loss of only Tmod4 results in severe depletion of actin filament compared to loss of only CapZ (Fig. 6.2), which confirms previous studies that suggest that nucleation of actin polymerization mainly occurs from the pointed end (Littlefield et al., 2001). Interestingly, nemaline bodies similar to that of the *nebulin* mutant (*buf*) were observed in the absence of Tmod4. Thirdly, ablation of Tmod4 and Nebulin exacerbates the

formation of nemaline bodies and as a result the sarcomere structure is severely disrupted, however, fragments of thin filament are still observed (Fig. 6.4). Finally, loss of CapZ in either the *nebulin* mutant or the Tmod4 morphant abolished the formation of nemaline bodies and implies that CapZ is involved in the formation of nemaline bodies (Fig. 6.4).

The findings from these knock down experiments illustrates the importance of CapZ, Nebulin and Tmod in maintaining the integrity and stability of the sarcomere. These thin filament associated proteins act in concert to define and maintain the length of the actin filament within striated muscle. However, a number of questions have arisen from these studies such as how are nemaline bodies formed and why do nemaline bodies only form in Tmod4 morphants and *nebulin* mutants? How does the loss of CapZ affect their formation? How are Nebulin and CapZ able to stabilize the thin filament and the Z-line? By comparing the knock down and mutant phenotypes that have been generated, in combination with what is already known about these thin filament associated proteins, it is possible to provide some explanations as to how Nebulin, Tmod and CapZ are involved in maintaining the integrity of the sarcomere and will be discussed herein.

In both zebrafish and mouse *nebulin* mutants the thin filaments still form, however, the length of the filaments is affected (Bang et al., 2006; Witt et al., 2006). Both these vertebrate mutants support the widely accepted theory that Nebulin is required to precisely define the length of the actin filament. Nebulin has also been shown to increase the affinity for Tmod to cap the pointed end of the thin filament (McElhinny et al., 2005).Therefore it is likely that in the absence of Nebulin, Tropomyosin may be able to assist in elongation of the thin filament to the approximate length, however, as the actin filament is partially uncapped at the pointed end aberrant elongation of the thin filament occurs at this end. Although the assembly of the

sarcomere is not grossly affected in zebrafish *nebulin* mutants, it could be speculated that the integrity of the sarcomere is lost once the muscle starts to function due to the longer actin filament. Witt and colleagues (2006) have proposed that the longer actin filament slips and extends further into the Z-line than it should, thus more α-actinin is recruited to the Z-line to link the extra thin filaments and eventually gives rise to nemaline bodies.

It has been well established that CapZ stably caps the barbed end of the thin filament and is thought to tether the thin filament to the Z-line. As previously mentioned from analysis of the zebrafish *sne* mutant, it has been hypothesized that loss of CapZ reduces the strength of the link between the thin filament and the Z-line. Sarcomere assembly still proceeds as Nebulin may be able to compensate for the lack of CapZ and partially cap the barbed end of the filament and secure it to the Z-line. However, as soon as muscle contraction begins, the link between the Z-line and the thin filament is not strong enough to endure the force generated resulting in loss of sarcomeric integrity. When both CapZ and Nebulin are depleted the thin filament is completely de-stabilized. Even though the actin filament should still nucleate from Tmod, at least CapZ or the C-terminus of Nebulin are required for the filament to become stable. It could be that the loss of the thin filament in these double loss of function embryos causes the Z-line to collapse: As there is no thin filament for α-actinin to cross link with, the Z-line becomes unstable and therefore disintegrates. This interpretation is supported by Tmod4 and CapZ double knockdowns, which also lack thin filaments and Z-lines.

In the Nebulin and Tmod4 double loss of function embryos thin filaments were still observed even though the sarcomere had become disorganized (Fig. 6.4). In these mutants CapZ is still present and therefore in theory a small amount of actin filament polymerization should be

able to occur, however, without the other capping protein (Tmod) or Nebulin to define the other end of the thin filament the lengths would be random. Once the muscle starts to contract, as speculated in the *nebulin* mutant, the actin filaments slip into the Z-line leading to the accumulation of α-actinin and thus the production of dense Z-line bodies. As these Z-bodies enlarge they disrupt the sarcomere structure and the titin cross-links are pulled apart, leading to Z-line disintegration and disorganization of the sarcomere.

Loss of Tmod4 on its own produces a similar phenotype to the *nebulin* mutant, however, the phenotype is more severe, probably because nucleation of the thin filament occurs predominantly from Tmod (Fig. 6.2). Those filaments that do form will be longer than normal as Nebulin cannot cap the actin filament. Therefore it is proposed that during muscle contraction, as in the *nebulin* mutant, the elongated filaments will be pushed into the Z-line and attract the accumulation of α-actinin which tries to cross-link the extra thin filament, thereby giving rise to nemaline bodies.

The lack of nemaline bodies in the Tmod4 and CapZ double knockdown, and Nebulin and CapZ loss of function embryos may be due to the loss of thin filament that in turn results in the loss of the Z-line, rather than a direct consequence of CapZ itself. As no thin filaments are produced in these double mutants α-actinin cannot cross-link either the thin filaments to each other or to titin and the Z-line is destabilized. Therefore nemaline bodies cannot form, unlike in the single mutants or the Tmod4 and Nebulin double loss of function embryos where thin filaments were observed. Although CapZ has been shown to interact with α-actinin it is unlikely that it is responsible for α-actinin localization to the Z-line, as in *sne* mutants α-actinin can localize to the Z-line in the absence of functional CapZ.

A number of key experiments are still required to support the role of CapZ, Nebulin and Tmod in sarcomere integrity and in the formation of nemaline bodies. The phenotypes of the double mutants must be examined at much earlier stages of development to confirm that the sarcomere assembles, and that its integrity is compromised due to the lack of the thin filament associated proteins. Conclusive evidence is required to establish that in Nebulin and Tmod4 double loss of function embryos the thin filaments are longer. The localization of CapZ in the mutants that form nemaline bodies will also assist in ruling out the possibility that CapZ directly induces nemaline body formation.

Studies in various model organisms have investigated how thin filament associated proteins regulate thin filament formation and integrity. Many of the results support the findings that we have observed from the knockdowns of these proteins in zebrafish, however, unlike our experiments most studies have only focused on Tmod or Nebulin. The findings of these studies compared to the results obtained in zebrafish are discussed herein.

Most of the research performed on Nebulin has shown that it is important in precisely defining the length of the thin filament. However, there is conflicting evidence in the literature regarding whether loss of Nebulin increases or decreases actin filament length and whether it is involved in assembly of the sarcomere. In 2006 two different laboratories generated nebulin knock out mice (Bang et al., 2006; Witt et al., 2006). Both sets of researchers produced knock out mice with very similar phenotypes and concluded that a lack of Nebulin results in shorter thin filaments. Witt and colleagues (2006) also observed that about 15% of the Z-lines were abnormally wide and nemaline rods had formed. They speculated that the nemaline bodies form

as actin filament capping by CapZ is perturbed upon loss of Nebulin. Therefore thin filaments polymerize into the Z-line and trigger the recruitment of more Z-line proteins, resulting in widening of the Z-lines. Our model of nemaline body formation, however, suggests that the thin filament aberrantly extends from the pointed end rather than the barbed end, from a lack of Nebulin. This theory is consistent with studies that have shown that CapZ is far more stable at capping the actin filament than Tmod, so it seems far more likely that Tmod capping is perturbed from the lack of Nebulin. Additionally, the interpretation that longer thin filaments exist in the muscle of these mutants may not be correct. To observe the structure of mouse muscle the muscle tissues are first isolated and then stretched. Therefore it is possible that the stretching of the muscle induces slight changes in the muscle architecture that are not representative of the *in vivo* structure. Indeed, in the previous year McElhinney and colleagues (2005) used siRNA to knockdown Nebulin in cultured rat cardiomyocytes and found that the filaments were longer at the pointed end. They also showed that striated thin filaments, Z-lines, Titin and thick filaments failed to assemble in fetal skeletal myocytes depleted of Nebulin and concluded that Nebulin plays a role in sarcomere assembly. Although longer filaments are observed in the zebrafish *nebulin* mutant, both mouse and zebrafish mutant models are still able to assemble sarcomeric components and do not support these latter conclusions. As these knockdowns were done in cultured myocytes they may produce very different outcomes to experiments performed *in vivo*.

Many studies on Tmod have been based in cultured cardiomyocytes and therefore have looked at Tmod1. It has been shown that overexpression of *tmod* in cardiomyocytes results in shorter actin filaments (Littlefield et al., 2001; Sussman et al., 1998). This result was replicated in *Drosophila* by transient overexpression of the *tmod* homologue *sanpodo* in indirect flight muscles (Mardahl-Dumesnil and Fowler, 2001). Conversely, reduced expression of *tmod* in

cardiomyocytes resulted in thin filament elongation. (Sussman et al., 1998). All the studies to date support a model for Tmod in regulating thin filament length by preventing polymerization and depolymerization. Recently a Tmod1 mouse knock out was generated, however, the null mice die due to heart abnormalities at E10-10.5. (Fritz-Six et al., 2003), and therefore detailed analysis of myofibril assembly and maturation could not be assessed. As an alternative to the mouse mutant, Tmod1 mouse knock out ES cells were used to examine the loss of Tmod1 in cardiomyocytes derived from embryoid bodies (Ono et al., 2005). In these embryoid bodies the sarcomere assembles normally in the null myofibrils, however, surprisingly, the actin thin filaments still have uniform lengths. These findings may be unique to embryoid bodies as they completely contradict the previous studies mentioned. Further research is therefore required to reach a consensus on the function of Tmod in regulating thin filament assembly *in vivo*.

Despite the discrepancies in the different loss of function models for Nebulin and Tmod, most of these models still support the hypothesis that Nebulin acts as a template for actin polymerization (presumably through its internal super-repeats) as well as being able to assist in terminating the end regions (McElhinny et al., 2001; Witt et al., 2006) by interacting with Tmod and CapZ. The different mutant models generated will no doubt prove to be useful tools in ultimately determining how the interactions between Nebulin, Tmod and CapZ define thin filament length.

The results from the zebrafish double loss of function experiments may also provide further insight on how the sarcomere assembles *in vivo*. As outlined in the introduction the latest model for myofibrillogenesis is the Sanger premyofibril model. This model proposes that myofibrillogenesis begins with the formation of premyofibrils consisting of I-Z-I bodies that

interdigitate with non-muscle myosin II. Titin and muscle myosin are then expressed and titin and the thin filament in I-Z-I bodies are responsible for integrating and aligning muscle myosin filaments within the sarcomere. In light of our double knockdown studies (CapZ and Tmod4 or CapZ and Nebulin double loss of function embryos) the loss of thin filament does not affect the organization of the thick filaments (Fig. 6.4). One of the most striking and unexpected results is that thick filaments are still positioned in an ordered block within the sarcomere in the absence of thin filaments. This indicates that the thin filament is not required for the incorporation and alignment of thick filaments within the sarcomere. Clearly the sarcomere is non-functional without thin filament and therefore it is likely that the thick filaments eventually disassemble in these double loss of function embryos. This phenomenon was also observed in *ex vivo* experiments on sea bass muscle. When the extracted muscle was incubated with proteases that ablated Z-lines or thin filament, the thick filament was still arranged in ordered blocks within the sarcomere after 24 hpf (Taylor et al., 1997). Of course the results described may not truly reflect what would happen *in vivo*, however, it does support the hypothesis that titin and M-line proteins may be more important in the assembly and maintenance of the thick filament than thin filament components.

The assembly and maintenance of myofibrils and sarcomeres is an extremely complex process and involves many proteins that cooperate together to make up a functioning muscle cell. It is evident that there is still intense debate on exactly how the sarcomere assembles and functions, and a consensus has still not been reached on the function of many sarcomeric proteins. Although *in vitro* studies have been invaluable in defining certain aspects of striated muscle assembly, further *in vivo* studies will be vital in gaining a greater understanding of muscle assembly and maintenance in vertebrates. Zebrafish are excellent for further investigation in this

field and there are now a number of mutants available that are defective in sarcomeric proteins. Further analysis of zebrafish muscle mutants will no doubt be beneficial to our understanding of vertebrate myofibrillogenesis and may also assist in unraveling the molecular nature of human myopathies.

7.6 CapZ and the intermediate filament protein desmin

Desmin is one of the earliest known myogenic markers that is expressed in both cardiac and skeletal muscle. Along with other costameric and intermediate proteins it is thought to be important in transducing the force generated by the sarcomere across the entire length of the myofibril and also between the sarcomere and the sarcolemma. Desmin is attached to the sarcomere at the Z-line and has previously been shown to bind to α-actinin and nebulin (Bang et al., 2001), however, a direct interaction with capZ has not been identified. Intriguingly the targeted mouse knock out of desmin produced a very similar phenotype to the *sne* mutant; TEM of different muscle tissues indicated that the early stages of muscle formation were normal, however weight bearing muscles such as the soleus and diaphragm lost their structure over time and the pathology worsened from increased muscle usage. The muscle structure degenerated and lateral alignment of myofibrils was observed (Li et al., 1997). Due to the striking similarity between the zebrafish *capzα1* mutant and the mouse desmin knockout I wanted to investigate whether CapZ and Desmin acted together to maintain the structural integrity of the muscle in zebrafish. As predicted the knock down of Desmin in zebrafish produces a very similar phenotype to the mouse mutant and the zebrafish *sne* mutant, characterized by wavy fibrils that were misaligned within each somite (Fig. 6.8). Intriguingly, antibody staining of Desmin in the *sne* mutants showed that protein levels were greatly diminished and, unlike in wild type controls, Desmin staining was absent in the myofibrils and greatly reduced in the myoseptum (Fig. 6.11).

This result clearly demonstrates that there is some connection between CapZ and Desmin, however, the exact molecular mechanisms behind this result are still unknown and many more questions need to be addressed such as: Does CapZ regulate Desmin expression or is it required for Desmin to localize to the Z-lines and the myoseptum? Moreover, does CapZ directly interact with Desmin and stabilize its attachment to the Z-line? It is tempting to speculate that the loss of CapZ at the Z-line disrupts localization of Desmin and therefore lack of this filament protein contributes to the misalignment of Z-lines between myofibrils and the gradual disintegration of myofibrillar organization upon muscle function. Further experiments will therefore be required to uncover the true nature of the interaction between CapZ and Desmin.

7.7 CapZ and motoneuron development

The involvement of CapZ in motoneuron development was investigated following the finding that the neurally expressed protein V-1 binds to CapZ (Taoka et al., 2003). Interestingly, knockdown of CapZα1 by using the ATG MO resulted in the formation of additional axonal exit points from spinal cord motoneurons at 4 dpf (Fig. 6.14). This finding indicates that CapZ is involved in axonal projection. Indeed, the movement of the growth cone at the tip of the axon relies on actin based motility and is guided along specific pathways by cues emitted from the surrounding tissues. Guidance molecules include netrins, semaphorins and slits, which act as attractants and repellants in defining the path of the axon (Dickson, 2002). They achieve this by regulating actin dynamics at the barbed end and thus affect the formation of filopodia in the growth cone. Additional axonal exit points have also been observed in the zebrafish mutant *sidetracked*. This mutant was found to have a mutation in *plexin A3*, a receptor for semaphorin guidance molecules (Palaisa and Granato, 2007).

Proteins that affect actin dynamics may be regulated by the guidance molecules. One example is the Arp2/3 complex which is a regulator of CapZ. The Arp2/3 complex consists of Arp (actin related protein) 2 and 3 along with five other subunits Arpc1-5 (Machesky et al., 1994). It is activated by a member of the WASP family (Wiscott Aldrich Syndrome Protein) and nucleates new actin filament assemblies. In addition to creating a branched network of filaments it can also cap the pointed ends of actin filaments (Mullins et al., 1998).One could speculate that loss of CapZ affects the correct formation of filopodia as the growth cone is unable to respond to the guidance cues, therefore the axons project aberrantly. It will be interesting to determine whether the axonal projection defect is also observed in other neurons at earlier stages of development.

7.8 Conclusions

In this thesis I have described the positional cloning and characterization of the zebrafish muscle mutant *sne*. The *sne* allele is hypomorphic and has a mutation in *capzα1*, which induces a muscle specific phenotype. Analysis of this mutant indicates that CapZ plays an important role in myofibrillar and sarcomeric integrity. Moreover, knockdown of the other subunits of CapZ suggest that different isoforms of CapZ have different roles and are required at very early stages of development. CapZ, Nebulin and Tmod double loss of function experiments illustrate the importance of these proteins in collaboratively instigating actin thin filament assembly and maintenance *in vivo*. Further research into these proteins in zebrafish will no doubt broaden our understanding of how the thin filament is maintained in skeletal muscle, and may also establish how the sarcomere assembles in vertebrates.

The various phenotypes of the capZ subunit morphants have revealed additional roles for CapZ in interaction with the costameric network and its importance in cell motility. To extend our knowledge on the roles of CapZ in zebrafish development, it will be essential to establish the existence of all isoforms, their localization and whether they have non-overlapping functions. The results presented in this thesis indicate that CapZ is involved in many aspects of development. Further characterization of this complex will not only provide insight into how CapZ maintains the muscle architecture but will also be necessary to unravel the additional roles of CapZ in vertebrate development.

References

Adams, J. C. and Watt, F. M. (1993). Regulation of development and differentiation by the extracellular matrix. *Development* **117**, 1183-98.

Agarkova, I. and Perriard, J. C. (2005). The M-band: an elastic web that crosslinks thick filaments in the center of the sarcomere. *Trends Cell Biol* **15**, 477-85.

Almenar-Queralt, A., Gregorio, C. C. and Fowler, V. M. (1999). Tropomodulin assembles early in myofibrillogenesis in chick skeletal muscle: evidence that thin filaments rearrange to form striated myofibrils. *J Cell Sci* **112 (Pt 8)**, 1111-23.

Alric, S., Froeschle, A., Piquemal, D., Carnac, G. and Bonnieu, A. (1998). Functional specificity of the two retinoic acid receptor RAR and RXR families in myogenesis. *Oncogene* **16**, 273-82.

Amacher, S. L., Draper, B. W., Summers, B. R. and Kimmel, C. B. (2002). The zebrafish T-box genes no tail and spadetail are required for development of trunk and tail mesoderm and medial floor plate. *Development* **129**, 3311-23.

Amacher, S. L. and Kimmel, C. B. (1998). Promoting notochord fate and repressing muscle development in zebrafish axial mesoderm. *Development* **125**, 1397-406.

Amatruda, J. F., Gattermeir, D. J., Karpova, T. S. and Cooper, J. A. (1992). Effects of null mutations and overexpression of capping protein on morphogenesis, actin distribution and polarized secretion in yeast. *J Cell Biol* **119**, 1151-62.

Amsterdam, A., Nissen, R. M., Sun, Z., Swindell, E. C., Farrington, S. and Hopkins, N. (2004). Identification of 315 genes essential for early zebrafish development. *Proc Natl Acad Sci U S A* **101**, 12792-7.

Antin, P. B., Forry-Schaudies, S., Friedman, T. M., Tapscott, S. J. and Holtzer, H. (1981). Taxol induces postmitotic myoblasts to assemble interdigitating microtubule-myosin arrays that exclude actin filaments. *J Cell Biol* **90**, 300-8.

Appel, B., Korzh, V., Glasgow, E., Thor, S., Edlund, T., Dawid, I. B. and Eisen, J. S. (1995). Motoneuron fate specification revealed by patterned LIM homeobox gene expression in embryonic zebrafish. *Development* **121**, 4117-25.

Arber, S., Halder, G. and Caroni, P. (1994). Muscle LIM protein, a novel essential regulator of myogenesis, promotes myogenic differentiation. *Cell* **79**, 221-31.

Arber, S., Hunter, J. J., Ross, J., Jr., Hongo, M., Sansig, G., Borg, J., Perriard, J. C., Chien, K. R. and Caroni, P. (1997). MLP-deficient mice exhibit a disruption of cardiac cytoarchitectural organization, dilated cardiomyopathy, and heart failure. *Cell* **88**, 393-403.

Babcock, G. G. and Fowler, V. M. (1994). Isoform-specific interaction of tropomodulin with skeletal muscle and erythrocyte tropomyosins. *J Biol Chem* **269**, 27510-8.

Bahler, M., Eppenberger, H. M. and Wallimann, T. (1985). Novel thick filament protein of chicken pectoralis muscle: the 86 kd protein. I. Purification and characterization. *J Mol Biol* **186**, 381-91.

Balza, R. O., Jr. and Misra, R. P. (2006). Role of the serum response factor in regulating contractile apparatus gene expression and sarcomeric integrity in cardiomyocytes. *J Biol Chem* **281**, 6498-510.

Bang, M. L., Centner, T., Fornoff, F., Geach, A. J., Gotthardt, M., McNabb, M., Witt, C. C., Labeit, D., Gregorio, C. C., Granzier, H. et al. (2001a). The complete gene sequence of titin, expression of an unusual approximately 700-kDa titin isoform, and its interaction with obscurin identify a novel Z-line to I-band linking system. *Circ Res* **89**, 1065-72.

Bang, M. L., Gregorio, C. and Labeit, S. (2002). Molecular dissection of the interaction of desmin with the C-terminal region of nebulin. *J Struct Biol* **137**, 119-27.

Bang, M. L., Li, X., Littlefield, R., Bremner, S., Thor, A., Knowlton, K. U., Lieber, R. L. and Chen, J. (2006). Nebulin-deficient mice exhibit shorter thin filament lengths and reduced contractile function in skeletal muscle. *J Cell Biol* **173**, 905-16.

Bang, M. L., Mudry, R. E., McElhinny, A. S., Trombitas, K., Geach, A. J., Yamasaki, R., Sorimachi, H., Granzier, H., Gregorio, C. C. and Labeit, S. (2001b). Myopalladin, a novel 145-kilodalton sarcomeric protein with multiple roles in Z-disc and I-band protein assemblies. *J Cell Biol* **153**, 413-27.

Barden, J. A., Miki, M., Hambly, B. D. and Dos Remedios, C. G. (1987). Localization of the phalloidin and nucleotide-binding sites on actin. *Eur J Biochem* **162**, 583-8.

Barresi, M. J., Stickney, H. L. and Devoto, S. H. (2000). The zebrafish slow-muscle-omitted gene product is required for Hedgehog signal transduction and the development of slow muscle identity. *Development* **127**, 2189-99.

Bassett, D. I., Bryson-Richardson, R. J., Daggett, D. F., Gautier, P., Keenan, D. G. and Currie, P. D. (2003). Dystrophin is required for the formation of stable muscle attachments in the zebrafish embryo. *Development* **130**, 5851-60.

Bassett, D. I. and Currie, P. D. (2003). The zebrafish as a model for muscular dystrophy and congenital myopathy. *Hum Mol Genet* **12 Spec No 2**, R265-70.

Baxendale, S., Davison, C., Muxworthy, C., Wolff, C., Ingham, P. W. and Roy, S. (2004). The B-cell maturation factor Blimp-1 specifies vertebrate slow-twitch muscle fiber identity in response to Hedgehog signaling. *Nat Genet* **36**, 88-93.

Beall, C. J., Sepanski, M. A. and Fyrberg, E. A. (1989). Genetic dissection of Drosophila myofibril formation: effects of actin and myosin heavy chain null alleles. *Genes Dev* **3**, 131-40.

Beam, K. G. (1988). Duchenne muscular dystrophy. Localizing the gene product. *Nature* **333**, 798-9.

Beattie, C. E. (2000). Control of motor axon guidance in the zebrafish embryo. *Brain Res Bull* **53**, 489-500.

Bennett, A. J. and Bagshaw, C. R. (1986). The mechanism of regulatory light chain dissociation from scallop myosin. *Biochem J* **233**, 179-86.

Bilak, S. R., Sernett, S. W., Bilak, M. M., Bellin, R. M., Stromer, M. H., Huiatt, T. W. and Robson, R. M. (1998). Properties of the novel intermediate filament protein synemin and its identification in mammalian muscle. *Arch Biochem Biophys* **355**, 63-76.

Black, B. L. and Olson, E. N. (1998). Transcriptional control of muscle development by myocyte enhancer factor-2 (MEF2) proteins. *Annu Rev Cell Dev Biol* **14**, 167-96.

Blagden, C. S., Currie, P. D., Ingham, P. W. and Hughes, S. M. (1997). Notochord induction of zebrafish slow muscle mediated by Sonic hedgehog. *Genes Dev* **11**, 2163-75.

Blanchard, A., Ohanian, V. and Critchley, D. (1989). The structure and function of alpha-actinin. *J Muscle Res Cell Motil* **10**, 280-9.

Bodine, S. C., Latres, E., Baumhueter, S., Lai, V. K., Nunez, L., Clarke, B. A., Poueymirou, W. T., Panaro, F. J., Na, E., Dharmarajan, K. et al. (2001). Identification of ubiquitin ligases required for skeletal muscle atrophy. *Science* **294**, 1704-8.

Bouvard, D., Brakebusch, C., Gustafsson, E., Aszodi, A., Bengtsson, T., Berna, A. and Fassler, R. (2001). Functional consequences of integrin gene mutations in mice. *Circ Res* **89**, 211-23.

Broschat, K. O. (1990). Tropomyosin prevents depolymerization of actin filaments from the pointed end. *J Biol Chem* **265**, 21323-9.

Bulfield, G., Siller, W. G., Wight, P. A. and Moore, K. J. (1984). X chromosome-linked muscular dystrophy (mdx) in the mouse. *Proc Natl Acad Sci U S A* **81**, 1189-92.

Capetanaki, Y. (2002). Desmin cytoskeleton: a potential regulator of muscle mitochondrial behavior and function. *Trends Cardiovasc Med* **12**, 339-48.

Carlier, M. F. (1998). Control of actin dynamics. *Curr Opin Cell Biol* **10**, 45-51.

Carlsson, L., Li, Z., Paulin, D. and Thornell, L. E. (1999). Nestin is expressed during development and in myotendinous and neuromuscular junctions in wild type and desmin knock-out mice. *Exp Cell Res* **251**, 213-23.

Casella, J. F. and Torres, M. A. (1994). Interaction of Cap Z with actin. The NH2-terminal domains of the alpha 1 and beta subunits are not required for actin capping, and alpha 1 beta and alpha 2 beta heterodimers bind differentially to actin. *J Biol Chem* **269**, 6992-8.

Centner, T., Yano, J., Kimura, E., McElhinny, A. S., Pelin, K., Witt, C. C., Bang, M. L., Trombitas, K., Granzier, H., Gregorio, C. C. et al. (2001). Identification of muscle specific ring finger proteins as potential regulators of the titin kinase domain. *J Mol Biol* **306**, 717-26.

Chen, E. H. and Olson, E. N. (2004). Towards a molecular pathway for myoblast fusion in Drosophila. *Trends Cell Biol* **14**, 452-60.

Chen, M. J., Shih, C. L. and Wang, K. (1993). Nebulin as an actin zipper. A two-module nebulin fragment promotes actin nucleation and stabilizes actin filaments. *J Biol Chem* **268**, 20327-34.

Chen, S. and Kimelman, D. (2000). The role of the yolk syncytial layer in germ layer patterning in zebrafish. *Development* **127**, 4681-9.

Chen, W., Burgess, S. and Hopkins, N. (2001). Analysis of the zebrafish smoothened mutant reveals conserved and divergent functions of hedgehog activity. *Development* **128**, 2385-96.

Choi, J., Costa, M. L., Mermelstein, C. S., Chagas, C., Holtzer, S. and Holtzer, H. (1990). MyoD converts primary dermal fibroblasts, chondroblasts, smooth muscle, and retinal pigmented

epithelial cells into striated mononucleated myoblasts and multinucleated myotubes. *Proc Natl Acad Sci U S A* **87**, 7988-92.

Christiansen, J. H., Coles, E. G. and Wilkinson, D. G. (2000). Molecular control of neural crest formation, migration and differentiation. *Curr Opin Cell Biol* **12**, 719-24.

Clark, K. A., McElhinny, A. S., Beckerle, M. C. and Gregorio, C. C. (2002). Striated muscle cytoarchitecture: an intricate web of form and function. *Annu Rev Cell Dev Biol* **18**, 637-706.

Conley, C. A., Fritz-Six, K. L., Almenar-Queralt, A. and Fowler, V. M. (2001). Leiomodins: larger members of the tropomodulin (Tmod) gene family. *Genomics* **73**, 127-39.

Cooper, B. J., Winand, N. J., Stedman, H., Valentine, B. A., Hoffman, E. P., Kunkel, L. M., Scott, M. O., Fischbeck, K. H., Kornegay, J. N., Avery, R. J. et al. (1988). The homologue of the Duchenne locus is defective in X-linked muscular dystrophy of dogs. *Nature* **334**, 154-6.

Cooper, J. A. and Schafer, D. A. (2000). Control of actin assembly and disassembly at filament ends. *Curr Opin Cell Biol* **12**, 97-103.

Cortes, F., Daggett, D., Bryson-Richardson, R. J., Neyt, C., Maule, J., Gautier, P., Hollway, G. E., Keenan, D. and Currie, P. D. (2003). Cadherin-mediated differential cell adhesion controls slow muscle cell migration in the developing zebrafish myotome. *Dev Cell* **5**, 865-76.

Costa, M. L., Escaleira, R. C., Rodrigues, V. B., Manasfi, M. and Mermelstein, C. S. (2002). Some distinctive features of zebrafish myogenesis based on unexpected distributions of the muscle cytoskeletal proteins actin, myosin, desmin, alpha-actinin, troponin and titin. *Mech Dev* **116**, 95-104.

Coutelle, O., Blagden, C. S., Hampson, R., Halai, C., Rigby, P. W. and Hughes, S. M. (2001). Hedgehog signalling is required for maintenance of myf5 and myoD expression and timely terminal differentiation in zebrafish adaxial myogenesis. *Dev Biol* **236**, 136-50.

Cox, P. R. and Zoghbi, H. Y. (2000). Sequencing, expression analysis, and mapping of three unique human tropomodulin genes and their mouse orthologs. *Genomics* **63**, 97-107.

Craig, R. and Lehman, W. (2001). Crossbridge and tropomyosin positions observed in native, interacting thick and thin filaments. *J Mol Biol* **311**, 1027-36.

Craig, R. and Offer, G. (1976). Axial arrangement of crossbridges in thick filaments of vertebrate skeletal muscle. *J Mol Biol* **102**, 325-32.

Craig, S. W. and Pardo, J. V. (1983). Gamma actin, spectrin, and intermediate filament proteins colocalize with vinculin at costameres, myofibril-to-sarcolemma attachment sites. *Cell Motil* **3**, 449-62.

Currie, P. D. and Ingham, P. W. (1996). Induction of a specific muscle cell type by a hedgehog-like protein in zebrafish. *Nature* **382**, 452-5.

Dabiri, G. A., Turnacioglu, K. K., Sanger, J. M. and Sanger, J. W. (1997). Myofibrillogenesis visualized in living embryonic cardiomyocytes. *Proc Natl Acad Sci U S A* **94**, 9493-8.

Dai, K. S. and Liew, C. C. (2001). A novel human striated muscle RING zinc finger protein, SMRZ, interacts with SMT3b via its RING domain. *J Biol Chem* **276**, 23992-9.

Danowski, B. A., Imanaka-Yoshida, K., Sanger, J. M. and Sanger, J. W. (1992). Costameres are sites of force transmission to the substratum in adult rat cardiomyocytes. *J Cell Biol* **118**, 1411-20.

Davies, K. E. and Nowak, K. J. (2006). Molecular mechanisms of muscular dystrophies: old and new players. *Nat Rev Mol Cell Biol* **7**, 762-73.

Davis, J. S. (1988). Assembly processes in vertebrate skeletal thick filament formation. *Annu Rev Biophys Biophys Chem* **17**, 217-39.

Davis, R. L., Weintraub, H. and Lassar, A. B. (1987). Expression of a single transfected cDNA converts fibroblasts to myoblasts. *Cell* **51**, 987-1000.

Delling, U., Tureckova, J., Lim, H. W., De Windt, L. J., Rotwein, P. and Molkentin, J. D. (2000). A calcineurin-NFATc3-dependent pathway regulates skeletal muscle differentiation and slow myosin heavy-chain expression. *Mol Cell Biol* **20**, 6600-11.

den Hertog, D., van Zante-de Fokkert, J. I., Sjamaar, S. A. and Beusmans, R. (2005). Optimal working zone division for safe track maintenance in The Netherlands. *Accid Anal Prev* **37**, 890-3.

Devoto, S. H., Melancon, E., Eisen, J. S. and Westerfield, M. (1996). Identification of separate slow and fast muscle precursor cells in vivo, prior to somite formation. *Development* **122**, 3371-80.

Devoto, S. H., Stoiber, W., Hammond, C. L., Steinbacher, P., Haslett, J. R., Barresi, M. J., Patterson, S. E., Adiarte, E. G. and Hughes, S. M. (2006). Generality of vertebrate developmental patterns: evidence for a dermomyotome in fish. *Evol Dev* **8**, 101-10.

Dickson, B. J. (2002). Molecular mechanisms of axon guidance. *Science* **298**, 1959-64.

Dlugosz, A. A., Antin, P. B., Nachmias, V. T. and Holtzer, H. (1984). The relationship between stress fiber-like structures and nascent myofibrils in cultured cardiac myocytes. *J Cell Biol* **99**, 2268-78.

Dome, J. S., Mittal, B., Pochapin, M. B., Sanger, J. M. and Sanger, J. W. (1988). Incorporation of fluorescently labeled actin and tropomyosin into muscle cells. *Cell Differ* **23**, 37-52.

Donner, K., Ollikainen, M., Ridanpaa, M., Christen, H. J., Goebel, H. H., de Visser, M., Pelin, K. and Wallgren-Pettersson, C. (2002). Mutations in the beta-tropomyosin (TPM2) gene--a rare cause of nemaline myopathy. *Neuromuscul Disord* **12**, 151-8.

dos Remedios, C. G., Chhabra, D., Kekic, M., Dedova, I. V., Tsubakihara, M., Berry, D. A. and Nosworthy, N. J. (2003). Actin binding proteins: regulation of cytoskeletal microfilaments. *Physiol Rev* **83**, 433-73.

Driever, W., Solnica-Krezel, L., Schier, A. F., Neuhauss, S. C., Malicki, J., Stemple, D. L., Stainier, D. Y., Zwartkruis, F., Abdelilah, S., Rangini, Z. et al. (1996). A genetic screen for mutations affecting embryogenesis in zebrafish. *Development* **123**, 37-46.

Du, A., Sanger, J. M., Linask, K. K. and Sanger, J. W. (2003). Myofibrillogenesis in the first cardiomyocytes formed from isolated quail precardiac mesoderm. *Dev Biol* **257**, 382-94.

Du, S. J., Devoto, S. H., Westerfield, M. and Moon, R. T. (1997). Positive and negative regulation of muscle cell identity by members of the hedgehog and TGF-beta gene families. *J Cell Biol* **139**, 145-56.

Edmondson, D. G. and Olson, E. N. (1989). A gene with homology to the myc similarity region of MyoD1 is expressed during myogenesis and is sufficient to activate the muscle differentiation program. *Genes Dev* **3**, 628-40.

Ehler, E., Horowits, R., Zuppinger, C., Price, R. L., Perriard, E., Leu, M., Caroni, P., Sussman, M., Eppenberger, H. M. and Perriard, J. C. (2001). Alterations at the intercalated disk associated with the absence of muscle LIM protein. *J Cell Biol* **153**, 763-72.

Ekker, M., Wegner, J., Akimenko, M. A. and Westerfield, M. (1992). Coordinate embryonic expression of three zebrafish engrailed genes. *Development* **116**, 1001-10.

Ekker, S. C., Ungar, A. R., Greenstein, P., von Kessler, D. P., Porter, J. A., Moon, R. T. and Beachy, P. A. (1995). Patterning activities of vertebrate hedgehog proteins in the developing eye and brain. *Curr Biol* **5**, 944-55.

Ericson, J., Thor, S., Edlund, T., Jessell, T. M. and Yamada, T. (1992). Early stages of motor neuron differentiation revealed by expression of homeobox gene Islet-1. *Science* **256**, 1555-60.

Fallon, J. R. and Nachmias, V. T. (1980). Localization of cytoplasmic and skeletal myosins in developing muscle cells by double-label immunofluorescence. *J Cell Biol* **87**, 237-47.

Fassler, R., Rohwedel, J., Maltsev, V., Bloch, W., Lentini, S., Guan, K., Gullberg, D., Hescheler, J., Addicks, K. and Wobus, A. M. (1996). Differentiation and integrity of cardiac muscle cells are impaired in the absence of beta 1 integrin. *J Cell Sci* **109 (Pt 13)**, 2989-99.

Faulkner, G., Pallavicini, A., Comelli, A., Salamon, M., Bortoletto, G., Ievolella, C., Trevisan, S., Kojic, S., Dalla Vecchia, F., Laveder, P. et al. (2000). FATZ, a filamin-, actinin-, and telethonin-binding protein of the Z-disc of skeletal muscle. *J Biol Chem* **275**, 41234-42.

Faulstich, H., Zobeley, S., Heintz, D. and Drewes, G. (1993). Probing the phalloidin binding site of actin. *FEBS Lett* **318**, 218-22.

Felsenfeld, A. L., Walker, C., Westerfield, M., Kimmel, C. and Streisinger, G. (1990). Mutations affecting skeletal muscle myofibril structure in the zebrafish. *Development* **108**, 443-59.

Ferrari, M. B., Ribbeck, K., Hagler, D. J. and Spitzer, N. C. (1998). A calcium signaling cascade essential for myosin thick filament assembly in Xenopus myocytes. *J Cell Biol* **141**, 1349-56.

Fischer, R. S. and Fowler, V. M. (2003). Tropomodulins: life at the slow end. *Trends Cell Biol* **13**, 593-601.

Fowler, V. M. (1990). Tropomodulin: a cytoskeletal protein that binds to the end of erythrocyte tropomyosin and inhibits tropomyosin binding to actin. *J Cell Biol* **111**, 471-81.

Fowler, V. M. (1996). Regulation of actin filament length in erythrocytes and striated muscle. *Curr Opin Cell Biol* **8**, 86-96.

Fowler, V. M. (1997). Capping actin filament growth: tropomodulin in muscle and nonmuscle cells. *Soc Gen Physiol Ser* **52**, 79-89.

Fowler, V. M., Greenfield, N. J. and Moyer, J. (2003). Tropomodulin contains two actin filament pointed end-capping domains. *J Biol Chem* **278**, 40000-9.

Fowler, V. M., McKeown, C. R. and Fischer, R. S. (2006). Nebulin: does it measure up as a ruler? *Curr Biol* **16**, R18-20.

Frank, D., Kuhn, C., Katus, H. A. and Frey, N. (2006). The sarcomeric Z-disc: a nodal point in signalling and disease. *J Mol Med* **84**, 446-68.

Fritz-Six, K. L., Cox, P. R., Fischer, R. S., Xu, B., Gregorio, C. C., Zoghbi, H. Y. and Fowler, V. M. (2003). Aberrant myofibril assembly in tropomodulin1 null mice leads to aborted heart development and embryonic lethality. *J Cell Biol* **163**, 1033-44.

Fujigasaki, H., Song, S. Y., Kobayashi, T. and Yamakuni, T. (1996). Murine central neurons express a novel member of the cdc10/SWI6 motif-containing protein superfamily. *Brain Res Mol Brain Res* **40**, 203-13.

Fyrberg, C., Ketchum, A., Ball, E. and Fyrberg, E. (1998). Characterization of lethal Drosophila melanogaster alpha-actinin mutants. *Biochem Genet* **36**, 299-310.

Galbiati, F., Engelman, J. A., Volonte, D., Zhang, X. L., Minetti, C., Li, M., Hou, H., Jr., Kneitz, B., Edelmann, W. and Lisanti, M. P. (2001). Caveolin-3 null mice show a loss of caveolae, changes in the microdomain distribution of the dystrophin-glycoprotein complex, and t-tubule abnormalities. *J Biol Chem* **276**, 21425-33.

Geisler, R., Rauch, G. J., Geiger-Rudolph, S., Albrecht, A., van Bebber, F., Berger, A., Busch-Nentwich, E., Dahm, R., Dekens, M. P., Dooley, C. et al. (2007). Large-scale mapping of mutations affecting zebrafish development. *BMC Genomics* **8**, 11.

Gilbert, R., Kelly, M. G., Mikawa, T. and Fischman, D. A. (1996). The carboxyl terminus of myosin binding protein C (MyBP-C, C-protein) specifies incorporation into the A-band of striated muscle. *J Cell Sci* **109 (Pt 1)**, 101-11.

Goff, D. J., Galvin, K., Katz, H., Westerfield, M., Lander, E. S. and Tabin, C. J. (1992). Identification of polymorphic simple sequence repeats in the genome of the zebrafish. *Genomics* **14**, 200-2.

Gonsior, S. M., Gautel, M. and Hinssen, H. (1998). A six-module human nebulin fragment bundles actin filaments and induces actin polymerization. *J Muscle Res Cell Motil* **19**, 225-35.

Granato, M., van Eeden, F. J., Schach, U., Trowe, T., Brand, M., Furutani-Seiki, M., Haffter, P., Hammerschmidt, M., Heisenberg, C. P., Jiang, Y. J. et al. (1996). Genes controlling and mediating locomotion behavior of the zebrafish embryo and larva. *Development* **123**, 399-413.

Granger, B. L. and Lazarides, E. (1980). Synemin: a new high molecular weight protein associated with desmin and vimentin filaments in muscle. *Cell* **22**, 727-38.

Greenfield, N. J. and Fowler, V. M. (2002). Tropomyosin requires an intact N-terminal coiled coil to interact with tropomodulin. *Biophys J* **82**, 2580-91.

Gregorio, C. C., Trombitas, K., Centner, T., Kolmerer, B., Stier, G., Kunke, K., Suzuki, K., Obermayr, F., Herrmann, B., Granzier, H. et al. (1998). The NH2 terminus of titin spans the Z-disc: its interaction with a novel 19-kD ligand (T-cap) is required for sarcomeric integrity. *J Cell Biol* **143**, 1013-27.

Gregorio, C. C., Weber, A., Bondad, M., Pennise, C. R. and Fowler, V. M. (1995). Requirement of pointed-end capping by tropomodulin to maintain actin filament length in embryonic chick cardiac myocytes. *Nature* **377**, 83-6.

Gros, J., Manceau, M., Thome, V. and Marcelle, C. (2005). A common somitic origin for embryonic muscle progenitors and satellite cells. *Nature* **435**, 954-8.

Grove, B. K., Kurer, V., Lehner, C., Doetschman, T. C., Perriard, J. C. and Eppenberger, H. M. (1984). A new 185,000-dalton skeletal muscle protein detected by monoclonal antibodies. *J Cell Biol* **98**, 518-24.

Groves, J. A., Hammond, C. L. and Hughes, S. M. (2005). Fgf8 drives myogenic progression of a novel lateral fast muscle fibre population in zebrafish. *Development* **132**, 4211-22.

Gruen, M., Prinz, H. and Gautel, M. (1999). cAPK-phosphorylation controls the interaction of the regulatory domain of cardiac myosin binding protein C with myosin-S2 in an on-off fashion. *FEBS Lett* **453**, 254-9.

Guyon, J. R., Mosley, A. N., Jun, S. J., Montanaro, F., Steffen, L. S., Zhou, Y., Nigro, V., Zon, L. I. and Kunkel, L. M. (2005). Delta-sarcoglycan is required for early zebrafish muscle organization. *Exp Cell Res* **304**, 105-15.

Haffter, P., Granato, M., Brand, M., Mullins, M. C., Hammerschmidt, M., Kane, D. A., Odenthal, J., van Eeden, F. J., Jiang, Y. J., Heisenberg, C. P. et al. (1996). The identification of genes with unique and essential functions in the development of the zebrafish, Danio rerio. *Development* **123**, 1-36.

Hagiwara, Y., Sasaoka, T., Araishi, K., Imamura, M., Yorifuji, H., Nonaka, I., Ozawa, E. and Kikuchi, T. (2000). Caveolin-3 deficiency causes muscle degeneration in mice. *Hum Mol Genet* **9**, 3047-54.

Halpern, M. E., Thisse, C., Ho, R. K., Thisse, B., Riggleman, B., Trevarrow, B., Weinberg, E. S., Postlethwait, J. H. and Kimmel, C. B. (1995). Cell-autonomous shift from axial to paraxial mesodermal development in zebrafish floating head mutants. *Development* **121**, 4257-64.

Hamade, A., Deries, M., Begemann, G., Bally-Cuif, L., Genet, C., Sabatier, F., Bonnieu, A. and Cousin, X. (2006). Retinoic acid activates myogenesis in vivo through Fgf8 signalling. *Dev Biol* **289**, 127-40.

Hart, M. C. and Cooper, J. A. (1999). Vertebrate isoforms of actin capping protein beta have distinct functions In vivo. *J Cell Biol* **147**, 1287-98.

Hart, M. C., Korshunova, Y. O. and Cooper, J. A. (1997a). Mapping of the mouse actin capping protein alpha subunit genes and pseudogenes. *Genomics* **39**, 264-70.

Hart, M. C., Korshunova, Y. O. and Cooper, J. A. (1997b). Vertebrates have conserved capping protein alpha isoforms with specific expression patterns. *Cell Motil Cytoskeleton* **38**, 120-32.

Hatta, K. (1992). Role of the floor plate in axonal patterning in the zebrafish CNS. *Neuron* **9**, 629-42.

Hatta, K., Bremiller, R., Westerfield, M. and Kimmel, C. B. (1991). Diversity of expression of engrailed-like antigens in zebrafish. *Development* **112**, 821-32.

Hein, S., Kostin, S., Heling, A., Maeno, Y. and Schaper, J. (2000). The role of the cytoskeleton in heart failure. *Cardiovasc Res* **45**, 273-8.

Henry, C. A. and Amacher, S. L. (2004). Zebrafish slow muscle cell migration induces a wave of fast muscle morphogenesis. *Dev Cell* **7**, 917-23.

Higashijima, S., Hotta, Y. and Okamoto, H. (2000). Visualization of cranial motor neurons in live transgenic zebrafish expressing green fluorescent protein under the control of the islet-1 promoter/enhancer. *J Neurosci* **20**, 206-18.

Hinits, Y. and Hughes, S. M. (2007). Mef2s are required for thick filament formation in nascent muscle fibres. *Development* **134**, 2511-9.

Hirsinger, E., Stellabotte, F., Devoto, S. H. and Westerfield, M. (2004). Hedgehog signaling is required for commitment but not initial induction of slow muscle precursors. *Dev Biol* **275**, 143-57.

Ho, R. K. (1992). Cell movements and cell fate during zebrafish gastrulation. *Dev Suppl*, 65-73.

Hoffman, E. P., Monaco, A. P., Feener, C. C. and Kunkel, L. M. (1987). Conservation of the Duchenne muscular dystrophy gene in mice and humans. *Science* **238**, 347-50.

Hollway, G. E. and Currie, P. D. (2003). Myotome meanderings. Cellular morphogenesis and the making of muscle. *EMBO Rep* **4**, 855-60.

Holtzer, H., Hijikata, T., Lin, Z. X., Zhang, Z. Q., Holtzer, S., Protasi, F., Franzini-Armstrong, C. and Sweeney, H. L. (1997). Independent assembly of 1.6 microns long bipolar MHC filaments and I-Z-I bodies. *Cell Struct Funct* **22**, 83-93.

Hopmann, R., Cooper, J. A. and Miller, K. G. (1996). Actin organization, bristle morphology, and viability are affected by actin capping protein mutations in Drosophila. *J Cell Biol* **133**, 1293-305.

Horowits, R., Luo, G., Zhang, J. Q. and Herrera, A. H. (1996). Nebulin and nebulin-related proteins in striated muscle. *Adv Biophys* **33**, 143-50.

Hubbard, T. J., Aken, B. L., Beal, K., Ballester, B., Caccamo, M., Chen, Y., Clarke, L., Coates, G., Cunningham, F., Cutts, T. et al. (2007). Ensembl 2007. *Nucleic Acids Res* **35**, D610-7.

Hug, C., Jay, P. Y., Reddy, I., McNally, J. G., Bridgman, P. C., Elson, E. L. and Cooper, J. A. (1995). Capping protein levels influence actin assembly and cell motility in dictyostelium. *Cell* **81**, 591-600.

Hug, C., Miller, T. M., Torres, M. A., Casella, J. F. and Cooper, J. A. (1992). Identification and characterization of an actin-binding site of CapZ. *J Cell Biol* **116**, 923-31.

Huxley, A. F. and Niedergerke, R. (1954). Structural changes in muscle during contraction; interference microscopy of living muscle fibres. *Nature* **173**, 971-3.

Huxley, H. and Hanson, J. (1954). Changes in the cross-striations of muscle during contraction and stretch and their structural interpretation. *Nature* **173**, 973-6.

Ingham, P. W. and McMahon, A. P. (2001). Hedgehog signaling in animal development: paradigms and principles. *Genes Dev* **15**, 3059-87.

Ivanenkov, V. V., Jamieson, G. A., Jr., Gruenstein, E. and Dimlich, R. V. (1995). Characterization of S-100b binding epitopes. Identification of a novel target, the actin capping protein, CapZ. *J Biol Chem* **270**, 14651-8.

Jin, J. P. and Wang, K. (1991). Cloning, expression, and protein interaction of human nebulin fragments composed of varying numbers of sequence modules. *J Biol Chem* **266**, 21215-23.

Johnson, S. L., Midson, C. N., Ballinger, E. W. and Postlethwait, J. H. (1994). Identification of RAPD primers that reveal extensive polymorphisms between laboratory strains of zebrafish. *Genomics* **19**, 152-6.

Johnston, J. J., Kelley, R. I., Crawford, T. O., Morton, D. H., Agarwala, R., Koch, T., Schaffer, A. A., Francomano, C. A. and Biesecker, L. G. (2000). A novel nemaline myopathy in the Amish caused by a mutation in troponin T1. *Am J Hum Genet* **67**, 814-21.

Kanki, J. P. and Ho, R. K. (1997). The development of the posterior body in zebrafish. *Development* **124**, 881-93.

Karpati, G. (2002). Structural and Molecular Basis of Skeletal Muscle Disease. Uppsala, Sweden: ISN Neuropath press.

Kazmierski, S. T., Antin, P. B., Witt, C. C., Huebner, N., McElhinny, A. S., Labeit, S. and Gregorio, C. C. (2003). The complete mouse nebulin gene sequence and the identification of cardiac nebulin. *J Mol Biol* **328**, 835-46.

Kilby, P. M., Van Eldik, L. J. and Roberts, G. C. (1997). Identification of the binding site on S100B protein for the actin capping protein CapZ. *Protein Sci* **6**, 2494-503.

Kimmel, C. B., Ballard, W. W., Kimmel, S. R., Ullmann, B. and Schilling, T. F. (1995). Stages of embryonic development of the zebrafish. *Dev Dyn* **203**, 253-310.

Kimmel, C. B., Kane, D. A., Walker, C., Warga, R. M. and Rothman, M. B. (1989). A mutation that changes cell movement and cell fate in the zebrafish embryo. *Nature* **337**, 358-62.

Kimmel, C. B. and Law, R. D. (1985). Cell lineage of zebrafish blastomeres. II. Formation of the yolk syncytial layer. *Dev Biol* **108**, 86-93.

Kimmel, C. B., Warga, R. M. and Schilling, T. F. (1990). Origin and organization of the zebrafish fate map. *Development* **108**, 581-94.

Knapik, E. W., Goodman, A., Atkinson, O. S., Roberts, C. T., Shiozawa, M., Sim, C. U., Weksler-Zangen, S., Trolliet, M. R., Futrell, C., Innes, B. A. et al. (1996). A reference cross DNA panel for zebrafish (Danio rerio) anchored with simple sequence length polymorphisms. *Development* **123**, 451-60.

Knapik, E. W., Goodman, A., Ekker, M., Chevrette, M., Delgado, J., Neuhauss, S., Shimoda, N., Driever, W., Fishman, M. C. and Jacob, H. J. (1998). A microsatellite genetic linkage map for zebrafish (Danio rerio). *Nat Genet* **18**, 338-43.

Knappeis, G. G. and Carlsen, F. (1968). The ultrastructure of the M line in skeletal muscle. *J Cell Biol* **38**, 202-11.

Knudsen, K. A. (1992). Fusion of myoblasts. In *Membrane fusion*, (ed. J. Wilschut and D. Hoekstra), pp. 601-626: Marcel Decker.

Kong, Y., Flick, M. J., Kudla, A. J. and Konieczny, S. F. (1997). Muscle LIM protein promotes myogenesis by enhancing the activity of MyoD. *Mol Cell Biol* **17**, 4750-60.

Koretz, J. F. (1979). Effects of C-protein on synthetic myosin filament structure. *Biophys J* **27**, 433-46.

Kostyukova, A. S., Choy, A. and Rapp, B. A. (2006). Tropomodulin binds two tropomyosins: a novel model for actin filament capping. *Biochemistry* **45**, 12068-75.

Kostyukova, A. S. and Hitchcock-DeGregori, S. E. (2004). Effect of the structure of the N terminus of tropomyosin on tropomodulin function. *J Biol Chem* **279**, 5066-71.

LaBonne, C. and Bronner-Fraser, M. (1999). Molecular mechanisms of neural crest formation. *Annu Rev Cell Dev Biol* **15**, 81-112.

Laing, N. G., Wilton, S. D., Akkari, P. A., Dorosz, S., Boundy, K., Kneebone, C., Blumbergs, P., White, S., Watkins, H., Love, D. R. et al. (1995). A mutation in the alpha tropomyosin gene TPM3 associated with autosomal dominant nemaline myopathy NEM1. *Nat Genet* **10**, 249.

Lassar, A. B., Buskin, J. N., Lockshon, D., Davis, R. L., Apone, S., Hauschka, S. D. and Weintraub, H. (1989). MyoD is a sequence-specific DNA binding protein requiring a region of myc homology to bind to the muscle creatine kinase enhancer. *Cell* **58**, 823-31.

Lazarides, E. (1980). Desmin and intermediate filaments in muscle cells. *Results Probl Cell Differ* **11**, 124-31.

Lazarides, E. (1982). Intermediate filaments: a chemically heterogeneous, developmentally regulated class of proteins. *Annu Rev Biochem* **51**, 219-50.

Le Dourain, N. and Kalcheim, C. (1999). The neural crest. New York: Cambridge University Press.

Lewis, K. E., Currie, P. D., Roy, S., Schauerte, H., Haffter, P. and Ingham, P. W. (1999). Control of muscle cell-type specification in the zebrafish embryo by Hedgehog signalling. *Dev Biol* **216**, 469-80.

Li, Z., Mericskay, M., Agbulut, O., Butler-Browne, G., Carlsson, L., Thornell, L. E., Babinet, C. and Paulin, D. (1997). Desmin is essential for the tensile strength and integrity of myofibrils but not for myogenic commitment, differentiation, and fusion of skeletal muscle. *J Cell Biol* **139**, 129-44.

Littlefield, R., Almenar-Queralt, A. and Fowler, V. M. (2001). Actin dynamics at pointed ends regulates thin filament length in striated muscle. *Nat Cell Biol* **3**, 544-51.

Littlefield, R. and Fowler, V. M. (1998). Defining actin filament length in striated muscle: rulers and caps or dynamic stability? *Annu Rev Cell Dev Biol* **14**, 487-525.

Loh, S. H., Chan, W. T., Gong, Z., Lim, T. M. and Chua, K. L. (2000). Characterization of a zebrafish (Danio rerio) desmin cDNA: an early molecular marker of myogenesis. *Differentiation* **65**, 247-54.

Lukoyanova, N., VanLoock, M. S., Orlova, A., Galkin, V. E., Wang, K. and Egelman, E. H. (2002). Each actin subunit has three nebulin binding sites: implications for steric blocking. *Curr Biol* **12**, 383-8.

Luther, P. and Squire, J. (1978). Three-dimensional structure of the vertebrate muscle M-region. *J Mol Biol* **125**, 313-24.

Machesky, L. M., Atkinson, S. J., Ampe, C., Vandekerckhove, J. and Pollard, T. D. (1994). Purification of a cortical complex containing two unconventional actins from Acanthamoeba by affinity chromatography on profilin-agarose. *J Cell Biol* **127**, 107-15.

Makita, R., Mizuno, T., Koshida, S., Kuroiwa, A. and Takeda, H. (1998). Zebrafish wnt11: pattern and regulation of the expression by the yolk cell and No tail activity. *Mech Dev* **71**, 165-76.

Mardahl-Dumesnil, M. and Fowler, V. M. (2001). Thin filaments elongate from their pointed ends during myofibril assembly in Drosophila indirect flight muscle. *J Cell Biol* **155**, 1043-53.

Markwald, R. R. (1973). Distribution and relationship of precursor Z material to organizing myofibrillar bundles in embryonic rat and hamster ventricular myocytes. *J Mol Cell Cardiol* **5**, 341-50.

Maruyama, K., Kimura, S., Kuroda, M. and Handa, S. (1977). Connectin, an elastic protein of muscle. Its abundance in cardiac myofibrils. *J Biochem (Tokyo)* **82**, 347-50.

Masaki, T. and Takaiti, O. (1974). M-protein. *J Biochem (Tokyo)* **75**, 367-80.

McElhinny, A. S., Kazmierski, S. T., Labeit, S. and Gregorio, C. C. (2003). Nebulin: the nebulous, multifunctional giant of striated muscle. *Trends Cardiovasc Med* **13**, 195-201.

McElhinny, A. S., Kolmerer, B., Fowler, V. M., Labeit, S. and Gregorio, C. C. (2001). The N-terminal end of nebulin interacts with tropomodulin at the pointed ends of the thin filaments. *J Biol Chem* **276**, 583-92.

McElhinny, A. S., Schwach, C., Valichnac, M., Mount-Patrick, S. and Gregorio, C. C. (2005). Nebulin regulates the assembly and lengths of the thin filaments in striated muscle. *J Cell Biol* **170**, 947-57.

McKay, R. T., Tripet, B. P., Hodges, R. S. and Sykes, B. D. (1997). Interaction of the second binding region of troponin I with the regulatory domain of skeletal muscle troponin C as determined by NMR spectroscopy. *J Biol Chem* **272**, 28494-500.

McKenna, N., Meigs, J. B. and Wang, Y. L. (1985). Identical distribution of fluorescently labeled brain and muscle actins in living cardiac fibroblasts and myocytes. *J Cell Biol* **100**, 292-6.

McKenna, N. M., Johnson, C. S. and Wang, Y. L. (1986). Formation and alignment of Z lines in living chick myotubes microinjected with rhodamine-labeled alpha-actinin. *J Cell Biol* **103**, 2163-71.

McNally, E. M., de Sa Moreira, E., Duggan, D. J., Bonnemann, C. G., Lisanti, M. P., Lidov, H. G., Vainzof, M., Passos-Bueno, M. R., Hoffman, E. P., Zatz, M. et al. (1998). Caveolin-3 in muscular dystrophy. *Hum Mol Genet* **7**, 871-7.

Melby, A. E., Warga, R. M. and Kimmel, C. B. (1996). Specification of cell fates at the dorsal margin of the zebrafish gastrula. *Development* **122**, 2225-37.

Milligan, R. A. (1996). Protein-protein interactions in the rigor actomyosin complex. *Proc Natl Acad Sci U S A* **93**, 21-6.

Mizuno, T., Yamaha, E., Kuroiwa, A. and Takeda, H. (1999). Removal of vegetal yolk causes dorsal deficencies and impairs dorsal-inducing ability of the yolk cell in zebrafish. *Mech Dev* **81**, 51-63.

Molkentin, J. D., Black, B. L., Martin, J. F. and Olson, E. N. (1995). Cooperative activation of muscle gene expression by MEF2 and myogenic bHLH proteins. *Cell* **83**, 1125-36.

Morris, G. E. (2001). The role of the nuclear envelope in Emery-Dreifuss muscular dystrophy. *Trends Mol Med* **7**, 572-7.

Mues, A., van der Ven, P. F., Young, P., Furst, D. O. and Gautel, M. (1998). Two immunoglobulin-like domains of the Z-disc portion of titin interact in a conformation-dependent way with telethonin. *FEBS Lett* **428**, 111-4.

Mullins, R. D., Heuser, J. A. and Pollard, T. D. (1998). The interaction of Arp2/3 complex with actin: nucleation, high affinity pointed end capping, and formation of branching networks of filaments. *Proc Natl Acad Sci U S A* **95**, 6181-6.

Munsterberg, A. E., Kitajewski, J., Bumcrot, D. A., McMahon, A. P. and Lassar, A. B. (1995). Combinatorial signaling by Sonic hedgehog and Wnt family members induces myogenic bHLH gene expression in the somite. *Genes Dev* **9**, 2911-22.

Nave, R., Furst, D. O. and Weber, K. (1989). Visualization of the polarity of isolated titin molecules: a single globular head on a long thin rod as the M band anchoring domain? *J Cell Biol* **109**, 2177-87.

Newey, S. E., Howman, E. V., Ponting, C. P., Benson, M. A., Nawrotzki, R., Loh, N. Y., Davies, K. E. and Blake, D. J. (2001). Syncoilin, a novel member of the intermediate filament superfamily that interacts with alpha-dystrobrevin in skeletal muscle. *J Biol Chem* **276**, 6645-55.

Nigro, V., de Sa Moreira, E., Piluso, G., Vainzof, M., Belsito, A., Politano, L., Puca, A. A., Passos-Bueno, M. R. and Zatz, M. (1996). Autosomal recessive limb-girdle muscular dystrophy, LGMD2F, is caused by a mutation in the delta-sarcoglycan gene. *Nat Genet* **14**, 195-8.

Nixon, S. J., Wegner, J., Ferguson, C., Mery, P. F., Hancock, J. F., Currie, P. D., Key, B., Westerfield, M. and Parton, R. G. (2005). Zebrafish as a model for caveolin-associated muscle disease; caveolin-3 is required for myofibril organization and muscle cell patterning. *Hum Mol Genet* **14**, 1727-43.

Noguchi, T. and Tanaka, T. (1982). The M1 and M2 subunits of rat pyruvate kinase are encoded by different messenger RNAs. *J Biol Chem* **257**, 1110-3.

Norris, W., Neyt, C., Ingham, P. W. and Currie, P. D. (2000). Slow muscle induction by Hedgehog signalling in vitro. *J Cell Sci* **113 (Pt 15)**, 2695-703.

Nowak, K. J. and Davies, K. E. (2004). Duchenne muscular dystrophy and dystrophin: pathogenesis and opportunities for treatment. *EMBO Rep* **5**, 872-6.

Nowak, K. J., Wattanasirichaigoon, D., Goebel, H. H., Wilce, M., Pelin, K., Donner, K., Jacob, R. L., Hubner, C., Oexle, K., Anderson, J. R. et al. (1999). Mutations in the skeletal muscle alpha-actin gene in patients with actin myopathy and nemaline myopathy. *Nat Genet* **23**, 208-12.

Nusslein-Volhard, C. (1994). Of flies and fishes. *Science* **266**, 572-4.
Nusslein-Volhard, C. and Wieschaus, E. (1980). Mutations affecting segment number and polarity in Drosophila. *Nature* **287**, 795-801.

O'Neill, A., Williams, M. W., Resneck, W. G., Milner, D. J., Capetanaki, Y. and Bloch, R. J. (2002). Sarcolemmal organization in skeletal muscle lacking desmin: evidence for cytokeratins associated with the membrane skeleton at costameres. *Mol Biol Cell* **13**, 2347-59.

Ober, E. A. and Schulte-Merker, S. (1999). Signals from the yolk cell induce mesoderm, neuroectoderm, the trunk organizer, and the notochord in zebrafish. *Dev Biol* **215**, 167-81.

Obermann, W. M., Gautel, M., Steiner, F., van der Ven, P. F., Weber, K. and Furst, D. O. (1996). The structure of the sarcomeric M band: localization of defined domains of myomesin, M-protein, and the 250-kD carboxy-terminal region of titin by immunoelectron microscopy. *J Cell Biol* **134**, 1441-53.

Obermann, W. M., Gautel, M., Weber, K. and Furst, D. O. (1997). Molecular structure of the sarcomeric M band: mapping of titin and myosin binding domains in myomesin and the identification of a potential regulatory phosphorylation site in myomesin. *Embo J* **16**, 211-20.

Ohtsuka, H., Yajima, H., Maruyama, K. and Kimura, S. (1997). The N-terminal Z repeat 5 of connectin/titin binds to the C-terminal region of alpha-actinin. *Biochem Biophys Res Commun* **235**, 1-3.

Ojima, K., Lin, Z. X., Zhang, Z. Q., Hijikata, T., Holtzer, S., Labeit, S., Sweeney, H. L. and Holtzer, H. (1999). Initiation and maturation of I-Z-I bodies in the growth tips of transfected myotubes. *J Cell Sci* **112 (Pt 22)**, 4101-12.

Ono, Y., Schwach, C., Antin, P. B. and Gregorio, C. C. (2005). Disruption in the tropomodulin1 (Tmod1) gene compromises cardiomyocyte development in murine embryonic stem cells by arresting myofibril maturation. *Dev Biol* **282**, 336-48.

Oppenheimer, J. M. (1936). Transplantation experiments on developing teleosts (fundulus and perca). *Journal of Experimental Zoology* **72**, 409-437.

Palaisa, K. A. and Granato, M. (2007). Analysis of zebrafish sidetracked mutants reveals a novel role for Plexin A3 in intraspinal motor axon guidance. *Development* **134**, 3251-7.

Palmgren, S., Ojala, P. J., Wear, M. A., Cooper, J. A. and Lappalainen, P. (2001). Interactions with PIP2, ADP-actin monomers, and capping protein regulate the activity and localization of yeast twinfilin. *J Cell Biol* **155**, 251-60.

Papa, I., Astier, C., Kwiatek, O., Raynaud, F., Bonnal, C., Lebart, M. C., Roustan, C. and Benyamin, Y. (1999). Alpha actinin-CapZ, an anchoring complex for thin filaments in Z-line. *J Muscle Res Cell Motil* **20**, 187-97.

Pardo, J. V., Siliciano, J. D. and Craig, S. W. (1983). A vinculin-containing cortical lattice in skeletal muscle: transverse lattice elements ("costameres") mark sites of attachment between myofibrils and sarcolemma. *Proc Natl Acad Sci U S A* **80**, 1008-12.

Parsons, M. J., Campos, I., Hirst, E. M. and Stemple, D. L. (2002). Removal of dystroglycan causes severe muscular dystrophy in zebrafish embryos. *Development* **129**, 3505-12.

Pashmforoush, M., Pomies, P., Peterson, K. L., Kubalak, S., Ross, J., Jr., Hefti, A., Aebi, U., Beckerle, M. C. and Chien, K. R. (2001). Adult mice deficient in actinin-associated LIM-domain protein reveal a developmental pathway for right ventricular cardiomyopathy. *Nat Med* **7**, 591-7.

Pelin, K., Hilpela, P., Donner, K., Sewry, C., Akkari, P. A., Wilton, S. D., Wattanasirichaigoon, D., Bang, M. L., Centner, T., Hanefeld, F. et al. (1999). Mutations in the nebulin gene associated with autosomal recessive nemaline myopathy. *Proc Natl Acad Sci U S A* **96**, 2305-10.

Perry, S. V. (2001). Vertebrate tropomyosin: distribution, properties and function. *J Muscle Res Cell Motil* **22**, 5-49.

Person, V., Kostin, S., Suzuki, K., Labeit, S. and Schaper, J. (2000). Antisense oligonucleotide experiments elucidate the essential role of titin in sarcomerogenesis in adult rat cardiomyocytes in long-term culture. *J Cell Sci* **113 Pt 21**, 3851-9.

Peterson, R. T., Shaw, S. Y., Peterson, T. A., Milan, D. J., Zhong, T. P., Schreiber, S. L., MacRae, C. A. and Fishman, M. C. (2004). Chemical suppression of a genetic mutation in a zebrafish model of aortic coarctation. *Nat Biotechnol* **22**, 595-9.

Petrof, B. J., Shrager, J. B., Stedman, H. H., Kelly, A. M. and Sweeney, H. L. (1993). Dystrophin protects the sarcolemma from stresses developed during muscle contraction. *Proc Natl Acad Sci U S A* **90**, 3710-4.

Porter, G. A., Dmytrenko, G. M., Winkelmann, J. C. and Bloch, R. J. (1992). Dystrophin colocalizes with beta-spectrin in distinct subsarcolemmal domains in mammalian skeletal muscle. *J Cell Biol* **117**, 997-1005.

Porter, G. A., Scher, M. G., Resneck, W. G., Porter, N. C., Fowler, V. M. and Bloch, R. J. (1997). Two populations of beta-spectrin in rat skeletal muscle. *Cell Motil Cytoskeleton* **37**, 7-19.

Postlethwait, J. H., Johnson, S. L., Midson, C. N., Talbot, W. S., Gates, M., Ballinger, E. W., Africa, D., Andrews, R., Carl, T., Eisen, J. S. et al. (1994). A genetic linkage map for the zebrafish. *Science* **264**, 699-703.

Pourquie, O. (2001). Vertebrate somitogenesis. *Annu Rev Cell Dev Biol* **17**, 311-50.

Pourquie, O. (2003). Vertebrate somitogenesis: a novel paradigm for animal segmentation? *Int J Dev Biol* **47**, 597-603.

Pownall, M. E., Gustafsson, M. K. and Emerson, C. P., Jr. (2002). Myogenic regulatory factors and the specification of muscle progenitors in vertebrate embryos. *Annu Rev Cell Dev Biol* **18**, 747-83.

Pyle, W. G., Hart, M. C., Cooper, J. A., Sumandea, M. P., de Tombe, P. P. and Solaro, R. J. (2002). Actin capping protein: an essential element in protein kinase signaling to the myofilaments. *Circ Res* **90**, 1299-306.

Pyle, W. G., La Rotta, G., de Tombe, P. P., Sumandea, M. P. and Solaro, R. J. (2006). Control of cardiac myofilament activation and PKC-betaII signaling through the actin capping protein, CapZ. *J Mol Cell Cardiol* **41**, 537-43.

Raeker, M. O., Su, F., Geisler, S. B., Borisov, A. B., Kontrogianni-Konstantopoulos, A., Lyons, S. E. and Russell, M. W. (2006). Obscurin is required for the lateral alignment of striated myofibrils in zebrafish. *Dev Dyn* **235**, 2018-29.

Rayment, I., Rypniewski, W. R., Schmidt-Base, K., Smith, R., Tomchick, D. R., Benning, M. M., Winkelmann, D. A., Wesenberg, G. and Holden, H. M. (1993). Three-dimensional structure of myosin subfragment-1: a molecular motor. *Science* **261**, 50-8.

Relaix, F., Rocancourt, D., Mansouri, A. and Buckingham, M. (2005). A Pax3/Pax7-dependent population of skeletal muscle progenitor cells. *Nature* **435**, 948-53.

Rhee, D., Sanger, J. M. and Sanger, J. W. (1994). The premyofibril: evidence for its role in myofibrillogenesis. *Cell Motil Cytoskeleton* **28**, 1-24.

Rhodes, S. J. and Konieczny, S. F. (1989). Identification of MRF4: a new member of the muscle regulatory factor gene family. *Genes Dev* **3**, 2050-61.

Robu, M. E., Larson, J. D., Nasevicius, A., Beiraghi, S., Brenner, C., Farber, S. A. and Ekker, S. C. (2007). p53 activation by knockdown technologies. *PLoS Genet* **3**, e78.

Rodaway, A., Takeda, H., Koshida, S., Broadbent, J., Price, B., Smith, J. C., Patient, R. and Holder, N. (1999). Induction of the mesendoderm in the zebrafish germ ring by yolk cell-derived TGF-beta family signals and discrimination of mesoderm and endoderm by FGF. *Development* **126**, 3067-78.

Root, D. D. and Wang, K. (2001). High-affinity actin-binding nebulin fragments influence the actoS1 complex. *Biochemistry* **40**, 1171-86.

Roy, S., Wolff, C. and Ingham, P. W. (2001). The u-boot mutation identifies a Hedgehog-regulated myogenic switch for fiber-type diversification in the zebrafish embryo. *Genes Dev* **15**, 1563-76.

Ruiz-Gomez, M., Coutts, N., Price, A., Taylor, M. V. and Bate, M. (2000). Drosophila dumbfounded: a myoblast attractant essential for fusion. *Cell* **102**, 189-98.

Saitoh, T., Hansen, L. A., Dobkins, K. R. and Terry, R. D. (1988). Increased Mr 60,000 protein phosphorylation is correlated with neocortical neurofibrillary tangles in Alzheimer's disease. *J Neuropathol Exp Neurol* **47**, 1-8.

Saude, L., Woolley, K., Martin, P., Driever, W. and Stemple, D. L. (2000). Axis-inducing activities and cell fates of the zebrafish organizer. *Development* **127**, 3407-17.

Schafer, D. A., Hug, C. and Cooper, J. A. (1995). Inhibition of CapZ during myofibrillogenesis alters assembly of actin filaments. *J Cell Biol* **128**, 61-70.

Schafer, D. A., Jennings, P. B. and Cooper, J. A. (1996). Dynamics of capping protein and actin assembly in vitro: uncapping barbed ends by polyphosphoinositides. *J Cell Biol* **135**, 169-79.

Schafer, D. A., Korshunova, Y. O., Schroer, T. A. and Cooper, J. A. (1994). Differential localization and sequence analysis of capping protein beta-subunit isoforms of vertebrates. *J Cell Biol* **127**, 453-65.

Schafer, D. A., Mooseker, M. S. and Cooper, J. A. (1992). Localization of capping protein in chicken epithelial cells by immunofluorescence and biochemical fractionation. *J Cell Biol* **118**, 335-46.

Schafer, D. A., Waddle, J. A. and Cooper, J. A. (1993). Localization of CapZ during myofibrillogenesis in cultured chicken muscle. *Cell Motil Cytoskeleton* **25**, 317-35.

Schultheiss, T., Lin, Z. X., Lu, M. H., Murray, J., Fischman, D. A., Weber, K., Masaki, T., Imamura, M. and Holtzer, H. (1990). Differential distribution of subsets of myofibrillar proteins in cardiac nonstriated and striated myofibrils. *J Cell Biol* **110**, 1159-72.

Seiler, S. H., Fischman, D. A. and Leinwand, L. A. (1996). Modulation of myosin filament organization by C-protein family members. *Mol Biol Cell* **7**, 113-27.

Sellers, J. R. (2000). Myosins: a diverse superfamily. *Biochim Biophys Acta* **1496**, 3-22.

Shih, J. and Fraser, S. E. (1996). Characterizing the zebrafish organizer: microsurgical analysis at the early-shield stage. *Development* **122**, 1313-22.

Shimada, T., Sasaki, N., Ohkura, R. and Sutoh, K. (1997). Alanine scanning mutagenesis of the switch I region in the ATPase site of Dictyostelium discoideum myosin II. *Biochemistry* **36**, 14037-43.

Shimoda, N., Knapik, E. W., Ziniti, J., Sim, C., Yamada, E., Kaplan, S., Jackson, D., de Sauvage, F., Jacob, H. and Fishman, M. C. (1999). Zebrafish genetic map with 2000 microsatellite markers. *Genomics* **58**, 219-32.

Shyy, J. Y. and Chien, S. (1997). Role of integrins in cellular responses to mechanical stress and adhesion. *Curr Opin Cell Biol* **9**, 707-13.

Sicinski, P., Geng, Y., Ryder-Cook, A. S., Barnard, E. A., Darlison, M. G. and Barnard, P. J. (1989). The molecular basis of muscular dystrophy in the mdx mouse: a point mutation. *Science* **244**, 1578-80.

Sizonenko, G. I., Karpova, T. S., Gattermeir, D. J. and Cooper, J. A. (1996). Mutational analysis of capping protein function in Saccharomyces cerevisiae. *Mol Biol Cell* **7**, 1-15.

Smith, M., Hickman, A., Amanze, D., Lumsden, A. and Thorogood, P. (1994). Trunk neural crest origin of caudal fin mesenchyme in the zebrafish Brachdanio rerio. *Proceedings: Biological Sciences* **256**, 137-145.

Sorimachi, H., Freiburg, A., Kolmerer, B., Ishiura, S., Stier, G., Gregorio, C. C., Labeit, D., Linke, W. A., Suzuki, K. and Labeit, S. (1997). Tissue-specific expression and alpha-actinin

binding properties of the Z-disc titin: implications for the nature of vertebrate Z-discs. *J Mol Biol* **270**, 688-95.

Sparrow, J. C., Nowak, K. J., Durling, H. J., Beggs, A. H., Wallgren-Pettersson, C., Romero, N., Nonaka, I. and Laing, N. G. (2003). Muscle disease caused by mutations in the skeletal muscle alpha-actin gene (ACTA1). *Neuromuscul Disord* **13**, 519-31.

Spemann, H. a. M., H. (1924). Induction of embryonic primordia by implantation of organizers from a different species. . New York: Hafner

Squire, J. M. (1997). Architecture and function in the muscle sarcomere. *Curr Opin Struct Biol* **7**, 247-57.

Srinivas, B. P., Woo, J., Leong, W. Y. and Roy, S. (2007). A conserved molecular pathway mediates myoblast fusion in insects and vertebrates. *Nat Genet* **39**, 781-6.

Steinbacher, P., Haslett, J. R., Six, M., Gollmann, H. P., Sanger, A. M. and Stoiber, W. (2006). Phases of myogenic cell activation and possible role of dermomyotome cells in teleost muscle formation. *Dev Dyn* **235**, 3132-43.

Steinmetz, M. O., Stoffler, D., Muller, S. A., Jahn, W., Wolpensinger, B., Goldie, K. N., Engel, A., Faulstich, H. and Aebi, U. (1998). Evaluating atomic models of F-actin with an undecagold-tagged phalloidin derivative. *J Mol Biol* **276**, 1-6.

Stellabotte, F., Dobbs-McAuliffe, B., Fernandez, D. A., Feng, X. and Devoto, S. H. (2007). Dynamic somite cell rearrangements lead to distinct waves of myotome growth. *Development* **134**, 1253-7.

Stern, H. M., Murphey, R. D., Shepard, J. L., Amatruda, J. F., Straub, C. T., Pfaff, K. L., Weber, G., Tallarico, J. A., King, R. W. and Zon, L. I. (2005). Small molecules that delay S phase suppress a zebrafish bmyb mutant. *Nat Chem Biol* **1**, 366-70.

Stickney, H. L., Barresi, M. J. and Devoto, S. H. (2000). Somite development in zebrafish. *Dev Dyn* **219**, 287-303.

Strunkelnberg, M., Bonengel, B., Moda, L. M., Hertenstein, A., de Couet, H. G., Ramos, R. G. and Fischbach, K. F. (2001). rst and its paralogue kirre act redundantly during embryonic muscle development in Drosophila. *Development* **128**, 4229-39.

Sussman, M. A., Baque, S., Uhm, C. S., Daniels, M. P., Price, R. L., Simpson, D., Terracio, L. and Kedes, L. (1998). Altered expression of tropomodulin in cardiomyocytes disrupts the sarcomeric structure of myofibrils. *Circ Res* **82**, 94-105.

Takada, F., Vander Woude, D. L., Tong, H. Q., Thompson, T. G., Watkins, S. C., Kunkel, L. M. and Beggs, A. H. (2001). Myozenin: an alpha-actinin- and gamma-filamin-binding protein of skeletal muscle Z lines. *Proc Natl Acad Sci U S A* **98**, 1595-600.

Tang, Z., Scherer, P. E., Okamoto, T., Song, K., Chu, C., Kohtz, D. S., Nishimoto, I., Lodish, H. F. and Lisanti, M. P. (1996). Molecular cloning of caveolin-3, a novel member of the caveolin gene family expressed predominantly in muscle. *J Biol Chem* **271**, 2255-61.

Taoka, M., Ichimura, T., Wakamiya-Tsuruta, A., Kubota, Y., Araki, T., Obinata, T. and Isobe, T. (2003). V-1, a protein expressed transiently during murine cerebellar development, regulates actin polymerization via interaction with capping protein. *J Biol Chem* **278**, 5864-70.

Taoka, M., Isobe, T., Okuyama, T., Watanabe, M., Kondo, H., Yamakawa, Y., Ozawa, F., Hishinuma, F., Kubota, M., Minegishi, A. et al. (1994). Murine cerebellar neurons express a novel gene encoding a protein related to cell cycle control and cell fate determination proteins. *J Biol Chem* **269**, 9946-51.

Taoka, M., Yamakuni, T., Song, S. Y., Yamakawa, Y., Seta, K., Okuyama, T. and Isobe, T. (1992). A rat cerebellar protein containing the cdc10/SWI6 motif. *Eur J Biochem* **207**, 615-20.

Tapscott, S. J. (2005). The circuitry of a master switch: Myod and the regulation of skeletal muscle gene transcription. *Development* **132**, 2685-95.

Taylor, R. G., Papa, I., Astier, C., Ventre, F., Benyamin, Y. and Ouali, A. (1997). Fish muscle cytoskeleton integrity is not dependent on intact thin filaments. *J Muscle Res Cell Motil* **18**, 285-94.

Thisse, C., Thisse, B., Schilling, T. F. and Postlethwait, J. H. (1993). Structure of the zebrafish snail1 gene and its expression in wild-type, spadetail and no tail mutant embryos. *Development* **119**, 1203-15.

Thomas, G. H. (2001). Spectrin: the ghost in the machine. *Bioessays* **23**, 152-60.

Tidball, J. G. (1991). Force transmission across muscle cell membranes. *J Biomech* **24 Suppl 1**, 43-52.

Tullio, A. N., Accili, D., Ferrans, V. J., Yu, Z. X., Takeda, K., Grinberg, A., Westphal, H., Preston, Y. A. and Adelstein, R. S. (1997). Nonmuscle myosin II-B is required for normal development of the mouse heart. *Proc Natl Acad Sci U S A* **94**, 12407-12.

Ursitti, J. A. and Fowler, V. M. (1994). Immunolocalization of tropomodulin, tropomyosin and actin in spread human erythrocyte skeletons. *J Cell Sci* **107 (Pt 6)**, 1633-9.

van der Ven, P. F., Bartsch, J. W., Gautel, M., Jockusch, H. and Furst, D. O. (2000). A functional knock-out of titin results in defective myofibril assembly. *J Cell Sci* **113 (Pt 8)**, 1405-14.

Van Der Ven, P. F., Obermann, W. M., Weber, K. and Furst, D. O. (1996). Myomesin, M-protein and the structure of the sarcomeric M-band. *Adv Biophys* **33**, 91-9.

Vera, C., Sood, A., Gao, K. M., Yee, L. J., Lin, J. J. and Sung, L. A. (2000). Tropomodulin-binding site mapped to residues 7-14 at the N-terminal heptad repeats of tropomyosin isoform 5. *Arch Biochem Biophys* **378**, 16-24.

Vigoreaux, J. O. (1994). The muscle Z band: lessons in stress management. *J Muscle Res Cell Motil* **15**, 237-55.

Volonte, D., Peoples, A. J. and Galbiati, F. (2003). Modulation of myoblast fusion by caveolin-3 in dystrophic skeletal muscle cells: implications for Duchenne muscular dystrophy and limb-girdle muscular dystrophy-1C. *Mol Biol Cell* **14**, 4075-88.

von Bulow, M., Rackwitz, H. R., Zimbelmann, R. and Franke, W. W. (1997). CP beta3, a novel isoform of an actin-binding protein, is a component of the cytoskeletal calyx of the mammalian sperm head. *Exp Cell Res* **233**, 216-24.

Vos, P., Hogers, R., Bleeker, M., Reijans, M., van de Lee, T., Hornes, M., Frijters, A., Pot, J., Peleman, J., Kuiper, M. et al. (1995). AFLP: a new technique for DNA fingerprinting. *Nucleic Acids Res* **23**, 4407-14.

Wakelam, M. J. (1985). The fusion of myoblasts. *Biochem J* **228**, 1-12.

Wang, K. (1996). Titin/connectin and nebulin: giant protein rulers of muscle structure and function. *Adv Biophys* **33**, 123-34.

Wang, K., McClure, J. and Tu, A. (1979). Titin: major myofibrillar components of striated muscle. *Proc Natl Acad Sci U S A* **76**, 3698-702.

Wang, K. and Wright, J. (1988). Architecture of the sarcomere matrix of skeletal muscle: immunoelectron microscopic evidence that suggests a set of parallel inextensible nebulin filaments anchored at the Z line. *J Cell Biol* **107**, 2199-212.

Warga, R. M. and Kimmel, C. B. (1990). Cell movements during epiboly and gastrulation in zebrafish. *Development* **108**, 569-80.

Warga, R. M. and Nusslein-Volhard, C. (1999). Origin and development of the zebrafish endoderm. *Development* **126**, 827-38.

Watchko, J. F., O'Day, T. L. and Hoffman, E. P. (2002). Functional characteristics of dystrophic skeletal muscle: insights from animal models. *J Appl Physiol* **93**, 407-17.

Way, M. and Parton, R. G. (1995). M-caveolin, a muscle-specific caveolin-related protein. *FEBS Lett* **376**, 108-12.

Wear, M. A., Yamashita, A., Kim, K., Maeda, Y. and Cooper, J. A. (2003). How capping protein binds the barbed end of the actin filament. *Curr Biol* **13**, 1531-7.

Wegner, A. (1982). Kinetic analysis of actin assembly suggests that tropomyosin inhibits spontaneous fragmentation of actin filaments. *J Mol Biol* **161**, 217-27.

Weinberg, E. S., Allende, M. L., Kelly, C. S., Abdelhamid, A., Murakami, T., Andermann, P., Doerre, O. G., Grunwald, D. J. and Riggleman, B. (1996). Developmental regulation of zebrafish MyoD in wild-type, no tail and spadetail embryos. *Development* **122**, 271-80.

Weintraub, H., Davis, R., Tapscott, S., Thayer, M., Krause, M., Benezra, R., Blackwell, T. K., Turner, D., Rupp, R., Hollenberg, S. et al. (1991). The myoD gene family: nodal point during specification of the muscle cell lineage. *Science* **251**, 761-6.

Williams, M. W. and Bloch, R. J. (1999). Differential distribution of dystrophin and beta-spectrin at the sarcolemma of fast twitch skeletal muscle fibers. *J Muscle Res Cell Motil* **20**, 383-93.

Williams, M. W., Resneck, W. G., Kaysser, T., Ursitti, J. A., Birkenmeier, C. S., Barker, J. E. and Bloch, R. J. (2001). Na,K-ATPase in skeletal muscle: two populations of beta-spectrin control localization in the sarcolemma but not partitioning between the sarcolemma and the transverse tubules. *J Cell Sci* **114**, 751-62.

Winegrad, S. (1999). Cardiac myosin binding protein C. *Circ Res* **84**, 1117-26.

Witt, C. C., Burkart, C., Labeit, D., McNabb, M., Wu, Y., Granzier, H. and Labeit, S. (2006). Nebulin regulates thin filament length, contractility, and Z-disk structure in vivo. *Embo J* **25**, 3843-55.

Wolff, C., Roy, S. and Ingham, P. W. (2003). Multiple muscle cell identities induced by distinct levels and timing of hedgehog activity in the zebrafish embryo. *Curr Biol* **13**, 1169-81.

Wolff, C., Roy, S., Lewis, K. E., Schauerte, H., Joerg-Rauch, G., Kirn, A., Weiler, C., Geisler, R., Haffter, P. and Ingham, P. W. (2004). iguana encodes a novel zinc-finger protein with coiled-coil domains essential for Hedgehog signal transduction in the zebrafish embryo. *Genes Dev* **18**, 1565-76.

Wright, W. E., Sassoon, D. A. and Lin, V. K. (1989). Myogenin, a factor regulating myogenesis, has a domain homologous to MyoD. *Cell* **56**, 607-17.

Yamashita, A., Maeda, K. and Maeda, Y. (2003). Crystal structure of CapZ: structural basis for actin filament barbed end capping. *Embo J* **22**, 1529-38.

Yang, C., Pring, M., Wear, M. A., Huang, M., Cooper, J. A., Svitkina, T. M. and Zigmond, S. H. (2005). Mammalian CARMIL inhibits actin filament capping by capping protein. *Dev Cell* **9**, 209-21.

Zhang, J. and King, M. L. (1996). Xenopus VegT RNA is localized to the vegetal cortex during oogenesis and encodes a novel T-box transcription factor involved in mesodermal patterning. *Development* **122**, 4119-29.

Zhou, Q., Chu, P. H., Huang, C., Cheng, C. F., Martone, M. E., Knoll, G., Shelton, G. D., Evans, S. and Chen, J. (2001). Ablation of Cypher, a PDZ-LIM domain Z-line protein, causes a severe form of congenital myopathy. *J Cell Biol* **155**, 605-12.

Appendix

Table 1. Sequences of indel primers used in the positional cloning of the *sne* mutant

Indel primer name	Sequence: Forward primer	Reverse primer
20.83	ATGGACGCAGTGGAGAAAAC	CAGCAGAAGCCCCTAATTCA
20.87	TGCTACGCCACTGCATAATC	GTGGCGACCCCTGATAAAT
20.97	TTTTCTCTGTGGCGATGACA	CCACTGATCAGGAAAATCTGC
21.01	TGCTACGCCACTGCATAATC	GTGGCGACCCCTGATAAAT
21.161	CAATTCGGTAATGGTTGTAGGC	TTTTGTTTTCGTATTGCATCTC
21.163	CACAAACTTTGGGATATTCAAGC	AAATCAAAGAGCATCAAACAAAA
21.18	TGAAGGCATTAAAATAAAAGACG	CCCAGGCAGGATGCTAAGT
21.196	TTTGAGTGAAAACTCTAATGAGCA	TTGGTGAGTTATGACAGGTTGTG
21.2	AGCAGGCATGCATGTTACAG	TTCAGCAACCTCACAAGTCA
21.22a	TGATCTATCCGCCCGTTAAG	CTGGCCATGGAATATTAGGC
21.22b	GGCTTGGACCTGAAAACAAG	ATGTCCTTCCATCTGCAACC
21.25	GGCATTAAAATAAAAGACGCACA	CCCAGGCAGGATGCTAAGTA
21.38	CCCATTCATCTCTGCATGTC	TGCAGAGTAAATCACACTCAATCA
21.46	GGCATAAAACACTGGTAAAAGCA	CAAATTTCTGGCCAAAAGAAA
21.63	TGGAATTATTCTGTATGGATGCAA	AATGGCTACATGCTGAACCAG
21.716	CAAGCCATCACATAGTCAAAAAG	TGACTTCTCATTCTTTTCTTGTTTT
21.76	CACGCAACACAAATAATTACCA	CTTCATTCGCCTGAGCAAA
21.762	TACCTCCCATTCGCTTCATT	GCCAGTCCGTTCTGTTATGG
21.765	AACAATGATGATGATAATGGTGATAA	TATTTCACACGCCTTCAACA
21.766	AGACTCCTTCGGCATAGCAA	TCGTTTCGGTTGAATTGACA
21.768	AGCAATGGCGGTAATCTGAC	CTGACCCAGGACCACAAAAT
21.77	GCTGTAAAGCAGCAGAAATGG	GGCTTTTTGTGAGGGAATGA
21.78	TTTGTAACATATCCGTCTCTCAAG	TGGAAAACAAATGCAAATGAA
21.79	CAGCATGCAAGAAGAGGAAA	TCCAGTGAATCTGTGTTTTATGC
21.86	TCCACCTTCTCTTCCGACAT	TTTGTTTCTGTCTTGCCTGAAC
22.09	TGCATGTGAAAACAAGATAATCA	CAATTTACCACAATAACCATCAAAA
22.16	TTTACACAGCGGATGCCTTT	GTCCAGCTGGGGTGAATATG
22.21	TGTTCAGCTAACAAAAAGTGGTG	TGTGATATTGCATGGCCCTA
22.5	GAAAAAGCTGCTCACCAACC	TCCAACCCTAATCAAACATGC
22.54	TGAAAGGAAGGAAGGACCAA	TCCTTTCATTTGAACGCTTCT
22.55	TGGATGGATGGATTAATAGATGG	TTAAAAATAGTGAGTGAAAAACTGACA
23	TGTGTTGATAGCAAGGCCAAT	GCATTTCAAAGCCTCATGAAT
23.17	GCAATGTGACCCAAACAGGT	GGTGTGAGGAATTGCAGGTT
23.3	TGGGCAGTTAAAATGTAAAGCA	ATCGGCCAGACGTAAAGAGA
23.34	TCTGTCAAAAGGACGTAGGC	AACGCCCTTTCAGCAATAGA
23.49	TGCCTTTTTATTTTTGGAAGGA	TTTTTGTGGCTGAATGATTTACA
24.11	CACACACACGAACCTAAGCA	AACTCCAGCAGAAGCACCAG
24.28	TGAAATTTTGTCAATTTCCACAT	AGGAAGTGCATCCACCAAAC
24.52	TGGGTTCACATCTTGAAATTCT	CAATTTGTTATTCTCAAGTCAAAATTC
25.01	TTCAGACTTCAACTGTATGTGTGTATG	GCGTTTTTAGACTCTGTGTTTGA
25.16	TCCGATATAGAGGGGGTTCA	ATGCTCTCAACTGGCTGGAT
25.67	AAAAGATTTGGGAGGGGTGT	CAGCCTTGAATAAATCTATTGTTGA
26.58	ACCGCGTCAGCTAAACTCTC	ACCAAACGAAAAAGCAATGG
27.36	AATGTAGCCGTGAAGGGATG	AGGGGCATCTTTTGAATGGT
28.14	TCAGAAGCAATCCATATGACAAA	CTGCAACAGCCAAATTTCAG
28.18	GGATGAGCATGCACAGAATG	TGCTTCACTGCTGTCTCTTG
28.37	ATTGTCGGTTTTGGGTGAAC	TGAACTGGGATGCAGAATGA
28.49	GCTGTCCTTTGCGAGTTTGT	CCGAGGGGGAAAACACTACT
28.68	TCATGCAACGTTACAGCAAA	CACACAAGTGCACTGTTAAATCT
28.73	GCACTGCTGTGTTCAGGATCT	TGAAGGGCAGGACAGAAAGT
28.98	TGATCTGATGAGGTCTGAAAACA	GCTGGAGGAAGTGTCTGGAG
29.15	TGACACAACTGGTTTTGCTTG	TAGGCTTTGAGCCAGCACTT
29.32	GAGAAGGTTGCTGGTTCGAG	ATGGATGCCCTTTCAGTCAG
29.51	TTGTGCTGTTTTCTCCACCA	TGGCTAATGCCTGTCTATGC
29.64	ATCCCAGGCTCTGTGTGAAT	GTGAAGAAAGCAGCTCACCA

Indel primer name	Sequence: Forward primer	Reverse primer
bx3.1	TCGCACAGGAATAGAATGAGC	AGACCTCCAGAGAGTTTAGAGACA
bx3.2	TCCAATCAGGAAGGGGTTATT	GCAGTGTTTGTGTTGTCAGGA
bx3.3	TTGTGATGGTATGATAACCTTGG	CAAGAGCAGAAAAGATATCCAAAGA
bx3.4	TTATCGTCCCATACCTAAGTGC	AATGGTGACAATTTGTATAAAGCA
bx3.5	CACAACATTTAAAGTTAATTCACACCA	TAAGGAAACCCCTGCCTGAT
bx3.6	ACCTGGCCTTCAGCAGAG	GATTTCCAGCAGCACAGTGA
bx3.7	TGAACTGTGCCTCAGTCGAG	TGGTGACCTCTGAAACAGAGAC
bx3.8	GCAATGACATGACCACATTGA	TGAACCTTAAAATAATGTGTGACCA
bx3.9	AAAAGCAGCCAATATCTCAAAAA	CCATTATGTTTATAACAAATTGCATTA
bx3.10	ACAGTCTGCAAGGTCCGATT	TTGGTGGTTTTCAGGGACTC
bx3.11	TGCATTCGATTAAGCAGCAG	GAGGGGCTAATAATTCAGACTTCA
bx3.12	AAGCTGTGTAGAATTGTCTTGAAAAA	AAAACAGGGGTGTCCAAACTT
bx3.13	TTGAGCTGAATTGGTTGCTG	CGTGCATCCATTGGAAATAA
bx3.14	ACAGAACACCCCAAAACTGC	TGACTACTTTTGGAAAATTGTAATTGA
bx3.15	CCGAAATTGGGAAGTGACAT	TTTGTTATGGTGAAGCTGCATT
bx3.16	CACTGATTTACAAACACCACAAGA	TTGTGTCGTGACAGTGCAGA
bx3.17	TCCCAAAAATCACATTTTCCA	TCTCTGTCCATCCGTCCTGT
bx3.18	GGACAGAGACAAACACACTGGAT	CCAACCATTCAACCATCAAC
bx3.19	GATGGTTGGATGGTCCAGTT	CCATCCATCCCTTTTTACCA
bx3.20	ATGGATGAAATGATGCATGG	TCTATCTGTCTACCTAGTGTGTCTGTC
cr38.1	GTTGAACACACGTCCACCAC	TTGTGAAAATTTCTTTGCTCTGTT
cr38.2	CGCTTTTATCCAAAGCGACT	CCTAATCTGCAATTGCCTCTC
cr38.3	TCTGTCTGAGCCAGCCTTCT	TTGCATACAAACCATTTTCCA
cr38.4	AGCAGTTTTCGGAGCCTACC	CTGGCAAAATCTCAGCCAAT

Table2. Sequences of primers used in amplification of *capzα1*and *capzβ* genomic and cDNA. The primer sequences used to amplify the actin control in the RT-PCR are also provided.

	Primer	Forward 5′′-3′	Reverse 5′-3′
capzα1	2	CAGCCAAGATGACCGACTTT	GGCTCAAACTTATGACCCTCA
	4	AGCATGGAGATCTGGGTCAG	AGGTTGAATGGAATCGCATC
	Fact3	TGTGCTCATTTTCCATTGATTT	AGGAAGAGGAAGTGGGTCGT
	Fact2	TGTAAAACGACGGCCAGTTGGT CAATCATTTCAATAACACC	AGGAAACAGCTATGACCATGTCG ATCTTGGTACGGGTGA
capzβ	capZb1 (RT-PCR)	CAGAATGAGCAGCAGTTGGA	GTGTGACCTGTCGGGTGAG
	capZb3 (genomic)	GCTCTGGAACCATGAACCTT	GAAAGAGAGACGGGTGGTGA
control	actin	GATCTTCACTCCCCTTGTTC	ACAGAGCAGAAGCCATGCTG

Table 3. Sequences of primers used to generate the template for the *capzα1, capzα2* and *capzβ in situ* probes.

Primer	Forward 5′-3′	Reverse 5′-3′
capZα1	TCTCCCCAAAAATGAAATTAAGA	TTATTCTGCCTTTTTGGTTATTAAA
capZα2	ATGAGGATGGAAACGTGCAG	AAAGGAGGCAGTCTCTTCAGC
capZβ	CAGAATGAGCAGCAGTTGGA	GTGTGACCTGTCGGGTGAG

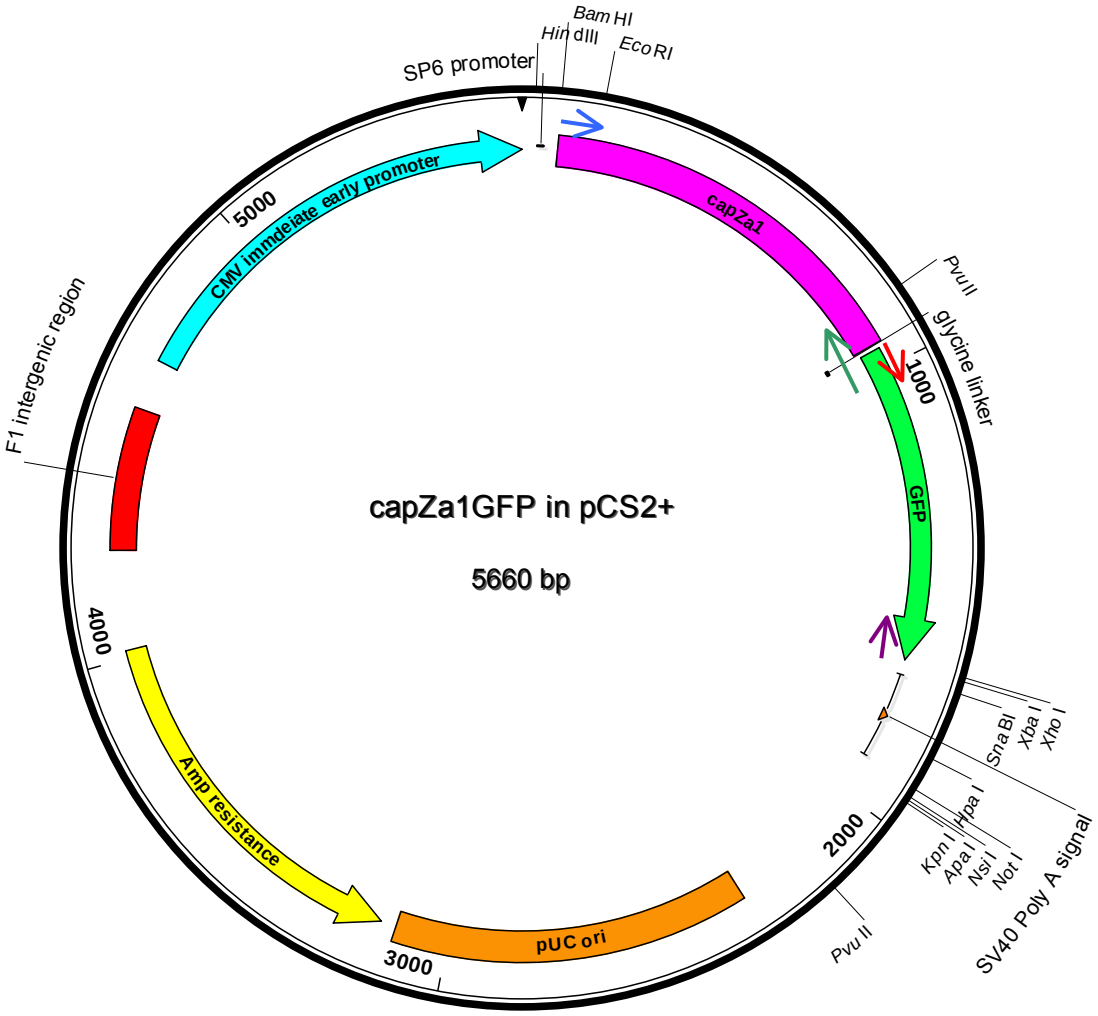

Fig 1. Plasmid map of capZα1-GFP pCS2+. The position of the capZORFF, GFPR1, GFPF2 and GFPR2 primers are represented by blue, red, green and purple arrows respectively.

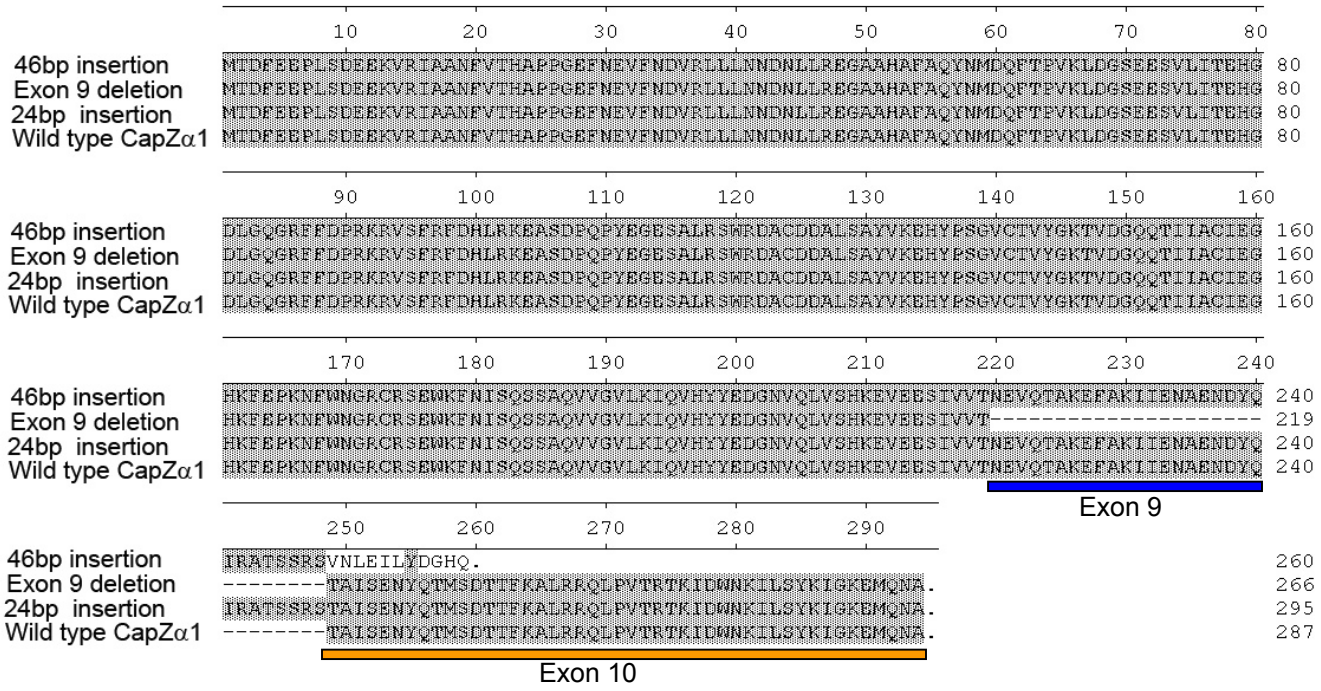

Fig. 2. Comparison of predicted CapZα1 *sne* mutant protein products with wild type CapZα1. The regions encoded by exon 9 and 10 are underlined in blue and orange respectively. The 46bp insertion of intron 9 produces a frame shift and exon 10 is not translated. The exon 9 deletion produces an in frame product where exon 10 is still translated. The 24bp insertion of intron 9 also produces an in frame product where exon 10 is translated, however, an additional eight amino acids are translated between exon 9 and 10.

Table 4. Number of experiments performed for all MOs used in this thesis. For each experiment approximately 50 embryos were injected. If over 90% of the embryos per MO experiment displayed similar phenotypes they were not scored on the basis of individual phenotype. All MOs were titrated to determine their optimum concentration prior to use.

Morpholino	Amount injected per embryo	Number of experiments performed
capZα1 ATG	5ng	4
capZα1 splice 1	4ng	3
capZα1 splice 2	10ng	5
capZα2 ATG	1.5ng	2
capZα2 splice	6ng	1
capZβ ATG	6ng	2*
capZβ splice	3ng	3*
Desmin ATG	3ng	2
Desmin splice	8ng	3
SK Tmod 4 and capZα1splice 2	3ng and 10ng	2
capZα1splice 2 injected into *buf* mutants	10ng	2
SK Tmod 4 injected into *buf* mutants	3ng	2

* Variable phenotypes were observed with these MOs. See appendix, Table 5 for specific descriptions

Table 5. List of phenotypes observed from capZβ ATG and splice MOs. All phenotypes were observed at 5dpf apart from capZβ splice 3ng on the 22/09/07 where phenotypes were observed at 48hpf.

	capZβ ATG 6ng 10/05/07	*capZβ ATG 6ng 20/05/07*	*capZβ splice 3ng (48 hpf) 22/09/06*	*capZβ splice 3ng 24/04/07*	*capZβ splice 3ng 20/05/07*
Severely truncated, heart edema and small brain	3	10	40		11
Truncated, curved axis, no heart edema		8		20	8
Straight axis, no swim bladder, reduced motility		1			
Straight axis, no swim bladder, frayed caudal fin, reduced motility		20			
Straight axis, no swim bladder, no heart edema, swim normally	32 (did not check for fin phenotype)			20	20 (12 of these look thinner than wild type)